

## (12) INTERNATIONAL APPLICATION PUBLISHED UNDER THE PATENT COOPERATION TREATY (PCT)

(12) World Intellectual Property Organization  
International Bureau(43) International Publication Date  
1 March 2001 (01.03.2001)

PCT

(10) International Publication Number  
WO 01/14824 A1

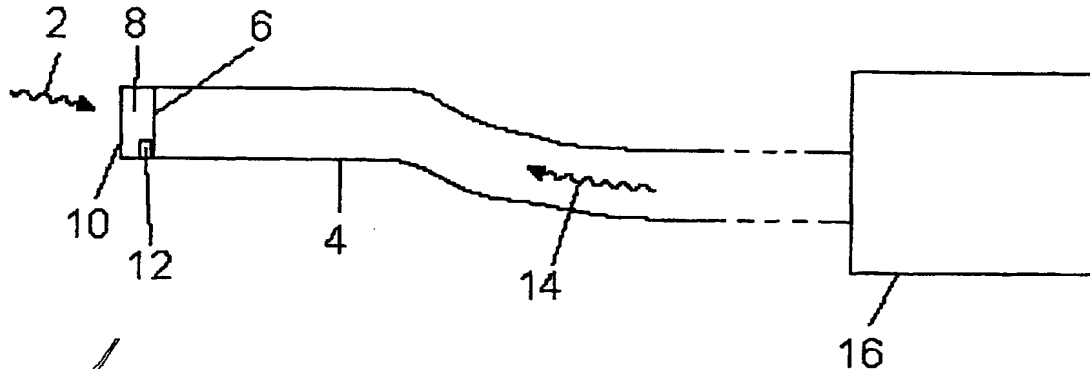
- (51) International Patent Classification<sup>7</sup>: G01B 9/02    (74) Agent: ELKINGTON AND FIFE; Prospect House, 8 Pembroke Road, Sevenoaks, Kent TN13 1XR (GB).
- (21) International Application Number: PCT/GB00/03238
- (22) International Filing Date: 18 August 2000 (18.08.2000)
- (25) Filing Language: English
- (26) Publication Language: English
- (30) Priority Data:  
9919688.3                          19 August 1999 (19.08.1999) GB
- (71) Applicant (for all designated States except US): UNIVERSITY COLLEGE LONDON [GB/GB]; Gower Street, London WC1E 6BT (GB).
- (72) Inventors; and
- (75) Inventors/Applicants (for US only): BEARD, Paul [GB/GB]; 41 Montrose House, Westferry Road, London E14 3SE (GB). MILLS, Timothy, Noel [GB/GB]; Flat 4, 45 Newman Street, London W1P 3PA (GB). DELPY, David [GB/GB]; 9 Keswick Avenue, Merton Park, London SW19 3JE (GB).
- (81) Designated States (national): AE, AG, AL, AM, AT, AU, AZ, BA, BB, BG, BR, BY, BZ, CA, CH, CN, CR, CU, CZ, DE, DK, DM, DZ, EE, ES, FI, GB, GD, GE, GH, GM, HR, HU, ID, IL, IN, IS, JP, KE, KG, KP, KR, KZ, LC, LK, LR, LS, LT, LU, LV, MA, MD, MG, MK, MN, MW, MX, MZ, NO, NZ, PL, PT, RO, RU, SD, SE, SG, SI, SK, SL, TJ, TM, TR, TT, TZ, UA, UG, US, UZ, VN, YU, ZA, ZW.
- (84) Designated States (regional): ARIPO patent (GH, GM, KE, LS, MW, MZ, SD, SL, SZ, TZ, UG, ZW), Eurasian patent (AM, AZ, BY, KG, KZ, MD, RU, TJ, TM), European patent (AT, BE, CH, CY, DE, DK, ES, FI, FR, GB, GR, IE, IT, LU, MC, NL, PT, SE), OAPI patent (BF, BJ, CF, CG, CI, CM, GA, GN, GW, ML, MR, NE, SN, TD, TG).

## Published:

— With international search report.

For two-letter codes and other abbreviations, refer to the "Guidance Notes on Codes and Abbreviations" appearing at the beginning of each regular issue of the PCT Gazette.

(54) Title: FABRICATION OF FABRY-PEROT POLYMER FILM SENSING INTERFEROMETERS



WO 01/14824 A1

(57) Abstract: A method of forming an interferometer film for an interferometer sensor comprises forming a parylene polymer layer (8) of substantially uniform thickness directly on an interferometer substrate (4, 45), the layer forming the interferometer film. Since the interferometer film (8) is formed directly onto the surface of the interferometer substrate, there is improved conformity between the two surfaces at the interface between the polymer layer and the substrate and improved uniformity in the thickness of the film.



# INTERNATIONAL SEARCH REPORT

Intern: ai Application No

PCT/GB 00/03238

## A. CLASSIFICATION OF SUBJECT MATTER

IPC 7 G01B9/02

According to International Patent Classification (IPC) or to both national classification and IPC

## B. FIELDS SEARCHED

Minimum documentation searched (classification system followed by classification symbols)

IPC 7 G01B

Documentation searched other than minimum documentation to the extent that such documents are included in the fields searched

Electronic data base consulted during the international search (name of data base and, where practical, search terms used)

EPO-Internal, PAJ, WPI Data

## C. DOCUMENTS CONSIDERED TO BE RELEVANT

Category °	Citation of document, with indication, where appropriate, of the relevant passages	Relevant to claim No.
A	US 5 311 485 A (KUZMENKO PAUL J ET AL) 10 May 1994 (1994-05-10) abstract; figures 1,2 column 3, line 58 ----	1,7,9
A	US 5 262 842 A (GAUGLITZ GUENTER ET AL) 16 November 1993 (1993-11-16) abstract; figure 1 ----	1,7,9
A	US 5 533 151 A (LEONARD JERRY) 2 July 1996 (1996-07-02) abstract; figure 10 -----	1,7,9

Further documents are listed in the continuation of box C.

Patent family members are listed in annex.

° Special categories of cited documents :

- "A" document defining the general state of the art which is not considered to be of particular relevance
- "E" earlier document but published on or after the international filing date
- "L" document which may throw doubts on priority, claim(s) or which is cited to establish the publication date of another citation or other special reason (as specified)
- "O" document referring to an oral disclosure, use, exhibition or other means
- "P" document published prior to the international filing date but later than the priority date claimed

- "T" later document published after the international filing date or priority date and not in conflict with the application but cited to understand the principle or theory underlying the invention
- "X" document of particular relevance; the claimed invention cannot be considered novel or cannot be considered to involve an inventive step when the document is taken alone
- "Y" document of particular relevance; the claimed invention cannot be considered to involve an inventive step when the document is combined with one or more other such documents, such combination being obvious to a person skilled in the art.
- "&" document member of the same patent family

Date of the actual completion of the international search

1 November 2000

Date of mailing of the international search report

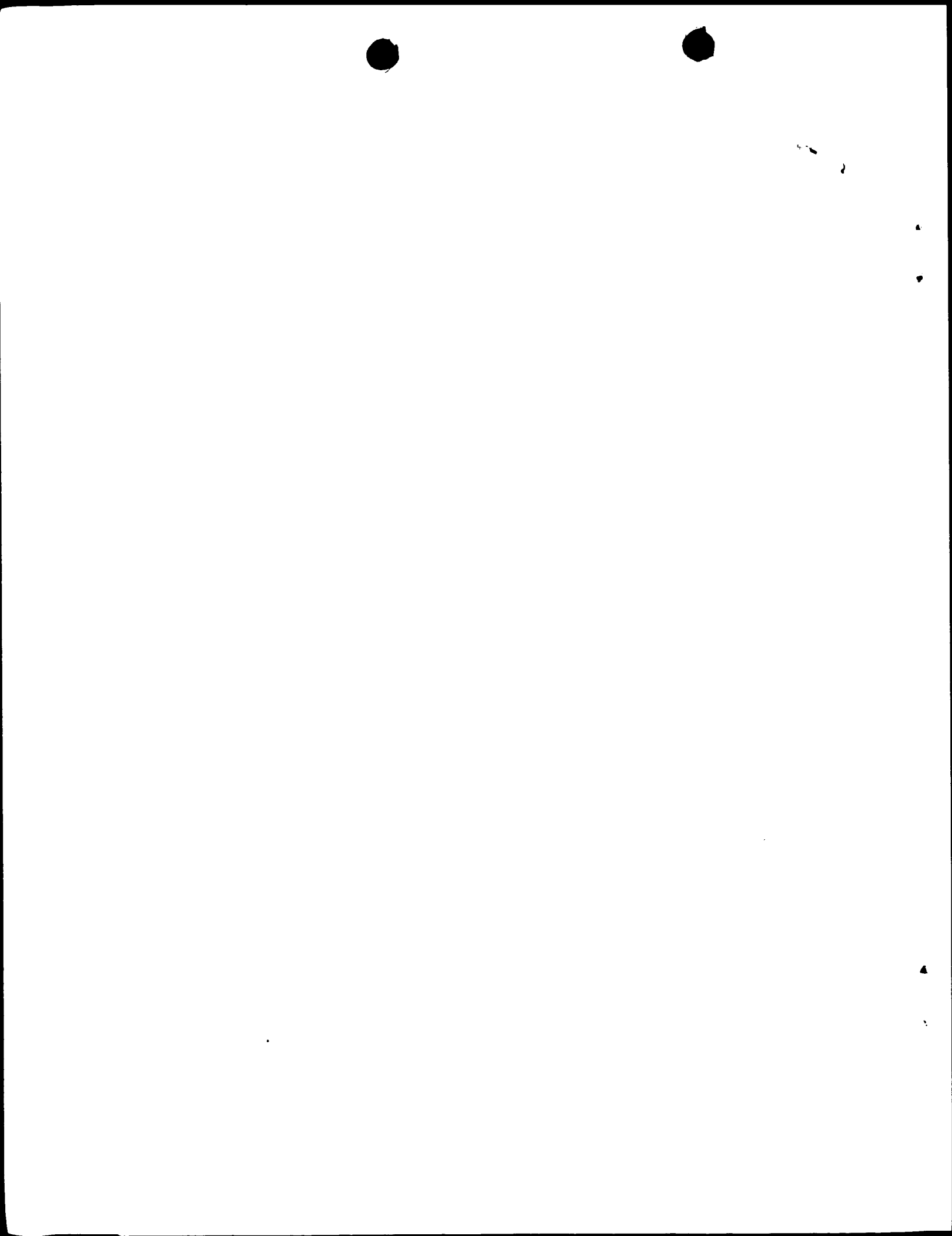
10/11/2000

Name and mailing address of the ISA

European Patent Office, P.B. 5818 Patentlaan 2  
NL - 2280 HV Rijswijk  
Tel. (+31-70) 340-2040, Tx. 31 651 epo nl,  
Fax: (+31-70) 340-3016

Authorized officer

Vorropoulos, G



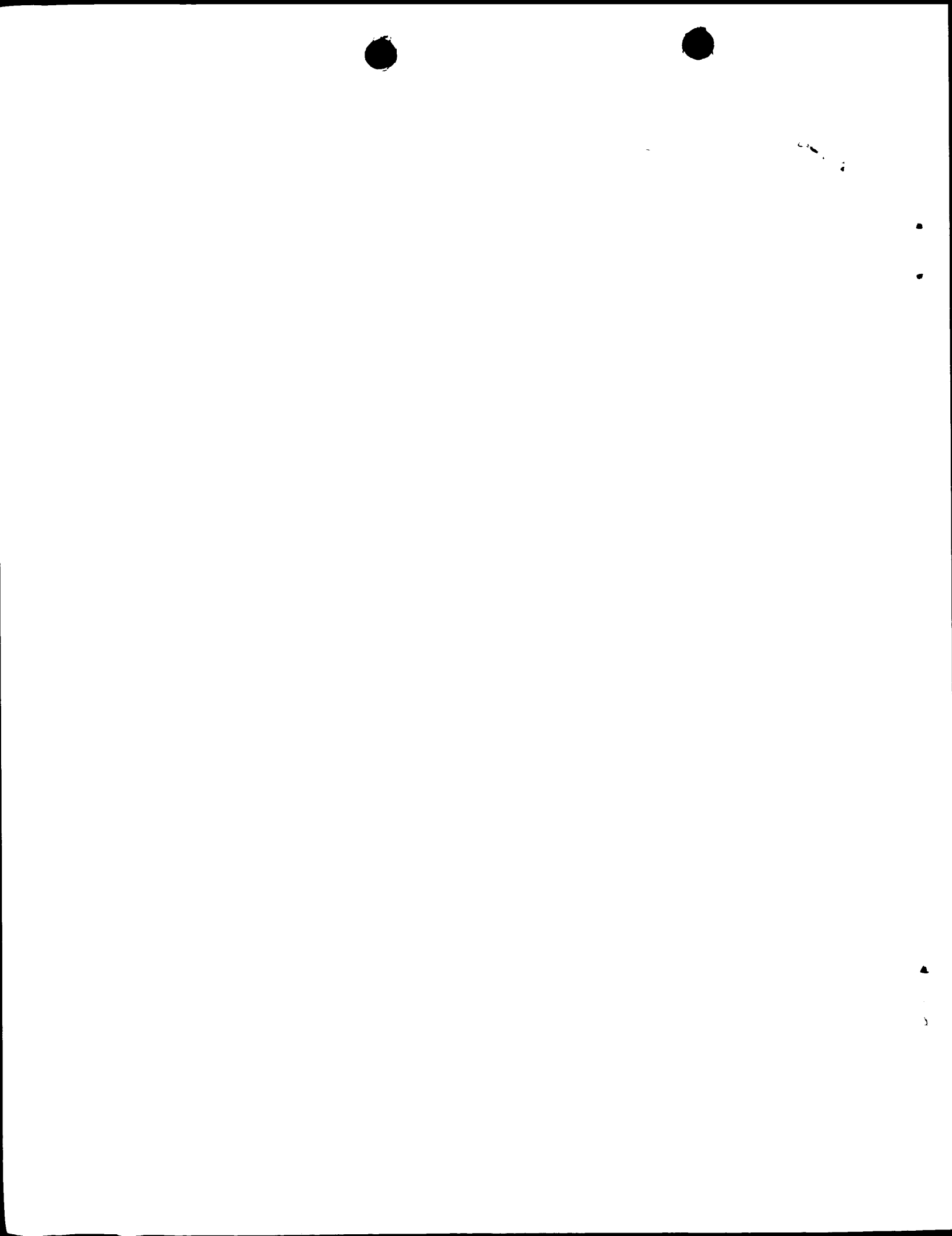
# INTERNATIONAL SEARCH REPORT

Information on patent family members

International Application No

PCT/GB 00/03238

Patent document cited in search report	Publication date	Patent family member(s)			Publication date
US 5311485	A 10-05-1994	NONE			
US 5262842	A 16-11-1993	DE	4033357 A	23-04-1992	
		EP	0481440 A	22-04-1992	
		JP	4285844 A	09-10-1992	
US 5533151	A 02-07-1996	NONE			



## PATENT COOPERATION TREATY

PCT

## INTERNATIONAL PRELIMINARY EXAMINATION REPORT

REC'D 05 APR 2001

## (PCT Article 36 and Rule 70)

Applicant's or agent's file reference NJE/G15565WO	<b>FOR FURTHER ACTION</b>	See Notification of Transmittal of International Preliminary Examination Report (Form PCT/IPEA/416)
International application No. PCT/GB00/03238	International filing date (day/month/year) 18/08/2000	Priority date (day/month/year) 19/08/1999
International Patent Classification (IPC) or national classification and IPC G01B9/02		
<p><b>Applicant</b> UNIVERSITY COLLEGE LONDON et al.</p> <p>1. This international preliminary examination report has been prepared by this International Preliminary Examining Authority and is transmitted to the applicant according to Article 36.</p> <p>2. This REPORT consists of a total of 4 sheets, including this cover sheet.</p> <p><input type="checkbox"/> This report is also accompanied by ANNEXES, i.e. sheets of the description, claims and/or drawings which have been amended and are the basis for this report and/or sheets containing rectifications made before this Authority (see Rule 70.16 and Section 607 of the Administrative Instructions under the PCT).</p> <p>These annexes consist of a total of sheets.</p> <p>3. This report contains indications relating to the following items:</p> <ul style="list-style-type: none"> <li>I    <input checked="" type="checkbox"/> Basis of the report</li> <li>II    <input type="checkbox"/> Priority</li> <li>III    <input type="checkbox"/> Non-establishment of opinion with regard to novelty, inventive step and industrial applicability</li> <li>IV    <input type="checkbox"/> Lack of unity of invention</li> <li>V    <input checked="" type="checkbox"/> Reasoned statement under Article 35(2) with regard to novelty, inventive step or industrial applicability; citations and explanations supporting such statement</li> <li>VI    <input type="checkbox"/> Certain documents cited</li> <li>VII    <input checked="" type="checkbox"/> Certain defects in the international application</li> <li>VIII    <input type="checkbox"/> Certain observations on the international application</li> </ul>		

Date of submission of the demand 13/02/2001	Date of completion of this report 03.04.2001
Name and mailing address of the international preliminary examining authority:  European Patent Office D-80298 Munich Tel. +49 89 2399 - 0 Tx: 523656 epmu d Fax: +49 89 2399 - 4465	Authorized officer Hiltner, K Telephone No. +49 89 2399 2198





# INTERNATIONAL PRELIMINARY EXAMINATION REPORT

International application No. PCT/GB00/03238

## I. Basis of the report

1. With regard to the **elements** of the international application (*Replacement sheets which have been furnished to the receiving Office in response to an invitation under Article 14 are referred to in this report as "originally filed" and are not annexed to this report since they do not contain amendments (Rules 70.16 and 70.17)*):

### Description, pages:

1-7                   as originally filed

### Claims, No.:

1-9                   as originally filed

### Drawings, sheets:

1/2,2/2               as originally filed

2. With regard to the **language**, all the elements marked above were available or furnished to this Authority in the language in which the international application was filed, unless otherwise indicated under this item.

These elements were available or furnished to this Authority in the following language: , which is:

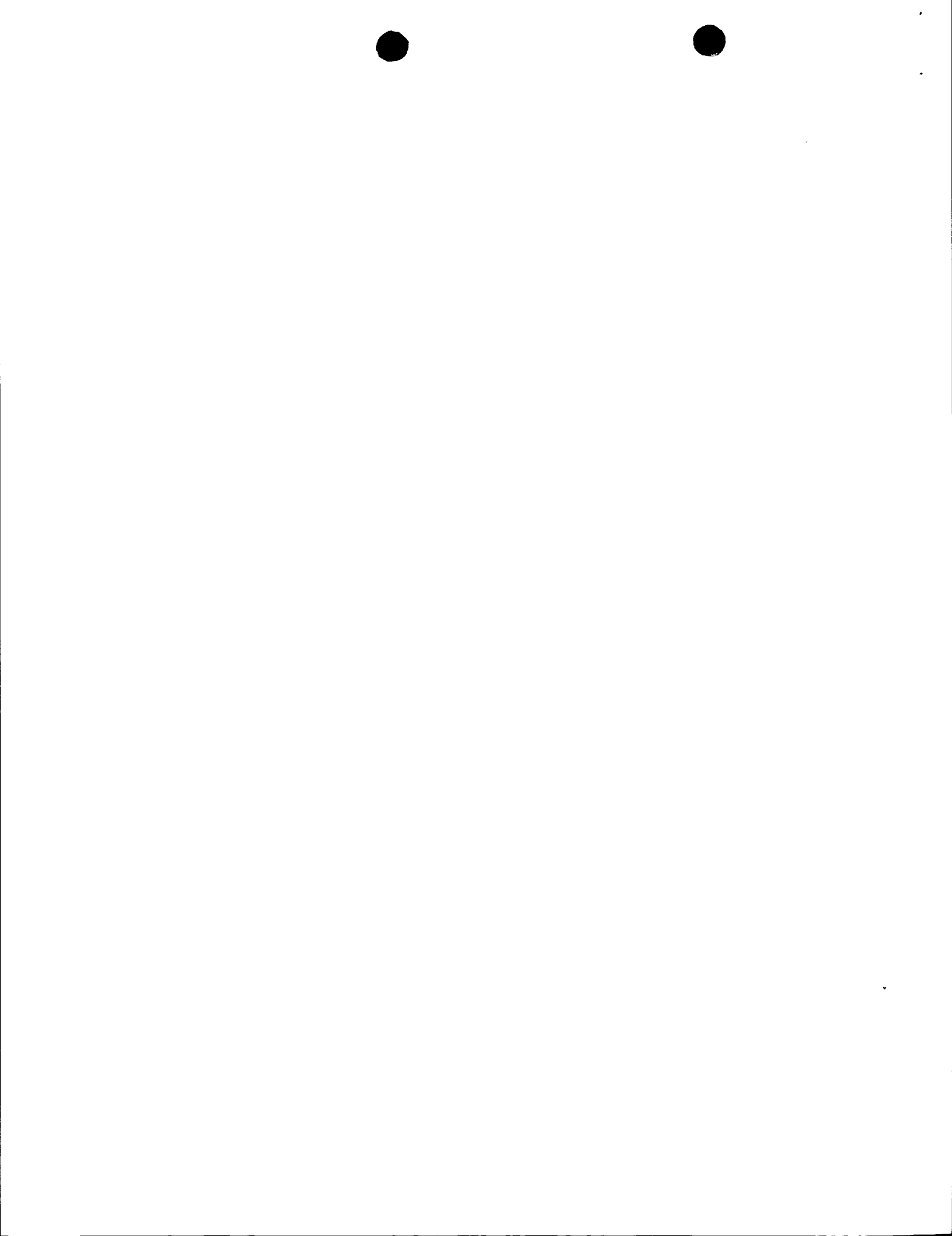
- the language of a translation furnished for the purposes of the international search (under Rule 23.1(b)).
- the language of publication of the international application (under Rule 48.3(b)).
- the language of a translation furnished for the purposes of international preliminary examination (under Rule 55.2 and/or 55.3).

3. With regard to any **nucleotide and/or amino acid sequence** disclosed in the international application, the international preliminary examination was carried out on the basis of the sequence listing:

- contained in the international application in written form.
- filed together with the international application in computer readable form.
- furnished subsequently to this Authority in written form.
- furnished subsequently to this Authority in computer readable form.
- The statement that the subsequently furnished written sequence listing does not go beyond the disclosure in the international application as filed has been furnished.
- The statement that the information recorded in computer readable form is identical to the written sequence listing has been furnished.

4. The amendments have resulted in the cancellation of:

- the description,       pages:
- the claims,              Nos.:



**INTERNATIONAL PRELIMINARY  
EXAMINATION REPORT**

International application No. PCT/GB00/03238

- the drawings,      sheets:
5.  This report has been established as if (some of) the amendments had not been made, since they have been considered to go beyond the disclosure as filed (Rule 70.2(c)):  
*(Any replacement sheet containing such amendments must be referred to under item 1 and annexed to this report.)*
6. Additional observations, if necessary:

**V. Reasoned statement under Article 35(2) with regard to novelty, inventive step or industrial applicability; citations and explanations supporting such statement**

1. Statement

Novelty (N)      Yes: Claims 1-9  
                      No: Claims

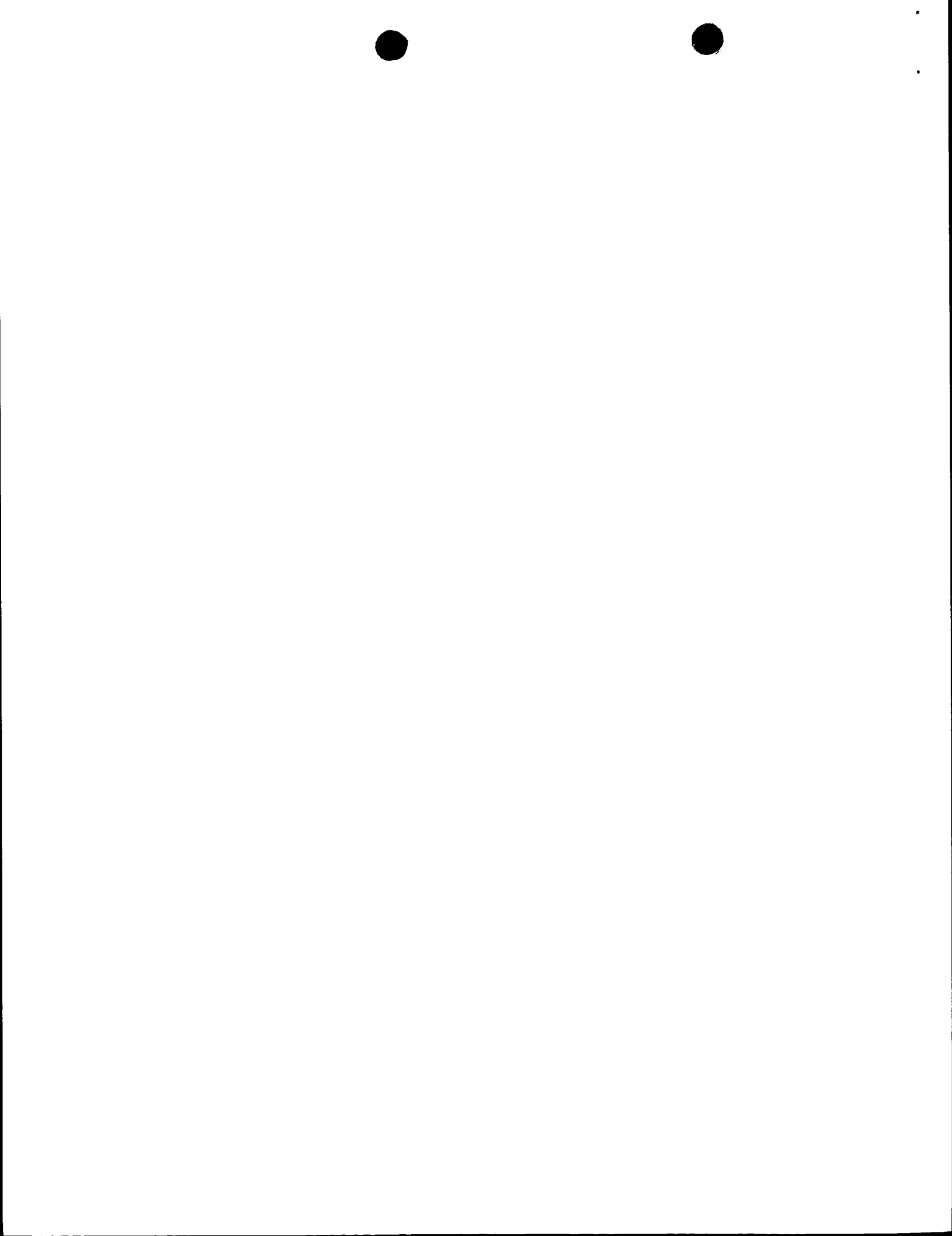
Inventive step (IS)      Yes: Claims 1-9  
                      No: Claims

Industrial applicability (IA)      Yes: Claims 1-9  
                      No: Claims

2. Citations and explanations  
**see separate sheet**

**VII. Certain defects in the international application**

The following defects in the form or contents of the international application have been noted:  
**see separate sheet**



**INTERNATIONAL PRELIMINARY  
EXAMINATION REPORT - SEPARATE SHEET**

---

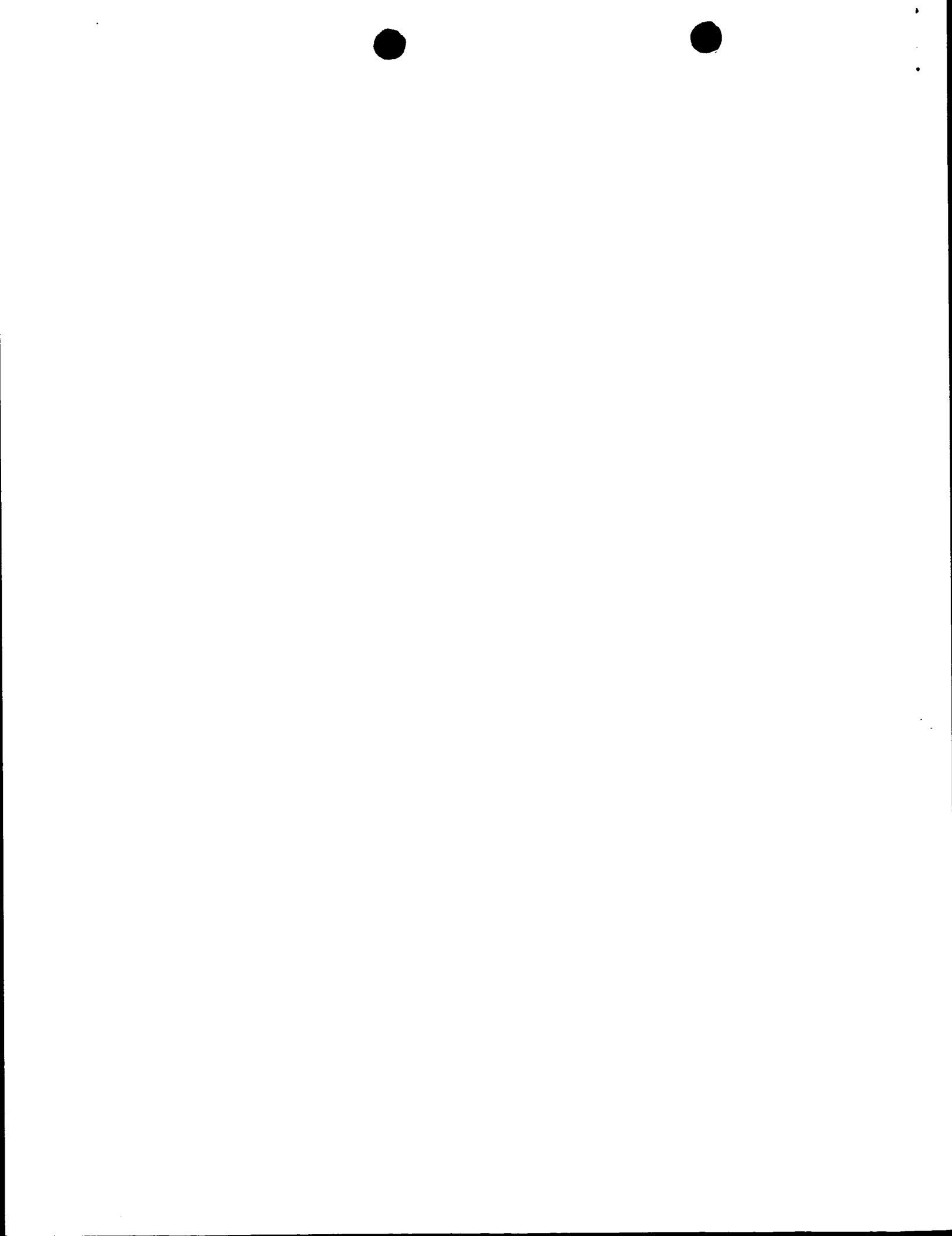
International application No. PCT/GB00/03238

re item V (Reasoned statement...):--

None of the three citations of the ISR provides a hint at the use of a parylene film formed on the interferometer substrate. The US-A-5 311 485 does not disclose any fibre coating, US-A-5 262 842 and US-A-5 533 151 do not disclose a Fabry-Perot interferometer having a cleaved fibre end with polymer disc, for which the parylene film would be advantageous. Claims 1 (method) and 7 (interferometer sensor) meet Art. 33(2),(3) PCT, the dependent claims 2-6,8,9, perforce, meet this Article. The industrial applicability of an interferometer sensor is evident.

re item VII (Certain defects..):--

Reference numerals mentioned in the description should be shown in a drawing, Rule 11.13 l) PCT. The deposition chamber should be designated by 22, inlet valve by 28.



## PATENT COOPERATION TREATY

## PCT

## INTERNATIONAL SEARCH REPORT

(PCT Article 18 and Rules 43 and 44)

Applicant's or agent's file reference	<b>FOR FURTHER ACTION</b> see Notification of Transmittal of International Search Report (Form PCT/ISA/220) as well as, where applicable, item 5 below.	
International application No.	International filing date (day/month/year)	(Earliest) Priority Date (day/month/year)
PCT/GB 00/03238	18/08/2000	19/08/1999
Applicant		
UNIVERSITY COLLEGE LONDON		

This International Search Report has been prepared by this International Searching Authority and is transmitted to the applicant according to Article 18. A copy is being transmitted to the International Bureau.

This International Search Report consists of a total of 2 sheets.

It is also accompanied by a copy of each prior art document cited in this report.

1. Basis of the report

- a. With regard to the **language**, the international search was carried out on the basis of the international application in the language in which it was filed, unless otherwise indicated under this item.
  - the international search was carried out on the basis of a translation of the international application furnished to this Authority (Rule 23.1(b)).
- b. With regard to any **nucleotide and/or amino acid sequence** disclosed in the international application, the international search was carried out on the basis of the sequence listing :
  - contained in the international application in written form.
  - filed together with the international application in computer readable form.
  - furnished subsequently to this Authority in written form.
  - furnished subsequently to this Authority in computer readable form.
  - the statement that the subsequently furnished written sequence listing does not go beyond the disclosure in the international application as filed has been furnished.
  - the statement that the information recorded in computer readable form is identical to the written sequence listing has been furnished
- 2.  Certain claims were found unsearchable (See Box I).
- 3.  Unity of invention is lacking (see Box II).

4. With regard to the title,

- the text is approved as submitted by the applicant.
- the text has been established by this Authority to read as follows:

5. With regard to the abstract,

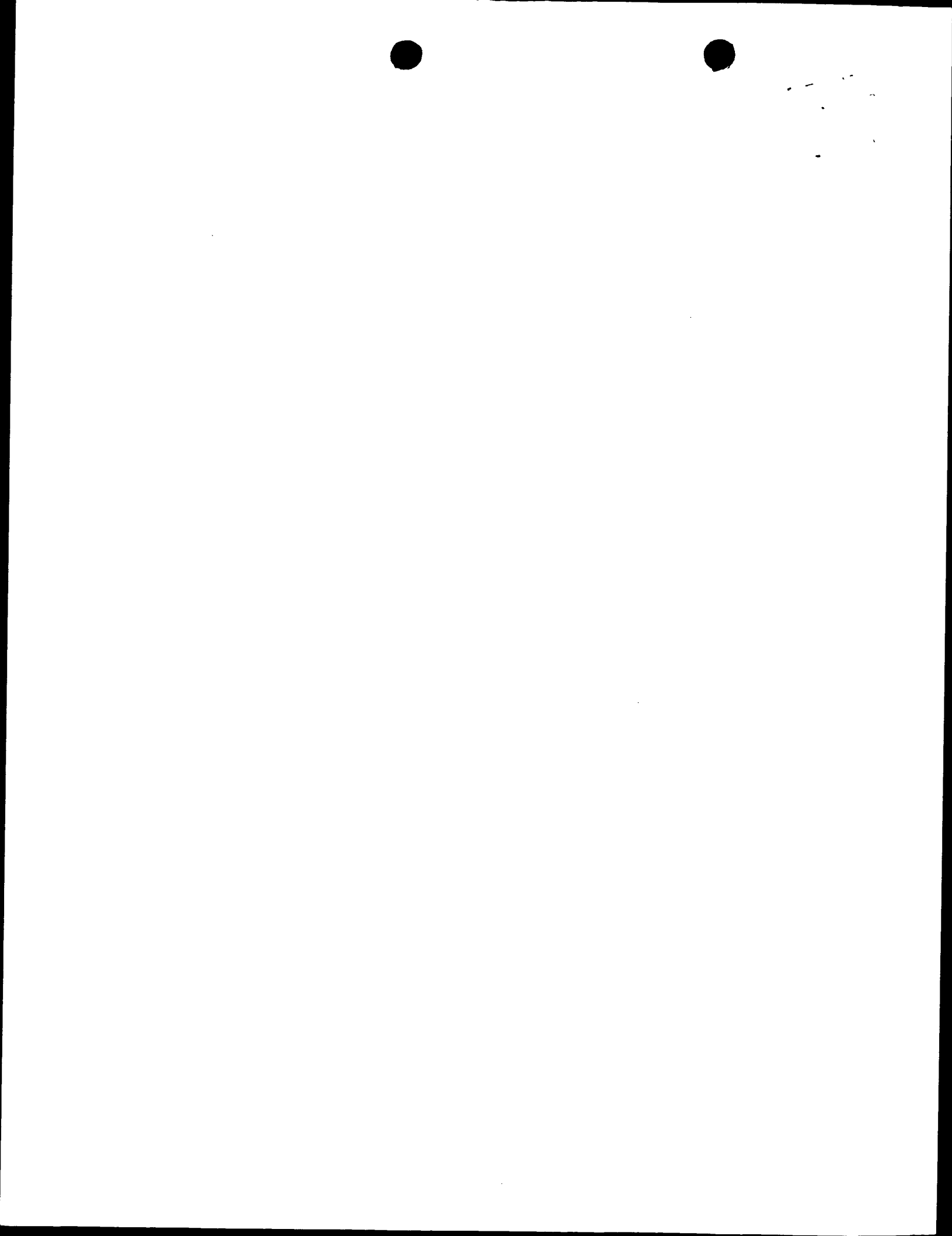
- the text is approved as submitted by the applicant.
- the text has been established, according to Rule 38.2(b), by this Authority as it appears in Box III. The applicant may, within one month from the date of mailing of this international search report, submit comments to this Authority.

6. The figure of the **drawings** to be published with the abstract is Figure No.

- as suggested by the applicant.
- because the applicant failed to suggest a figure.
- because this figure better characterizes the invention.

1

None of the figures.



## INTERNATIONAL SEARCH REPORT

International Application No

PCT/GB 00/03238

A. CLASSIFICATION OF SUBJECT MATTER  
IPC 7 G01B9/02

According to International Patent Classification (IPC) or to both national classification and IPC

## B. FIELDS SEARCHED

Minimum documentation searched (classification system followed by classification symbols)

IPC 7 G01B

Documentation searched other than minimum documentation to the extent that such documents are included in the fields searched

Electronic data base consulted during the international search (name of data base and, where practical, search terms used)

EPO-Internal, PAJ, WPI Data

## C. DOCUMENTS CONSIDERED TO BE RELEVANT

Category °	Citation of document, with indication, where appropriate, of the relevant passages	Relevant to claim No.
A ✓	US 5 311 485 A (KUZMENKO PAUL J ET AL) 10 May 1994 (1994-05-10) abstract; figures 1,2 column 3, line 58 ---	1,7,9
A ✓	US 5 262 842 A (GAUGLITZ GUENTER ET AL) 16 November 1993 (1993-11-16) abstract; figure 1 ---	1,7,9
A ✓	US 5 533 151 A (LEONARD JERRY) 2 July 1996 (1996-07-02) abstract; figure 10 -----	1,7,9

Further documents are listed in the continuation of box C.

Patent family members are listed in annex.

## ° Special categories of cited documents :

- "A" document defining the general state of the art which is not considered to be of particular relevance
- "E" earlier document but published on or after the international filing date
- "L" document which may throw doubts on priority claim(s) or which is cited to establish the publication date of another citation or other special reason (as specified)
- "O" document referring to an oral disclosure, use, exhibition or other means
- "P" document published prior to the international filing date but later than the priority date claimed

"T" later document published after the international filing date or priority date and not in conflict with the application but cited to understand the principle or theory underlying the invention

"X" document of particular relevance; the claimed invention cannot be considered novel or cannot be considered to involve an inventive step when the document is taken alone

"Y" document of particular relevance; the claimed invention cannot be considered to involve an inventive step when the document is combined with one or more other such documents, such combination being obvious to a person skilled in the art.

"&" document member of the same patent family

Date of the actual completion of the international search

1 November 2000

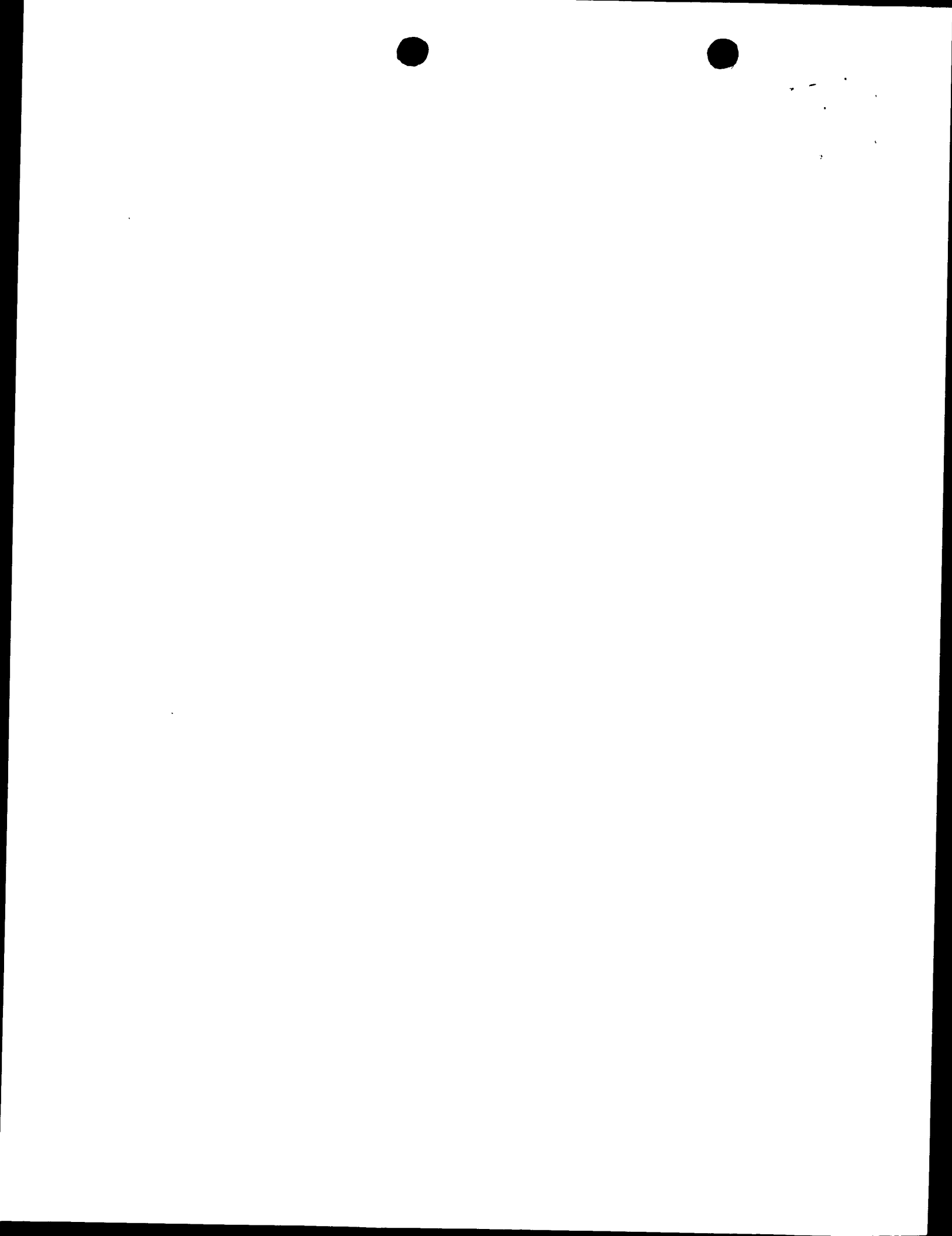
Date of mailing of the international search report

10/11/2000

Name and mailing address of the ISA  
European Patent Office, P.B. 5818 Patentlaan 2  
NL - 2280 HV Rijswijk  
Tel. (+31-70) 340-2040, Tx. 31 651 epo nl,  
Fax: (+31-70) 340-3016

Authorized officer

Vorropoulos, G



**INTERNATIONAL SEARCH REPORT**

Information on patent family members

International Application No

PCT/GB 00/03238

Patent document cited in search report	Publication date	Patent family member(s)			Publication date
US 5311485	A 10-05-1994	NONE			
US 5262842	A 16-11-1993	DE	4033357 A	23-04-1992	
		EP	0481440 A	22-04-1992	
		JP	4285844 A	09-10-1992	
US 5533151	A 02-07-1996	NONE			

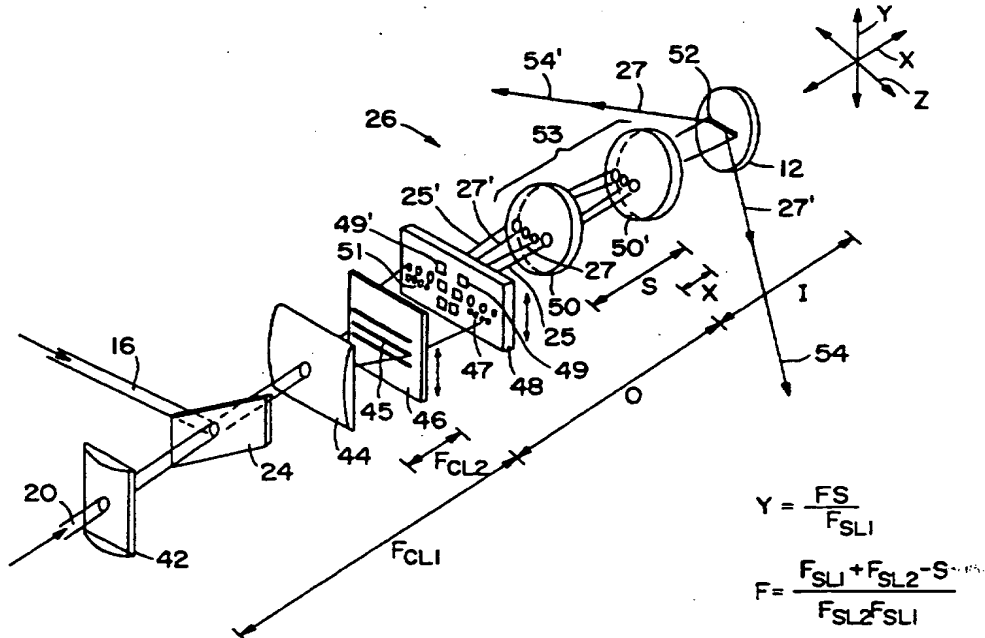




## INTERNATIONAL APPLICATION PUBLISHED UNDER THE PATENT COOPERATION TREATY (PCT)

(51) International Patent Classification <sup>6</sup> : <b>G01B 9/02</b>		A1	(11) International Publication Number: <b>WO 96/23197</b>
			(43) International Publication Date: <b>1 August 1996 (01.08.96)</b>
(21) International Application Number: <b>PCT/US96/00552</b>		(81) Designated States: JP, European patent (AT, BE, CH, DE, DK, ES, FR, GB, GR, IE, IT, LU, MC, NL, PT, SE).	
(22) International Filing Date: <b>16 January 1996 (16.01.96)</b>		Published <i>With international search report.</i>	
(30) Priority Data: 08/377,310 24 January 1995 (24.01.95) US			
(71) Applicant: MASSACHUSETTS INSTITUTE OF TECHNOLOGY [US/US]; 77 Massachusetts Avenue, Cambridge, MA 02142 (US).			
(72) Inventors: ROGERS, John, A.; 7412 Berkeley Circle, Castle Rock, CO 80104 (US). NELSON, Keith, A.; 55 Clearwater Road, Newton, MA 02162 (US).			
(74) Agent: PRAHL, Eric, L.; Fish & Richardson P.C., 225 Franklin Street, Boston, MA 02110-2804 (US).			

(54) Title: DEVICE AND METHOD FOR TIME-RESOLVED OPTICAL MEASUREMENTS



## (57) Abstract

An optical modulating system (26) allows modulation of a single light beam (16) with a spatially filtering mask (47) to form a spatially periodic, time dependent excitation field. Once generated, the field can be used to induce a transient grating in a sample (12). The optical modulating system (26) is additionally configured to automatically orient a probe beam (20) at the Bragg angle, thereby allowing the intensity of the probe beam (20) to be maximized.

**FOR THE PURPOSES OF INFORMATION ONLY**

Codes used to identify States party to the PCT on the front pages of pamphlets publishing international applications under the PCT.

AM	Armenia	GB	United Kingdom	MW	Malawi
AT	Austria	GE	Georgia	MX	Mexico
AU	Australia	GN	Guinea	NE	Niger
BB	Barbados	GR	Greece	NL	Netherlands
BE	Belgium	HU	Hungary	NO	Norway
BF	Burkina Faso	IE	Ireland	NZ	New Zealand
BG	Bulgaria	IT	Italy	PL	Poland
BJ	Benin	JP	Japan	PT	Portugal
BR	Brazil	KE	Kenya	RO	Romania
BY	Belarus	KG	Kyrgyzstan	RU	Russian Federation
CA	Canada	KP	Democratic People's Republic of Korea	SD	Sudan
CF	Central African Republic	KR	Republic of Korea	SE	Sweden
CG	Congo	KZ	Kazakhstan	SG	Singapore
CH	Switzerland	LI	Liechtenstein	SI	Slovenia
CI	Côte d'Ivoire	LK	Sri Lanka	SK	Slovakia
CM	Cameroon	LR	Liberia	SN	Senegal
CN	China	LT	Lithuania	SZ	Swaziland
CS	Czechoslovakia	LU	Luxembourg	TD	Chad
CZ	Czech Republic	LV	Latvia	TG	Togo
DE	Germany	MC	Monaco	TJ	Tajikistan
DK	Denmark	MD	Republic of Moldova	TT	Trinidad and Tobago
EE	Estonia	MG	Madagascar	UA	Ukraine
ES	Spain	ML	Mali	UG	Uganda
FI	Finland	MN	Mongolia	US	United States of America
FR	France	MR	Mauritania	UZ	Uzbekistan
GA	Gabon			VN	Viet Nam

DEVICE AND METHOD FOR TIME-RESOLVED OPTICAL  
MEASUREMENTS

Field of the Invention

5        This invention relates to the measurement of material properties using time-dependent, spatially varying optical fields.

Background

Measurement techniques involving optical excitation and detection of material motions are extremely important from both purely scientific and applications-oriented points of view. In particular, techniques such as transient grating spectroscopy or impulsive stimulated scattering use laser light to both excite materials (e.g., polymer films) and to measure the resulting response. In these techniques, two excitation laser pulses are crossed in space and time in the sample. Overlap of the excitation pulses results in optical interference to produce an excitation field which has alternating "light" and "dark" regions, with the overall intensity of the field varying in a sinusoidal manner. The angle between the overlapping pulses determines the spatial frequency, i.e., the wavevector, of the alternating regions. The excitation field can induce a transient grating in the sample through several different mechanisms. For example, optical absorption of the excitation field can create electronic excited states which can decay through the emission of heat or light. For example, in Impulsive Stimulated Thermal Scattering ("ISTS") the optical energy of the light regions of the field is absorbed by the sample, resulting in the deposition of heat which is followed by thermal expansion of the irradiated regions. This results in the launching of coherent, counter-propagating ultrasonic phonons

- 2 -

having a wavevector with a spatial frequency and orientation matching the geometry of the excitation field. The sample can also be excited via a non-absorptive process. In Impulsive Stimulated Brillouin Scattering ("ISBS") or Impulsive Stimulated Raman Scattering ("ISRS"), for example, the sample is excited using a spatially varying optical intensity pattern, but the photons have a wavelength that is not absorbed by the film. In these techniques, optical energy is coupled directly into the film's acoustic field to excite acoustic processes. The excitation process takes advantage of the inherent spectral line width of the excitation pulses; higher-frequency photons from each excitation pulse are annihilated to create lower-frequency photons in the opposite excitation pulse. Counter-propagating acoustic phonons of the difference frequency and wavevector are then generated in the medium.

In ISTS, ISRS, ISBS, and other transient grating techniques, phonon propagation or electronic events may continue after the excitation pulses leave the sample, causing a time-dependent, spatially periodic variation in the material properties in the excited region. Because the relevant optical properties of the material are functions of the magnitude of this response, the time dependence of the excited region can be detected with an optical probe beam. The excited region of the sample functions as a transient diffraction grating, resulting in diffraction and modulation of the incident probe beam to produce a signal beam which can be detected and analyzed. In order to determine a particular property of the sample, such as the elastic moduli, it may be necessary to measure the sample's dispersion (i.e., the wavevector-dependent response).

- 3 -

In order to form the spatially varying optical excitation field using the conventional transient grating methodology, the excitation beam is split into two beams, which are then recombined in the sample using optical components such as mirrors, beam-splitters, lenses and mechanical delay stages. These components may also be used to adjust the angle between the excitation beams. Additional optical components are used to accurately adjust the angle, spatial overlap, and timing of the probe beam with respect to the excitation beams. However, even after careful adjustment, the signal diffracted by the induced transient grating is often weak, making both alignment and detection difficult.

Summary

15 In one aspect, the invention provides a method and apparatus for determining a property of a sample using the steps of: (a) providing a beam of radiation, and then passing the beam through a pattern on a diffracting mask to form at least two excitation sub-beams; (b) 20 overlapping at least two excitation sub-beams on a region of the sample with an imaging system to generate a spatially varying optical field which excites a transient grating in the region of the sample; (c) irradiating the transient grating with a probe beam oriented so that at 25 least a portion of the probe beam is diffracted by the transient grating; (d) detecting the diffracted portion of the probe beam with an optical detector to generate a light-induced signal; and (e) analyzing the light-induced signal from the optical detector to determine the 30 property of the sample.

By "sub-beam", as used herein, is meant an optical field resulting from diffraction of either an excitation or probe beam. The excitation and probe beams may have the same or different wavelengths; both beams may be 35 partially absorbed by the sample.

- 4 -

In preferred embodiments, the diffracting pattern includes alternating light-modulating regions having at least one spatial frequency, and the excitation beam is separated into at least a zeroth, +1, and -1 excitation 5 sub-beam following diffracting off of the light-modulating regions of the diffracting pattern. In this case, the overlapping step may further include the step of passing at least the +1 and -1 excitation sub-beams through the imaging system (e.g., a lens or series of 10 lenses) prior to overlapping these sub-beams on the sample. The imaging system then images at least one of the spatial frequencies of the light-modulating regions of the diffracting pattern onto the sample to form the spatially varying optical field. Preferably, at least 15 one of the spatial frequencies of the light-modulating region and the spatial varying optical field are equivalent.

In still other preferred embodiments, the probe and excitation beams are made collinear prior to step 20 (a). In this case, step (a) further comprises the step of separating the probe beam into at least two probe sub-beams by passing the probe beam through the diffracting pattern on the first mask. Here, the probe sub-beams preferably pass through the imaging system prior to 25 irradiating the grating induced in the region of the sample.

In other preferred embodiments, the excitation beam is focussed (e.g., cylindrically focussed) onto the diffracting pattern prior to step (a). In addition, the 30 imaging system is preferably a 1:1 imaging system. In this embodiment, the probe beam irradiates the transient grating at the Bragg angle.

In still other preferred embodiments, between steps (b) and (c), the excitation sub-beams are spatially 35 filtered with a second mask. Preferably, the first and

- 5 -

second masks are contained in a single unit, and the spatial filtering transmits the +1 and -1 excitation and probe sub-beams.

- In other embodiments, the analyzing step further
- 5 includes determining the dispersion of the sample. The dispersion may be used to determine the mechanical (e.g., adhesion, elastic moduli, stiffness, residual stress, and density), thermal, optical, or electronic properties of the sample. In this embodiment, the dispersion may be
- 10 determined following the step of inducing multiple transient gratings in the sample with a single spatial varying optical field having multiple spatial frequencies. Alternatively, the dispersion is determined following the steps of sequentially inducing multiple
- 15 transient gratings in the sample with multiple spatial varying optical fields, each of which has a single spatial frequency.

- In another aspect, the invention provides a method of diffracting a probe beam off a sample. The method
- 20 includes: (a) providing a beam of radiation, and then passing the beam through a pattern on a diffracting mask to form at least two excitation sub-beams; (b) overlapping at least two excitation sub-beams on a region of the sample with an imaging system to generate a
- 25 spatially varying optical field which excites a transient grating in the region of the sample; and (c) irradiating the transient grating with a probe beam oriented so that at least a portion of the probe beam is diffracted by the transient grating.

- 30 In another aspect, the invention provides an apparatus for diffracting a portion of a probe beam off a sample. The apparatus includes means for generating a probe optical beam and an excitation optical beam orientated along an optical axis, and a first diffracting
- 35 mask including an optical diffracting pattern. The

- 6 -

diffracting pattern is positioned along the optical axis and is configured so that, when irradiated with the excitation beam, the pattern diffracts the excitation beam to generate at least two excitation sub-beams. The 5 apparatus also include an imaging system containing at least one lens positioned along the optical axis. The imaging system is configured to focus the excitation sub-beams onto a region of the sample to generate a spatially varying optical field which excites a transient grating 10 which allows partial diffraction of the probe beam.

In preferred embodiments, the diffracting pattern includes a series of opaque regions spaced by a distance which allows diffraction of visible or infrared radiation. Alternatively, the diffracting pattern may 15 include a series of regions etched to a depth and spaced by a distance which allows diffraction of visible or infrared radiation. Preferably, the diffracting mask includes a plurality of diffracting patterns.

In another preferred embodiment, the apparatus 20 further includes a second, spatially filtering mask which includes a pair of openings. The openings are positioned along the optical axis so that the spatially filtering mask allows spatial filtering of the diffracted excitation sub-beams. Preferably, the spatial filtering 25 mask includes a plurality of pairs of openings, and the diffracting and spatial filtering masks are contained in a single unit.

Embodiments may include one of the following advantages. For example, a simple, linearly configured 30 optical system is provided which modulates a single beam with a filtering mask to form a spatially periodic, time-dependent excitation field which can then be used to induce a transient grating in a sample. The system can be additionally configured to orient a probe beam at the 35 Bragg (or phase-matching) angle using a simple optical

- 7 -

arrangement. This allows the diffraction efficiency of the induced grating, and the intensity of the diffracted probe beam, to be maximized.

Optical alignment of the system is both simple and quick. The user need only make the probe and excitation beam collinear prior to interaction with the masks. The masks and imaging optics are used to define the excitation pattern (i.e., wavevector) at the sample, set the timing such that the excitation pulses arrive at the sample at the same time, set the probe angle of incidence at the Bragg angle, and provide a beam to allow for facile signal location and amplification. During operation, the wavevector of the excited phonons can be adjusted simply by translating the masks. These masks are the only moving parts in the system, allowing the measurement technique to be easily automated while reducing the number of optics required in the optical modulating system.

When a thick grating is formed in the sample, automatic setting of the Bragg angle allows the diffraction efficiency of the grating to be maximized. This is particularly important, as diffraction efficiency for these gratings falls off rapidly at angles even within a fraction of a degree of the Bragg angle, regardless of the amplitude of the material response. Once irradiated, the optical modulating system generates multiple probe beams at the sample. One probe beam can serve to probe the transient grating, while another probe beam may serve as a "finder" beam to determine the position of the signal beam. This makes the practical matter of aligning weak signals into a detector trivial since the finder beam has a large optical intensity, and is thus easy to locate. This same finder beam may also be used for heterodyne amplification of weak signal beams.

- 8 -

Moreover, with this invention the excitation fields are not limited to simple sinusoidal patterns. For example, in some cases it may be desirable to induce material motions with more complex geometries or to 5 simultaneously excite material motions at multiple wavevectors using complex mask patterns.

Brief Description of the Drawings

Fig. 1 is a schematic drawing of the optical elements of a sample-measuring device according to the 10 invention;

Fig. 2 is a perspective view of the optical modulating system of the sample-measuring device;

Fig. 3 is an expanded view of the masks and imaging optics of the optical modulating system;

15 Figs. 4A and 4B are, respectively, a graph showing the spatial dependence of the modulating regions of the mask, and the spatial dependence of the excitation field generated using the diffracting mask of the optical modulating system;

20 Figs. 5A, and 5C are, respectively, the spatial dependencies of the excitation and probe fields after being diffracted by the first mask but prior to being filtered by the second mask, and after being diffracted by the first mask and filtered by the second mask;

25 Fig. 5B is the spatial transmission function of the spatial filtering mask;

30 Figs. 6A and 6B are, respectively, plots showing the time dependence of the diffracted signal from a thin grating generated in a film sample using the optical modulating system;

Figs. 7A and 7B are, respectively, plots showing the time dependence of the diffracted signal from a thick grating generated in salol using the optical modulating system.

- 9 -

Detailed Description

Referring to Fig. 1, an optical measurement system 10 used to excite a sample 12 and probe the resulting motions includes excitation 14 and probe 18 lasers which 5 produce, respectively, excitation 16 and probe 20 optical beams. The excitation beam is composed of a sequence of pulses, while the probe beam may contain sequences of pulses, or alternatively, optical waveforms having relatively long temporal durations. Prior to irradiating 10 the sample, the excitation beam 16 is reflected by a pair of optics 22, 24 which are highly reflective at the excitation beam wavelength and are oriented to direct the beam into an optical modulating system 26. The second high-reflecting optic 24 preferably reflects the 15 excitation beam efficiently, and is partially transparent to the probe beam. For example, this optic may be a beam splitter, dichroic mirror, or a thin film polarizer. The optic 24 allows the probe beam 20 to be oriented collinearly with the excitation beam 16 prior to entering 20 the optical modulating system 26.

The optical modulating system 26 modulates the single excitation beam 16 to produce a pair of spatially modulated excitation sub-beams 25, 25' which are recombined within or on the surface of the sample. The 25 optical modulating system is configured so that the timing and spatial positions of the pulses in the excitation sub-beams 25, 25' are overlapped, resulting in optical interference between the two sub-beams to produce a spatially varying optical field which is then used to 30 excite the sample 12. The single probe beam 20 is also spatially modulated by the optical modulating system 26, resulting in the generation of a pair of probe sub-beams 27, 27' which, when the probe wavelength is different than the excitation wavelength, spatially separate from 35 the excitation sub-beams 25, 25'. During the measurement

- 10 -

process, both probe sub-beams 27, 27' are diffracted from the transient grating excited in the sample, resulting in the generation of a pair of signal beams. A single signal beam 28 is measured by an optical detection system 30, which may include, for example, a photodetector electrically connected to a transient recording device. Measurement of the diffracted signal results in the generation of a status signal 32 which may be further processed by a computer and used to evaluate the material properties of the sample 12.

The elements of the optical modulating system 26 generate the spatially varying optical excitation field from a single excitation beam, and allow the Bragg angle of incidence of the probe beam to be automatically set. This permits data to be collected at a variety of excitation wavevectors with minimal alignment, thereby allowing the dispersive characteristics of the sample to be easily measured. Measurement of the dispersion allows, for example, material properties such as modulus of elasticity, thermal diffusion, adhesion, electronic transport, and stress to be determined in both bulk and thin film samples. In addition, the optical modulating system 26 has a simple, compact design with a minimal number of optical elements, and only one movable element. This allows the sample-measurement process to be easily automated and performed in a rapid fashion.

Referring now to Figs. 2 and 3, in a preferred embodiment, the elements of the optical modulating system 26 are preferably disposed in a linear arrangement along an axis (indicated in the figure by the x axis) to allow spatial modulation of the collinear excitation 16 and probe 20 beams. Prior to passing through the optic 24, the probe beam 20 is transmitted through a first cylindrical lens 42 (having a focal length indicated by "F<sub>c11</sub>") which focuses the beam so that it is elongated

- 11 -

along the z axis. Once overlapped, the excitation 16 and probe 20 beams are focussed with a second cylindrical lens 44 (having a focal length indicated by "F<sub>c12</sub>") onto a patterned region 45 of a first mask 46 which spatially 5 filters both beams. The mask 46 is positioned at the focal point (F<sub>c12</sub>) of the second cylindrical lens 44 so that the excitation beam is focussed to an elongated, elliptical spot which extends along the pattern 45, while the probe beam, previously focussed with the first 10 cylindrical lens 42, is focussed to a small circular spot in the center of the elongated excitation spot.

The patterned region 45 on the mask 46 may include, for example, an alternating periodic pattern of transmissive and opaque regions which filter the 15 intensity of the cylindrically focussed excitation beam. Alternatively, the pattern may include periodic regions of transparent glass etched to varying depths (e.g.,  $\lambda/4$ ) which filter the phase of the incident excitation field. In both cases, interaction of the excitation 16 and probe 20 beams with the patterned region 45 causes diffraction of these beams to form a series of sub-beams corresponding to different diffractive orders.

After being dispersed and separated following diffraction from the first mask 46, the diverging 25 excitation and probe sub-beams are spatially filtered by a second mask 48 which is displaced along the x axis from the first mask by a distance which allows clear spatial separation of the excitation and probe diffractive orders. This is the case when the wavelengths of the 30 excitation and probe beams are different; when the wavelengths are the same, the excitation and probe sub-beams are not separated. The second mask 48 includes multiple pairs of openings 49, 49' which allow transmission of the selected diffractive orders from both 35 the pump and probe beams. Preferably, the second mask is

- 12 -

configured so that each pair of openings corresponds to a separate patterned region on the first mask. The pairs of openings are brought into the beam path by translating the second mask vertically.

5        Each diffractive order represents a different Fourier component of the spatially varying pattern region 45 of the first mask 46. For example, the +1 and -1 orders of the excitation and probe fields are first order Fourier components, while higher (e.g., +/-2, +/-3) and 10 lower (e.g., the zeroth order) diffractive orders represent, respectively, high-frequency and DC Fourier components. Spatial filtering by the second mask 28 thus allows selected Fourier components of the diffracted field to pass; these components are then recombined on 15 the sample to form the desired excitation pattern.

The excitation 25, 25' and probe 27, 27' sub-beams are transmitted through the mask 40. The diffracted sub-beams diverge at angles of  $\theta$  (probe sub-beams) and  $\phi$  (excitation sub-beams), with each sub-beam representing 20 either the positive 47 (e.g., +1, +2) or negative 51 (e.g., -1, -2) orders of diffraction. The diffractive process depends on the spatial separation  $d$  (i.e., the "wavelength") of the light-modulating regions of the patterned region, and on the wavelengths of the incident 25 excitation and probe fields:

$$\begin{aligned} 2d \sin (\theta) &= n \lambda_{\text{probe}} \\ 2d \sin (\phi) &= n \lambda_{\text{excitation}} \end{aligned} \quad (1)$$

where  $n$  is the diffracted order. Thus, the divergence of the sub-beams is determined only by the excitation and probe wavelengths and the geometry of the patterned region.

30       Recombination of the transmitted diffracted orders of the excitation and probe beams is accomplished using an imaging system 53. This allows: 1) spatial

- 13 -

recombination of selected excitation sub-beams, resulting in the generation of a spatially varying optical field in or on the surface of the sample; and 2) the probe sub-beams to be automatically oriented so that they arrive at 5 the sample at the Bragg (i.e. phase-matching) angle. The imaging optics may consist of a single lens (Fig. 3) or two separate lenses 50, 50' having focal lengths of, respectively,  $F_{sl1}$  and  $F_{sl2}$  (Fig. 2).

In the case where two separate lenses are used, 10 the separation between the lenses, indicated by S in the figure, allows the imaging system to be used as a telescope to magnify or demagnify the field imaged onto the sample. This allows the spatial scale or size of the interference pattern at the sample to be adjusted by 15 changing the separation between the two imaging lenses. For example, if the interference pattern is demagnified on the sample, the separation between light and dark regions will be decreased, resulting in an increase in the excitation wavevector. Conversely, if the pattern is 20 magnified, the separation between light and dark regions is increased, and the spatial frequency of the excitation wavevector is decreased.

The actual imaging process occurs at a plane defined as the image plane, which is determined by the 25 focal length of a single lens or the equivalent focal length of the multiple-lens (e.g., a two-lens) imaging system. In the two-lens system, the effective focal length F of the imaging system is a function of  $F_{sl1}$ ,  $F_{sl2}$ , and S:

$$F = \frac{F_{sl1} + F_{sl2} - S}{F_{sl1}F_{sl2}} \quad (2)$$

- 14 -

The effective "position"  $X$  of the imaging system along the  $x$  axis is displaced from the second lens 50' by a distance related to  $F$ ,  $S$ , and the focal length  $F_{s11}$  of the first lens 50:

$$X = \frac{FS}{F_{s11}} \quad (3)$$

- 5        The patterned region on the mask, which represents the object to be imaged, is displaced from  $X$  by a distance  $O$ . The displacement  $I$  of the sample from  $X$  represents the displacement of the image plane, and is related to  $F$  and  $O$  by the equation:

$$\frac{1}{F} = \frac{1}{O} + \frac{1}{I} \quad (4)$$

- 10 which can be rewritten as

$$I = \frac{OF}{(O-F)} \quad (5)$$

- Thus, during imaging, the degree of magnification or demagnification  $M$  of the object, defined as  $M = I/O$ , can be adjusted by choosing a lens combination which gives the desired value of  $F$ , and by placing the sample at the  
15 appropriate distance  $I$  from  $X$ .

- In addition to imaging particular Fourier components of the patterned region onto the sample, the imaging optics can be configured to focus the transmitted probe beams onto the induced grating at the Bragg angle.  
20 Referring now to Fig. 3, in order for the probe beam 16 to satisfy the Bragg phase-matching criteria, excitation 20 and probe 16 beams having wavelengths  $\lambda_{ex}$  and  $\lambda_{pr}$  are spatially overlapped along an optical axis of the modulating system prior to irradiating the patterned

- 15 -

region 45 on the first mask 46. (In this embodiment, a single imaging lens is used, although it is understood that a multiple-lens imaging system, as shown in Fig. 2, may also be used.) Diffraction generates at least a 5 zeroth 65, +1 47, and -1 51 diffracted orders, with each order containing the excitation 25, 25' and probe 27, 27' sub-beams. The excitation and probe beams are separated, respectively, by angles  $\phi$  and  $\theta$  from the optical axis of the system. The second mask 48 is used to spatially 10 filter the zeroth order 65 and transmit the +1 47 and -1 51 orders onto an imaging lens 50 which is spaced a distance D from the first mask 46. The diffracted excitation and probe beams irradiate the lens, respectively, at distances  $z_1$  and  $z_2$  from the optical 15 axis. The beams are imaged onto the sample 12 which is spaced a distance D from the lens 50. In this configuration, the distances D and D' are related by the equation

$$\frac{1}{D'} = \frac{1}{f} - \frac{1}{D} \quad (6)$$

which can be rewritten as

$$D' = \frac{Df}{(D-f)} \quad (7)$$

20 Following focussing by the lens 50, the diffracted orders 47, 51 containing the probe and excitation sub-beams converge on the sample with angles  $\theta'$  and  $\phi'$ , which can be related to  $z_1$ ,  $z_2$ , D, and D':

$$\tan\phi' = \frac{z_1}{D'} = \frac{Dt\tan\phi}{D} \quad (8)$$

- 16 -

$$\tan\theta' = \frac{z_2}{D'} = \frac{Dt\tan\theta}{D'} \quad (9)$$

It can be shown, then, that

$$\frac{\sin\theta'}{\sin\phi'} = \frac{\lambda_e}{\lambda_p} \sqrt{\frac{M^2 [1 - (\frac{\lambda_e}{2d})^2] + (\frac{\lambda_e}{2d})^2}{M^2 [1 - (\frac{\lambda_p}{2d})^2] + (\frac{\lambda_p}{2d})^2}} \quad (10)$$

To satisfy the phase-matching criteria, it is required that

$$\frac{\sin\theta'}{\sin\phi'} = \frac{\lambda_e}{\lambda_p} \quad (11)$$

Two conditions must be met, therefore, for the Bragg phase-matching angle to be set independently of the mask pattern.

These conditions are:

M = 1 (i.e., a 1:1 imaging system), or the case when

$$M > \frac{(\frac{\lambda_e}{2d})}{\sqrt{1 + (\frac{\lambda_e}{2d})^2}} \quad (12)$$

10 and

$$M > \frac{(\frac{\lambda_p}{2d})}{\sqrt{1 + (\frac{\lambda_p}{2d})^2}} \quad (13)$$

- 17 -

hold for the imaging system. In addition, in the case where the excitation and probe wavelengths are equivalent, the Bragg angle for the system is automatically set using the optical modulating system.

5 Thus, by making the excitation and probe beams collinear prior to entering the optical modulating system, the probe beam is diffracted by the first mask to produce a pair of probe sub-beams which, when conditions (1) or (2) are satisfied, are automatically oriented at  
10 the Bragg angle.

Following interaction with the transient grating, the sub-beams incident on the sample are diffracted to generate a pair of signal beams 54, 54' which are spatially overlapped with the residual portions (i.e.,  
15 the non-diffracted components) of the opposing probe sub-beams. The presence of both diffracted (i.e., signal) and reflected (i.e., residual probe) beams is advantageous for two principal reasons. First, the residual beam may be used as a reference or "finder" beam  
20 which allows the spatial location of the signal (which is often weak and hard to see by eye) to be determined, thereby simplifying alignment of the diffracted beam into the detection apparatus. Second, the presence of both signal and reference beams allows for heterodyne  
25 amplification of the signal beam, i.e., the high-intensity residual beam may be used to optically interfere and "beat" against the weak diffracted signal beam, resulting in amplification of the signal. Although Figs. 2 and 3 show a sample which reflects the incident  
30 probe beams, transmissive samples may be monitored; the relative geometries for the excitation, probe, and signal beams are similar for such samples.

Referring now to Figs. 4A and 4B, the patterned region 68 of the first mask of the optical modulating  
35 system interacts with the incident excitation field to

- 18 -

produce multiple orders of excitation sub-beams, which can then be recombined to generate a spatially varying optical field at the sample. In a preferred embodiment, the patterned region 68 consists of alternating, equally spaced opaque regions 70, each having a width 76, which are separated from each other by neighboring transparent regions 72. The modulating regions 70 of the mask may consist, for example, of a series of opaque lines formed by deposition of an absorbing material, such as a thin metal film, on a glass substrate which is transparent to the excitation and probe laser wavelengths. Masks having this "square-wave" transmission profile include, in theory, an infinite number of spatial frequency components, and will thus produce an infinite number of diffracted orders, with the intensity of each order falling off as

$$I \sim \left[ \left( \frac{\sin(\frac{N\pi dp}{\lambda})}{\sin(\frac{\pi dp}{\lambda})} \right)^2 \frac{\sin(\frac{\pi sp}{\lambda})}{\frac{\pi sp}{\lambda}} \right]^2 \quad (14)$$

where  $\lambda$  is the wavelength of light,  $p = \sin \theta$ , where  $\theta$  is the diffracted angle,  $n$  is the diffracted order, and  $d$  is the width of the opaque regions, and  $s$  is the distance separating these regions. Multiple orders appear because Fourier decomposition of the square-wave pattern of the mask yields an infinite additive series of sine wave harmonics, with the fundamental frequency of the series equivalent to the inverse of the spacing 74.

Alternatively, the modulating regions 70 of the mask may be fabricated to have a different thickness relative to the transparent regions 72 so as to spatially modulate the phase of the excitation field. For example, if the region 70 of the pattern 68 is etched so that its thickness is  $\lambda/2$  less than the thickness of the adjacent

- 19 -

regions 72, then the portions of the cylindrically focussed excitation spot which propagate through regions 70 will be  $\pi$  out of phase relative to the adjacent portions of the excitation field following propagation 5 through the mask. Phase modulation, as opposed to amplitude modulation, may be desirable as a way of modulating the excitation field as the intensity of the field is not attenuated by the mask.

Both the amplitude and phase-modulating masks 10 diffract the excitation field into multiple sub-beams. Once when recombined in or on the sample, the excitation sub-beams result in an optical interference pattern in which the spatial separation 86 of the light 82 regions (or, alternatively, dark regions 84) of the optical 15 intensity pattern 80 is a function of the spacing 74 in the patterned region 68 and, as described above, the focal and geometric properties of the imaging system.

In general, the spacing 74 of the regions 70 on the pattern 68 is within a factor of between 1 and 1000 20 of the wavelength of the optical field 80 which is imaged in the sample; typically the spacing is between 1 and 100 microns. A single mask may include multiple patterns, with each pattern having a different spacing 74 between light-modulating regions 70 and thus corresponding to an 25 excitation field having a different wavevector. The multiple patterns are preferably placed as close together as possible; for typical beam geometries, individual patterns are preferably separated by distances of between about 300-700 microns. The width 76 of the modulating 30 regions is typically between 0.2 and 1.5 times the separation distance 74.

In the case where it is desirable to excite multiple acoustic modes in the sample, with each mode having a separate well-defined wavevector, a patterned 35 region on the mask may be fabricated to include multiple

- 20 -

low-frequency spatial frequency components (i.e., frequencies other than those used to construct the square wave edges). For example, the mask may have multiple square or sine waves, each having a different 5 periodicity. An excitation field having this pattern will excite multiple modes, allowing the dispersive (i.e., wavevector-dependent) properties of the sample to be determined using a single excitation pulse.

The shape of the modulating regions 70 of the 10 pattern 68 need not have a square-wave profile. For example, the pattern may vary sinusoidally along the z dimension. This geometry, as opposed to the square-wave pattern which essentially requires an infinite number of spatial frequencies to construct the sharp edges of the 15 waveform, contains only a single frequency component equal to the spatial frequency of the sine wave. The intensity of the field diffracted by the sine wave pattern is primarily distributed between a DC component (i.e., the zeroth order) and the +1 and -1 diffractive 20 orders. In this embodiment, therefore, a larger fraction of the incident excitation field is concentrated in the first-order excitation sub-beams.

In another embodiment, multiple masks, each having a different spatial frequency, may be stacked 25 sequentially along the z axis and used to generate an optical field containing multiple excitation wavevectors. In addition, other patterns, such as a series of concentric rings, may also be included on the mask and imaged onto the sample.

30 The patterned regions of amplitude and phase masks are fabricated using deposition techniques well-known in the art, such as chemical vapor deposition, RF and magnetron sputtering techniques, and standard micro-lithographic (i.e., photo-lithographic) techniques. 35 These methods are described, for example, in

- 21 -

Semiconductor Lithography: Principles, Practices, and Materials, Wayne M. Moreau (1988), and Wavefront Engineering for Photolithography, Mark D. Levinson, the contents of which are incorporated herein by reference.

- 5 Both square and sine wave patterned masks are also available commercially from, for example, Sine Patterns or Applied Image Inc. Phase-modulating masks may be formed, for example, using glass etching techniques known in the art, such as those described in the above-  
10 mentioned references.

Once the excitation and probe beams are diffracted from the patterned region of the first mask, the second mask is used to spatially filter the diffracted field to allow selection of the diffracted orders which are to be imaged onto the sample. Referring now to Figs. 5A and 5C, following diffraction by the first mask, the optical intensities of the diverging sub-beams, indicated by the ordinate axes in the figures, vary as a function of the divergence along the z axis. The figures represent the spatial intensity profile of the diffracted excitation and probe sub-beams measured along a plane which is adequately spaced from the first mask, thereby allowing clear separation of the diffracted orders and the sub-beams within each diffracted order. The zeroth diffracted orders 100, 102 of both the excitation and probe sub-beams, representing the spatial DC component of the diffracted field, do not diverge and remain spatially overlapped following interaction with the diffracting mask. The +1 and -1 orders, indicated, respectively, by brackets 104 and 104', contain the +1 and -1 probe 106, 106' and excitation 108, 108' sub-beams. The separations between the DC components 100, 102 and the excitation and probe sub-beams of the +1 and -1 orders, indicated by the arrows 103 and 105, are a function of the configuration  
30 of the pattern on the mask, the wavelengths of the  
35

- 22 -

excitation and probe fields, and the separation between the plane of the diffracted field and the mask. In the case where the pattern on the diffractive mask is configured to generate multiple diffractive orders (i.e., 5 a square wave diffracting pattern), probe 110, 110' and excitation 112, 112' sub-beams will be present in the +2 and -2 diffractive orders indicated, respectively, by the brackets 114 and 114'. Higher diffracted orders, although possible, are not shown in the figure.

10 The second mask is chosen to have a transmission function which spatially filters the diffracted pattern, thereby selecting, for example, a single pair of diffractive orders. Referring now to Figs. 5B and 5C, a mask which allows selection of the +1 and -1 diffractive 15 orders has non-transmissive regions 120, 122, 122' which block the DC and higher-order diffracted components, thereby preventing these sub-beams from propagating onto the sample. Transmissive regions 124, 124' are disposed to allow four beams, i.e., the +1 and -1 orders 104, 104', 20 each containing the excitation 108, 108' and probe 106, 106' sub-beams, to propagate onto the sample. In embodiments, the non-transmissive regions in the second mask may be composed of an absorbing or reflecting substrate, such as a metal or plastic plate, and the 25 transmissive regions may consist of apertures where the substrate has been removed.

The width of the transmissive region in the second mask, indicated by the arrow 126, is chosen to allow passage of both the excitation and probe sub-beams of the 30 selected diffraction order. This width is dependent on the cumulative spatial extension of the diffracted excitation and probe sub-beams, and, as described previously, is determined by the wavelengths of the excitation and probe fields, the spacing of the 35 modulating regions in the diffracting pattern, and the

- 23 -

separation between the dispersed fields and the first mask. Typically, the transmissive regions have widths of between 0.5 and 2.0 cm.

During operation, the diffractive patterned 5 regions on the first mask are aligned with respect to the spatial filtering patterns on the second mask so that the two masks can preferably move vertically and in concert, thereby allowing rapid, automated adjustment of the different excitation fields. The masks should be mounted 10 so that the diffracting and filtering patterns are aligned at the same height and positioned symmetrically along the optical axis of the system. For example, the two masks may be mounted on a mechanical translation stage whose position can be controlled manually or by 15 using a motorized drive and a computer. In this manner, data can be sequentially taken at a number of wavevectors to allow determination of various points along the dispersion curves of bulk and thin film samples.

Alternatively, in order to reduce the number of 20 components of the optical modulating system, both masks can be formed on a single substrate. For example, the diffracting, spatially periodic pattern may be formed on one surface of a glass plate, and the spatially filtering pattern may be formed on the opposing surface. In this 25 case, the diffracting and filtering patterns are positioned relative to each other as described above, and the substrate must be thick enough to allow the diffracted sub-beams to adequately disperse before impinging the spatially filtering surface.

Once data is collected for a particular 30 wavevector, the masks are translated so that new diffracting and filtering patterns are used to generate an excitation field at a new wavevector, and the data-collection process is repeated. Alternatively, a single 35 pattern containing several distinct spatial frequencies

- 24 -

may be used to modulate the incident excitation beam, and a second mask is used to select the desired Fourier components of the fields to be imaged onto the sample. In this embodiment, multiple excitation and probe beams, 5 each corresponding to a different excitation wavevector, are diffracted by the first mask, and are then recombined on the sample and used to generate multiple signal beams, which may then be detected and analyzed. This allows the entire dispersion of the sample to be determined during a 10 single excitation probe event.

The optical sources and detection electronics which may be used with the optical modulating system have been described previously in J.A. Rogers et al., J. Appl. Phys. 75:1 (1994) and A.R. Duggal et al., U.S.S.N. 15 07/910,762, the contents of which are incorporated herein by reference. Briefly, in order to impulsively generate material motions in a sample (using, e.g., ISTS or ISBS), the excitation beam is pulsed, and may be generated using a light source which is Q-switched, mode-locked, or both. 20 The pulse duration of the excitation field must be short enough to impulsively stimulate material motions in the film. For example, in order to excite acoustic processes, the output pulse preferably has a duration of between 100 picoseconds and 5 nanoseconds. The energy of 25 the output pulse is preferably between 0.1 and 5 millijoules. In addition, the repetition rate of the pulses must be high enough to allow suitable data averaging (when necessary), but low enough to allow the thermal properties of the sample to recover between laser 30 shots. Preferably, the repetition rate is between 1 and 2000 Hz, with the rate being adjusted for measurement of different types of samples. For samples which easily damage, such as thin polymer films, it may be preferable to reduce the repetition rate of the excitation laser.

- 25 -

In order to create excited-state transient gratings (e.g., gratings of electron-hole pairs, or other excitonic species), the carrier frequency of the excitation beam is such that it is absorbed by the  
5 sample. If the excitation wavelength is below the absorption energy of the sample, the beam may first be passed through one or more non-linear optical devices, such as a frequency-doubling or frequency-tripling crystal, which can be used to generate higher-order  
10 harmonics (e.g., second or third order harmonics) of the fundamental frequency. Alternatively, if the sample is excited using mechanisms which do not rely on optical absorption (e.g., ISRS or ISBS processes), the excitation light need not be absorbed by the sample.

15 Once excited, the time-dependent properties of the sample are recorded by monitoring the time-dependent diffraction of the probe beam, which is preferably derived from a continuous wave (cw) single-mode laser producing between 0.1 and 1 Watt in the visible frequency  
20 range (e.g., 514 nm) with a flat intensity profile. In certain embodiments, in order to measure the entire time dependence of the transient grating induced in the sample (which, e.g., may take place over several hundreds of microseconds), a well-defined probe waveform is generated  
25 by electro-optically modulating the cw probe beam with a light modulator which controls both the duration and shape of the probe waveform. Preferably, in this case, a probe pulse having a square-wave profile is generated. The waveform has a time duration slightly longer than the  
30 time-dependent motions in the film. The pulse preferably has a temporal duration on the order of between 1 and 100 microseconds. Alternatively, a Q-switched laser producing a pulse duration greater than about 100 ns may be used as the probe laser. In this case, the pulse may  
35 be frequency doubled or tripled prior to interacting with

- 26 -

the sample. In still other embodiments, the diffracted signal may be mapped out in a point-by-point basis, using a pulsed probe beam as described in Duggal et al., U.S.S.N. 07/910,762.

5       The probe waveform diffracted from the transient grating induced in the sample is preferably detected with a time-resolving photodetector. This allows the entire time dependence of the excited region of film to be measured with a single probe waveform. For especially  
10 weak signals, a lens may be used to focus the diffracted beam on the optically active region of the detector, thereby increasing the intensity of the signal. For particularly noisy or weak signals, signal-enhancing electronics, such as high-speed amplifiers, may be used  
15 in combination with the photodetector. For signals detected on a point-by-point basis, photodetectors having long time constants may be used to generate the light-induced signal.

Light sources other than Nd:YAG lasers may be used  
20 to optically excite the film. Suitable lasers include, among others, Nd:YLF, ion (e.g., argon and krypton), Ti:Sapphire, diode, CO<sub>2</sub>, holmium, excimer, dye, and metal-vapor lasers. Similarly, light sources other than cw argon ion lasers may be used as the probe laser.

25 Alternative lasers include diode and krypton ion lasers. Pulsed light sources which may be used to generate the probe beam include Q-switched Nd:YAG, Nd:YLF, Ti:Sapphire, diode, CO<sub>2</sub>, holmium, excimer, dye, and metal-vapor lasers.

30       The samples which may be monitored with the method and apparatus described herein may be bulk (e.g., solids such as metal or semiconductors), thin films (e.g., polyimide, semiconductor, or metal films), fluids, surfaces or other samples exhibiting time-dependent  
35 material motions. The material properties which can be

- 27 -

determined in these samples include mechanical, elastic, (depth-dependent and/or anisotropic) diffusive, adhesion-based, thermal (e.g., thermal diffusivities) and viscous properties associated with the damping of acoustic waves.

- 5 In addition, electron relaxation lifetimes, electron-hole recombination times, exciton lifetimes, and bi-exciton lifetimes may additionally be determined in, for example, metal and semiconductor samples.

In bulk systems the dispersion of the acoustic properties allows the frequency dependence of the mechanical (e.g., bulk or shear) modulus to be determined. Additionally, measurement of the thermal diffusion dynamics allows the thermal diffusivity for the bulk system to be determined. In thin film systems, the 15 acoustic information that is obtained allows determination of the degree of adhesion, delamination properties, and the elastic, shear, and longitudinal moduli, as well as anisotropies in these properties. Depth-dependent properties and residual stresses in thin 20 films can also be determined.

The following are examples of the use of the optical modulating system to generate and measure transient motions in bulk and thin film samples.

Examples

- 25 The material motions of thin polyimide film samples adhered to silicon substrates were measured by passing an excitation beam through the optical modulating system described herein, resulting in the excitation of a transient grating in the sample. Following excitation, 30 the temporal dynamics of the grating were monitored using a probe beam delivered to the sample using a separate optical system.

In the data reported, waveguide modes in the film were excited using a Q-switched, mode-locked, and cavity-dumped Nd:YAG laser. The output pulse had an energy of 1

- 28 -

millijoule, a wavelength of 1064 nm, a pulse duration of 100 ps, and a repetition rate of up to 1 kHz. The light from this laser was first attenuated and then passed through a lithium triborate (LBO) crystal to yield light at 532 nm, which was then mixed with the remnant 1064 nm radiation in a  $\beta$ -barium borate (BBO) crystal to yield excitation pulses of approximately 20 microjoules at 355 nm. This light was then attenuated to yield ~1 microjoule pulses that were used for excitation of the films.

The excitation pulses were focussed on the patterned region of the mask using a cylindrical lens having a focal length of 15 cm to produce a beam size of about 1 cm (z direction) by 300 microns (x direction).  
The patterned region permitted modulation of the amplitude of the excitation beam, and consisted of alternating light-absorbing regions spaced by transparent regions, resulting in a pattern having a square-wave spatial profile. In the patterned region, the light-absorbing regions were spaced by a distance of 6 microns, with each region having a width of 6 microns. The light-absorbing regions of the second patterned region of this same mask were spaced by a distance of 12 microns, with each region having a width of 12 microns. The second mask was spaced by a distance of 2 cm from the first mask, and contained a series of two square openings for spatial filtering of the diffracted excitation sub-beams. In the first series of openings, the transmitting regions had an area of 1 cm<sup>2</sup> and were spaced by a distance of 4 cm. The transmitting regions of the second series had an area of 1 cm and were spaced by a distance of 2 cm.

The imaging system used to image the spatial patterns of the masks onto the sample consisted of a single lens having a focal length of 20 cm. The lens was separated from the first mask by a distance of 40 cm.

- 29 -

- The imaging lens was displaced by a distance of 40 cm from the sample. Recombination of the excitation sub-beams using this imaging system and the two masks resulted in spatially varying optical excitations
- 5 patterns at the sample having wavevectors equal to the spatial frequency of the patterned regions of the masks.
- Material motions in the film were recorded in real-time by monitoring the time-dependent diffraction of a probe pulse spatially overlapped with the induced
- 10 transient grating. The probe pulse had a duration of about 150 ns, and was derived from Q-switched Nd:YAG laser. Prior to irradiating the sample, the probe beam was frequency-doubled to a wavelength of 532 nm. The probe beam was then focussed at an angle of 15° to a 100-
- 15 micron diameter spot on the transient grating. The diffracted component of the probe beam was measured with a fast amplified photodiode (Antel; 2 GHz bandwidth). The light-induced signal was then sent to a transient digitizer (Tektronics DSA 602A; 1 GHz bandwidth),
- 20 resulting in generation of digital signal for analysis. The combination of the photodiode and transient digitizer effectively provided a 1 GHz-bandwidth window through which the film's oscillatory and relaxational motions were monitored.
- 25 Data was generated by passing the excitation beam through the first set of patterns on the two masks, signal averaging for 20 laster shots, and then mechanically adjusting the masks so that the excitation beam was modulated by the second set of patterns.
- 30 Referring now to Figs. 6A and 6B, typical data taken from the silicon-bound polyimide films using the above-identified optical system illustrates the time-dependent nature of the measured signal. The oscillatory component of the data is due to the coherent, periodic motions of
- 35 the excited waveguide modes. The difference in frequency

- 30 -

between the two data scans is due to excitation of the film with different wavevectors. Damping of these modes, shown in the data (after several hundred nanoseconds) as a decrease in the amplitude of subsequent oscillations, 5 is due to viscous losses in the polyimide material. The two data scans, taken with different excitation wavevectors adjusted during a time period of just 19 seconds, demonstrate that the optical modulation system can be used to change the wavevector of the excitation 10 pattern in very rapid fashion, and can additionally be used to generate data having high signal-to-noise ratios.

In a separate experiment, the first and second masks described above were used to sequentially modulate the excitation and probe beams in order to monitor the 15 response of the liquid salol at room temperature. In this case, the sample was optically excited throughout the bulk (i.e., in the thick-grating regime) using the fundamental frequency from the Nd:YAG laser described above. The transient grating was probed using the output 20 from a cw single-mode Argon ion laser (Lexel 3500) producing 1 Watt at 514 nm with a flat intensity profile. This output was electro-optically modulated (Conoptics 380) to yield a square pulse having a temporal width of 100 microseconds. The signal beam was detected using the 25 photodetector and transient digitizer described above. In this experiment, the excitation and probe beams were made collinear prior to modulation with the diffracting and spatial filtering masks, and 1:1 imaging optics (i.e.  $M = 1$ ) were used, thereby ensuring that the phase- 30 matching criteria were satisfied by the probe beam.

Referring now to Figs. 7A and 7B, two sets of data were generated using a first mask with amplitude-modulating regions 6 microns wide, and 6 microns apart. The second mask used to filter the diffracted beam had 35 two openings, each with an area of  $1 \text{ cm}^2$  and spaced by a

- 31 -

distance of 4 cm. The first order diffracted components of the pattern on the first mask were imaged onto the sample, resulting in a sinusoidally varying excitation field having a spatial periodicity of 6 microns. The 5 diffracted signals were measured during short (i.e., 600 ns; Fig. 7A) and long (i.e., 110 microseconds; Fig. 7B) time windows.

The high signal-to-noise ratios of the data scans illustrates that the Bragg angle is accurately set using 10 the masks. (If the probe were not incident at the Bragg angle, the diffracted signal would be too weak to measure.) In the experiments, the residual probe sub-beam overlapped with the signal beam was used as a finder beam to allow facile alignment of the signal into the 15 photodetector. As before, the coherent oscillations in the data were due to the induced acoustic processes in the samples, while the long-time exponential decay is due to thermal diffusion.

Other embodiments are within the scope of the 20 following claims.

What is claimed is:

- 32 -

1. A method of determining a property of a sample, said method comprising:

(a) providing a beam of radiation and then passing the beam through a pattern on a diffracting mask to form 5 at least two excitation sub-beams;

(b) overlapping at least two excitation sub-beams on a region of the sample with an imaging system to generate a spatially varying optical field which excites a transient grating in the region of the sample;

10 (c) irradiating the transient grating with a probe beam oriented so that at least a portion of the probe beam is diffracted by the transient grating;

(d) detecting the diffracted portion of the probe beam with an optical detector to generate a light-induced 15 signal; and

(e) analyzing said light-induced signal from the optical detector to determine the property of the sample.

2. The method of claim 1, wherein the diffracting pattern comprises alternating light-modulating regions 20 having at least one spatial frequency, and the excitation beam is separated into at least a zeroth, +1, and -1 excitation sub-beam by diffracting the excitation beam off of the light-modulating regions of the diffracting pattern.

25 3. The method of claim 2, wherein said overlapping step further comprises the step of passing at least the +1 and -1 excitation sub-beams through the imaging system prior to overlapping the excitation sub-beams on the sample.

- 33 -

4. The method of claim 3, wherein the imaging system images at least one of the spatial frequencies of the light-modulating regions of the diffracting pattern onto the sample to form the spatially varying optical field.

5. The method of claim 4, wherein at least one of the spatial frequencies of the light-modulating region and the spatial varying optical field are equivalent.

6. The method of claim 1, wherein the excitation beam is focussed onto the diffracting pattern prior to step (a).

7. The method of claim 6, wherein the excitation beam is cylindrically focussed onto the diffracting pattern.

15 8. The method of claim 1, wherein the probe and excitation beams are made collinear prior to step (a).

9. The method of claim 8, wherein step (a) further comprises the step of separating the probe beam into at least two probe sub-beams by passing the probe beam through the diffracting pattern on the first mask.

10. The method of claim 8, wherein said probe sub-beams pass through the imaging system prior to irradiating the grating induced in the region of the sample.

25 11. The method of claim 10, wherein the imaging system is a 1:1 imaging system.

- 34 -

12. The method of claims 1 or 9, wherein between steps (b) and (c) said excitation sub-beams are spatially filtered with a second mask.

13. The method of claim 12, wherein the first and 5 second masks are comprised in a single unit.

14. The method of claim 12, wherein said spatial filtering transmits the +1 and -1 excitation and probe sub-beams.

15. The method of claim 1, wherein said analyzing 10 step further comprises determining the dispersion of the sample.

16. The method of claim 15, wherein the dispersion is used to determine the mechanical, thermal, optical, or electronic properties of the sample.

15 17. The method of claim 16, wherein the mechanical property is one of adhesion, elastic moduli, stiffness, residual stress, and density.

18. The method of claim 15, wherein the dispersion is determined following inducing multiple 20 transient gratings in the sample with a single spatial varying optical field having multiple spatial frequencies.

19. The method of claim 15, wherein the dispersion is determined following sequentially inducing 25 multiple transient gratings in the sample with multiple spatial varying optical fields, each having a single spatial frequency.

- 35 -

20. A method of diffracting a probe beam off a sample, said method comprising:

(a) providing a beam of radiation and then passing the beam through a pattern on a diffracting mask to form 5 at least two excitation sub-beams;

(b) overlapping at least two excitation sub-beams on a region of the sample with an imaging system to generate a spatially varying optical field which excites a transient grating in the region of the sample; and

10 (c) irradiating the transient grating with a probe beam oriented so that at least a portion of the probe beam is diffracted by the transient grating.

21. An apparatus for diffracting a portion of a probe beam off a sample, comprising:

15 means for generating a probe optical beam and an excitation optical beam orientated along an optical axis, a first diffracting mask comprising an optical diffracting pattern, said diffracting pattern being positioned along the optical axis and being configured so 20 that when irradiated with the excitation beam, said pattern diffracts the excitation beam to generate at least two excitation sub-beams;

an imaging system comprising at least one lens positioned along the optical axis, said imaging system 25 configured to focus the excitation sub-beams onto a region of the sample to generate a spatially varying optical field which excites a transient grating in the region of the sample, said grating allowing diffraction of a portion of the probe beam off of the excited region 30 of the sample.

22. The apparatus of claim 21, wherein said diffracting pattern comprises a series of opaque regions

- 36 -

spaced by a distance which allows diffraction of visible or infrared radiation.

23. The apparatus of claim 21, wherein said diffracting pattern comprises a series of regions etched 5 to a depth and spaced by a distance which allows diffraction of visible or infrared radiation.

24. The apparatus of claim 21, wherein said apparatus further comprises a second, spatially filtering mask comprising a pair of openings, said openings 10 positioned along the optical axis so that said spatially filtering mask allows spatial filtering of said diffracted excitation sub-beams.

25. The apparatus of claim 24, wherein the diffracting and spatial filtering masks are comprised in 15 a single unit.

26. The apparatus of claim 24, wherein said filtering mask comprises a plurality of pairs of opening.

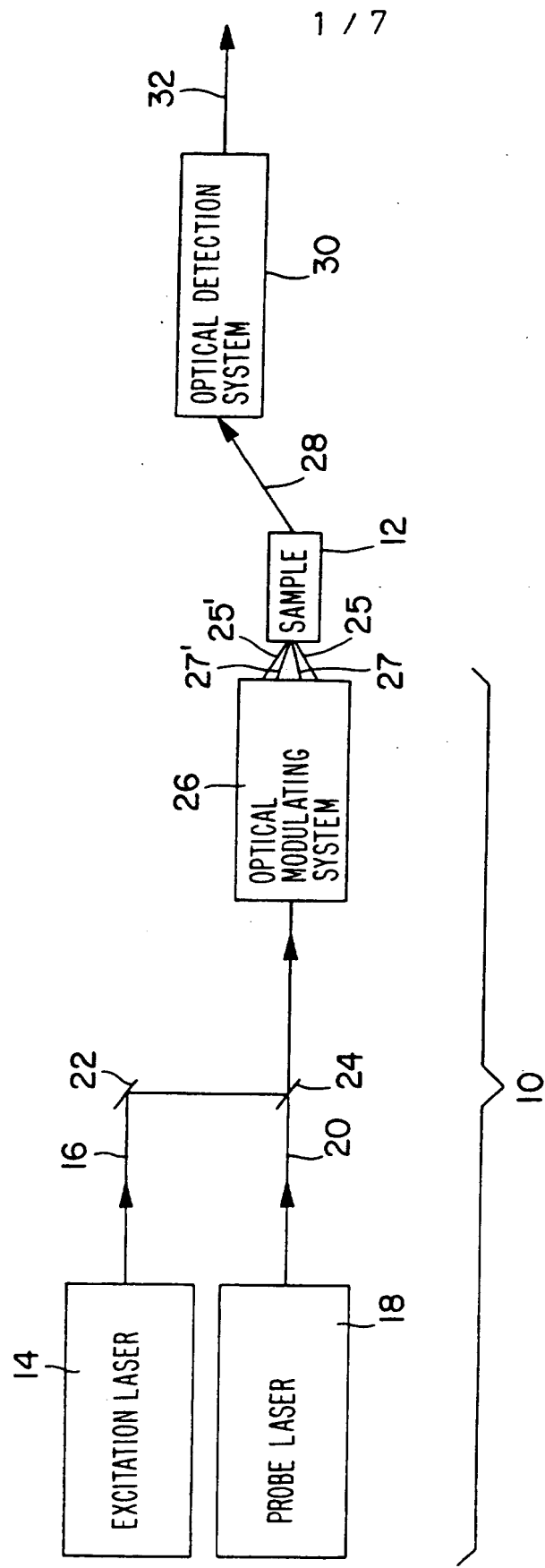


FIG. I

2 / 7

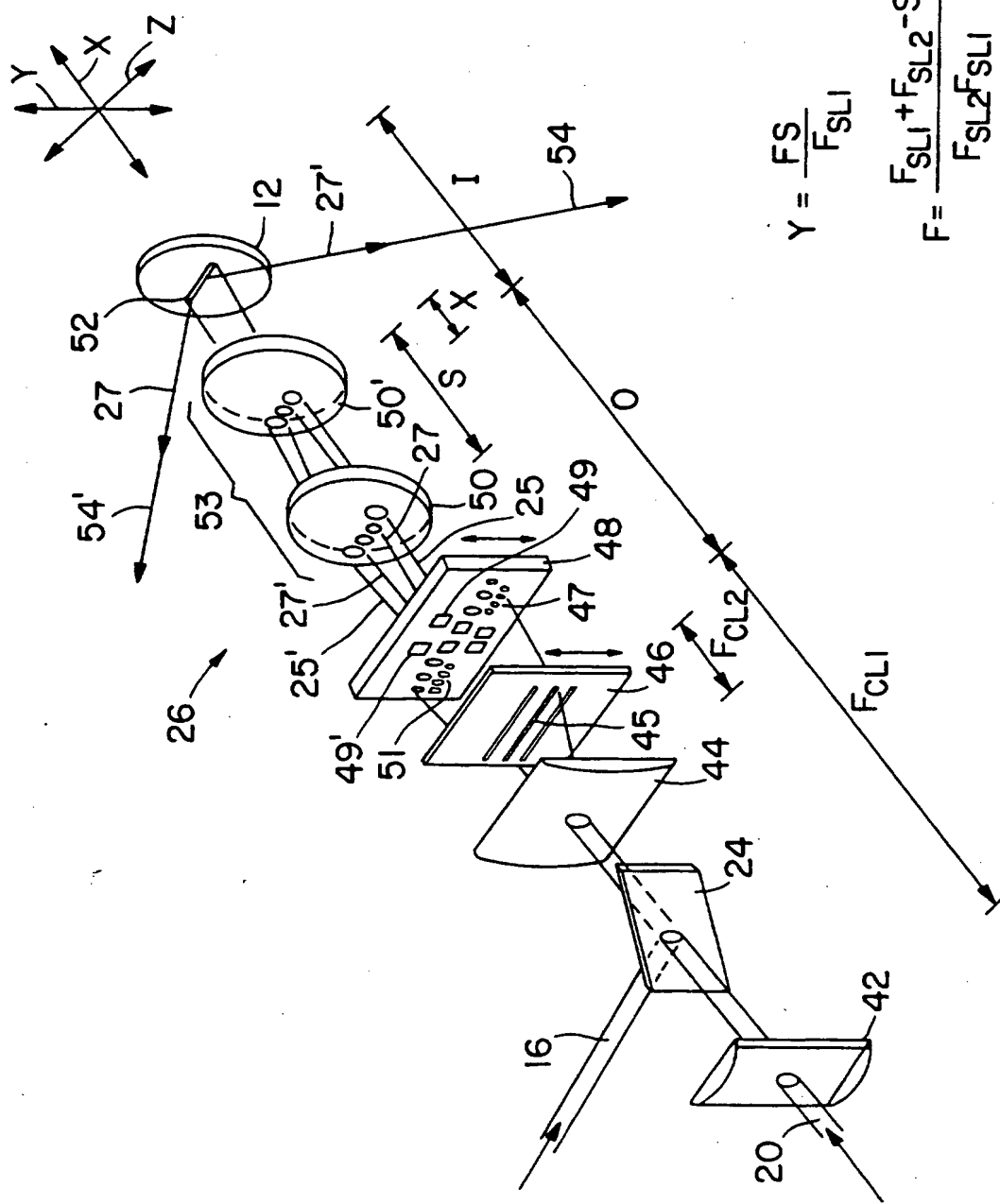


FIG. 2

SUBSTITUTE SHEET (RULE 26)

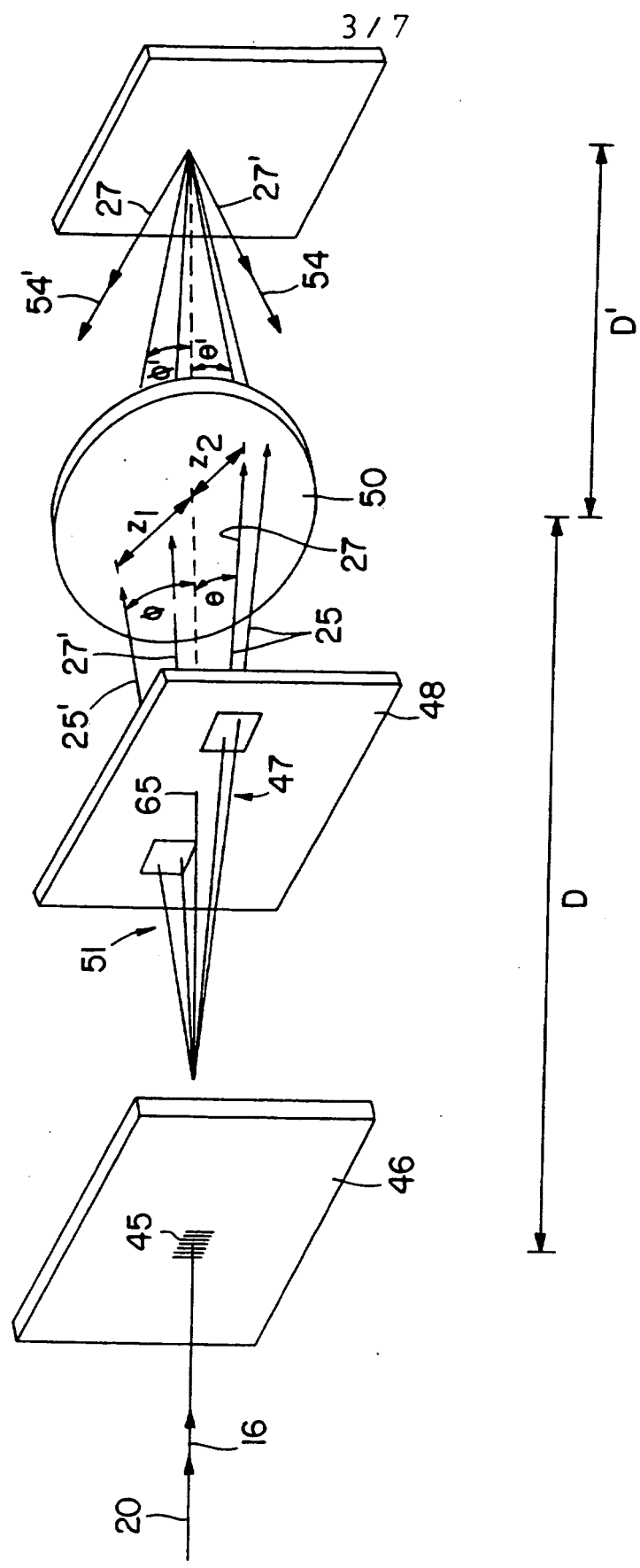


FIG. 3

SUBSTITUTE SHEET (RULE 26)

4 / 7

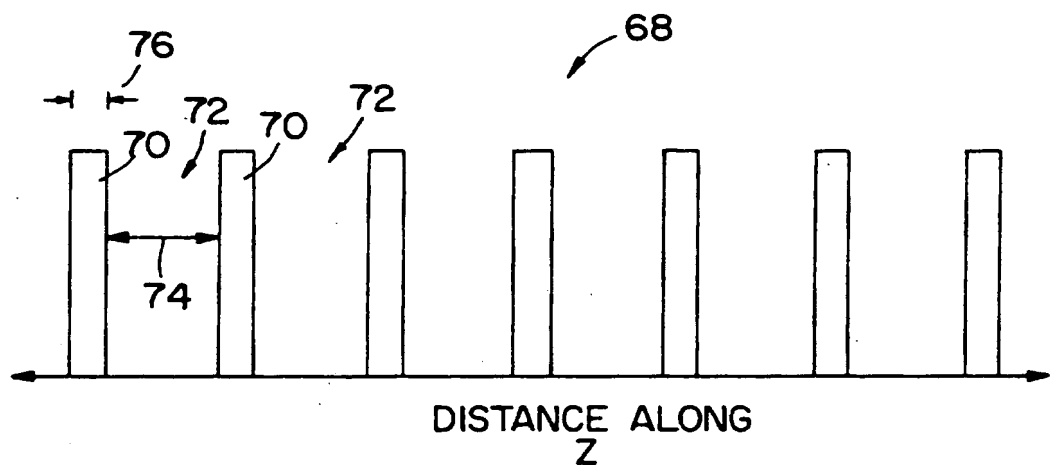


FIG. 4A

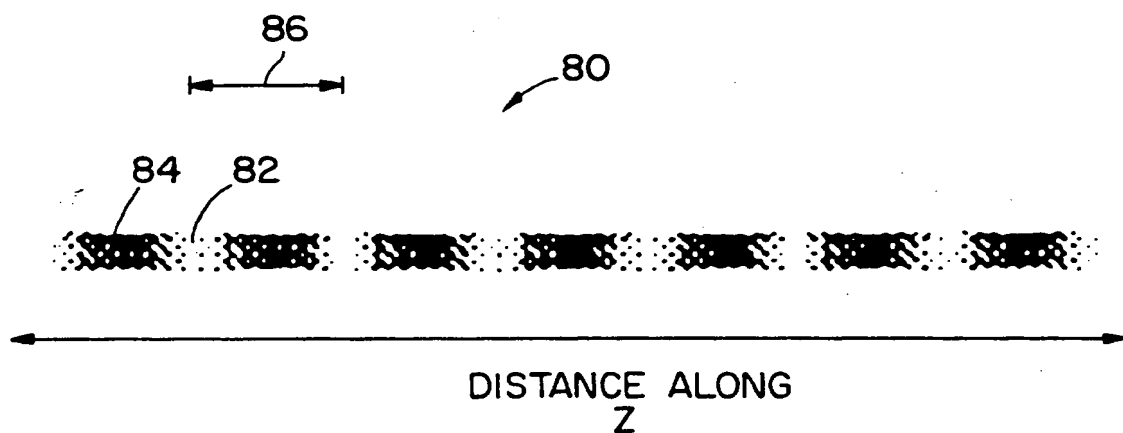


FIG. 4B

SUBSTITUTE SHEET (RULE 26)

5 / 7

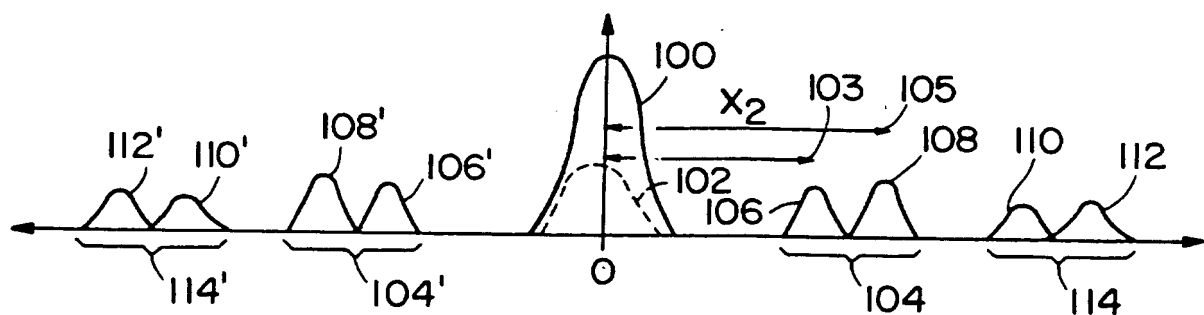


FIG. 5A

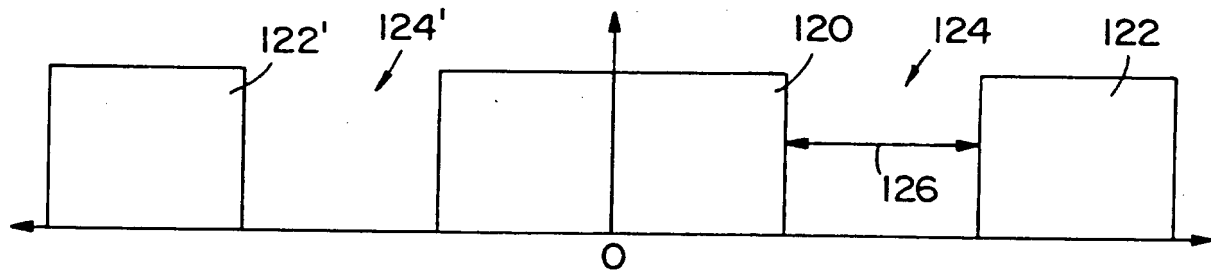


FIG. 5B

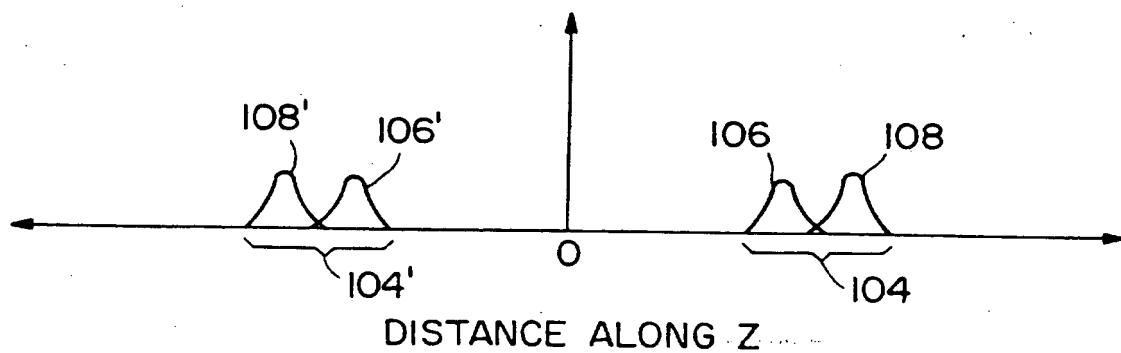


FIG. 5C

6 / 7

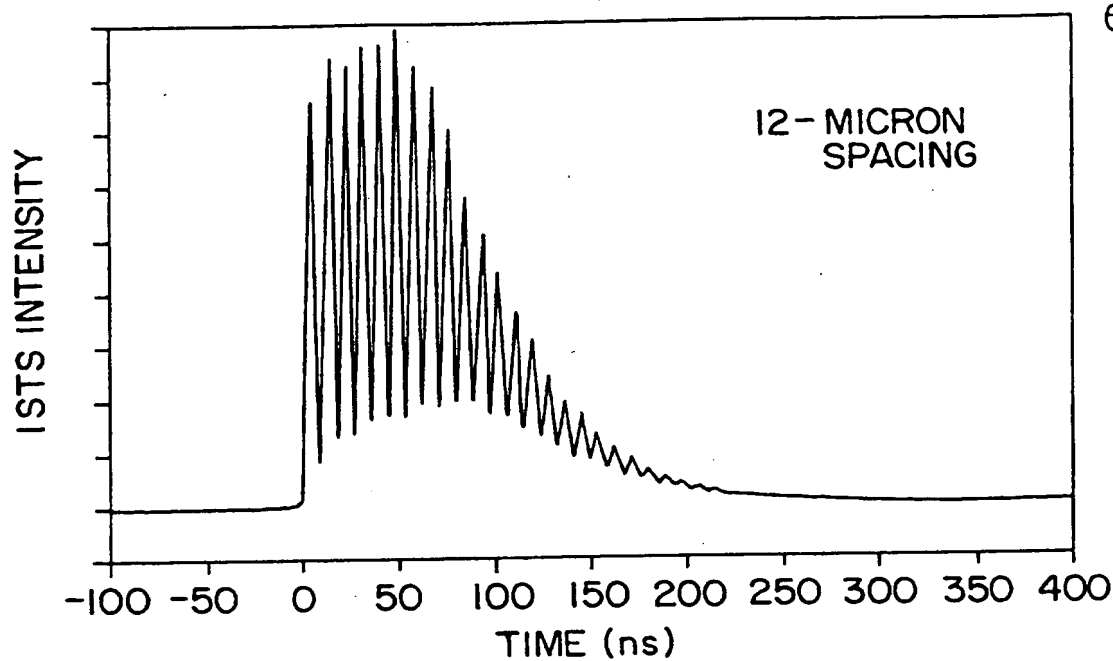


FIG. 6A

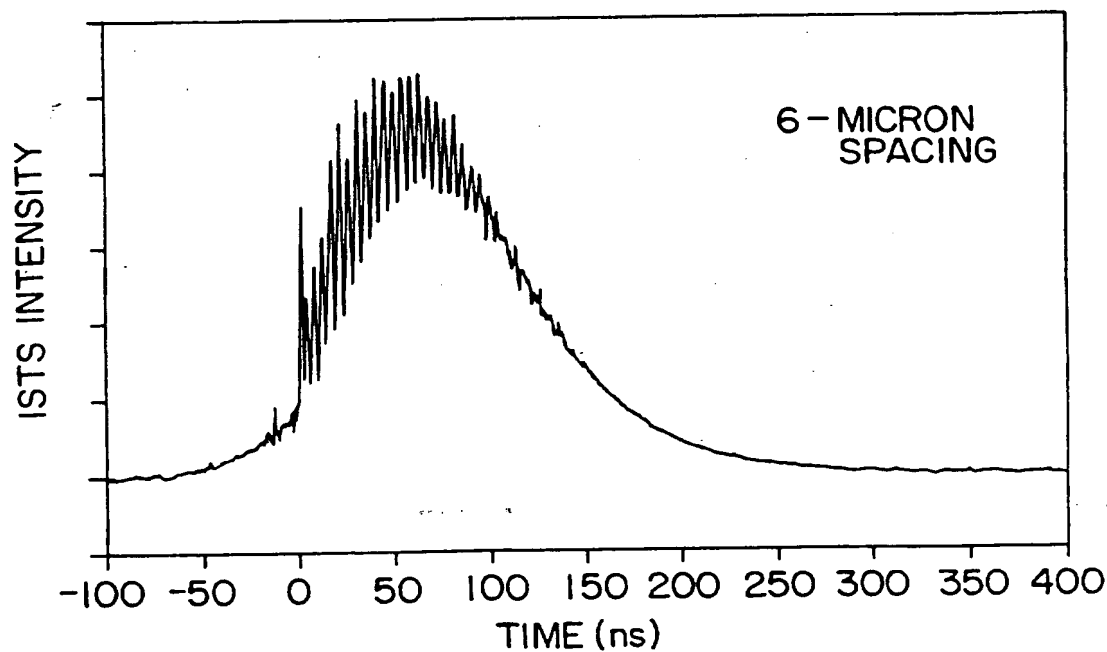


FIG. 6B

7 / 7

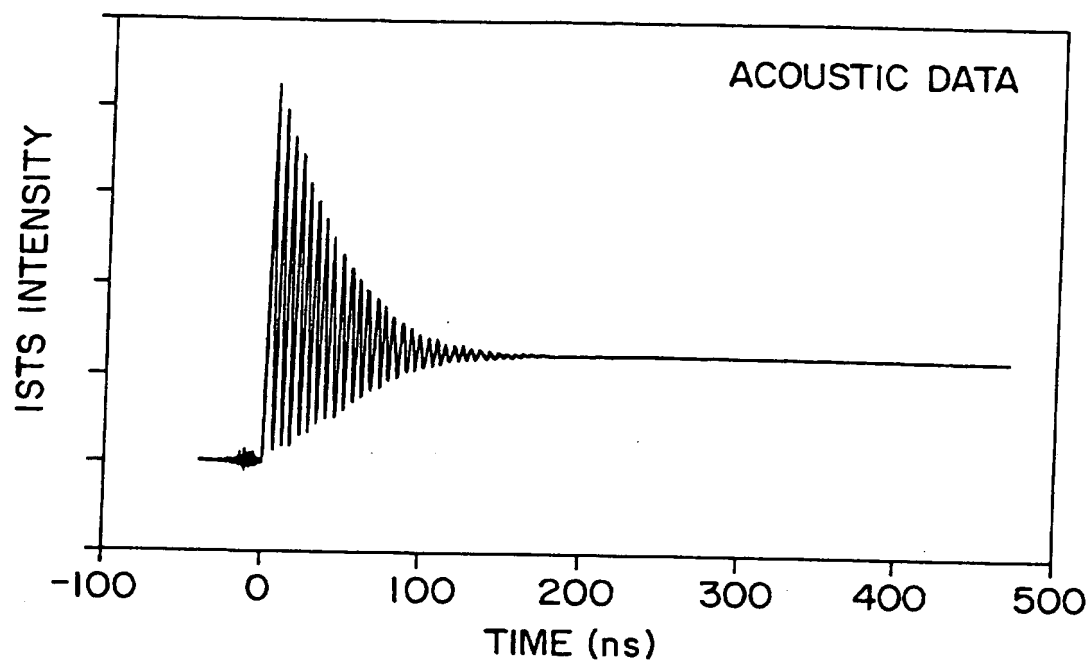


FIG. 7A

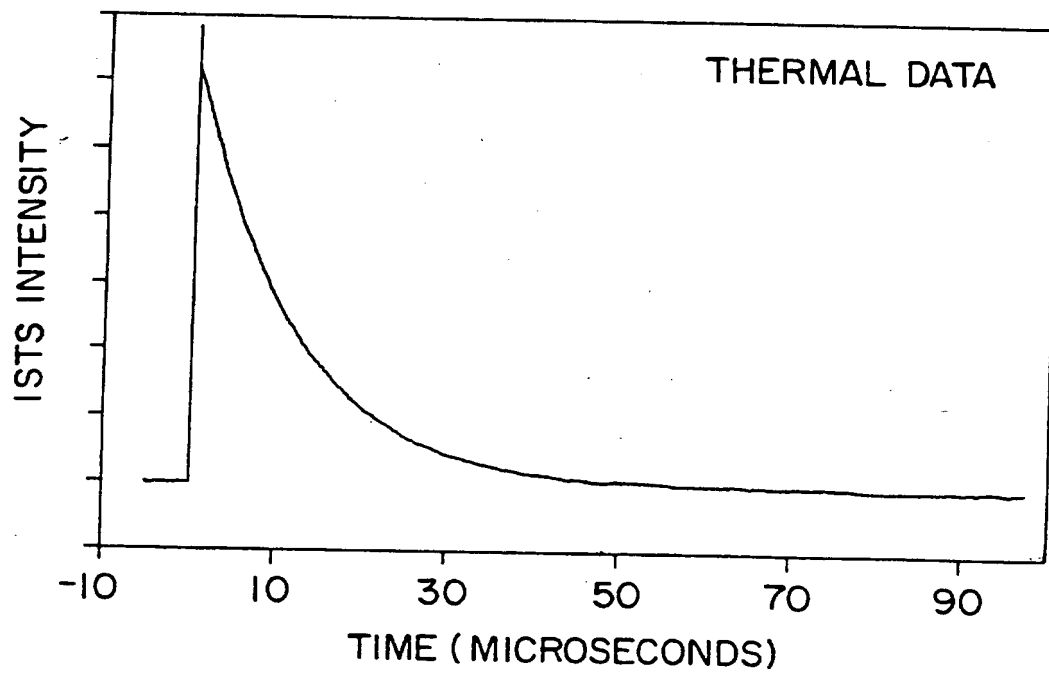


FIG. 7B

# INTERNATIONAL SEARCH REPORT

International application No.

PCT/US96/00552

## A. CLASSIFICATION OF SUBJECT MATTER

IPC(6) :G01B 9/02  
US CL :356/354, 356, 432, 237

According to International Patent Classification (IPC) or to both national classification and IPC

## B. FIELDS SEARCHED

Minimum documentation searched (classification system followed by classification symbols)

U.S. : 356/354, 356, 432, 237

Documentation searched other than minimum documentation to the extent that such documents are included in the fields searched

Electronic data base consulted during the international search (name of data base and, where practicable, search terms used)

APS

search terms: transient grating, probe beam, excitation beam, diffraction

## C. DOCUMENTS CONSIDERED TO BE RELEVANT

Category*	Citation of document, with indication, where appropriate, of the relevant passages	Relevant to claim No.
X	US, A, 5,344,236 [FISHMAN]06 SEPTEMBER 1994, figures 2 and 3	1-11, 15-23 ,
A, P	US, A, 5,479,256 [TAMAI EL AL] 26 DECEMBER 1995.	1-26

Further documents are listed in the continuation of Box C.  See patent family annex.

* Special categories of cited documents:	"T"	later document published after the international filing date or priority date and not in conflict with the application but cited to understand the principle or theory underlying the invention
"A" document defining the general state of the art which is not considered to be of particular relevance	"X"	document of particular relevance; the claimed invention cannot be considered novel or cannot be considered to involve an inventive step when the document is taken alone
"E" earlier document published on or after the international filing date	"Y"	document of particular relevance; the claimed invention cannot be considered to involve an inventive step when the document is combined with one or more other such documents, such combination being obvious to a person skilled in the art
"L" document which may throw doubts on priority claim(s) or which is cited to establish the publication date of another citation or other special reason (as specified)	"&"	document member of the same patent family
"O" document referring to an oral disclosure, use, exhibition or other means		
"P" document published prior to the international filing date but later than the priority date claimed		

Date of the actual completion of the international search

29 MARCH 1996

Date of mailing of the international search report

22 APR 1996

Name and mailing address of the ISA/US  
Commissioner of Patents and Trademarks  
Box PCT  
Washington, D.C. 20231

Faxsimile No. (703) 305-3230

Authorized officer

AMANDA MERLINO

Telephone No. (703) 305-3488

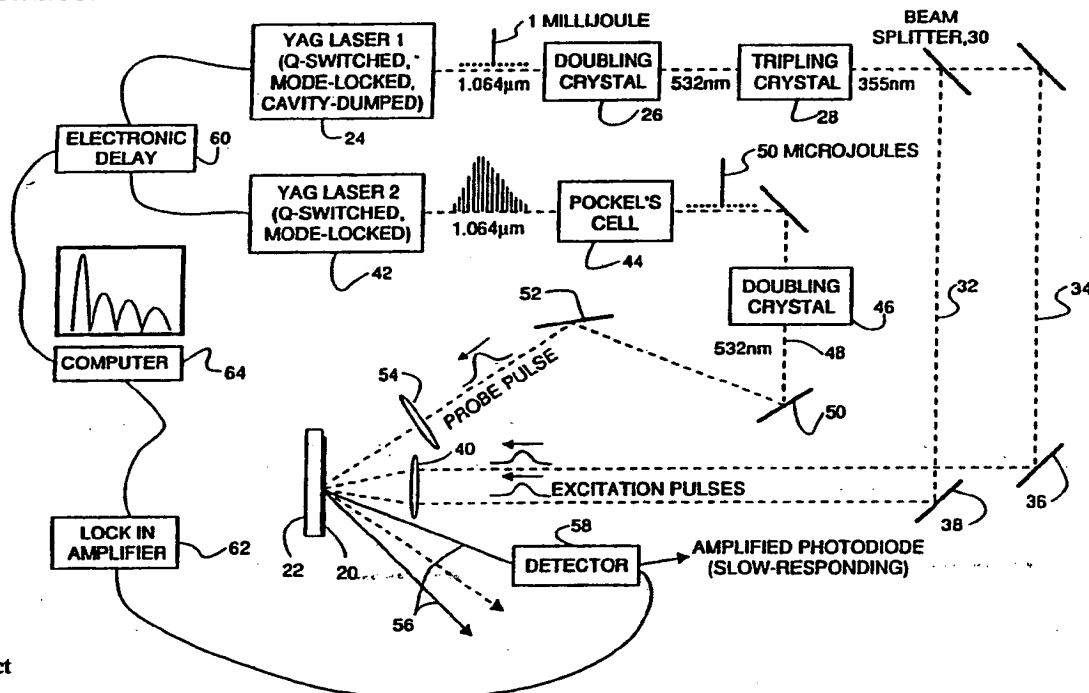
Form PCT/ISA/210 (second sheet)(July 1992)\*



## INTERNATIONAL APPLICATION PUBLISHED UNDER THE PATENT COOPERATION TREATY (PCT)

(51) International Patent Classification 5 :  G01J 3/30	A1	(11) International Publication Number: WO 93/01476  (43) International Publication Date: 21 January 1993 (21.01.93)
(21) International Application Number: PCT/US92/05679		(74) Agent: FEIGENBAUM, David, L.; Fish & Richardson, 225 Franklin Street, Boston, MA 02110-2804 (US).
(22) International Filing Date: 8 July 1992 (08.07.92)		(81) Designated States: JP, European patent (AT, BE, CH, DE, DK, ES, FR, GB, GR, IT, LU, MC, NL, SE).
(30) Priority data: 726,759 8 July 1991 (08.07.91) US		Published <i>With international search report.</i>
(71) Applicant: MASSACHUSETTS INSTITUTE OF TECHNOLOGY [US/US]; 77 Massachusetts Avenue, Cambridge, MA 02139 (US).		
(72) Inventors: NELSON, Keith, A. ; 55 Clearwater Road, Newton, MA 02162 (US). DUGGAL, Anil, R. ; 15 Alfred Road, Arlington, MA 02174 (US). ROGERS, John, A. ; 305 Memorial Drive, No. 617A, Cambridge, MA 02139 (US).		

## (54) Title: MEASUREMENT OF MATERIAL PROPERTIES WITH OPTICALLY INDUCED PHONONS



## (57) Abstract

Samples such as thin polymeric films (20) are analyzed using optically induced phonons by excitation of the sample using radiation (32, 34) preferably absorbed by the sample and probe radiation (48, 76) preferably not absorbed by the sample, that is diffracted from the surface of the sample. The pulse width of the probe is preferably on the order of the detectable diffraction signal so that the phonon decay from each excitation pulse can be detected (58, 72) and analyzed (64, 62, 37). The technique is applicable to various samples by inducing a ripple morphology on the sample surface and detection of light diffracted substantially from surface ripple.

**FOR THE PURPOSES OF INFORMATION ONLY**

Codes used to identify States party to the PCT on the front pages of pamphlets publishing international applications under the PCT.

AT	Austria	FI	Finland	ML	Mali
AU	Australia	FR	France	MN	Mongolia
BB	Barbados	GA	Gabon	MR	Mauritania
BE	Belgium	GB	United Kingdom	MW	Malawi
BF	Burkina Faso	GN	Guinea	NL	Netherlands
BG	Bulgaria	GR	Greece	NO	Norway
BJ	Benin	HU	Hungary	PL	Poland
BR	Brazil	IE	Ireland	RO	Romania
CA	Canada	IT	Italy	RU	Russian Federation
CF	Central African Republic	JP	Japan	SD	Sudan
CG	Congo	KP	Democratic People's Republic of Korea	SE	Sweden
CH	Switzerland	KR	Republic of Korea	SN	Senegal
CI	Côte d'Ivoire	LI	Liechtenstein	SU	Soviet Union
CM	Cameroon	LK	Sri Lanka	TD	Chad
CS	Czechoslovakia	LU	Luxembourg	TG	Togo
DE	Germany	MC	Monaco	US	United States of America
DK	Denmark	MG	Madagascar		

- 1 -

MEASUREMENT OF MATERIAL PROPERTIES  
WITH OPTICALLY INDUCED PHONONS

Field of the Invention

5 This invention relates to the measurement of material properties using optically induced phonons.

Background of the Invention

Laser Induced Phonons (LIPS) are produced by time-coincident laser pulses intersecting inside a sample, 10 setting up an optical interference pattern, i.e., alternating intensity peaks and nulls. Energy deposited into the system via optical absorption or stimulated Brillouin scattering results in the launching of counterpropagating ultrasonic waves (phonons) whose 15 wavelength and orientation match the interference pattern geometry. The mechanism by which LIPS ultrasonic waves are generated depends upon whether the sample is optically absorbing or transparent at the excitation wavelength. If the excitation pulses are absorbed e.g. 20 into high-lying vibronic levels, rapid radiationless relaxation and local heating at the interference maxima (the transient grating peaks) occurs. Thermal expansion then drives material in phase away from the grating peaks and toward the grating nulls, setting up 25 counterpropagating waves.

In samples which are transparent at the excitation wavelength, optical energy is coupled directly into the sample's acoustic field via stimulated Brillouin scattering. This process takes advantage of the inherent 30 spectral line width in 100-picosecond (psec) excitation pulses. Higher-frequency photons from each pulse are annihilated to create lower-frequency photons in the opposite pulse and phonons of the difference frequency and wave vector in the medium. Counterpropagating waves 35 (a standing wave) are thus produced.

SUBSTITUTE SHEET

- 2 -

In either case the acoustic wave propagation, which continues after the excitation pulses leave the sample, causes time-dependent, spatially periodic variations in the material density, and since the 5 sample's optical properties (real and imaginary parts of the index of refraction) are density-dependent, the irradiated region of the sample acts as a Bragg diffraction grating. This propagation of the optically excited ultrasonic waves can be optically monitored by 10 time-dependent Bragg diffraction of a variably delayed probe laser pulse.

Summary of the Invention

An object of the invention is to make LIPS (alternatively referred to herein as Impulsive Stimulated 15 Thermal Scattering or ISTS) measurements by reflectance of a probe beam from the sample surface without regard to the absorbance of the probe beam by the sample. Another object is to make LIPS measurements without regard to sample type or thickness. A particular object is the 20 analysis of thin, polymer samples by LIPS-reflectance with a non-absorbing probe laser.

The phenomenon which allows realization of these objects is believed to be the inducement of a physical surface morphology or 'ripple' in response to laser 25 excitation. It has been discovered that the surface ripple phenomenon can be selectively induced based on the nature of the sample, e.g. sample stiffness and thickness and the angle of incidence and wavelengths of the excitation radiation and selectively detected or analyzed 30 by control or monitoring of parameters such as angle of incidence, polarization and intensity of a probe beam reflected from the ripple morphology. The discovery enables advantages in terms of the samples that can be analyzed, including ultrathin polymer films, in terms of 35 the rate at which data can be obtained, such as obtaining

- 3 -

the full transient signal induced by each excitation laser shot, and in terms of the type and accuracy of data that can be obtained, including more accurate subtraction of probe pulse contribution from the signal and the 5 collection of new data such as acoustic dampings rates (attenuation), thermal conductivity and film delamination.

In a particular example, excitation of a sample using optically absorbing wavelengths can be used to 10 induce the physical morphology, preferably in the form of a periodic grating on the surface of a sample. The grating morphology can be interrogated by reflectance of a probe laser from the surface without regard to the probe laser wavelength and in particular, allowing the 15 use of a probe laser not substantially absorbed by the sample. The sample may be of various types. A particular example is the analysis of thin polymer films. The films, which may be UV-absorbing and visible-transmitting, may be excited by UV pulses and 20 interrogated by reflectance with visible pulses. For very thin samples, e.g., 500, 30, 10 or even  $1\mu\text{m}$  or less, this operational mode is particularly advantageous since, with a non-absorbing probe laser, sample heating which can easily damage thin samples, is reduced. It is also 25 an advantage that samples can be interchanged without the need for selecting new probe laser wavelengths. Alternatively, in the case of thin samples, e.g., polymer films, acoustic waves may also be excited through impulsive Brillouin scattering in which case the 30 excitation pulses need not be absorbed by the sample.

Another object is to make measurements quickly, with fewer laser shots, to make it possible to observe changing sample properties with high time resolution. Employing techniques of the invention, LIPS measurements 35 may be made in real time. An excitation pulse having a

## SUBSTITUTE SHEET

- 4 -

short pulse width compared with the phonon oscillation period may be employed in combination with a high power probe laser having a relatively long pulse width such that a substantial time-portion, in many cases all, of a  
5 sample's transient time dependent response from each excitation pulse can be measured. While a high power probe may be particularly useful in some circumstances, alternatively, it has been discovered that signal can be obtained using a relatively low power probe, e.g. about 1  
10 watt, provided by a CW source such as an argon ion laser. In either case, the probe signal from successive excitation pulses may be signal averaged to increase signal to noise. The detection electronics are selected so they have sufficiently fast response times to permit  
15 time resolution of the phonon oscillations. Operation in these modes is, again, particularly advantageous for thin, polymer samples since the number of excitation pulses can be reduced and thus the number of heating cycles, which can potentially damage thin, fragile  
20 samples can also be reduced. For a probe which has a short width compared to the lifetime of the transient response, a temporal delay between excitation and probe pulses may be varied to interrogate the sample at different time segment stages in its response evolution.

25 The term "polymers" as used herein refers to molecules composed of sequences of repeating monomer units connected by covalent bonds. A particular polymer is generally not made up of a single molecular species. Rather, polymers are mixtures of macromolecules with  
30 similar structures and molecular weights that exhibit some average characteristic properties. The polymers may be homopolymers or copolymers, linear or branched, cross-linked or bonded by electrostatic interaction such as hydrogen bonds. The polymers may be elastomers,  
35 thermoplastics and may include plasticizers, stabilizers,

- 5 -

anti-oxidants and lubricants. Polymers may be crystalline in the sense that long segments of linear polymer chains are oriented in a regular manner with respect to one another. Such crystalline regions of a polymer are 5 referred to as crystallites. Amorphous, noncrystalline regions generally lie between the crystallites and constitute defects in the crystalline structure.

A "sample" such as of a polymer may include additives, e.g., chromophores incorporated within the 10 polymer mass (typically not covalently bonded) for enhancing absorbance of the sample at a particular wavelength such as a desired excitation or probe wavelength. A "pure sample" as used herein contains no such additive.

15 The term "absorption", as used herein, includes absorption of electromagnetic radiation by ground or excited states of the sample molecule. Particular aspects of the invention use LIPS in the reflectance mode where the absorbance of the probe is less than the 20 absorbance of the excitation. Particularly the probe absorbance is 50%, 10% or even 1% or less than the excitation absorbance. In some cases, no absorbance of the probe beam by the sample can be detected. Molar absorptivities ( $E$ ) at the probe wavelength may be less 25 than 1000 or 100. Absorption may be less than about 10% of the maximum absorption (which may be relative to complete absorbance) in a wavelength region (e.g., UV, visible, infrared), typically less than 1%. The excitation wavelength is selected such that the 30 absorbance is sufficient to give rise to a periodic morphology on the sample surface, detectable as a diffraction signal.

In a particular aspect, the invention features an apparatus for measuring the properties of a sample of 35 material. The apparatus includes a first, excitation

#### SUBSTITUTE SHEET

- 6 -

source for producing excitation radiation adapted to impinge upon the sample of material. The excitation radiation is comprised of pulsed radiation composed of at least two component pulses which interfere within the  
5 sample. The excitation radiation is sufficient to induce a transient phonon in the material which gives rise to a transient, time dependent periodic ripple morphology on a surface of the sample. A second, probe source is provided for producing probe radiation arranged to  
10 reflect from the periodic ripple morphology on the surface of the sample to form a diffraction signal. A detector detects the diffraction signal from the probe source radiation reflected from the surface, and an analyzer selectively analyzes the diffraction signal  
15 formed by the transient ripple morphology.

In another particular aspect, a method for measuring the properties of a sample. The method includes impinging a pulse of excitation radiation upon the sample. The excitation radiation is composed of at  
20 least two component pulses which interfere within the sample and are selected to induce a transient phonon in the sample which gives rise to a transient, time dependent ripple morphology on a surface of the sample. Probe radiation is reflected from the periodic ripple  
25 morphology on the surface of the sample to form a diffraction signal. The diffraction signal from the probe source radiation reflected from the ripple morphology is selectively detected.

In another particular aspect, the invention  
30 features an apparatus for measuring the properties of a thin sample of polymeric material. The apparatus includes a first, excitation laser source for producing a pulse of radiation adapted to impinge upon the sample. The excitation source is a pulsed source composed of at  
35 least two component pulses which interfere within the

#### SUBSTITUTE SHEET

- 7 -

thin film. The excitation radiation is adapted to induce a transient phonon in the material. A second, probe laser source is provided for producing radiation. The probe radiation is of selected wavelength not substantially absorbed by the sample and arranged to reflect from the surface of the sample to form a diffraction signal. A detector detects the diffraction signal.

The features of the above aspects can be combined.

10 Apparatus features can be used in method inventions. In addition, in various aspects the invention may include one or more of the following features. The radiation from the probe source is absorbed about 50%, 10% or 1% or less than the radiation from the excitation source or

15 there is no detectable or substantial absorbance by the sample at the probe wavelength. The excitation source of radiation is in the ultraviolet. The probe source is in the visible. The sample is a thin sample, e.g., on the order of about 500, 30 or 10  $\mu\text{m}$  or less, and the

20 excitation radiation is absorbed by the sample. The sample is a thin polymeric film. The film is a free-standing film or disposed on a support. The probe radiation is diffracted from the surface of the sample.

25 The probe beam and detector are for detecting a substantial time-portion of the time-dependent diffraction signal, induced by each excitation pulse such as the entire detectable time-dependent diffraction induced by each excitation pulse. The probe radiation is of a selected pulse width and the detector is adapted to

30 detect the time dependent diffraction for the duration of the probe pulse. The excitation pulse width is on the order of psec duration and the probe pulse width is on the order of nanosecond (nsec) duration (e.g. generally greater than 10 nsec, e.g. around 100 ns). The detector

35 has a time resolution on the order of 1 nsec. A signal

#### SUBSTITUTE SHEET

- 8 -

averaging means is provided for signal averaging the diffracted radiation from multiple excitation pulses. The probe pulse has a peak power output (power during the laser on-time) of about 1000 watts or greater, such as 5 around 10,000 watts. The probe laser is a Q-switched YAG laser. The excitation pulse is generated from a pulsed laser and the probe pulse can be generated from a CW laser having for example a laser power output of around 1 watt, such as a gated argon ion laser. The polymer 10 sample is a pure polymer sample.

Various aspects may also include one or more of the following features. The diffraction signal is analyzed to selectively analyze diffraction from surface ripple. The analyzer includes a polarizer for 15 determining change of polarization of the probe beam after diffraction to selectively analyze diffraction from the surface morphology. The analyzer may also be for analyzing the signal as a function of wavevector to selectively analyze diffraction signal from the ripple 20 morphology. The angle of incidence of the probe beam and/or the excitation beam or the wavelength of the excitation beam may be varied to optimize diffraction from the ripple morphology. The diffraction signal is produced by reflection of the probe beam from the back 25 surface of a sample, opposite the radiation sources or the front surface or both. The system is adapted for determining adhesion and/or thermal diffusion of the polymer sample on a substrate surface from the diffraction signal.

30 The invention has many advantages and applications. It is demonstrated below that ISTS experiments with real-time data acquisition rates are possible and can be applied to studying the pseudo-Rayleigh acoustic modes that propagate in thin film 35 coatings. Real-time data acquisition can be crucial in

SUBSTITUTE SHEET

- 9 -

avoiding optical damage to polymer films. The diffracted ISTS signal arises predominantly from corrugation or ripple displacements at the film surface and the film/substrate ripple due to the propagating pseudo-Rayleigh modes. The relative contribution of each acoustic mode to the ISTS signal depends on the efficiency with which each mode is excited by the excitation pulses and on the efficiency with which each mode diffracts the probe beam due to surface and interface ripple. A formalism is developed to quantify both of these factors. Using this formalism a method for extracting the elastic constants of the film by analyzing the dispersion of the pseudo-Rayleigh modes is described and applied to the polyimide/silicon system.

The techniques have wide applications in nondestructive, real-time characterization of thin films. For many applications, such as monitoring thin-film fabrication and cure or determination of the spatial uniformity of coatings, it is not necessary to determine elastic moduli but merely to monitor changes in acoustic frequency. Finally, characterization of thermal diffusion rates will present a similar range of applications in polymeric, diamond, and other thin films. Other types of materials can be studied, for example, single crystal Fe films and amorphous, plasma deposited carbon films.

The invention includes methods of use of the techniques described. Still other objects, features and advantages follow.

30 Detailed Description

We first briefly describe the drawings.

Drawings

Figs. 1 to 1c illustrate schematically, the surface ripple morphology phenomenon included in the present invention;

- 10 -

Fig. 2 is a schematic of a measurement apparatus according to the invention; Fig. 2a is an absorbance spectrum of a polymeric sample; Fig. 2b is a plot of the intensity verses time, raw data, from the experimental setup in Fig. 2; and Fig. 2c is a plot of the processed data;

Fig. 3 is a schematic of an alternative measurement apparatus according to the invention; Fig. 3a is a plot of the intensity verses time, raw data, from the experimental setup in Fig. 3; Fig. 3b is a plot of the probe pulse intensity; Fig. 3c is a plot of the processed data from Fig. 3a and Fig. 3d is a plot of processed data taken under the conditions of Fig. 3a, but from a single excitation shot;

Fig. 4 is a plot of intensity versus time raw data, and Fig. 4a is a plot of the processed data from an experimental set up similar to Fig. 3, with an acoustic wavevector of  $0.60 \mu\text{m}^{-1}$ ;

Fig. 5 is a plot of intensity versus time, raw data, from an experimental set up using a CW probe laser while Fig. 5a is a plot similar to Fig. 5 but from a single excitation shot;

Fig. 6 is a plot of intensity versus time, raw data, from an experimental set up using a CW probe laser to obtain thermal data;

Fig. 7 illustrates the system geometry used in the theoretical calculations, wherein the film fills the space between  $y=0$  and  $y=-h$  and the substrate fills the area from  $y=0$  to  $y=+H$  and the acoustic wavevector set up by the pump beams is in the z direction;

Fig. 8 is a plot of pseudo-Rayleigh mode dispersion generated using substrate elastic parameters  $v_{Ls} = 8945 \text{ m/s}$ ,  $v_{Ts} = 5341 \text{ m/s}$ ,  $\rho_s = 2.33 \text{ g/cm}^3$  and film elastic parameters  $v_{Lf} = 1300 \text{ m/s}$ ,  $v_{Tf} = 700 \text{ m/s}$ ,  $\rho_f = 1.45 \text{ g/cm}^3$ , with the acoustic wavevector given by  $q$ , the

SUBSTITUTE SHEET

- 11 -

film thickness is  $h$ , and  $v_{Rs}$  and  $v_{Rf}$  are the substrate and film Rayleigh surface velocities respectively;

Fig. 9 is a schematic illustration of the beam paths for the four components of first order ripple 5 diffraction that contribute to ISTS signal, wherein parts A and B describe the different paths for the two orders of diffraction observed experimentally;

Fig. 10 illustrates material displacements, generated using the optimized (for the system studied) 10 elastic constants, for the first eight pseudo-Rayleigh modes on a  $1\mu m$  film coating an infinite substrate at a  $qh$  value of 2.5, with the scale factors (A) for each mode determined such that the largest component of displacement in the mode which is driven most efficiently 15 is equal to one and the ripple amplitude (R) for each mode given relative to the maximum displacement amplitude for that mode;

Fig. 11 is a plot of the film surface ripple amplitude versus  $qh$  and velocity for a given ISTS heat 20 input using the optimized (for the system studied) elastic constants wherein each symbol represents a different mode dispersion curve to facilitate comparison with Fig. 14 and the units of the z axis are arbitrary;

Fig. 12 is a plot of the film-substrate interface 25 ripple amplitude versus  $qh$  and velocity using the same parameters as Fig. 11 and the units of the z axis are the same as those given in Fig. 11;

Fig. 13 is a plot of lattice distortion of the first two modes at  $qh=0.8$ , which, upon comparison with 30 Fig. 11 indicates the existence of a crossover;

Fig. 14 is experimental data (symbols) and theoretical pseudo-Rayleigh mode dispersion curves (solid lines) for pyralin films on silicon substrates with various film thicknesses ( $h$ ) in microns; the elastic 35 parameters used in generating the dispersion curves were

SUBSTITUTE SHEET

- 12 -

optimized to best fit the data that fall on the lowest two velocity curves;

Fig. 15 is a plot of dispersion curves for the first 30 normal modes for a  $3\mu\text{m}$  film on a  $330\mu\text{m}$  substrate  
5 using the optimized elastic constants for the pyralin/silicon system; the existence of modes is illustrated with velocities above  $v_{Ts}$  which was the cut-off value for the pseudo-Rayleigh modes calculated for an infinite substrate as in Figs. (6) and (12);

10 Fig. 16 is a dispersion curve plot of velocity versus wavevector for a tightly bound film-substrate system, while Fig. 16a is a similar plot for a freestanding film;

15 Fig. 17 is a series of dispersion curve plots of velocity versus wavevector;

Fig. 18 illustrates the system geometry for an analysis of thermal diffusion.

#### General Description

Referring to Figs. 1-1c, a sample 2, typically a  
20 thin  $T_1$ , e.g.  $5\mu\text{m}$  thick or less, polymer thin film is provided having a front exposed surface 3 and a back surface 5 which is disposed on a substrate 6. (It will be understood that the film could be, as well, a free standing film, without substrate 6.) As shown in Fig.  
25 1a, the sample is excited by impinging a pair of excitation beams 7,9 from sources  $E_1$ ,  $E_2$ . The wavelength of radiation from  $E_1$  and  $E_2$  is selected such that it is absorbed by the sample. The beams 7,9 interfere within an overlap region 11 within the bulk of the sample,  
30 causing rapid local heating in a periodic fashion. Upon such excitation, a periodic ripple-like morphology 13 is generated at the surface 3. The morphology has a peak to trough height,  $H$ , that is at a maximum soon after absorption of the excitation wavelengths and then  
35 oscillates and decays with time. In particular

**SUBSTITUTE SHEET**

- 13 -

experiments, as discussed below, maximum heights  $H$ , are estimated on the order of 5-10 nanometer (nm). As shown in Fig. 1b, the morphology 13 may be interrogated by a probe laser pulse 15, from a source  $P_1$ , by diffraction of 5 the pulse in the reflection mode from the surface 3. The diffracted beam 15' is detected by a detector D, positioned on the same side of the sample as the source  $P_1$ . The angle of incidence of the probe,  $\theta_i$ , and angle of diffraction  $\theta_r$ , may be varied and selected based on the 10 spacing of the periodic morphology. The source  $P_1$  is preferably selected such that the wavelength of the probe pulse is not substantially absorbed by the sample. As illustrated, a component 15'' of the beam 15 may be transmitted through the sample. The pulse 15 is 15 typically selected such that its duration is long compared to the excitation pulse and the lifetime of the periodic morphology. The pulse may be from a pulsed probe laser of selected pulse width and energy or a continuous wave laser, for example. The detector is 20 adapted to receive the signal pulse 15', which is the diffracted beam component from the sample surface, for analyzing the characteristics of the morphology over the course of its existence from each excitation. As illustrated in Fig. 1c, after analysis, the sample 2 25 returns to its original state.

The excitation wavelength is preferably in the ultraviolet (about 100-400nm), but may be, e.g., in the visible (about 410-800nm), infrared (about 0.1-50 $\mu$ ) or beyond. The probe is preferably in the visible, but 30 maybe in other regions, e.g. infrared or ultraviolet, depending on sample absorbance. The excitation and probe radiation may be in the same wavelength region. An advantage of the invention is that the sample may be probed with a laser wavelength independent of the sample 35 absorption; greater flexibility is provided in the choice

#### SUBSTITUTE SHEET

- 14 -

of the probe laser. In particular, it is advantageous to employ a probe laser emitting visible light which can be easily aligned in manufacturing applications. As further discussed in the examples, analysis times can be reduced 5 by employing a probe pulse width as long as the transient decay of the induced phonons, so that the entire morphology decay is detected from each excitation.

A particular advantage is the analysis of thin films, especially thin polymer films, e.g. 10 $\mu\text{m}$  thickness 10 or less, or even 1 $\mu\text{m}$  thickness or less. Typical polymer samples include visible wavelength transmitting polymers such as polyethylene, polyurethane and polyimides. Polymer films which may be analyzed include molecular films such as Langmuir-Blodgett films or biological 15 films. The films analyzed may be supported on a substrate or may be freestanding films. In the case of films on a substrate, the support provides both mechanical rigidity and can reduce sample damage when the support acts as a heat sink. Sample supports include 20 silicon or glass. Applications for the system include analysis of polymer protective coatings on silicon substrates and various applications to polymers in polymer processing, including in-situ processing during e.g. extrusion. In the latter case, the analysis may be 25 carried out at various points in the extruder to determine the progress of the operation and to modify the extrusion in response to the data obtained. Other polymer applications include polymer curing and polymer loading (analysis of properties under mechanical load).

30 The properties that can be measured by analysis of the raw data include acoustic speeds, determined from the frequency of surface oscillations; attenuation rates determined from decay of the signal; thermal expansion and thermal diffusion rates; thermal expansion 35 coefficients and heat capacities can be determined from

SUBSTITUTE SHEET

- 15 -

signal intensities cases where standard samples are run; compressibility and elastic modulus may be determined from acoustic speed and sample thickness frequency dependencies. Calculation of many properties from the 5 raw data is known in the art, and is further discussed in *Journal of Chemical Physics* 94, 7677 (1991) and Farnell et al., "Elastic Wave Propagation in Thin Layers", *Physical Acoustics*, (W.P. Mason, R.N. Thurston Eds.) 935FF, Academic Press, NY, 1972. A particular method for 10 measuring thermal diffusion is discussed below. Calculation of excitation efficiencies is also discussed below.

Example 1

Short Probe Pulse

15 Referring to Fig. 2, an apparatus 2 for measuring the properties of a thin film of polymeric material 20, such as a thin (about 2.2 micron) film of Pyralin® 2555 (a polyimide polymer available from E.I. DuPont de Nemour, Wilmington, DE; other Pyralin materials may be 20 also available for study, e.g. PI 2525, PI 2545, PI 2611) on a silicon substrate 22, includes a first laser 24 such as a YAG laser that produces a beam at a wavelength of about 1.064 micron and an energy of about 1 millijoule. The pulse width is on the order of picoseconds, in this 25 example 100 psec. The beam is modified by crystals, 26,28 for frequency doubling and tripling to produce an excitation beam wavelength in the ultraviolet at about 355 nanometers. Another preferred wavelength is about 266 nanometers. The beam from the laser is split by a 30 beam splitter 30 into component beams 32, 34 which are directed by reflecting optics 36, 38 toward a focusing element 40 (about 30 cm focal length cylindrical focus) which focuses component beams 32, 34 such that they overlap in time and location within the sample 20. 35 Typically, the spot size on the sample is selected to

**SUBSTITUTE SHEET**

- 16 -

avoid excessive heating and damage therefrom, e.g., the spot size may be 100 microns to 1 millimeter with an energy of about 10  $\mu\text{J}$ . In this example, the spot size was about 100  $\mu\text{m}$  high and 2 mm wide (cylindrical focus).

- 5 The probe laser 42 is a YAG laser for probing the surface morphology by reflectance. The output beam from the laser 42 passes through a Pockel's cell 44 to isolate a particular pulse with an energy of, for example, about 50 microjoules. The probe beam is passed through a doubling
- 10 crystal 46 to produce a probe pulse 48 having a wavelength generally not absorbed by the sample 20 such as a probe pulse in the visible range, e.g. 532 nm, as in this example. The probe pulse 48 is directed to the sample by optical reflectors 50, 52 and focused by
- 15 focusing element 54 (about 20 cm focal length) such that the beam impinges upon the sample surface at angle  $\theta_I$  about 45° from normal to the unperturbed sample surface. Diffracted beams 56, arising from the morphology at the sample surface, may be detected at angle  $\theta_R$  about 45°, by
- 20 a detector 58 such as an amplified photodiode. The pulses from the excitation laser 24 and probe laser 42 are electronically delayed to probe the surface morphology as a function of time. A delay control 60 times the sequential pulses of the lasers. Typically,
- 25 the excitation laser pulses at about 1 kilohertz. The probe laser pulses at delay times (from the excitation pulse) varying from the nanosecond range to 40 microseconds or more, depending on the properties of the sample to be determined. The probe pulse width is short
- 30 relative to the period of the phonon oscillations so that each probe pulse thus represents a single measurement of the instantaneous diffraction signal. The signal detected by the detector 58 is filtered via a lock-in amplifier 62 and passed to an analysis means 64, e.g., a
- 35 microprocessor, which also receives the pulse delay

SUBSTITUTE SHEET

- 17 -

information and which converts the raw data via Fourier transform to a spectrum of intensity versus frequency.

Referring to Fig. 2a an absorbance spectrum of a thin film of Pyralin® is shown. At the excitation wavelength of 355 nm, the material is highly absorbing. At the probe wavelength of 532 nm, on the other hand, radiation is not substantially absorbed.

Referring to Fig. 2b, the raw LIPS data for the thin Pyralin® sample is shown as a plot of the intensity versus time, being the delay between the excitation beam pulse and the probe beam pulse. In Fig. 2c, the processed data is shown after compilation with the Fast Fourier Transform algorithm (FFT). The analysis time for this measurement was about 10 minutes using about 150,000 excitation and probe pulses. The data may be analyzed to yield material properties as described above.

#### Example 2

##### Long Probe Pulse

Referring now to Fig. 3, in an alternative mode, a probe laser 70 is adapted to provide a probe beam having a relatively long pulse width such that a substantial time-portion of the transient grating can be measured from each excitation pulse. The probe pulse is typically of longer duration than the excitation probe pulse and may be as long or longer than the detectable diffraction signal from the sample surface. In this example, like numbers refer to the same elements as described in Example 1, Fig. 2. The probe laser 70 may be a YAG laser operated in the Q-switch mode with energy of about 3 millijoules in a pulse width of about 300 nanoseconds. (The peak power, therefore, was on the order of 10,000 watts. Lower power operation, e.g., down to around 1000 watts is believed to be highly practical. Power requirements may be dependent on signal strength which may vary with the sample.) In this case, the probe laser

SUBSTITUTE SHEET

- 18 -

beam 76 impinges upon the sample surface simultaneously with the excitation beams and the full time dependent response from each excitation pulse is recorded. (If signal persists after 300 ns, the probe pulse can be 5 delayed as discussed in Example 1.) The detector 72 is a fast response (370 psec) amplified photodiode (model ARX-SA, Antel Optronics, Inc., 3325B Mainway, Burlington, Ontario, CANADA). The signal is received by a transient digitizer 74 with a 1 GHz bandwidth (digital signal 10 analyzer model 602, Tektronix, Inc., P.O. Box 500, Beaverton, OR 97077). The 1 GHz bandwidth and fast photodetector provide about 1 nsec time resolution, so that acoustic waves of up to 1 GHz frequency can be time resolved. The detector and electronics are generally 15 selected to be as fast as the sample response of interest. A polarizer (thin film) is preferably positioned between lens 54 and the sample.

Referring to Fig. 3a a plot of raw data the transient signal from a single excitation pulse is shown. 20 An advantage of operation in this mode is that, rather than probe a single time point of the transient morphology as in the embodiment of Fig. 2, the diffraction signal from the full duration of the transient morphology produced by each excitation pulse is 25 detected. The time required for signal detection is therefore considerably reduced. Fig. 3a also illustrates the probe pulse profile (which can be subtracted from the raw data prior to processing). In Fig. 3b, the processed data (without subtraction of the probe pulse profile) is 30 shown. This data was collected in about 15 seconds, using about 500 excitation shots, the signals from which were collected and signal averaged. Pyralin films of various thicknesses have been studied, e.g. from about 0.92 to 5.81 micron (spin coated on a 330 micron thick

SUBSTITUTE SHEET

- 19 -

silicon wafer with thickness determined within  $\pm 0.05$  micron by mechanical stylus profilometer).

Referring particularly to Fig. 3a, the oscillations in the data are due to acoustic oscillations initiated by the crossed excitation pulses. The signal intensity depends on the induced time-dependent material displacements (which are described in more detail in the sections that follow), weighted by the probe pulse intensity envelop which is shown in Fig. 3b. In Fig. 3a, the first part (-85 ns) of the probe pulse arrive at the sample before the excitation pulse, so there is no signal other than that due to parasitically scattered probe light. The excitation pulses heat the sample and initiate acoustic oscillations which are observed in the data. There is also a nonoscillatory component of the signal due to steady-state thermal expansion in the heated regions of the sample. This component finally decays as thermal diffusion washes away the spatially periodic variation in sample temperature. Thermal decay is not observed in these experiments because at these wavevectors, the timescale for thermal diffusion is much longer than the length of the Q-switched probe pulse. Instead, the signal in Fig. 3a disappears as the probe pulse ends. (As discussed below, with a larger temporal probe pulse, such as a CW probe pulse, longer sample excitation signals may be detected.)

From the data in Fig. 3a, the frequency of the surface acoustic wave can be extracted. In the Fourier transform of the data shown in Fig. 3c, the acoustic response is dominated by one mode with a frequency of 113  $\pm 2$  MHz. The dc component of the transform (not shown) is 30 times larger than the acoustic peak. In Fig. 3d the Fourier transform of diffracted signal is shown taken under identical conditions as the data in Fig. 3a, but with only one laser shot, i.e., no averaging. While this

SUBSTITUTE SHEET

- 20 -

spectrum is noisier than the spectrum of the averaged data, the position of the main peak is identical. (The extra noise seen in Fig. 3d is believed to be due to self-modelocking within the one Q-switched probe pulse.)

- 5 The data clearly illustrates the ability to perform true one-laser shot experiments. Best results can be obtained with a smooth probe pulse temporal profile.

In Figs. 4 and 4a, ISTS raw data and its Fourier transform, are shown respectively for the same sample at 10 a larger scattering wavevector. It can clearly be seen that there are at least two surface acoustic modes which contribute to the signal.

To insure that the signal was due to the polyimide film, control experiments were performed on uncoated 15 silicon wafers. No signal from the silicon surface could be detected.

Further, it is possible to distinguish between scattering due to modulation of the dielectric constant through elasto-optic coupling and diffraction due to 20 surface and interface ripple through analysis of the polarization properties of the diffracted light and the acoustic wavevector dependence of the diffracted signal intensity. Pseudo-Rayleigh waves have both transverse and longitudinal character, and therefore give rise to 25 modulation of both diagonal and off-diagonal elements of the dielectric tensor of a thin film through elasto-optic coupling. If elasto-optic coupling is a significant source of diffraction, then a component of the diffracted probe beam should be polarized at an angle 90° relative 30 to the incident probe beam (depolarized or VH scattering). The magnitude of this component relative to the non-depolarized diffracted component depends on the square of the ratio of off-diagonal to the diagonal elasto-optic coupling coefficients. By contrast, for a

#### SUBSTITUTE SHEET

- 21 -

coplanar scattering geometry surface ripple does not rotate the polarization of the diffracted light.

In addition, if elasto-optic coupling were the dominant diffraction mechanism, the signal intensity 5 would be independent of scattering wavevector  $q$  since the acoustic strain induced through bulk ISTS excitation is  $q$ -independent. By contrast, surface ripple arises from components of the acoustic displacement rather than strain and should thus vary as  $q^{-1}$ . Signal from surface 10 ripple depends on the square of the displacement, and as detailed below the signal intensity due to surface ripple decreases approximately as  $q^{-2}$ .

In experiments performed above, no depolarized component of the diffracted signal was detected. It was 15 also observed that the diffracted signal intensity decreases sharply as the  $q$  is increased. This indicates that the diffracted signals are due predominantly to surface and interface ripple induced by the pseudo-Rayleigh waves.

20

### Example 3

#### CW Probe

A further embodiment employs a continuous wave probe pulse from, e.g., a CW argon laser generating a CW beam of known duration in place of the YAG laser in 25 Example 2. The probe laser wavelength may be in the visible, 514 nm, and probe pulse width controlled by an EO modulator (in place of the doubling crystal shown in Fig. 3). (No electronic delay is necessary for the CW experiments.) This embodiment, similar to that of 30 Example 2, allows the transient response from each excitation shot to be completely detected. In this method the probe beam has a time-independent profile, thus enabling reduction in noise contribution when subtracting the probe beam profile from the detected 35 signal.

**SUBSTITUTE SHEET**

- 22 -

Referring to Figs. 5 and 5a, raw data from an unsupported polyimide film using a YAG laser excitation source at  $\lambda=266$  nm, 100 psec (a quadrupling crystal is used in place of tripling crystal 28) and a gated (500 5  $\mu$ sec) small frame argon ion CW probe (about 50 - 100 micron beam size, with single line power of about 1 watt) is illustrated for 200 signal averaged excitation shots and a single excitation shot, respectively. Despite the relatively low intensity, about 50 to 100 times lower 10 than the Q-switched probe used in the experiments above, good data was obtained. Care should be taken to efficiently gate the beam to avoid overexposure which can lead to damage of the sample. In these experiments, a Q-polarizer was placed before the EO gate.

15 An advantage of the gated CW probe is that thermal processes which occur on timescales larger than acoustic processes can be efficiently monitored. Likewise, the long temporal widths available with the CW probe allows the entirety of the sample acoustic profile to be 20 detected. In addition, by including frequency dependent loss modulus, the experiments can account for acoustic dampings. Referring to Fig. 6, a thermal decay curve of the polyimide sample over a microsecond time scale is shown. Similar data can be obtained from a single 25 excitation shot.

#### Theoretical Treatment and Parameter Optimization

A discussion of the features of the data obtained and a theoretical analysis that leads to optimization of the experiment for detecting signal predominately from 30 the induced surface ripple, follows.

In ISTS, two ultrashort laser excitation pulses are crossed temporally and spatially at the sample. An optical interference pattern characterized by scattering wavevector  $q$  is formed, where  $q$  is the difference between

**SUBSTITUTE SHEET**

- 23 -

the wavevectors of the crossed pulses. The scattering wavevector magnitude  $q$  associated with each excitation angle  $\theta_x$  can be calculated according to:

$$q = \frac{4\pi \sin\left(\frac{\theta_x}{2}\right)}{\lambda} \quad (1)$$

5 where  $\lambda$  is the wavelength of the excitation light. Experimentally, referring particularly to the data obtained in the experiments performed as discussed with respect to Fig. 3 et seq., data can be recorded as a function of the excitation angle  $\theta$  for all the Pyralin/Si  
10 sample thicknesses. The angles used in this study are  $0.48^\circ$ ,  $0.68^\circ$ ,  $0.72^\circ$ ,  $0.92^\circ$ ,  $1.07^\circ$ ,  $1.17^\circ$ ,  $1.62^\circ$ ,  $1.67^\circ$ ,  $1.77^\circ$ ,  $1.93^\circ$ ,  $2.37^\circ$ ,  $3.40^\circ$ ,  $3.92^\circ$ , and  $5.85^\circ$ . (These angles may be measured mechanically using a calibrated rotation stage and are accurate to  $\pm 0.05^\circ$ .) The  
15 corresponding scattering wavevectors according to (a) are  $0.15$ ,  $0.21$ ,  $0.22$ ,  $0.28$ ,  $0.33$ ,  $0.36$ ,  $0.50$ ,  $0.52$ ,  $0.55$ ,  $0.60$ ,  $0.73$ ,  $1.05$ ,  $1.21$ , and  $1.81$  inverse microns. These are accurate to  $\pm 0.01$  inverse microns. The wavevectors were chose to lie along a crystal axis of the silicon  
20 substrate. However, experiments performed with a wavevector magnitude of  $0.52\mu\text{m}^{-1}$  on a  $5.81\mu\text{m}$  Pyralin film sample showed no dependence on wavevector direction.

### I. Surface Ripple Amplitude

An order of magnitude estimate can be made for the  
25 surface ripple generated in an ISTS experiment by calculating the magnitude of the temperature grating set up by the excitation laser pulses and then relating this to a displacement amplitude using the linear thermal expansion coefficient. The temperature change  $\Delta T$  for  
30 light impinging on the surface (in the  $y=-h$  plane) in the

SUBSTITUTE SHEET

- 24 -

y direction and setting up a grating of wavevector  $\mathbf{q}$  in the z direction can be written as in eqs (2-3).

$$\Delta T(y, z) = A e^{-\zeta y} [1 + e^{iqz}] \quad (2)$$

$$A = \frac{1}{\rho C} P_a (1 - R) I_E \zeta e^{-\zeta h} \quad (3)$$

5 Here,  $2.303\zeta$  is the material absorption coefficient,  $I_E$  is the total energy per unit area of the excitation laser pulses,  $\rho$  is the mass density,  $C$  is the heat capacity per unit mass,  $R$  is the reflectivity for the material/air interface and  $P_a$  is the fraction of absorbed light that  
 10 is converted to heat. An upper limit for the average value of the temperature increase over the thickness of the film can be estimated with (2) by setting  $P_a = 1$  and  $R=0$ . For these experiments,  $I_E=1.6 \text{ mJ/cm}^2$  and  $\zeta=1.3\mu\text{m}^{-1}$ . Using values of  $\rho = 1\text{g/cm}^3$  and  $C = 2.3\text{J/(g.K)}$  which are  
 15 typical for polymers leads to an average temperature increase of approximately 8 K for a  $4\mu\text{m}$  thick film.

This temperature change can be related to the change in the y-direction length of a volume element  $\delta L_y(y, z)$  using the linear thermal expansion coefficient  $\alpha_T$   
 20 as in eq. (4).

$$\delta L_y(y, z) = \alpha_T \Delta T(y, z) dy \quad (4)$$

For the general case, the total surface ripple  $R_{rip}(z)$  can be found by integrating this expression over the sample thickness. For a thin film of thickness  $h$  attached to a  
 25 nonabsorbing substrate as in these experiments the integration extends only over the thickness of the film. Performing this integration leads to eq. (5).

- 25 -

$$R_{rip}(z) = \frac{1}{\rho C} P_a (1-R) I_E (1-e^{-\zeta h}) \alpha_T [1 + e^{iqz}] \quad (5)$$

Using a typical polymeric value of  $\alpha_T = 80 \times 10^{-6}$  m/(m.K)<sup>16</sup> for the linear thermal expansion coefficient yields an upper-limit estimate of 0.005 microns for the surface 5 corrugation amplitude excited by ISTS. This estimation assumes that neighboring volume elements slide by one another, and does not consider the effects of stress that will tend to reduce the corrugation. For this reason, expression (5) does not show the expected 1/q dependence.

## 10 II. Theory

In order to extract the elastic constants of the thin film from the pseudo-Rayleigh mode frequencies measured at different scattering wavevector magnitudes q, the dispersion of  $\omega(q)$  for the various modes is to be 15 understood. In fact, the frequency depends only on the product qh, where h is the film thickness, so that the results of measurements on films of different thickness can be compared. As mentioned earlier, the ISTS excitation efficiencies and the probe diffraction 20 efficiencies for each of the modes are to be determined. The ISTS signal expected from a supported film is derived below treating the excitation then the probing process. An isotropic theory is used since no effects of the elastic anisotropy of silicon or the film were observed.

### 25 A. ISTS Excitation of the System

Starting with the equations of thermoelasticity for an isotropic, elastic, and homogeneous medium:

$$c_{44} \nabla^2 u + (c_{11} - c_{44}) \nabla(\nabla \cdot u) = \gamma \nabla T + \rho \frac{\partial^2 u}{\partial t^2} \quad (6)$$

- 26 -

$$\kappa \nabla^2 T - C_s \rho \frac{\partial T}{\partial t} - \eta \kappa \nabla \cdot \frac{\partial u}{\partial t} = -Q \quad (7)$$

In these expressions  $u$  is a vector describing the material displacements,  $T$  is the fluctuation in temperature relative to the equilibrium temperature,  $\rho$  is the equilibrium density, and  $c_{44}$  and  $c_{11}$  are the elastic constants which are related to the bulk longitudinal and transverse acoustic velocities according to  $v_L = (c_{11}/\rho)^{1/2}$  and  $v_T = (c_{44}/\rho)^{1/2}$ .  $\gamma$  is a constant related to the elastic constants and the coefficient of linear volume expansion  $\alpha_T$  by  $\gamma = (3c_{11} - 4c_{44})\alpha_T$ .  $\kappa$  is the thermal conductivity,  $\eta = \gamma T_0 / \kappa$  and  $C_s$  is the constant strain specific heat per unit mass. Finally,  $Q$  represents the absorbed heat per unit time per unit volume derived from the excitation laser pulses.

If  $u$  is expressed in terms of longitudinal ( $\phi$ ) and transverse ( $\psi$ ) potentials,

$$u = \nabla \phi + \nabla \times \psi \quad \nabla \cdot \psi = 0 \quad (8)$$

then equations (6) and (7) can be rewritten as follows.

$$\kappa \nabla^2 T - C_s \rho \frac{\partial T}{\partial t} = -Q \quad (9)$$

$$20 \quad \nabla^2 \phi - \frac{1}{c_{11}} \frac{\partial^2 \phi}{\partial t^2} = \frac{\gamma}{\rho c_{11}} T \quad (10)$$

$$\nabla^2 \psi - \frac{1}{c_{44}} \frac{\partial^2 \psi}{\partial t^2} = 0 \quad (11)$$

SUBSTITUTE SHEET

- 27 -

It is assumed that longitudinal compressions do not cause substantial changes in temperature ( $\eta \sim 0$  in eq. (7)).

Note that for a bulk system, the last two equations describe uncoupled longitudinal and transverse acoustic modes respectively. Since the laser heating enters through eq. (9) which is only directly coupled to eq. (10), ISTS only excites longitudinal acoustic modes in bulk isotropic systems. However, this simple picture breaks down for a thin film, since boundary conditions must be satisfied. In particular, for a thin film in intimate contact with a substrate, the material displacements and the normal components of the stress must be continuous across the interface and the normal components of the stress at any free surface must vanish.

These boundary conditions lead to coupling between the longitudinal and transverse potentials so that every surface acoustic mode has both longitudinal and transverse character.

The film/substrate system geometry is depicted in Fig. 7. The substrate fills the region from  $y=0$  to  $y=+H$  and the film fills the region from  $y=0$  to  $y=-h$ . It is assumed that the ISTS excitation beams form an infinite uniform grating pattern with wavevector  $q$  in the  $z$  direction which is independent of  $x$  and damped along  $y$  due to optical absorption. In this analysis,  $H$  is considered infinite so that the substrate fills the whole  $y>0$  half space. (The corrections that occur when the finite size of the substrate is explicitly accounted for is discussed below.)

The first step in solving equations (9)-(11) is to determine the temperature distribution set up by the excitation pulses. The dynamics of thermal diffusion take place on a much longer timescale than the acoustic dynamics. Thus, for analyzing the excitation of the film-substrate system,  $\kappa$  can be set to zero in eq. (9).

#### SUBSTITUTE SHEET

- 28 -

In ISTS, the excitation laser pulse duration is short compared to the acoustic oscillation period. Here it is assumed that conversion of optical energy to heat through molecular electronic and vibrational relaxation also occurs on a fast time scale relative to the acoustic oscillation period so that the time dependence of  $Q$  in eq. (9) can be approximated by a delta-function at zero time. More gradual thermalization will reduce all the acoustic amplitudes but should not affect the relative amplitudes of the different modes substantially.

Equation (9) is solved for the temperature distribution set up by the laser excitation beams to yield eq. (12).

$$T(y, z, t) = A e^{-\zeta(y+h)} [1 + e^{iqz}] \theta(t) \quad (12)$$

Here,  $\theta(t)$  is the Heaviside step function which turns on at  $t=0$ , and  $A$  and  $\zeta$  were introduced in eqs (2-3). since the film absorbs strongly and the silicon substrate reflects the 355nm excitation light used in these experiments,  $T(y, z, t)$  is only nonzero in the film (for  $-h < y < 0$ ).

With this functional form for the temperature distribution, equations (10) and (11) can be solved using transform techniques. Since the temperature distribution is independent of  $x$ , all derivatives with respect to  $x$  are neglected. From the geometry of the system and the nature of the temperature distribution given in (12), a Laplace transform for the time variable and exponential Fourier transform for the  $z$  coordinate are the natural choices. (Notation is such that  $S$  is the Laplace variable conjugate to  $t$  and  $k$  is the Fourier variable conjugate to  $z$ .) The transformed solutions for the potentials  $\phi$  and  $\Psi$  are then found to be,

SUBSTITUTE SHEET

- 29 -

$$\phi(k, y, s) = \begin{cases} A_\phi(k, s) \exp\left(y\sqrt{k^2 + \frac{s^2}{v_{Lf}^2}}\right) + B_\phi(k, s) \exp\left(-y\sqrt{k^2 + \frac{s^2}{v_{Lf}^2}}\right) \\ + \frac{A\gamma}{ps} e^{-\zeta y} \left[ \frac{\delta(k)}{-s^2 + \zeta^2 v_{Lf}^2} + \frac{\delta(k-q)}{-k^2 v_{Lf}^2 + \zeta^2 v_{Lf}^2 - s^2} \right] & -h < y < 0 \\ C_\phi(k, s) \exp\left(y\sqrt{k^2 + \frac{s^2}{v_{Ls}^2}}\right) + D_\phi(k, s) \exp\left(-y\sqrt{k^2 + \frac{s^2}{v_{Ls}^2}}\right) & H > y > 0 \end{cases} \quad (13)$$

$$\psi(k, y, s) = \begin{cases} A_\psi(k, s) \hat{x} \exp\left(y\sqrt{k^2 + \frac{s^2}{v_{Tf}^2}}\right) + B_\psi(k, s) \hat{x} \exp\left(-y\sqrt{k^2 + \frac{s^2}{v_{Tf}^2}}\right) \\ + C_\psi(k, s) \hat{x} \exp\left(y\sqrt{k^2 + \frac{s^2}{v_{Ts}^2}}\right) + D_\psi(k, s) \hat{x} \exp\left(-y\sqrt{k^2 + \frac{s^2}{v_{Ts}^2}}\right) & -h < y < 0 \\ & H > y > 0 \end{cases}$$

(14)

where  $k$  is the Fourier transform variable conjugate to  $z$  and  $s$  is the Laplace variable conjugate to time. In  
5 these expressions,  $v_{Lf}$ ,  $v_{Tf}$ ,  $v_{Ls}$ , and  $v_{Ts}$  are the bulk longitudinal and transverse velocities in the film and substrate respectively. In taking the Laplace transform, the initial conditions that there is no displacement or motion at  $t=0$  when the laser pulses first arrive at the

**SUBSTITUTE SHEET**

- 30 -

sample have been used. Note that choosing the only nonzero component of  $\Psi$  to lie along the  $x$  axis allows for trivial satisfaction of the gauge  $\nabla \cdot \Psi = 0$  used here.

Finally, all but the third term in the expression for the longitudinal potential in the film are homogeneous solutions to the equations of motion. This third term is the particular solution of equation (10) and can be thought of as driving the motion of the film and giving rise to a response consisting of a longitudinal disturbance propagating along  $z$ , a periodic stress pulse propagating along  $y$ , and a dc response.

The variables  $A_\phi(k,s)$ ,  $B_\phi(k,s)$ ,  $D_\phi(k,s)$  etc. are potential constants which are determined by imposing the necessary boundary conditions and physical realizability requirements. For the system of Fig. 7 with  $H$  infinite, the terms involving  $C_\phi(k,s)$  and  $C^*(k,s)$  represent physically unreasonable solutions. For this reason, they are set to zero. The other six constants are determined with the boundary conditions. As stated earlier, these are that  $u$  and the normal components of the stress are continuous at  $y=0$  and that the normal components of the stress vanish for  $y=-h$ . The stress tensor is calculated using the Duhamel-Neumann relation shown in eq. (15) in order to properly take into account the contribution from the temperature grating.

$$\sigma_{ij} = c_{44} \left( \frac{\partial u_i}{\partial x_j} + \frac{\partial u_j}{\partial x_i} \right) + [(c_{11} - 2c_{44}) \nabla \cdot u - \gamma T] \delta_{ij} \quad (15)$$

Using equations (8), (15) and (12)-(14), the boundary conditions can be imposed. The six relations thus derived are most conveniently expressed in matrix form,

#### SUBSTITUTE SHEET

- 31 -

$$\underline{C} \underline{D} = \underline{F}$$

(16)

$$\underline{C} = \begin{pmatrix} (1+p^2)e^{-nkh} & (1+p^2)e^{nkh} & 2ip e^{-pkh} & -2ip e^{pkh} & 0 & 0 \\ 2ine^{-nkh} & -2ine^{nkh} & -(1+p^2)e^{-pkh} & -(1+p^2)e^{pkh} & 0 & 0 \\ 1+p^2 & 1+p^2 & 2ip & -2ip & -(1+r^2)g & 2irg \\ 2in & -2in & -(1+p^2) & -(1+p^2) & 2img & (1+r^2)g \\ -1 & -1 & -ip & ip & 1 & -ir \\ in & -in & -1 & -1 & im & 1 \end{pmatrix} \quad (17)$$

$$\underline{D} = \begin{pmatrix} A_\phi \\ B_\phi \\ A_\psi \\ B_\psi \\ D_\phi \\ D_\psi \end{pmatrix}$$

(18)

SUBSTITUTE SHEET

- 32 -

$$\begin{aligned}
 & \left. \left( \frac{-(\delta(k) + \delta(k-q))}{k^2} + \frac{v_{L'}^2}{k^2} \left( \frac{-(v_{L'}^2 - 2v_{T'}^2)}{v_{L'}^2} + \frac{\zeta^2}{k^2} \right) \left( \frac{\delta(k)}{v^2 + \frac{v_{L'}^2 \zeta^2}{k^2}} + \frac{\delta(k-q)}{v^2 + v_{L'}^2 \left( \frac{\zeta^2 - k^2}{k^2} \right)} \right) \right. \right. \\
 & \quad \left. \left. \frac{2\zeta v_{T'}^2}{ik^3} \left( \frac{\delta(k)}{v^2 + \frac{v_{L'}^2 \zeta^2}{k^2}} + \frac{\delta(k-q)}{v^2 + v_{L'}^2 \left( \frac{\zeta^2 - k^2}{k^2} \right)} \right) \right) \right. \\
 & \quad \left. \left. \frac{-e^{-\zeta d} (\delta(k) + \delta(k-q))}{k^2} + \frac{e^{-\zeta d} v_{L'}^2}{k^2} \left( \frac{-(v_{L'}^2 - 2v_{T'}^2)}{v_{L'}^2} + \frac{\zeta^2}{k^2} \right) \left( \frac{\delta(k)}{v^2 + \frac{v_{L'}^2 \zeta^2}{k^2}} + \frac{\delta(k-q)}{v^2 + v_{L'}^2 \left( \frac{\zeta^2 - k^2}{k^2} \right)} \right) \right) \right. \\
 F = \frac{iA\gamma}{v_{T'}^2 \rho k v} & \left. \left. \frac{2e^{-\zeta d} \zeta v_{T'}^2}{ik^3} \left( \frac{\delta(k)}{v^2 + \frac{v_{L'}^2 \zeta^2}{k^2}} + \frac{\delta(k-q)}{v^2 + v_{L'}^2 \left( \frac{\zeta^2 - k^2}{k^2} \right)} \right) \right. \right. \\
 & \quad \left. \left. \frac{-e^{-\zeta d} v_{T'}^2}{k^2} \left( \frac{\delta(k)}{v^2 + \frac{v_{L'}^2 \zeta^2}{k^2}} + \frac{\delta(k-q)}{v^2 + v_{L'}^2 \left( \frac{\zeta^2 - k^2}{k^2} \right)} \right) \right. \right. \\
 & \quad \left. \left. \frac{e^{-\zeta d} \zeta v_{T'}^2}{k^3} \left( \frac{\delta(k)}{v^2 + \frac{v_{L'}^2 \zeta^2}{k^2}} + \frac{\delta(k-q)}{v^2 + v_{L'}^2 \left( \frac{\zeta^2 - k^2}{k^2} \right)} \right) \right) \right) \quad (19)
 \end{aligned}$$

(20)

$$n = \sqrt{1 - \frac{v^2}{v_{L'}^2}}$$

SUBSTITUTE SHEET

- 33 -

$$p = \sqrt{1 - \frac{v^2}{v_{Tf}^2}} \quad (21)$$

$$m = \sqrt{1 - \frac{v^2}{v_{Ts}^2}} \quad (22)$$

$$r = \sqrt{1 - \frac{v^2}{v_{Ls}^2}} \quad (23)$$

$$g = \frac{\rho_s v_{Ts}^2}{\rho_f v_{Tf}^2} \quad (24)$$

5 and  $\rho_f$  and  $\rho_s$  are the densities in the film and substrate respectively. The first two rows of the matrix equation ensure that the yy and the yz components of the stress respectively are zero at the surface of the film. The next two rows require continuity of the yy and yz  
 10 components of the stress respectively at the interface. Finally, the last two rows require that the z and y components of the material velocities respectively are continuous at the interface. For notational convenience, the k and s dependence of the potential constants has  
 15 been dropped. Also, the Laplace variable s has been written as  $s^2 = -\omega^2 = -v^2 K^2$  where w is the real frequency and v is the velocity of the acoustic mode solutions. This transformation limits the possible solutions to strictly

#### SUBSTITUTE SHEET

- 34 -

pseudo-Rayleigh modes with velocities below the transverse velocity of the substrate. A continuum of "leaky mode" solutions with complex frequency are also possible for velocities greater than  $v_{Ts}$ . These solutions  
5 are damped as energy is "lost" to the semi-infinite substrate. Normal mode solutions of eq. (16) occur when

$$\det(\underline{C})=0 \quad (25)$$

Aside from  $kh$  and  $v$ , the matrix  $C$  only contains constants related to the film and the substrate. All of the laser  
10 and optical properties appear in the column matrix  $F$ . Thus, eq. (25) can be solved to yield the dispersion relations ( $qh$  vs.  $v$  where  $q$  is the acoustic wavevector) for the various pseudo-Rayleigh modes irrespective of the ISTS excitation source.

15 An example of typical dispersion curves for the substrate loading case (ie.  $v_{Ts} > v_{Tf}$ ) is shown for the lowest 16 modes in Fig. 8. As  $qh$  approaches zero only one mode, whose velocity approaches only one mode whose velocity approaches that of the substrate pure Rayleigh mode  $v_{Rs}$ , exists. At large  $qh$ , this lowest mode approaches the pure Rayleigh surface mode of the film with velocity  $v_{Rf}$ . Each of the higher velocity modes, often called Sezawa modes, has a limiting  $qh$  value below it does not propagate. At this  $qh$  value, the velocity of  
20 each mode is equal to the substrate transverse velocity  $v_{Ts}$ . As shown in Fig. 8, as  $qh$  is increased, these modes all asymptotically approach the film transverse velocity.  
25

In order to solve for the displacements of a particular mode  $j$  excited through ISTS, one must solve  
30 the full eq. (16) for the potential constants at the  $qh$  value and velocity of interest. It can be shown using

SUBSTITUTE SHEET

- 35 -

eqs. (8) and (13-14) that the normal mode displacements  $u^j$  with wavevector  $q$  obey the following equation

$$u^j(q, y, z, t) = [u_y^j(q, y)\hat{y} + u_z^j(q, y)\hat{z}]e^{iqz}e^{iv_j qt} \quad (26)$$

where

$$u_y^j(q, y) = \begin{cases} qn_j [\bar{A}_\phi^j e^{yqn_j} - \bar{B}_\phi^j e^{-yqn_j}] + iq [\bar{A}_\psi^j e^{yqp_j} + \bar{B}_\psi^j e^{-yqp_j}] & -h < y < 0 \\ -qm_j \bar{D}_\phi^j e^{-yqm_j} + iq \bar{D}_\psi^j e^{-yq\varphi_j} & y > 0 \end{cases} \quad (27)$$

SUBSTITUTE SHEET

- 36 -

$$u_z^j(q,y) = \begin{cases} iq\left[\tilde{A}_\phi^j e^{yqn_j} + \tilde{B}_\phi^j e^{-yqn_j}\right] + qp_j\left[-\tilde{A}_\psi^j e^{yqp_j} + \tilde{B}_\psi^j e^{-yqp_j}\right] & -h < y < 0 \\ iq\tilde{D}_\phi^j e^{-yqm_j} + qr_j\tilde{D}_\psi^j e^{-yqr_j} & y > 0 \end{cases} \quad (28)$$

In these expressions, the tildes denote the residue of the quantity evaluated at the appropriate pole. Note that the material displacements oscillate with frequency 5  $\omega_j = v_j q$ . Examples of the pseudo-Rayleigh displacements for various modes at one  $qh$  value are showing in Fig. 8. The total displacements at a particular wavevector and sample thickness will be the sum of the  $u_j$  values for each pseudo-Rayleigh mode plus a nonoscillatory term due to 10 steady-state thermal expansion.

#### B. Probe Diffraction

In this section, an analysis is presented of diffraction appropriate for the ISTS experiments described here in which ripple effects were found to 15 dominate. The equations below are the reflected and transmitted first order diffracted components of light from a corrugated half space, modified to deal with the case of arbitrary indices of refraction on either side of the corrugated interface, and to the case of standing 20 wave corrugation. In addition, index modulation

- 37 -

contributions to the phase are neglected. The results are,

$$E_z = \pm \hat{a} \sqrt{I_0} e^{i\alpha z} e^{-in_1 k_i R_0} J_1(\alpha_1) \left( \frac{(1+r(\theta_i)) \cos \theta_d - (1-r(\theta_i)) \cos \theta_i}{2 \cos \theta_i} \mp \frac{q(1+r(\theta_i)) (\sin \theta_d + \sin \theta_i)}{2n_1 k_i \cos \theta_i (\cos \theta_d + \cos \theta_i)} \right) \quad (29a)$$

$$\alpha_1 = \delta(t) n_1 k_i (\cos \theta_d + \cos \theta_i) \quad (29b)$$

20

$$\sin \theta_{d \pm 1} = \sin \theta_i \pm \frac{q}{n_1 k_i} \quad (29c)$$

$$E_z = \mp \hat{a} \sqrt{I_0} e^{i\alpha z} e^{-in_2 k_i R_0 / n_1} J_1(\alpha'_1) \left( \frac{(1+r(\theta_i)) \frac{n_2}{n_1} \cos \theta_i + (1-r(\theta_i)) \cos \theta_i}{2 \cos \theta_i} \mp \frac{q(1+r(\theta_i)) \left( \frac{n_2}{n_1} \sin \theta_i + \sin \theta_i \right)}{2n_1 k_i \cos \theta_i \left( \frac{n_2}{n_1} \cos \theta_i - \cos \theta_i \right)} \right) \quad (30a)$$

- 38 -

$$\alpha'_1 = \delta(t) n_1 k_i \left( \frac{n_2}{n_1} \cos \theta_i - \cos \theta'_i \right) \quad (30b)$$

$$\sin \theta_{i\pm 1} = \frac{n_1}{n_2} \sin \theta_i \pm \frac{q}{n_2 k_i} \quad (30c)$$

In these equations,  $I_o$  is the intensity of the probe measured in medium 1, and  $k_i$  is the wavevector of the probe measured in vacuum.  $\theta_i$  is the angle of the probe relative to the corrugated interface,  $a$  is the unit vector representing the polarization of the probe,  $r$  is the reflection coefficient for transmission from medium 1 to medium 2, and  $R_o$  is the distance from the point at which the diffraction is generated to the detector.

Also,  $q$  is the wavevector of the corrugation, and  $\delta(t)$  is the time dependent amplitude of the corrugation.

Finally, the upper signs refer to the +1 diffracted order, while the lower signs refer to -1 diffracted order.

For a thin supported film, there are four sources of first order ripple diffraction which must be considered. These are shown schematically in Fig. 9. Parts A and B of this figure represent the probe and diffracted beam paths for the two final signal directions seen experimentally. The first three paths show the components involving diffraction from the film surface ripple. The fourth path describes the component arising from diffraction from the interface ripple. In general,

- 39 -

all four components contribute to the diffracted signal in the two signal directions.

The electric fields at the detector associated with these four diffraction contributions can be obtained 5 using eqs. (29-30), Snell's Law, and taking into account reflective losses at the film-air interface. In the following, it is assumed that all light striking the film-substrate interface is reflected. In addition, due to the spatial size of the probe pulse, the thickness of 10 the film, the index of refraction of the film, the wavevector of the corrugation, and the angle of incidence, it is a good approximation to assume that all of the diffracted beams give in Fig. 9a or 9b emerge from the same point on the film and travel parallel to one 15 another. The results, written in terms of sums over pseudo-Rayleigh mode amplitudes, are shown in the following equations.

$$E_1 = \mp \hat{a} \sqrt{I_0} K_1 e^{i\omega t} e^{-ik_i R_o} \sum_{j=0}^N u_j^j y(q, y = -h) \sin(v_j qt) \quad (31a)$$

$$K_1 = k_i (\cos \theta_d + \cos \theta_i) \left[ \frac{(1 + r(\theta_i)) \cos \theta_d - (1 - r(\theta_i)) \cos \theta_i}{4 \cos \theta_i} \pm \frac{q(1 + r(\theta_i)) (\sin \theta_d + \sin \theta_i)}{4 k_i \cos \theta_i (\cos \theta_d + \cos \theta_i)} \right] \quad (31b)$$

$$\sin \theta_{d \pm 1} = \sin \theta_i \pm \frac{q}{k_i} \quad (31c)$$

$$E_2 = \mp \hat{a}'(\theta_i) \sqrt{I_0} K_2 e^{i\omega t} e^{-ik_i R_o} e^{-ink_i h_2} \sum_{j=0}^N u_j^j y(q, y = -h) \sin(v_j qt) \quad (32a)$$

- 40 -

$$K_2 = k_i(n \cos \theta_i - \cos \theta_i) \left[ \frac{(1+r(\theta_i))n \cos \theta_i + (1-r(\theta_i))\cos \theta_i}{4 \cos \theta_i} \mp \frac{q(1+r(\theta_i))(n \sin \theta_i + \sin \theta_i)}{4k_i \cos \theta_i (n \cos \theta_i - \cos \theta_i)} \right] \quad (32b)$$

$$\sin \theta_{i\pm 1} = \frac{1}{n} \sin \theta_i \pm \frac{q}{nk_i} \quad (32c)$$

$$h_2 = \frac{2h}{\cos \theta_{i\pm 1}} \quad (32d)$$

$$E_3 = \mp \hat{a}_i(\theta_i) \sqrt{I_0} K_3 e^{i\omega t} e^{-ik_i R_0} e^{-ink_i h_3} \sum_{j=0}^N u_j^j (q, y = -h) \sin(v_j q t) \quad (33a)$$

$$K_3 = k_i(\cos \theta_i - n \cos \theta_{rfr}) \left[ \frac{(1+r'(\theta_{rfr}))\cos \theta'_i + n(1-r'(\theta_{rfr}))\cos \theta_{rfr}}{4 \cos \theta_{rfr}} \mp \frac{q(1+r'(\theta_{rfr}))(\sin \theta'_i + n \sin \theta_{rfr})}{4k_i \cos \theta_{rfr} (\cos \theta'_i - n \cos \theta_{rfr})} \right] \quad (33b)$$

$$\sin \theta'_{i\pm 1} = n \sin \theta_{rfr} \pm \frac{q}{k_i} \quad (33c)$$

$$h_3 = \frac{2h}{\cos \theta_{rfr}} \quad (33d)$$

(33d)

## SUBSTITUTE SHEET

- 41 -

$$\theta_{rfr} = \sin^{-1} \left( \frac{1}{n} \sin \theta_i \right) \quad (33e)$$

$$E_4 = \mp \hat{t}(\theta_i) t'(\theta'_d) \sqrt{I_0} K_4 e^{i\omega t} e^{-ik_i R_o} e^{-ink_i h_4} \sum_{j=0}^N u_j y(q, y=0) \sin(v_j q t) \quad (34a)$$

$$K_4 = nk_i (\cos \theta'_d + \cos \theta_{rfr}) \left[ \frac{n \cos \theta'_d}{2 \cos \theta_{rfr}} \pm \frac{q (\sin \theta'_d + \sin \theta_{rfr})}{2k_i \cos \theta_{rfr} (\cos \theta'_d + \cos \theta_{rfr})} \right] \quad (34b)$$

$$\sin \theta'_{d\pm 1} = \sin \theta_{rfr} \pm \frac{q}{nk_i} \quad (34c)$$

$$h_4 = \frac{h}{\cos \theta_{rfr}} + \frac{h}{\cos \theta'_{d\pm 1}} \quad (34d)$$

Here,  $j$  runs from 0 to  $N$  and represents the mode solutions for  $j > 0$  and the dc term for  $j=0$  (ie.  $v_0=0$ ). Also,  $t$  is the transmission coefficient for passage from the air into the film, and  $t'$  is the transmission coefficient for passage from the film into the air. Finally, in these expressions the small-argument expansion of the Bessel function ( $J_1(x) \sim x/2$  for  $x \ll 1$ )

- 42 -

has been used since the rippled amplitude (as estimated in section IV) times the grating wavevector magnitude is small compared to one for all excitation geometries investigated in this experiment.

5       The signal intensity can be written as the square of the sum of the four electric fields given in eqs. (31-34). The resulting intensity will exhibit varying interference effects depending on the probing angle and wavelength, the index of refraction and thickness of the  
10 film, and the grating excitation wavevector. For the purpose of analyzing the relative intensities of the various pseudo-Rayleigh modes in an ISTS experiment, the only important interference occurs between the E-fields derived from the surface ripple ( $E_1-E_3$ ) and the field  
15 derived from the interface ripple ( $E_4$ ). Such interference can cause a mode with a large surface corrugation amplitude to only appear as a weak Fourier component in the experimentally measured diffraction signal and vice-versa. The final ISTS intensity ( $I$ ) can  
20 be written in a manner which emphasizes this effect as

$$I = I_0 \left[ \sum_j \left[ (F(n, h, k_i, q, \theta_i) u_j^j(q, y = -h) + G(n, h, k_i, q, \theta_i) u_j^j(q, y = 0)) \sin(v_j q t) \right] \times c.c. \right] \quad (35)$$

where  $F$  and  $G$  are functions determined by summing terms in equations (31-34). This expression was obtained by averaging over an optical cycle with the assumption that  
25 acoustic terms are constant over this interval. It can be seen that, in general, the measured signal consists of a dc term, a series of heterodyned components oscillating at the pseudo-Rayleigh mode frequencies which arise from a beating against the dc term, and terms oscillating at sums and differences of the normal mode frequencies.  
30

SUBSTITUTE SHEET

- 43 -

C. Qualitative Considerations

The relative intensities of the various modes seen with ISTS depend on two factors - the extent to which the different modes are excited by the pump pulses and the efficiency with which the surface and interface mode displacements diffract the probe pulse. Both of these factors can be quantified at a particular  $q_h$  value by solving the full matrix eq. (16) for each mode. This was done using the elastic constants found for the Pyralin/silicon system as described below. Aside from an arbitrary laser-intensity dependent constant factor, the only additional input parameter needed to perform this computation was the Pyralin absorption coefficient  $\zeta$ . This was measured to be  $1.3\mu\text{m}^{-1}$  using a Pyralin film coated onto a fused silica substrate. Fig. 10 shows the results of the calculations at  $q_h=2.5$ . This figure shows material displacements for the first eight modes that exist at this value of  $q_h$ . The relative excitation efficiencies for the different modes are indicated by the relative amplitudes  $A$ . ( $A = 1$  for the mode with the largest displacements.) The surface ripple amplitude relative to the maximum amplitude for each mode is given by  $R$ . Modes with large values of the produce  $AR$  contribute most to ISTS signal. There are several guidelines that can be determined through a study of these and other figures that allow for an understanding of the level of excitation and the resulting diffraction efficiency of a particular mode. First, modes with fewer spatial modulations along the  $y$  direction are excited more strongly than those with many nodes along  $y$ . This is reasonable since the heating excitation mechanism will tend to displace material in only one direction for a give value of  $z$ . Next, lower velocity modes in general have larger peak displacements than high velocity modes. This is due to the fact that as the mode velocity is

SUBSTITUTE SHEET

- 44 -

increased and approaches the substrate transverse velocity, the mode displacements become spread out over both the film and far into the substrate. This leads to small peak displacement amplitudes compared to those of  
5 the low-velocity modes whose displacements are well localized in the film. Finally, it is evident that some modes involve much more surface and interface ripple than others. Since detection results predominantly from diffraction from surface and interface ripple, only modes  
10 with significant surface displacements along y are detected. With these guidelines, it is possible to qualitatively explain relative signal amplitudes from the various modes over a wide range of  $qh$ . For purposes of data analysis, the calculations provide a clear  
15 indication of which modes in a thin film are likely to be observed in ISTS data. In most of the data, only one or two frequency components are observed predominantly. Dispersion curves like those in Fig. 8 can be fit to the frequency values determined from the data, which the  
20 elastic moduli as adjustable parameters to be deduced from the best fit. To do this correctly it is essential to know which modes are under observation, i.e. which of the many dispersion curves should be fit to the experimentally determined frequency values. Another  
25 qualitative consideration that explains why ripple amplitude is small for modes with large velocities (which explains drop off for modes at a given  $qh$  and for all modes as  $qh$  is decreased to small values) is that modes are fast because they involve substantial motion in the  
30 substrate which is very stiff compared to the film (i.e. it is motion in the substrate that "speeds the mode  $1\phi$ "). Since the substrate is very stiff, equal energy deposition will result in smaller displacements for fast modes.

#### SUBSTITUTE SHEET

- 45 -

Fig. 10 illustrates bulk and surface ripple amplitudes for a single value of wavevector  $q$ , given the film thickness  $h$ . Fig. 11 is a three-dimensional plot showing the calculated film surface ripple (the product 5 AR) excited through ISTS as a function of  $qh$  and velocity for the various modes in 1  $\mu\text{m}$  film. Fig. 12 displays the analogous results for the interface ripple. The x-y plane of these figures shows the mode velocity dispersion as in Fig. 8, while the z axis shows the relative ripple 10 displacements for a given energy density of the ISTS excitation pulses. Note that since the displacements associated with each pseudo-Rayleigh mode are different, the relative ripple displacements for the film surface and the film - substrate interface are also different.

15 Both, however, exhibit the same general trend of decreasing ripple amplitude with increasing  $qh$ . For fixed  $h$  as in this simulation, this corresponds to decreasing mode displacement amplitude with increasing wavevector which, as discussed earlier, is expected for 20 ISTS excitation. In addition to this decrease in amplitude which is approximately like  $1/q$  for values of  $qh$  above 1, there is a distinct decrease in the magnitude of the surfaces ripple for small values of  $qh$ . This decrease is attributed to the fact that as  $q$  is decreased 25 to values near zero, even the lowest modes take on large velocities. Thus, as discussed above, these modes are not well localized and so have small peak displacements. For this reason, the ripple due to such modes is small.

In addition to the decrease in surface ripple at 30 both high and very low values of  $q$ , it is seen in Fig. 11 that there is a "cross-over" near  $qh=1.5$  where, upon increase in  $qh$ , the surface ripple due to mode two becomes small and that due to mode one becomes large. This occurs because the character of these two modes 35 switch in this region. This "crossover" is evident from

SUBSTITUTE SHEET

- 46 -

the dispersion curves of Fig. 14, in which there is an "avoided crossing" of the first two frequencies, and through a comparison of modes one and two at  $qh=2.5$  given in Fig. 10 and at  $qh=0.8$  given in Fig. 13. (The presence 5 of this cross over effect is a property of ripple phenomena.)

The relative contribution of each pseudo-Rayleigh mode to ISTS signal can be calculated using eq. (16) and the ripple information contained in Figs. (11-12). The 10 resulting mode intensity ratios can then be compared to the ratios found in the raw ISTS data for each value of  $qh$  and  $h$ . When the interface displacements are not negligibly small compared to the surface displacements, interference effects between these two contributions to 15 diffracted signal become important so that with different experimental conditions - such as probe angle of incidence or film thickness - ISTS data can show vastly different mode intensity ratios (cf. eq. 35).

Conversely, when one or the other set of displacements 20 dominates, interference effects can be ignored and the resulting mode intensity ratios become independent of the precise experimental conditions and mimic the behavior of the relevant ripple displacements. From Figs. (11-12) it is clear that the theoretical surface displacements are 25 over an order of magnitude larger than the interface displacements for the two lowest velocity modes with  $qh$  values above -0.5, while for the other modes and at lower  $qh$ , the surface and interface displacements are of the same order. Calculations performed at other film 30 thicknesses between 1 and 5  $\mu\text{m}$  show this same general behavior. Thus, for the samples examined in this study, one would expect the relative intensities of the two lowest modes to mirror the relative intensities shown in figure 9 for  $qh>0.5$ . (An analysis of the complete mode

SUBSTITUTE SHEET

- 47 -

intensity spectrum requires the full solution of eq.  
(35).)

D. Quantitative Analysis of ISTS Data

As stated earlier, the dc term dominates the ISTS  
5 signal for these experiments. In fact the power in the  
zero-frequency peak of the Fourier transforms ranged from  
30 to 200 times greater than the acoustic peaks. Thus,  
the heterodyne terms in equation (35) dominate and the  
frequencies of the most intense Fourier peaks will  
10 correspond to the fundamental pseudo-Rayleigh mode  
frequencies  $\omega_j$ .

The values of  $\omega_j$  found for all the scattering  
wavevectors and sample thicknesses in this study were  
converted to phase velocities and plotted versus  $qh$ . The  
15 results are showing in Fig. 14. In cases where multiple  
modes were excited, only those with Fourier transformed  
intensities greater than half that of the largest were  
plotted. In addition, to eliminate the possibility of  
spurious peaks due to sample imperfections, data points  
20 were taken at several spots on each sample and only  
frequencies that were consistent from spot to spot on the  
same were kept. The estimated experimental uncertainties  
for the velocities range from 1% at the highest  $qh$  values  
to 5% at the lowest  $qh$  values observed for each sample.  
25 The  $qh$  values are accurate to  $\pm 0.1$ . The main source of  
error results from uncertainties in the scattering  
wavevector which are derived from uncertainties in the  
mechanical measurement of the scattering angle. This  
error can be substantially reduced by deducing the  
30 scattering wavevector directly from ISTS data taken with  
a well characterized reference sample.

The solution for the pseudo-Rayleigh mode  
dispersion for this system requires the density and the  
longitudinal and transverse velocities for both the  
35 silicon and the Pyralin as inputs. For silicon,  $\rho_s = 2.33$

SUBSTITUTE SHEET

- 48 -

g/cm and the isotropic velocities are  $v_L = 8945 \text{ m/s}$ , and  $v_T = 5341 \text{ m/s}$ . For Pyralin, the values given by Dupont for the density and Young's modulus ( $Y$ ) are  $1.45 \text{ g/cm}^3$  and  $2.4 \text{ GPa}$  respectively.<sup>22</sup> To the inventor's knowledge,  
 5 there is no reported measurement of Poisson's ration ( $\nu$ ) for this film. All three of these values are necessary to obtain the longitudinal and transverse velocities for the film according to eqs. (36) and (37).

$$v_T^2 = \frac{Y}{2\rho(1+\nu)} \quad (36)$$

$$v_L^2 = \frac{Y}{\rho(1+\nu)} \left[ 1 + \frac{\nu}{1-2\nu} \right] \quad (37)$$

Different sets of dispersion curves were generated by solving eq. (25) using the silicon and Pyralin parameters given above and varying Poisson's ration for Pyralin from 0 to 0.5. None of these theoretical data sets were able  
 15 to fit the experimental data adequately. The experimental data was thus fit numerically using the Marquardt-Levenberg nonlinear least squares algorithm and allowing all three of the Pyralin parameters to vary. In performing such a calculation, one must assign each  
 20 experimental point to a particular dispersion curve. This was fairly straightforward for the data shown in Fig. 14 since the experimental points group together into well-defined curves resembling the pseudo-Rayleigh dispersion curves. The theoretical results shown in  
 25 Figs. 11 and 12 and discussed above indicate that the lowest velocity pseudo-Rayleigh modes should give rise to the strongest signals for most of the wavevectors used. It was therefore assumed that the two lowest-velocity

SUBSTITUTE SHEET

- 49 -

sets of data points correspond to the two lowest-velocity pseudo-Rayleigh dispersion curves. The Pyralin velocities ( $^vL_f$  and  $^vT_f$ ) parameters were adjusted to fit the points on these lowest-velocity curves with the 5 density fixed at the measured value of  $1.45 \text{ g/cm}^3$ . Fig. 14 shows the data points and the fit. Using the values obtained, the other pseudo-Rayleigh dispersion curves were calculated and plotted on Fig. 14. The agreement between these higher-velocity pseudo-Rayleigh dispersion 10 curves and the higher-velocity data points is excellent, with no further adjusting of any parameters.

The Pyralin velocity parameters determined from the fit are  $^vL_f = 2650 \text{ m/sec}$  and  $^vT_f = 1160 \text{ m/sec}$ . While it is never certain that the global minimum in the value 15 of  $\chi^2$  using nonlinear least squares fitting routines is reached, these values correspond to the lowest minimum found after starting from many different initial guesses for the parameter values. Varying either of the Pyralin velocity parameters by 10% led to substantially worse 20 fits. Varying the substrate parameters by the same amount led to worse fits for values of  $qh < 1$ , but did not affect the quality of the fits at higher  $qh$  values. It is thus estimated that the overall uncertainties in the pyralin velocity parameter values to be  $\pm 5\%$ .

25 The relative intensities of the two lowest modes can be compared to the film surface displacements of Fig. 11 for  $qh > 0.5$ . Experimentally, Fig. 14 shows that at least one of these two modes is present for all the samples. According to figure 9, the second lowest mode 30 should dominate from  $qh \sim 0.5$  to  $qh \sim 1.5$  while at higher  $qh$  values, i.e. above the crossover discussed earlier, the lowest mode should have a higher intensity. Upon examination of figure 12, this qualitative behavior definitely obtains since, for all the samples, the 35 density of observed data points is much higher for the

#### SUBSTITUTE SHEET

- 50 -

second mode than for the first qh values less than the crossover, while at higher qh values the only observed data points correspond to the first mode. A quantitative mode intensity analysis is possible by accurately fixing  
5 or measure the probe angle of incidence  $\theta_i$  since, according to eqs (29-34), changes in  $\theta_i$  significantly change the values of F and G in eq. (35) which in turn can change the final mode intensities seen in an ISTS experiment.

10 The outlying high velocity data points observed are not strictly pseudo-Rayleigh surface modes but rather represent modes which arise from interactions with the free substrate boundary. Their counterparts for the semi-infinite substrate are known as "leaky" modes which  
15 are damped due to the fact that they lose energy to the semi-infinite substrate as they propagate. The behavior of the modes can be elucidated by treating the finite size of the substrate explicitly. This is demonstrated below.

20 The solution for the transient grating excitation of a thin film coating is generalized to include the effects of a substrate with finite thickness. The formal solution for the displacement potentials is still given by eqs. (13-14). However, now the finite substrate has a  
25 free boundary at  $y=H$  (cf. Fig. 7) which is ignored for the semi-infinite system. For this reason, the  $C_\phi$  and  $C_y$  terms of eq. (13-14) are no longer unphysical and must be retained in order that the normal components of the stress at this new surface can be fixed to zero.

30 With the two new boundary condition equations and the two new unknown potential constants, eq. (16) becomes an 8x8 matrix equation. Using the Duhamel-Neumann expression for the stress (eq.) 15), and assuming as

SUBSTITUTE SHEET

- 51 -

before that there is no heating of the silicon, it can be shown that the new matrix equation takes the form

$$\underline{C}^f \underline{D}^f = \underline{F}^f \quad (38)$$

where

**SUBSTITUTE SHEET**

- 52 -

$$\underline{C'} = \begin{pmatrix} (1+p^1)e^{-\omega H} & (1+p^2)e^{-\omega H} & 2ip e^{-\omega H} & -2ip e^{-\omega H} & 0 & 0 & 0 \\ 2im e^{-\omega H} & -2im e^{-\omega H} & -(1+p^1)e^{-\omega H} & 0 & 0 & 0 & 0 \\ 1+p^2 & 1+ip & -2ip & -(1+r^1)g & 2irg & -(1+r^1)g & -2irg \\ 1+p^1 & -2in & -(1+p^3) & 2img & (1+r^1)g & -2img & (1+r^1)g \\ 2in & -1 & -ip & 1 & -ir & 1 & ir \\ 1+ip & -1 & -1 & im & 1 & -im & 1 \\ -1 & -in & 0 & -g(1+r^1)e^{-\omega H} & 2igre^{-\omega H} & -g(1+r^1)e^{-\omega H} & -2igre^{-\omega H} \\ in & 0 & 0 & 2igme^{-\omega H} & g(1+r^1)e^{-\omega H} & -2igme^{-\omega H} & g(1+r^1)e^{-\omega H} \\ 0 & 0 & 0 & 0 & 0 & 0 & 0 \end{pmatrix}$$

(39)

$$\underline{D'} = \begin{pmatrix} A' \\ B' \\ A' \\ B' \\ D' \\ D' \\ C' \\ C' \end{pmatrix}$$

(40)

SUBSTITUTE SHEET

- 53 -

$$\begin{aligned}
 F = \frac{i\Lambda\gamma}{v_{\text{II}}^2 \rho k v} & \left[ \begin{array}{l}
 \frac{-(\delta(k) + \delta(k-q))}{k^2} + \frac{v_{\text{I}}^2}{k^2} \left( \frac{-(v_{\text{I}}^2 - 2v_{\text{II}}^2)}{v_{\text{I}}^2} + \frac{\zeta^2}{k^2} \left( \frac{\delta(k)}{v^2 + \frac{v_{\text{I}}^2 \zeta^2}{k^2}} + \frac{\delta(k-q)}{v^2 + v_{\text{I}}^2 \left( \frac{\zeta^2 - k^2}{k^2} \right)} \right) \right) \\
 \frac{2\zeta v_{\text{II}}^2}{ik^3} \left( \frac{\delta(k)}{v^2 + \frac{v_{\text{I}}^2 \zeta^2}{k^2}} + \frac{\delta(k-q)}{v^2 + v_{\text{I}}^2 \left( \frac{\zeta^2 - k^2}{k^2} \right)} \right) \\
 \frac{-e^{-\zeta d} (\delta(k) + \delta(k-q))}{k^2} + \frac{e^{-\zeta d} v_{\text{I}}^2}{k^2} \left( \frac{-(v_{\text{I}}^2 - 2v_{\text{II}}^2)}{v_{\text{I}}^2} + \frac{\zeta^2}{k^2} \left( \frac{\delta(k)}{v^2 + \frac{v_{\text{I}}^2 \zeta^2}{k^2}} + \frac{\delta(k-q)}{v^2 + v_{\text{I}}^2 \left( \frac{\zeta^2 - k^2}{k^2} \right)} \right) \right) \\
 \frac{2e^{-\zeta d} v_{\text{II}}^2}{ik^3} \left( \frac{\delta(k)}{v^2 + \frac{v_{\text{I}}^2 \zeta^2}{k^2}} + \frac{\delta(k-q)}{v^2 + v_{\text{I}}^2 \left( \frac{\zeta^2 - k^2}{k^2} \right)} \right) \\
 \frac{-e^{-\zeta d} v_{\text{II}}^2}{k^2} \left( \frac{\delta(k)}{v^2 + \frac{v_{\text{I}}^2 \zeta^2}{k^2}} + \frac{\delta(k-q)}{v^2 + v_{\text{I}}^2 \left( \frac{\zeta^2 - k^2}{k^2} \right)} \right) \\
 \frac{e^{-\zeta d} v_{\text{II}}^2}{k^2} \left( \frac{\delta(k)}{v^2 + \frac{v_{\text{I}}^2 \zeta^2}{k^2}} + \frac{\delta(k-q)}{v^2 + v_{\text{I}}^2 \left( \frac{\zeta^2 - k^2}{k^2} \right)} \right) \\
 0 \\
 0
 \end{array} \right] \quad (41)
 \end{aligned}$$

SUBSTITUTE SHEET

- 54 -

Information is extracted from this matrix equation with the same techniques that were used for the 6x6 equation in the main text. The resulting dispersion curves for the thirty lowest velocity modes of a system composed of 3  $\mu\text{m}$  Pyralin film on a 330 $\mu\text{m}$  silicon substrate are showing in Fig. A1. One can see that relaxing the semi-infinite substrate assumption give rise to extra plate modes propagating predominantly within the substrate with velocities above the substrate transverse velocity  $v_{T_s}$  which was, in the semi-infinite case, the cutoff for propagating modes of the system. The dispersion curves for velocities sufficiently below the  $v_{T_s}$  are almost identical to those for the pseudo-Rayleigh modes calculated using the semi-infinite substrate system and shown in Fig. 14. The only differences occur at phase velocities near the cut-off and, for the lowest velocity mode, at very low ( $<0.2$ )  $q_h$  values. This behavior is expected and confirms that the semi-infinite substrate approximation is adequate to explain nearly all of the pseudo-Rayleigh modes seen in these experiments.

The extra plate modes above  $v_{T_s}$  are produced as a result of acoustic reflections from the free substrate surface. They can be obtained within the semi-infinite substrate approximation as well, but only as "leaky" modes with finite lifetime due to energy flow into the infinite substrate. The existence of these modes for the Pyralin/silicon system used in these experiments provides an explanation for the ISTS data points occurring above  $v_{T_f}$  in Fig. 14.

### 30 E. Discussion

The values of  $v_{Lf} = 2650 \pm 130 \text{ m/sec}$  and  $v_{Tf} = 1160 \pm 60 \text{ m/sec}$  deduced in this study for Pyralin 2555 combined with the density of  $1.45 \text{ g/cm}^3$  correspond to a Young's modulus of  $5.4 \pm 0.5 \text{ GPa}$  and a Poisson's ratio of

SUBSTITUTE SHEET

- 55 -

0.38 $\pm$ 0.02. (The uncertainties given for Young's modulus and the Poisson ratio are calculated from the uncertainties for  $v_{Lf}$  and  $v_{Tf}$  determined from the study above and do not account for uncertainties in the film density.) To the inventor's knowledge, this represents the first measurement of Poisson's ratio in this material. This value for Young's modulus is over 100% higher than the previously measured value of 2.4 GPa. The value of Young's modulus can depend very sensitively on the method of film curing. Thus, the difference is believed due to intrinsic difference in sample characteristics.

Polyimide films can exhibit variation in the degree of chain orientation and in density as a function of depth. These measurements yield values which are averaged over the film thickness and so do not provide direct information about depth dependences. Measurements of thinner films may yield different parameters, indicative of differences in film properties very close to the substrate surface. By tilting the grating wavevector so that it has a component perpendicular to the film, it is possible to determine separate in-plane and out-of-plane elastic moduli. The theoretical treatment outlined here could be generalized to take this into account.

In general, there are several different protocols available for extracting the elastic parameters from ISTS data on thin supported films. One method, which was demonstrated above, involves determining the mode velocities at a range of  $q_h$  values - by either changing scattering angle or sample thickness or both - and then varying the elastic parameters until a good match between theoretical dispersion curves and data is obtained. Experimental error can be reduced with improved accuracy of the scattering wavevector measurement and an analysis

#### SUBSTITUTE SHEET

- 56 -

along these lines with fewer  $q_h$  values and higher accuracy can be achieved. An alternative or complementary method involves using the relative ISTS signal intensity information obtained for the different 5 modes at each  $q_h$  values. As discussed, a quantitative analysis of the relative intensities requires accurate specification of the incident probe angle, the indices of refraction of the film and substrate, and the film thickness. The first parameter is easily determined in 10 the ISTS experiment. The indices of refraction and film thickness can be measured by other techniques, or treated as free parameters in a fitting scheme. The elastic parameters may be extracted using data from only one  $q_h$  value at which multiple modes are observed, by fitting 15 both the pseudo-Rayleigh mode velocities and relative intensities. With efficient computing algorithms to accomplish fitting, the elastic parameters may be extracted with the same real-time rates demonstrated for the data acquisition. Generally, the experiment can be 20 optimized with an improved probe pulse temporal profile.

#### E. Determination of Adhesion Quality

In the analysis described above, the film and substrate were modeled such that together they form an acoustic waveguide and together determine the frequencies 25 of the acoustic waveguide modes that propagate in the film-substrate system. Referring to Figs. 16 and 16a, comparing the dispersion curves for a tightly bound film-substrate system with a system in which the substrate is removed (which would be equivalent to a film-substrate 30 system with a substrate that has a very low stiffness) it is seen that the waveguide frequencies change dramatically. These changes can be used to detect regions where the film has become debound from the substrate by sampling the film at various locations.

SUBSTITUTE SHEET

- 57 -

Further, the degree of film substrate adhesion can be determined. For example, the absence of a substrate is equivalent to the case where the film is no longer stuck to the substrate. If the film is slightly stuck but not tightly bound, the acoustic waveguide frequencies are intermediate between the case where the substrate is present and where it is removed. By measuring the actual positions of the frequencies, the degree of adhesion can be determined. In the adhesion model, two parameters are introduced ( $k_z$ ,  $k_y$ , further discussed below). One is a spring stiffness parameter per unit area for motions parallel to the plane of the film ( $k_z$ ). The other is a spring stiffness parameter per unit area for motions perpendicular to the film ( $k_y$ ). Although each parameter affects the waveguide frequencies, for films with intermediate degrees of adhesion, we expect that since the film is in contact with the substrate, the stiffness parameter ( $k_y$ ) for motions perpendicular to the film will be large (i.e. close to the tightly bound case).

Referring to Fig. 17 only the stiffness parameter for motions parallel to the plane ( $k_z$ ) of the film has been varied. (The plot wherein  $k_z = \infty$  corresponds to the tightly bound case, Fig. 16, and the case wherein  $k_z = 0$  corresponds to the case of a film on a frictionless surface.) As can be seen from this figure, there is a smooth variation in the acoustic waveguide mode frequencies between the tightly bound case and the frictionless interface case (i.e. the case where there is no resistance to film motions parallel to the plane of the film but there is resistance to motions perpendicular to the film). The waveguide frequencies are most sensitive to changes in the adhesion at small wavevector times thickness values. Therefore, this region can be probed (by varying the wavevector of the excitation).

SUBSTITUTE SHEET

- 58 -

The plots in Figs. 16 and 17 were generated by computer algorithm using inputs as follows.

$$\sigma_{yy}(d^+) - \sigma_{yy}(d^-) \quad (42)$$

$$\sigma_{yz}(d^+) = \sigma_{yz}(d^-) \quad (42a)$$

$$[u_z(d^+) - u_z(d^-)] K_z - \frac{1}{2} (\sigma_{yz}(d^+) + \sigma_{yz}(d^-)) = 0 \quad (42b)$$

$$[u_y(d^+) - u_y(d^-)] K_y - \frac{1}{2} (\sigma_{yy}^+ + \sigma_{yy}^-) = 0 \quad (42c)$$

where  $J_{ij}$  is the stress tensor;  $u_i$  is the displacement vector;  $k_z$  is an elastic stiffness/unit area for motion along the z axis;  $k_y$  is an elastic stiffness/unit area for motion along the y axis (perpendicular to the plane of the sample surface). These boundary conditions are used with the equations of motion to determine acoustic mode dispersion and excitation efficiency. (Discussion of models for a different purpose can be found in F.J. Margetan et al., Journal of Nondestructive Evaluation, Vol. 7, Nos. 3 and 4, 1988, p. 131.)

An inertial mass term was used to describe excess mass at the crack tip is dropped for the adhesion model.

#### F. Analysis of Thermal Diffusion Data

Referring to Fig. 18, the following is a derivation of a technique for measurement of thermal diffusion, using boundary conditions for a thin film. Starting with the equation of motion:

SUBSTITUTE SHEET

- 59 -

$$\frac{\partial^2 T}{\partial y^2} + \frac{\partial^2 T}{\partial z^2} - \frac{cp}{\kappa} \frac{\partial T}{\partial t} = -\frac{Q}{\kappa} \quad (43)$$

$Q$  represents the heat source;  $K$  is the thermal conductivity;  $C$  is the heat capacity per unit mass; and  $\rho$  is the density.

5 It is assumed that heat flow occurs within the film and out of the film into the air and substrate. The heat flow out of the film obeys Newton's laws of heat propagation (i.e. heat flow is proportional to the temperature gradient leaving the following boundary  
10 conditions on heat flow:

$$\left. \frac{\partial T}{\partial y} \right|_{y=0} = hT \quad \left. \frac{\partial T}{\partial y} \right|_{y=d} = h'T \quad (44)$$

In the above, the  $z$  axis is in the plane of film and the  $y$  axis parallel to the film thickness with the origin,  $y=0$ , of the film surface and where the film  
15 thickness is  $y=d$ ,  $h$  and  $h'$  relate to the degree of thermal coupling between the film and air and film and substrate, respectively. For ISTS excitation:

With  $Q=A(1+e^{iqz})(e^{-\xi y})\gamma(t)$ , the transformed solution (using transforms above) is:

$$T(s, k, y) = B(s, k) \exp\left\{-y\left(k^2 + \frac{cps}{\kappa}\right)\right\} + C(s, k) \exp\left\{y\left(k^2 + \frac{cps}{\kappa}\right)\right\} \quad (45)$$

SUBSTITUTE SHEET

- 60 -

$$-\frac{A}{k} e^{-\zeta y} \left[ \frac{\delta(k) + \delta(k - \beta)}{\zeta^2 - k^2 - \frac{cps}{\kappa}} \right] \quad (46)$$

where A is the amplitude factor related to excitation pulse intensity and optical absorption coefficient, q is the wavevector and  $\zeta$  is the optical absorption coefficient. Applying the boundary conditions and inverting the transform yields

$$T(y, z, t) = \left[ 1 + \exp\left(\frac{-\zeta^2}{cp} t\right) e^{i\beta z} \right] \sum_n \exp\left(\frac{-\kappa r_n^2}{cpd^2} t\right) F(y, r_n) \quad (47)$$

with

$$\tan r_n = \frac{(h - h')r_n d}{hh'd^2 + r_n^2} \quad (48)$$

and

$$\bar{F}(y, r_n) = \frac{2A}{cp\left(\zeta^2 + \frac{r_n^2}{d^2}\right)} \left\{ \frac{(h + \zeta)\left(\frac{r_n}{d} \cos \frac{r_n(y-d)}{d} + h' \sin \frac{r_n(y-d)}{d}\right) - e^{-\zeta d}(h' + \zeta)\left(\frac{r_n}{d} \cos \frac{r_n y}{d} + h \sin \frac{r_n y}{d}\right)}{\left[2 - d(h' - h) \sin r_n + (h' - h)\left(\frac{d}{r_n} - d \cot r_n\right) \cos r_n\right]} \right\} \quad (49)$$

SUBSTITUTE SHEET

- 61 -

In the quasi-static limit, the displacements are related to the temperature as follows:

$$\nabla^2 \phi = \alpha_T T \quad (50)$$

$$\vec{u} = \nabla \phi + \nabla \times \vec{\psi} \quad \text{with } \nabla \cdot \vec{\psi} = 0 \text{ and } \nabla^2 \vec{\psi} = 0 \quad (50a)$$

5 where  $\alpha_T$  is the coefficient of thermal expansion and  $\vec{u}$  is the displacement.

In this limit, the temporal dependence of  $\vec{u}$  is determined by the temporal dependence of  $T$ . Thus, the signal is a sum of exponentials with the same decay rate 10 in equation (46). The different decay rates can be extracted with a linear prediction routine. With the rates determined in this manner, comparison can be made to theory to determine:

$$\frac{kq^2}{cp} + \frac{Kt_n^2 f}{cp} \quad (51)$$

15 by changing  $q$  and  $d$ , then, predictions can be made for the form of the experimental decay. In this way, equation (51) can be compared to experimental values to determine the accuracy of the calculated values.

#### Further Embodiments

20 It will be evident from the above that the invention enables many embodiments and advantages. While the experiments may be carried out on thin films to particular advantage as discussed above where surface ripple is the predominant phenomenon leading to

SUBSTITUTE SHEET

- 62 -

diffraction of the probe, the ripple effect may also be induced on thicker samples. The experiment can be optimized to selectively analyze diffraction from ripple over diffraction from bulk, refractive index  
5 modification. The ripple effect can be preferentially detected by maximizing the amount of reflected light by increasing the incident angle of the probe beam. The optimum incident angle may be determined based on sample thickness and the refractive index to enable a large  
10 incident angle while avoiding substantial losses due to total internal refraction. The detection of diffraction from the ripple effect can also be optimized on freestanding samples by detection of transmitted and reflected probe radiation and subtracting the former,  
15 which contains bulk-properties information, from the latter, which contains ripple information. (It will also be understood that for thin films, ripple from both sides of a film can be detected, even for films on a substrate, in which case ripple of the sample-substrate interface  
20 can be detected.) The presence of signal induced from bulk properties can also be detected by study of the polarization of the diffracted beam. A polarizer can be positioned after the probe focusing optic (e.g. optic 54) and another polarizer positioned before the detector  
25 (e.g. detector 58). As discussed above bulk properties vary the incident polarization. The polarization can be studied as a function of incident angle to determine the optimum angle for detecting ripple induced diffraction. Further, the excitation radiation can be optimized to  
30 enhance the diffraction signal arising from ripple. The wavevector dependence of the signal can be studied (e.g. with a computer) to determine that the diffraction signal is predominately from ripple. Generally, a smaller excitation wavevector (longer excitation wavelength or  
35 smaller angle of incidence of the excitation beams)

SUBSTITUTE SHEET

- 63 -

enhances the ripple effect. In the experiments on the sample as described above, the maximum wavevector for which signal was obtained was about  $q=1.81\mu\text{m}^{-1}$ . Larger maximum wavevectors can be used if a less stiff sample or 5 higher intensity probe laser is used.

Other embodiments are within the scope of the following claims.

What is claimed is:

**SUBSTITUTE SHEET**

- 64 -

Claims

1. An apparatus for measuring the properties of a sample of material, comprising:

a first, excitation source for producing  
5 excitation radiation adapted to impinge upon said sample of material, said excitation radiation comprising pulsed radiation composed of at least two component pulses which interfere within said sample, said excitation radiation being sufficient to induce a transient phonon in said  
10 material which gives rise to a transient, time dependent periodic ripple morphology on a surface of said sample,

a second, probe source for producing probe radiation arranged to reflect from the periodic ripple morphology on the surface of said sample to form a  
15 diffraction signal,

a detector for detecting the diffraction signal from said probe source radiation reflected from said surface, and

an analyzer for selectively analyzing said  
20 diffraction signal formed by said transient ripple morphology.

2. The apparatus of claim 1 wherein said probe source produces radiation that is not substantially absorbed by said sample.

25 3. The apparatus of claim 1 wherein said probe source produces radiation that is absorbed about 10% or less than said radiation from said excitation source.

4. The apparatus of claim 3 wherein said probe source produces radiation that is absorbed about 1% or  
30 less than said radiation from said excitation source.

SUBSTITUTE SHEET

- 65 -

5. The apparatus of claim 1 wherein said excitation source radiation comprises ultraviolet radiation absorbed sufficiently by said sample to induce heating that gives rise to said phonon and ripple 5 morphology.

6. The apparatus of claim 5 wherein said probe source radiation comprises visible radiation not substantially absorbed by said sample.

7. The apparatus of claim 1 wherein said sample 10 comprises a thin sample of about 500  $\mu\text{m}$  or less.

8. The apparatus of claim 7 wherein said thin sample is about 10  $\mu\text{m}$  or less.

9. The apparatus of claim 1 wherein said sample comprises a thin polymeric film.

15 10. The apparatus of claim 9 wherein said film comprises a free-standing film.

11. The apparatus of claim 9 where said film is disposed on a support.

12. The apparatus of claim 1 wherein said 20 analyzer includes a polarizer for determining change of polarization of said probe beam after diffraction from said surface to selectively analyze diffraction from said ripple morphology.

13. The apparatus of claim 1 wherein said 25 analyzer is for analyzing said signal as a function of the wavevector and to selectively analyze diffraction signal from said ripple morphology.

SUBSTITUTE SHEET

- 66 -

14. The apparatus of claim 1 further including a probe beam and detector constructed for detecting and resolving a substantial time-portion of the time-dependent diffraction induced by each excitation pulse.

5 15. The apparatus of claim 14 wherein said probe radiation is of a selected pulse width and said detector is adapted to detect the time-dependent diffraction for the duration of said probe pulse.

10 16. The apparatus of claim 15 wherein said detector is constructed to detect the entire detectable time-dependent diffraction induced by each excitation pulse.

15 17. The apparatus of claim 16 wherein said excitation radiation has a pulse width on the order of psec duration and the probe radiation pulse width is on the order of nsec duration.

18. The apparatus of claim 17 wherein said detector has a time resolution on the order of 1 nsec.

20 19. The apparatus of claim 14 wherein said probe pulse has a peak power output of about 1000 watts or greater.

20. The apparatus of claim 19 wherein said laser comprises a Q-switch YAG laser.

25 21. The apparatus of claim 14 wherein said excitation pulse is generated from a pulsed laser and said probe pulse is generated from a CW laser.

SUBSTITUTE SHEET

- 67 -

22. A method for measuring the properties of a sample comprising:

impinging a pulse of excitation radiation upon said sample, said excitation radiation being composed of  
5 at least two component pulses which interfere within said sample, and being selected to induce a transient phonon in said sample which gives rise to a transient, time dependent ripple morphology on a surface of said sample,  
reflecting probe radiation from the periodic  
10 ripple morphology on the surface of said sample to form a diffraction signal, and

selectively detecting the diffraction signal from said probe source radiation reflected from said ripple morphology.

15 23. The method of claim 22 wherein said sample is about 500  $\mu\text{m}$  thick or less.

24. The method of claim 23 wherein said sample is about 10  $\mu\text{m}$  thick or less.

25. The method of claim 24 wherein said sample is  
20 a pure polymer sample.

26. The method of claim 25 comprising selecting excitation radiation that is absorbed by the sample.

27. The method of claim 26 comprising selecting probe radiation that is absorbed less than said  
25 excitation radiation.

28. The method of claim 27 comprising selecting probe radiation that is not substantially absorbed by said sample.

SUBSTITUTE SHEET

- 68 -

29. The method of claim 28 wherein said excitation radiation comprises UV radiation and said probe radiation comprises visible radiation.

30. The method of claim 22 comprising detecting 5 and resolving a substantial time-portion of the time-dependent diffraction induced by each excitation pulse.

31. The method of claim 30 wherein said probe source is a CW laser.

32. The method of claim 30 further comprising:  
10 providing a probe source having a power output of about 1000 watts or greater, and  
detecting and resolving a substantial time-portion of the time-dependent diffraction induced by each excitation pulse.

15 33. The method of claim 30 further including signal averaging the diffracted radiation from multiple excitation pluses.

34. The method of claim 22 further comprising analyzing said signal to selectively analyze diffraction 20 from said ripple.

35. The method of claim 32 comprising analyzing the polarization of said diffracted radiation.

36. The method of claim 34 comprising analyzing the diffracted radiation as a function of wavevector.

25 37. The method of any one of claims 33 to 35 including optimizing the diffraction from said ripple by varying the angle of incidence of said probe beam.

SUBSTITUTE SHEET

- 69 -

38. The method of any one of claims 33 to 35 including optimizing the diffraction from said ripple by varying the wavelength or angle of incidence of said excitation radiation.

5 39. An apparatus for measuring the properties of a thin sample of polymeric material comprising:

a first, excitation laser source for producing a pulse of radiation adapted to impinge upon said sample, said excitation source comprising a pulsed source

10 composed of at least two component pulses which interfere within said thin film, said excitation radiation adapted to induce a transient phonon in said material,

a second, probe laser source for producing radiation, said probe radiation being of selected

15 wavelength not substantially absorbed by said sample and arranged to reflect from the surface of said sample to form a diffraction signal, and

a detector for detecting the diffraction signal.

40. The apparatus of claim 39 further including a  
20 probe beam and detector constructed for detecting and resolving a substantial time-portion of the time-dependent diffraction induced by each excitation pulse.

41. The apparatus of claim 40 further including a signal average for signal averaging signal from multiple  
25 excitation pulses.

42. The apparatus of claim 40 wherein said excitation pulse is on the order of psec duration and the probe pulse on the order of nsec duration.

43. The apparatus of claim 42 wherein the probe  
30 laser source peak power is about 1000 watts or more.

**SUBSTITUTE SHEET**

- 70 -

44. The apparatus of claim 43 wherein the peak power is about 10,000 watts.

45. The apparatus of claim 43 wherein said laser is a YAG Q-switched laser.

5 46. The apparatus of claim 45 wherein said detector has a response time on the order of 1 nsec.

47. The apparatus of claim 39 wherein said diffracted radiation is reflected from the back surface of said sample opposite said radiation sources.

10 48. The apparatus of claim 39 wherein said probe source is a CW laser.

49. The apparatus of claim 48 wherein said probe source is a gated argon ion laser.

50. The apparatus of any one of claims 39 or 48  
15 wherein said probe has a power output of around 1 watt.

51. The apparatus of claim 39 including an analyzer adapted for determining the adhesion of said polymer sample on a substrate surface from said diffraction signal.

20 52. The apparatus of claim 39 including an analyzer adapted for determining the thermal diffusion of said sample from said diffraction signal.

SUBSTITUTE SHEET

1/24

FIG 1c

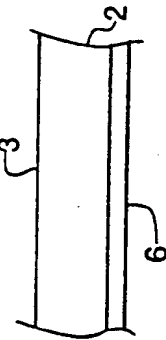


FIG 1b

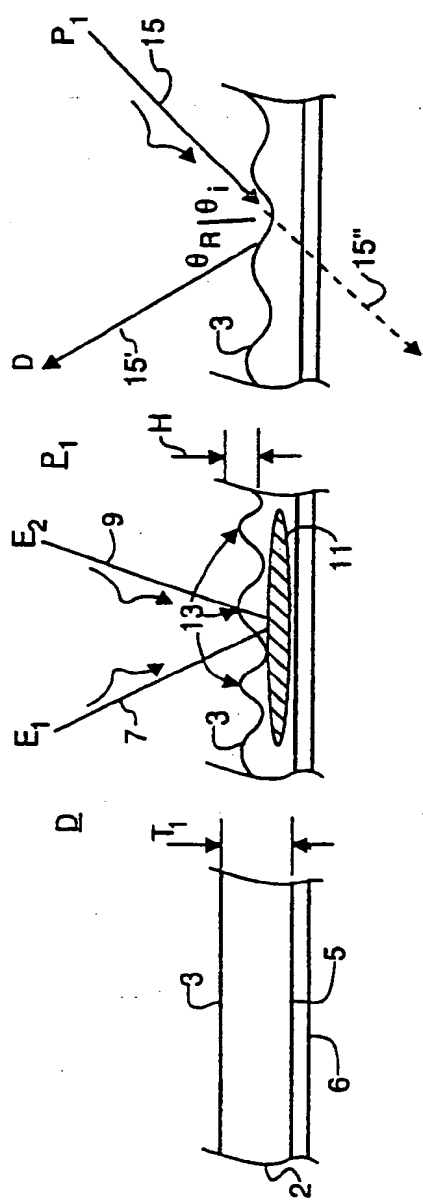
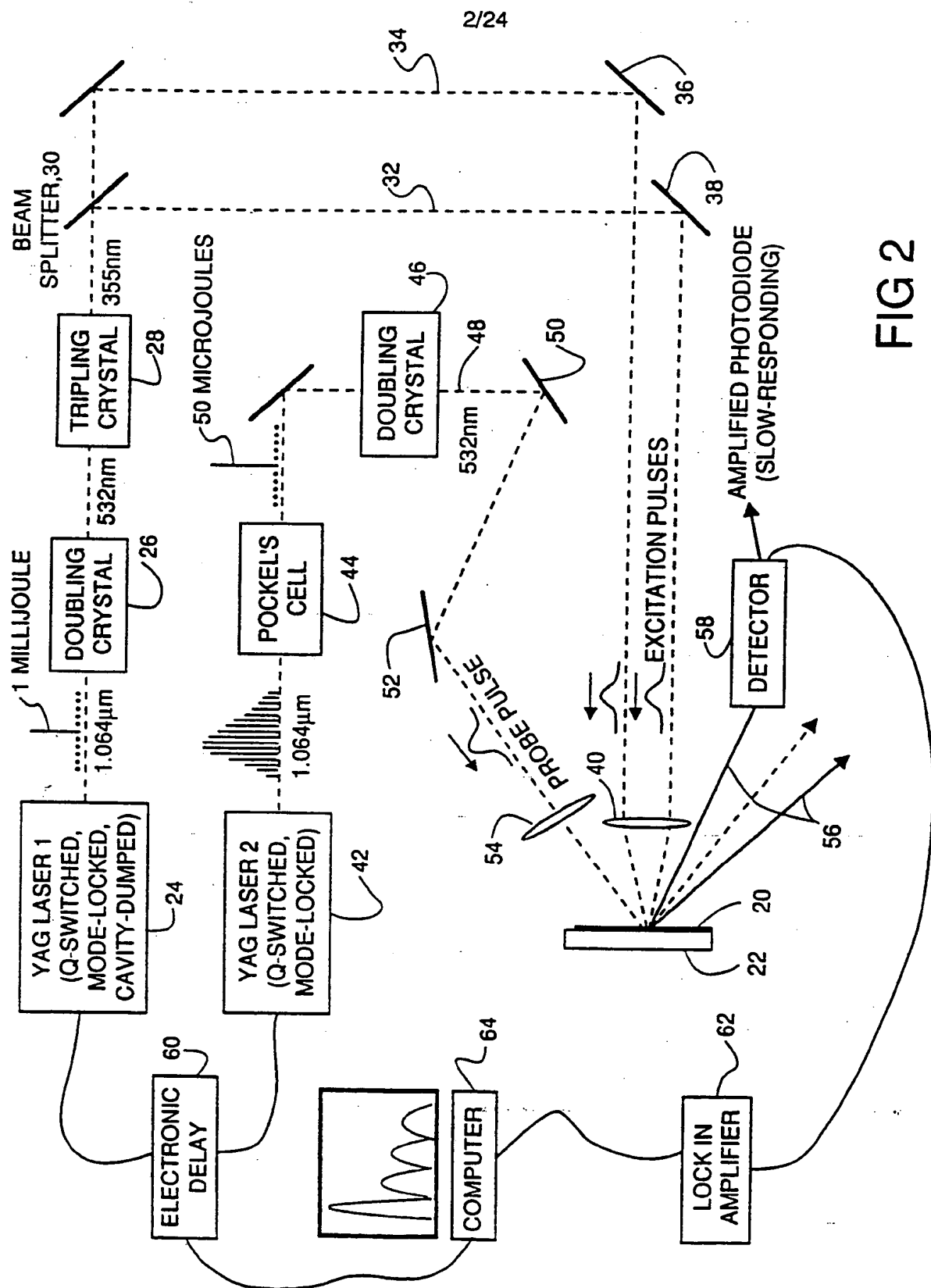


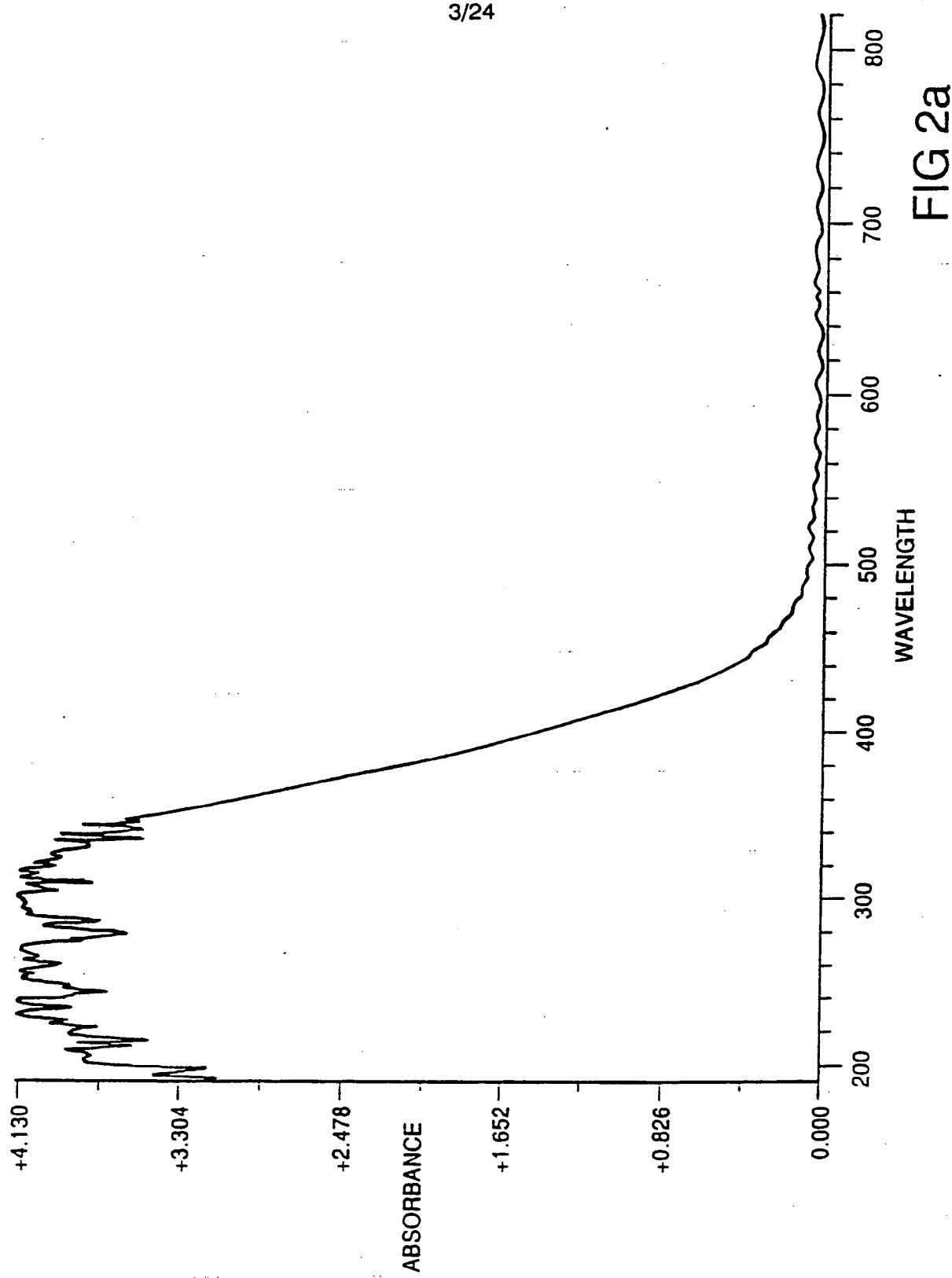
FIG 1

SUBSTITUTE SHEET

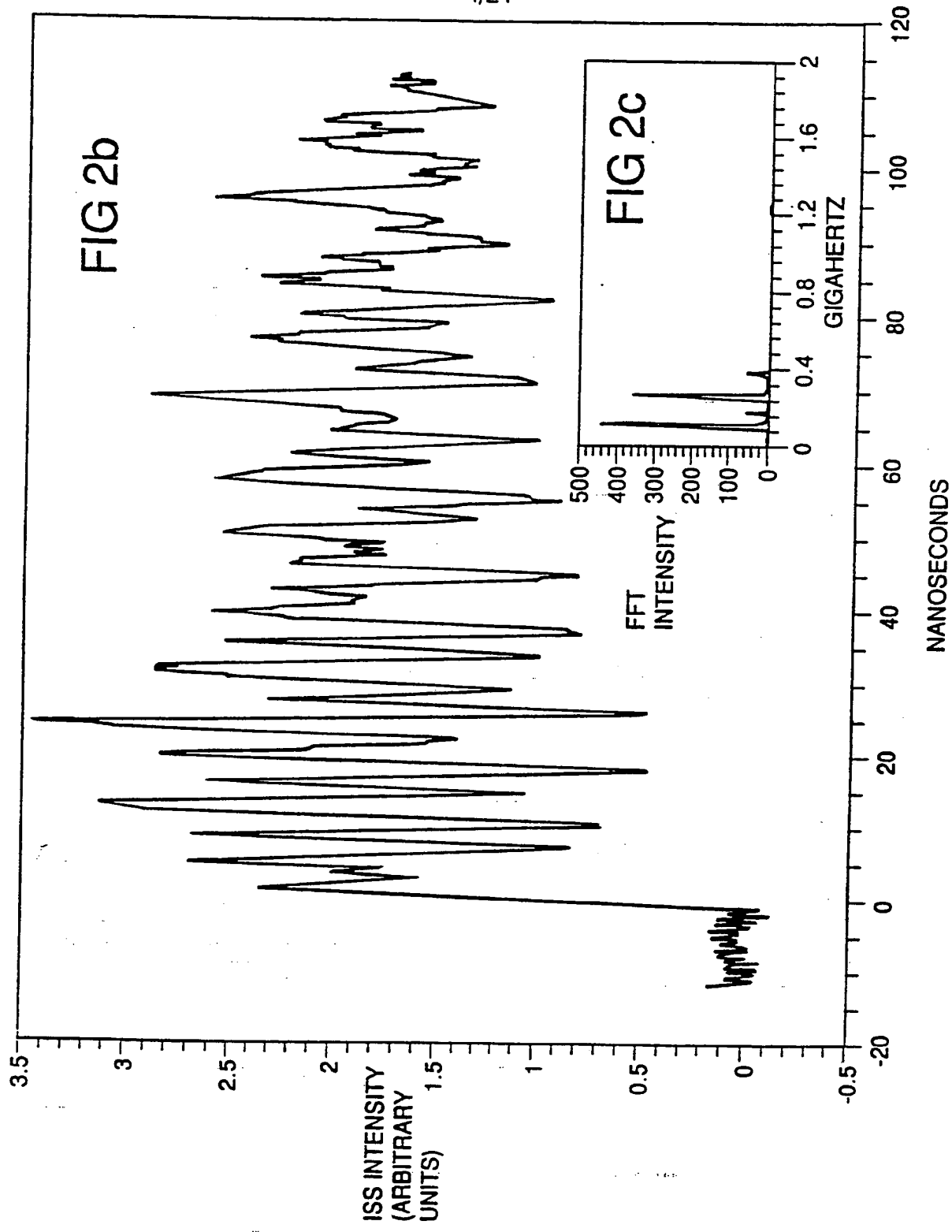


SUBSTITUTE SHEET

3/24

**SUBSTITUTE SHEET**

4/24



SUBSTITUTE SHEET

5/24

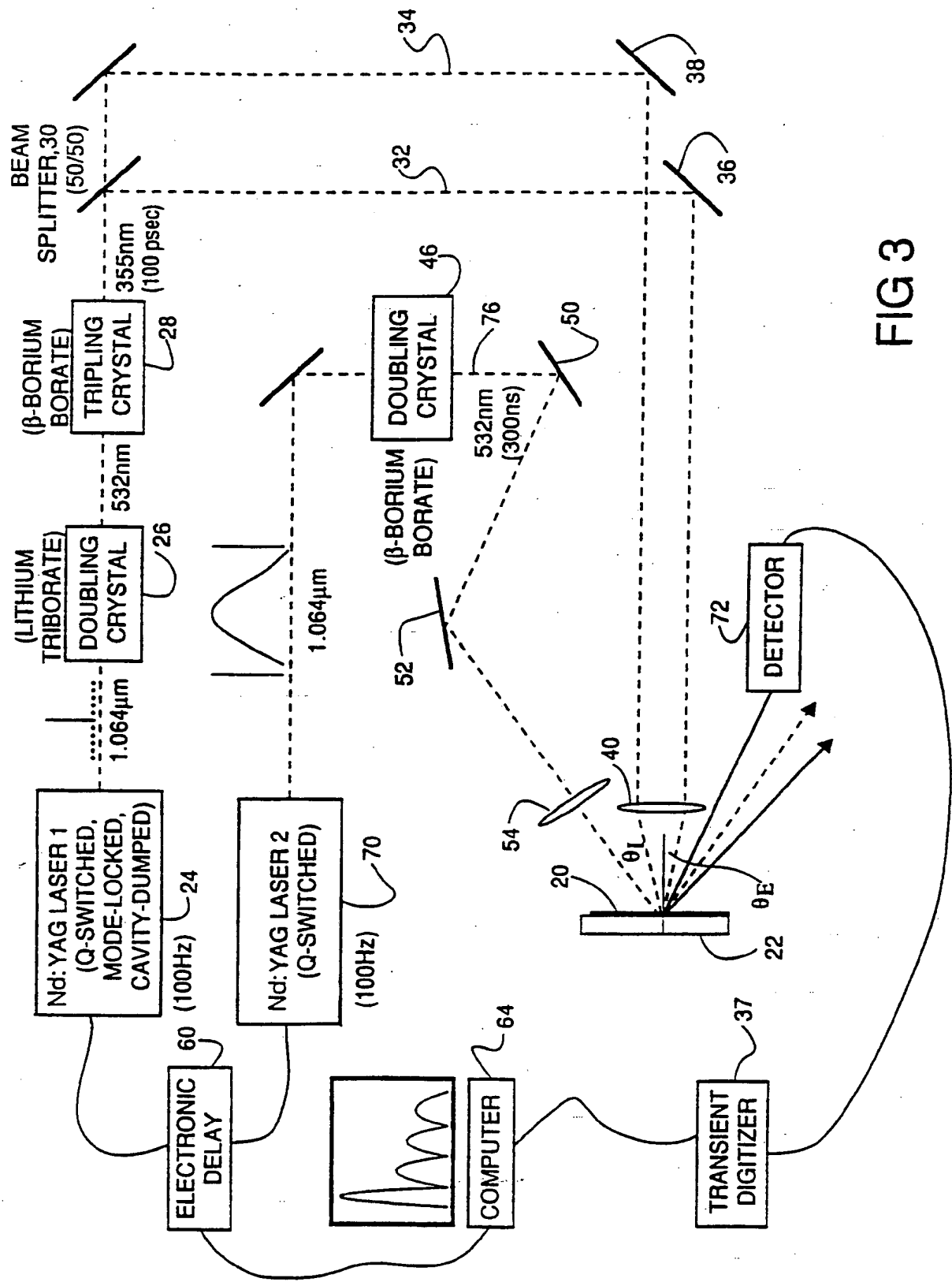
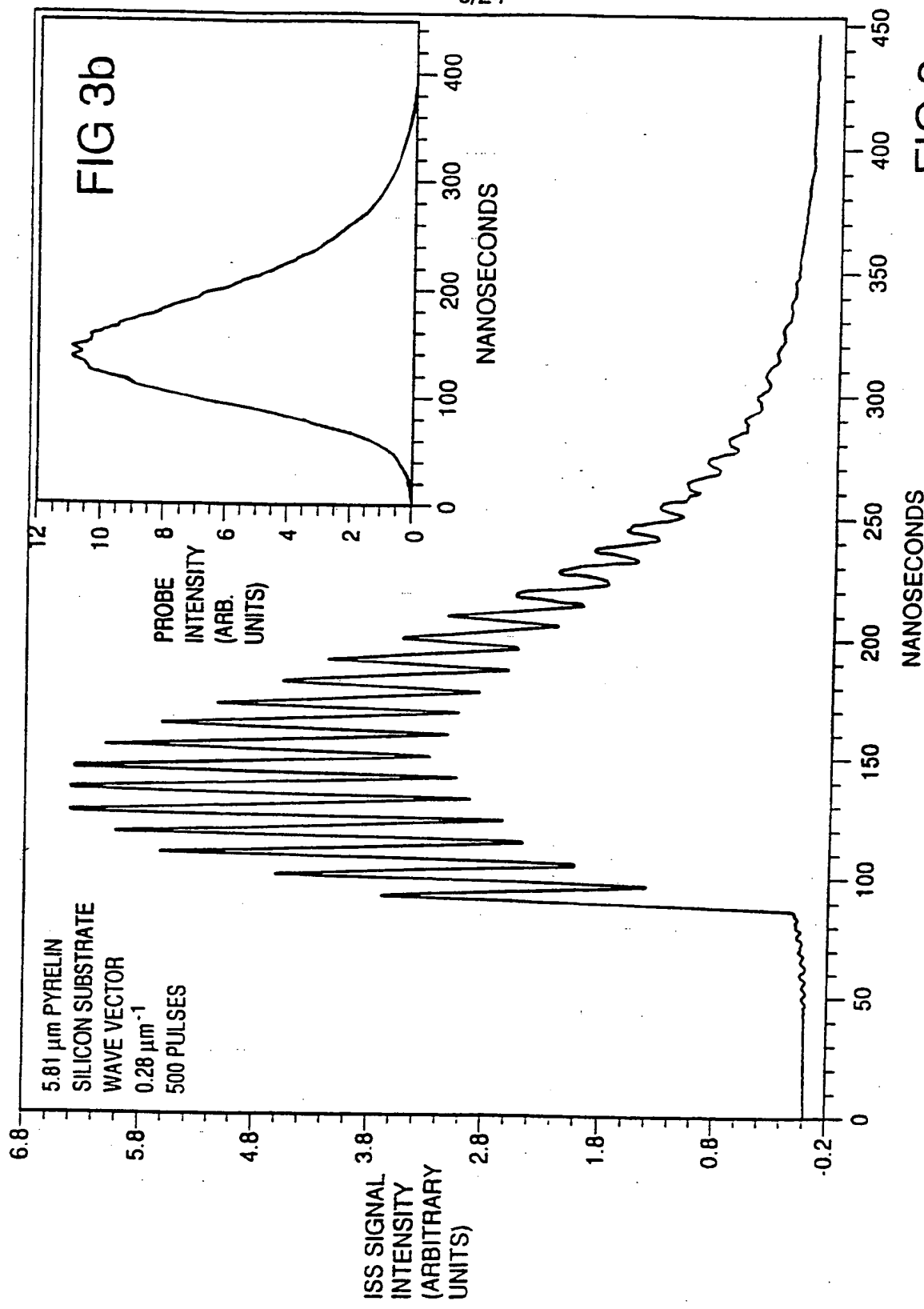
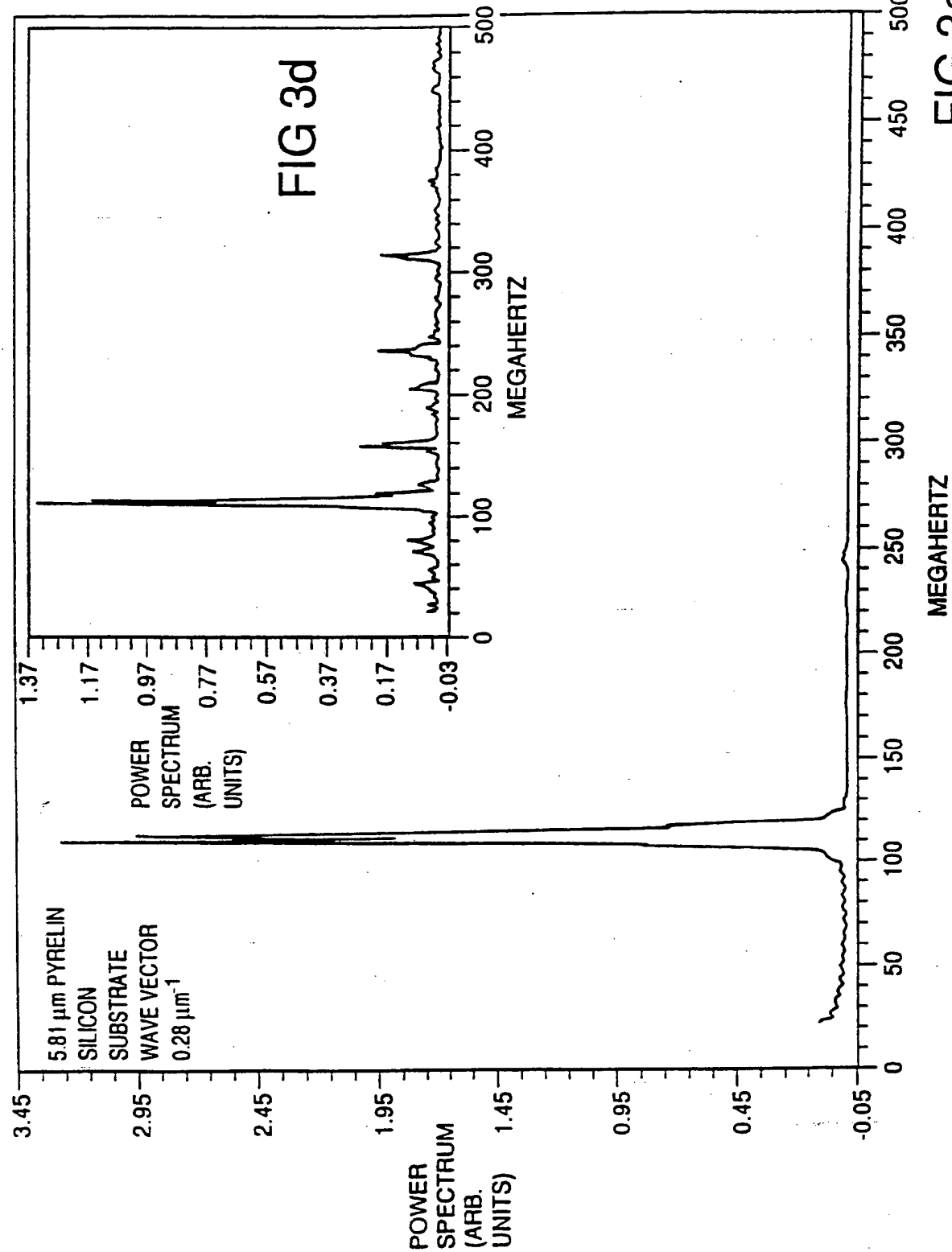


FIG 3

6/24

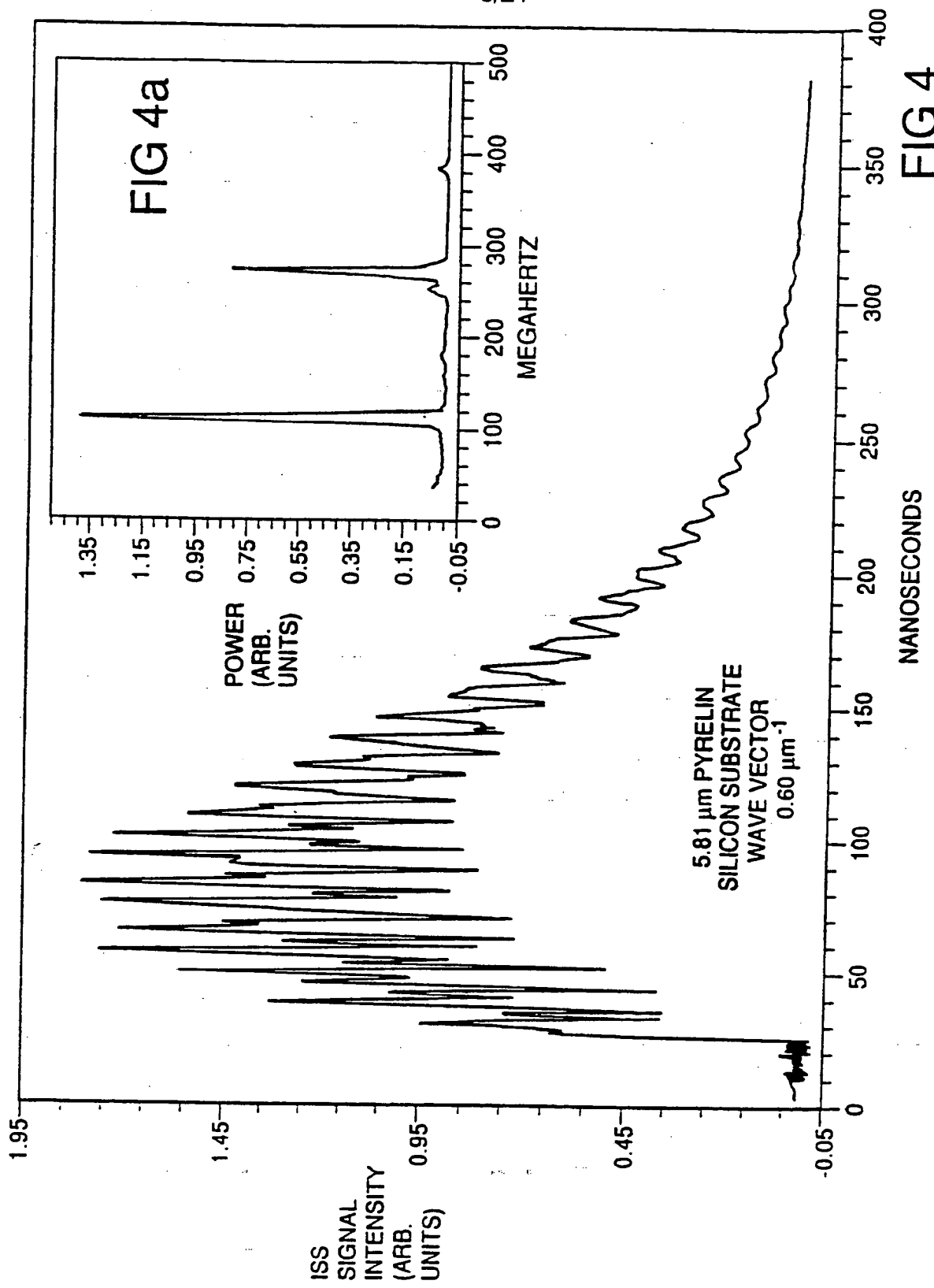
**FIG 3a****SUBSTITUTE SHEET**

7/24



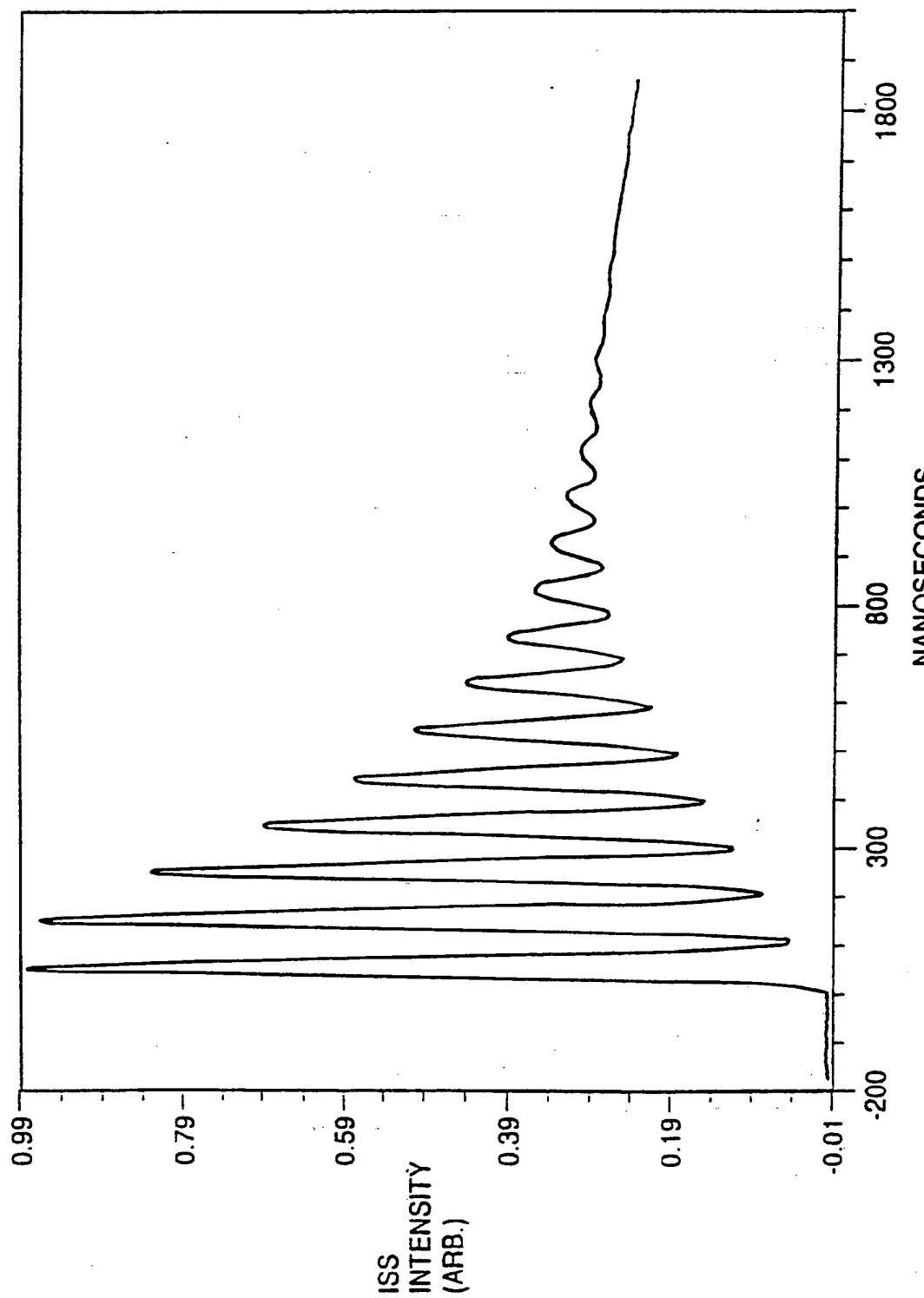
SUBSTITUTE SHEET

8/24

**SUBSTITUTE SHEET**

9/24

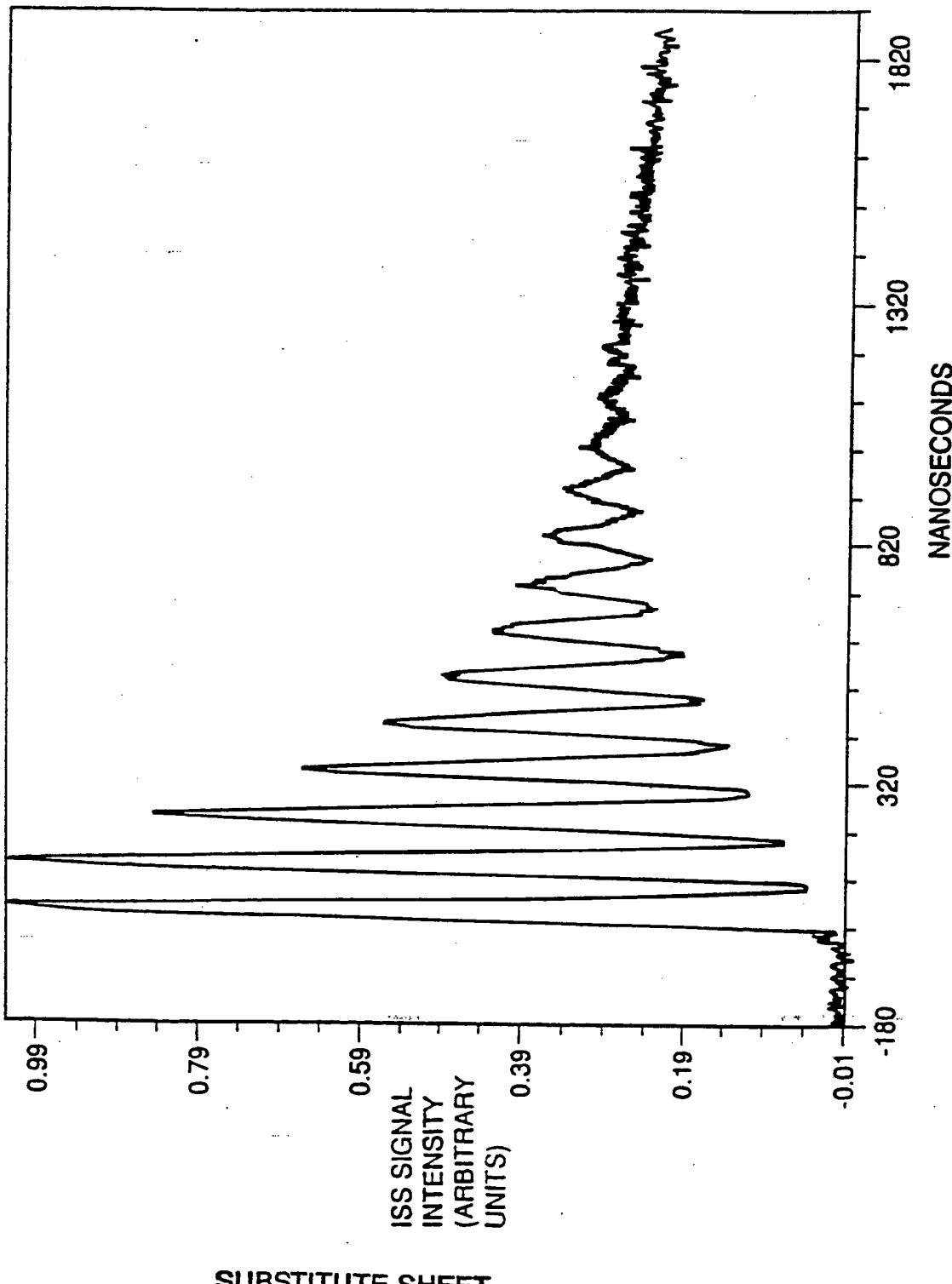
FIG 5



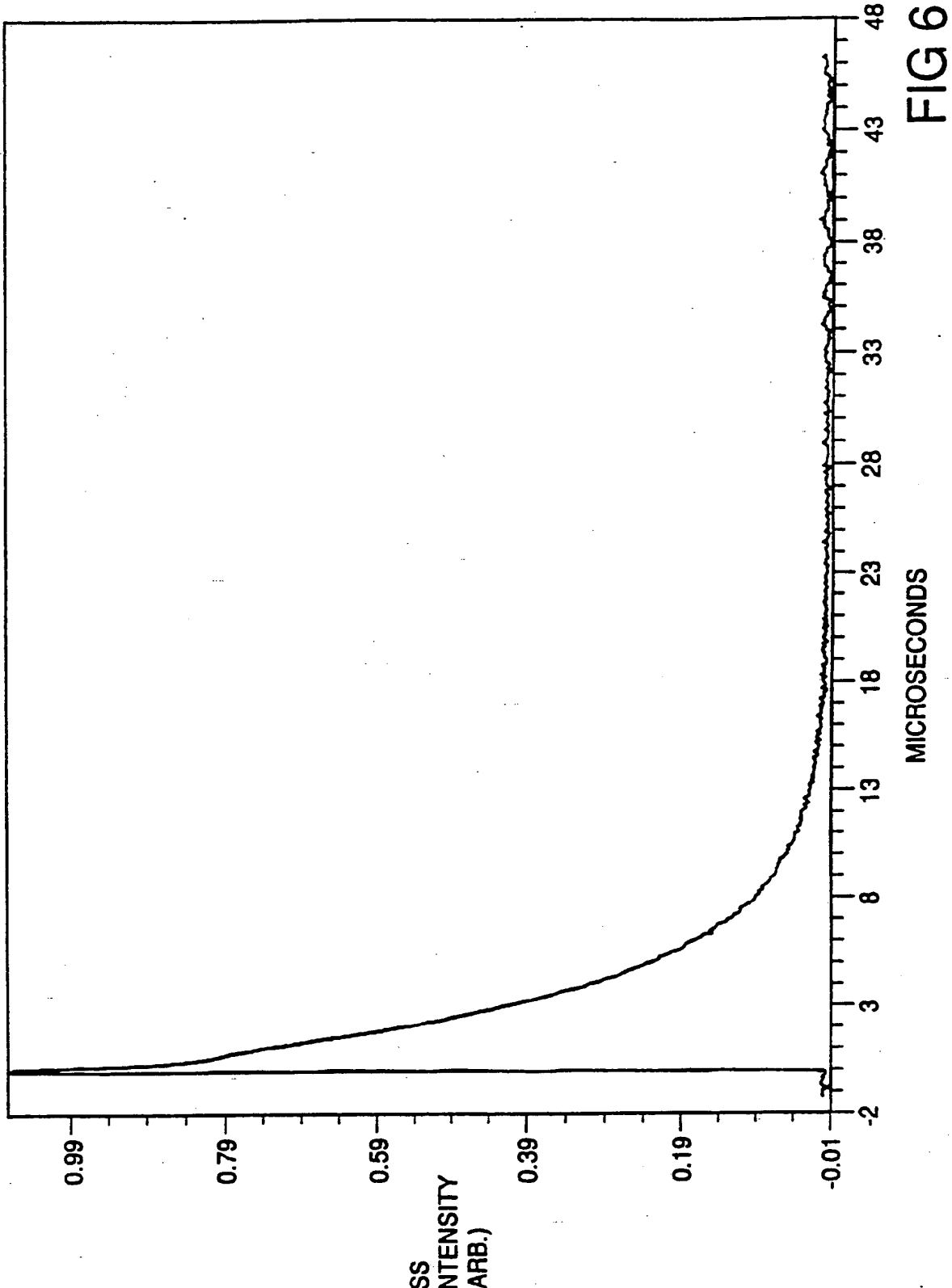
SUBSTITUTE SHEET

10/24

FIG 5a



11/24

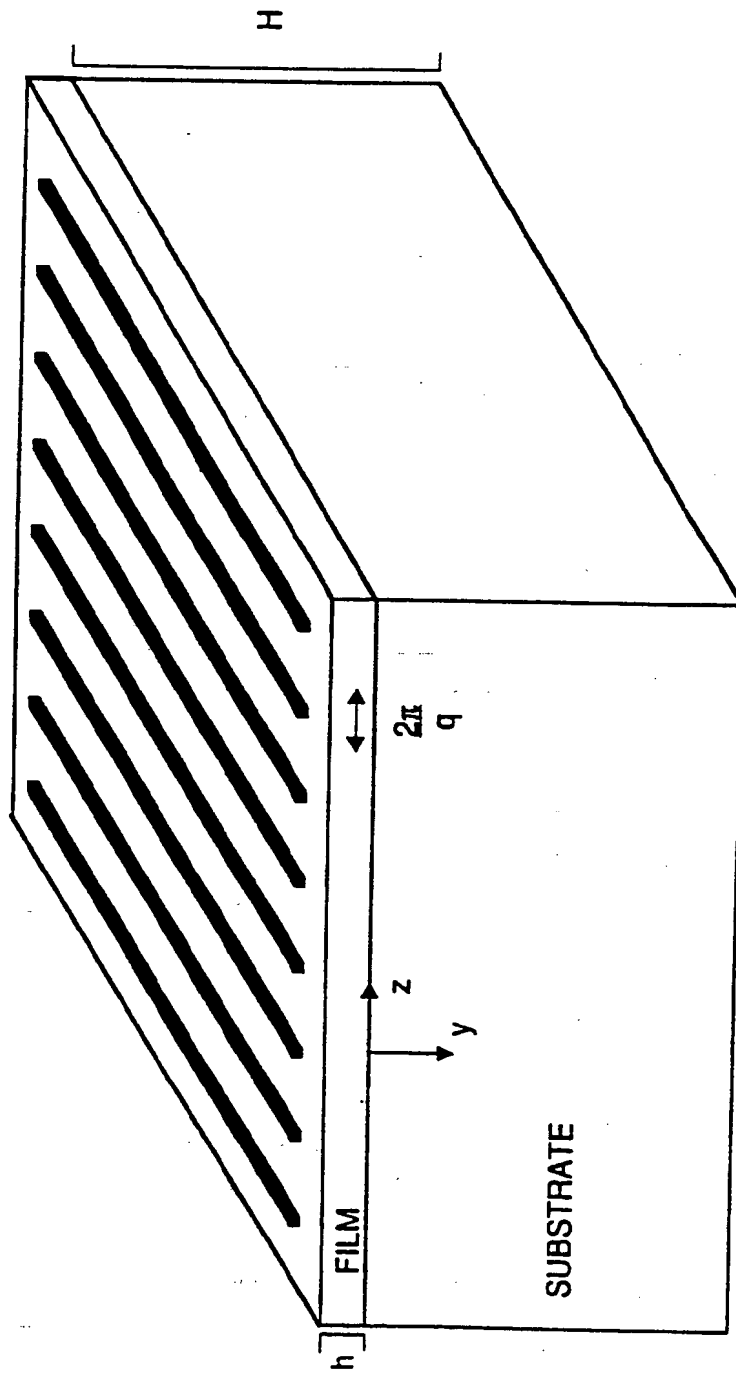


SUBSTITUTE SHEET

FIG 6

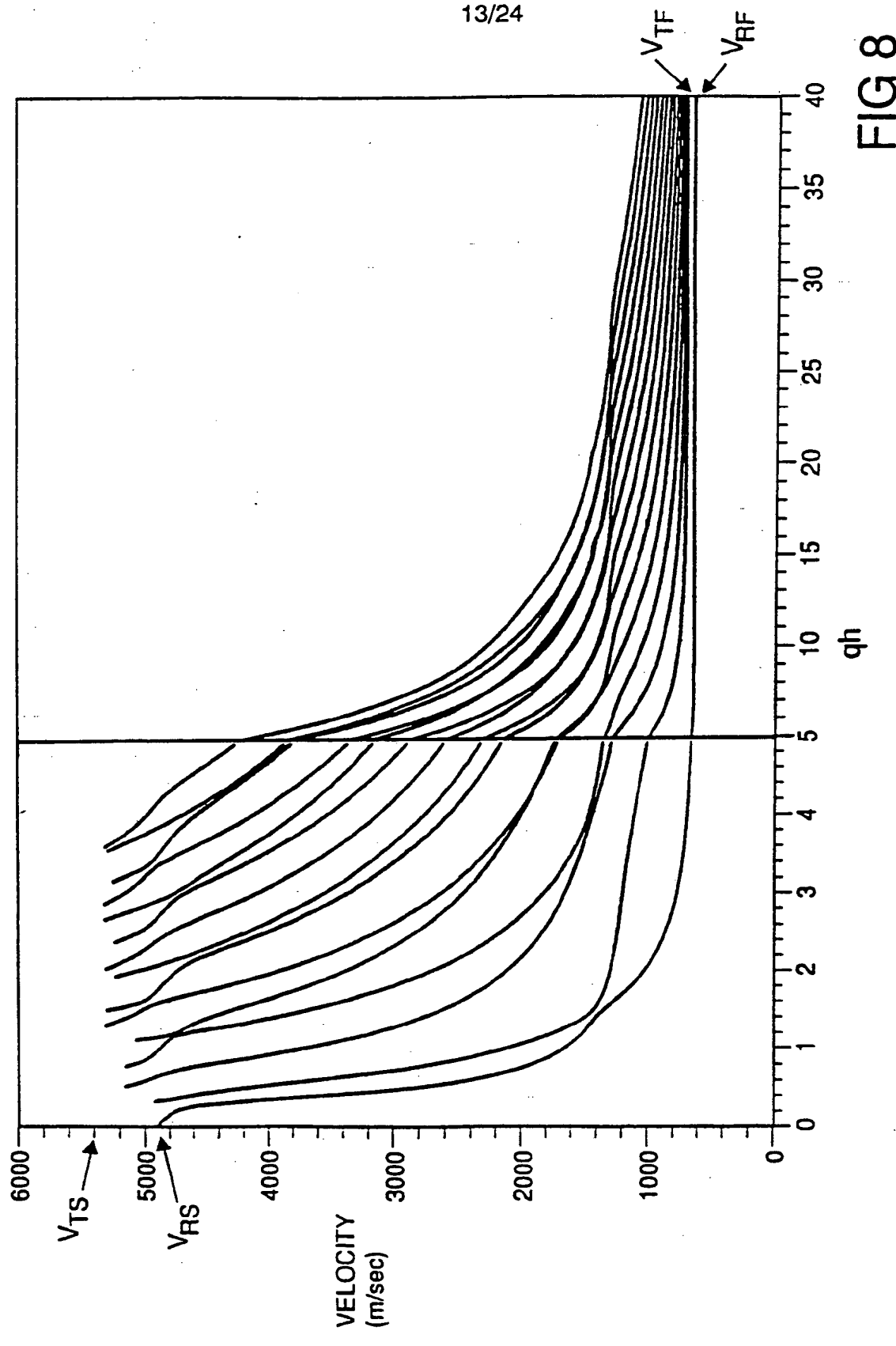
12/24

FIG 7



SUBSTITUTE SHEET

13/24



SUBSTITUTE SHEET

FIG 8

14/24

FIG. 9A

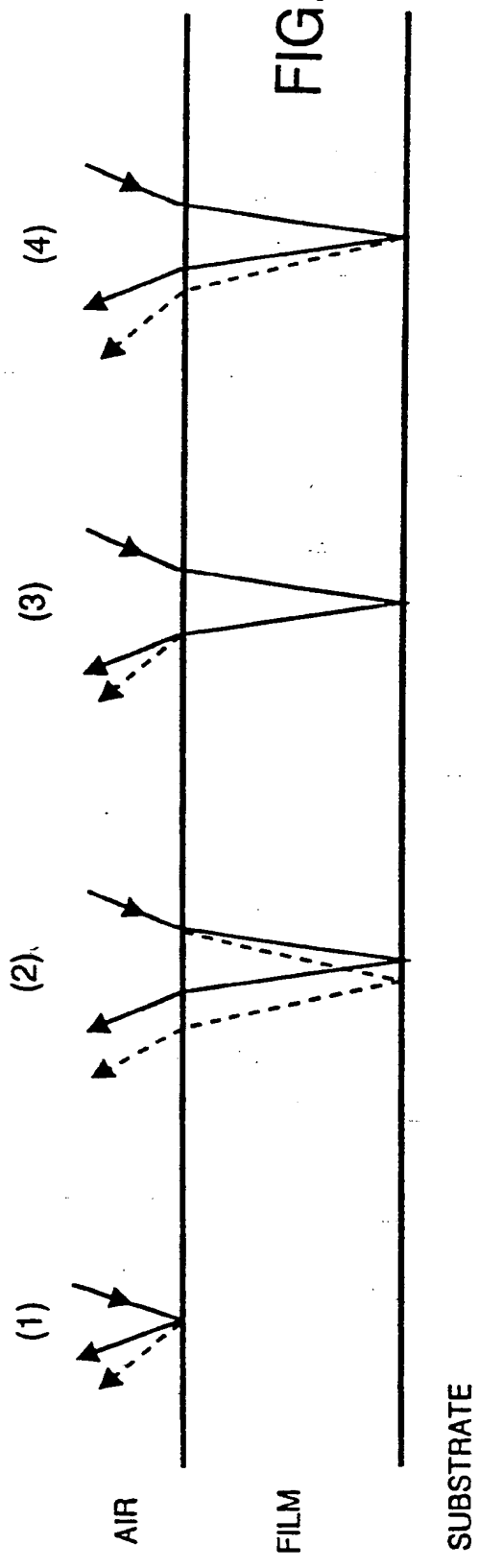
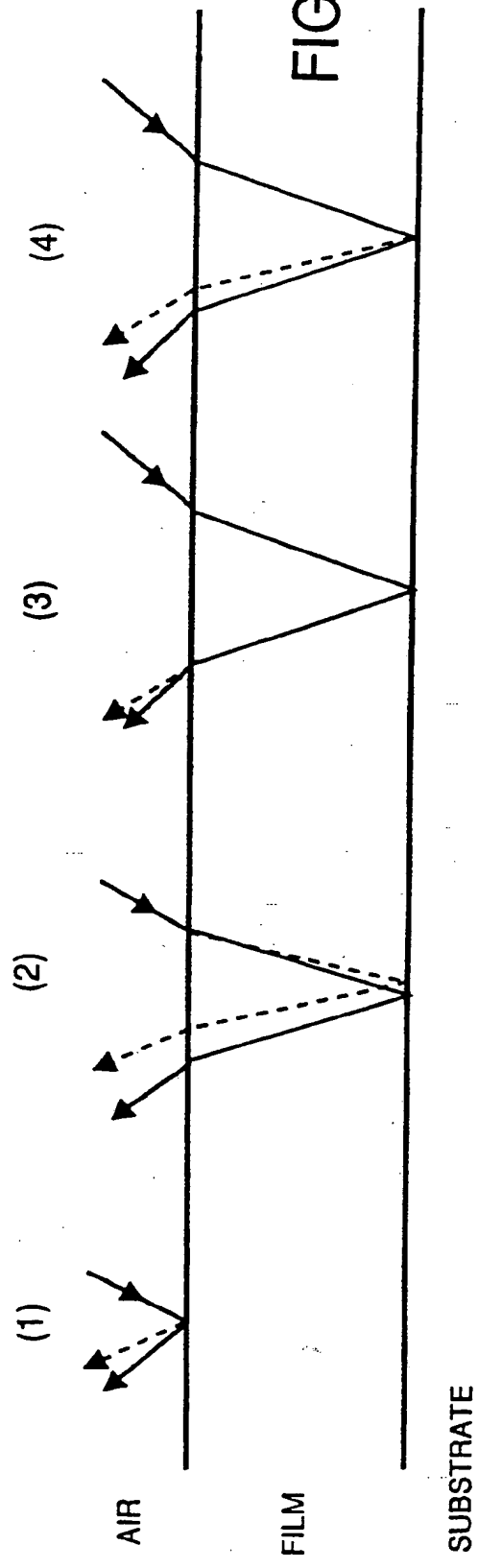
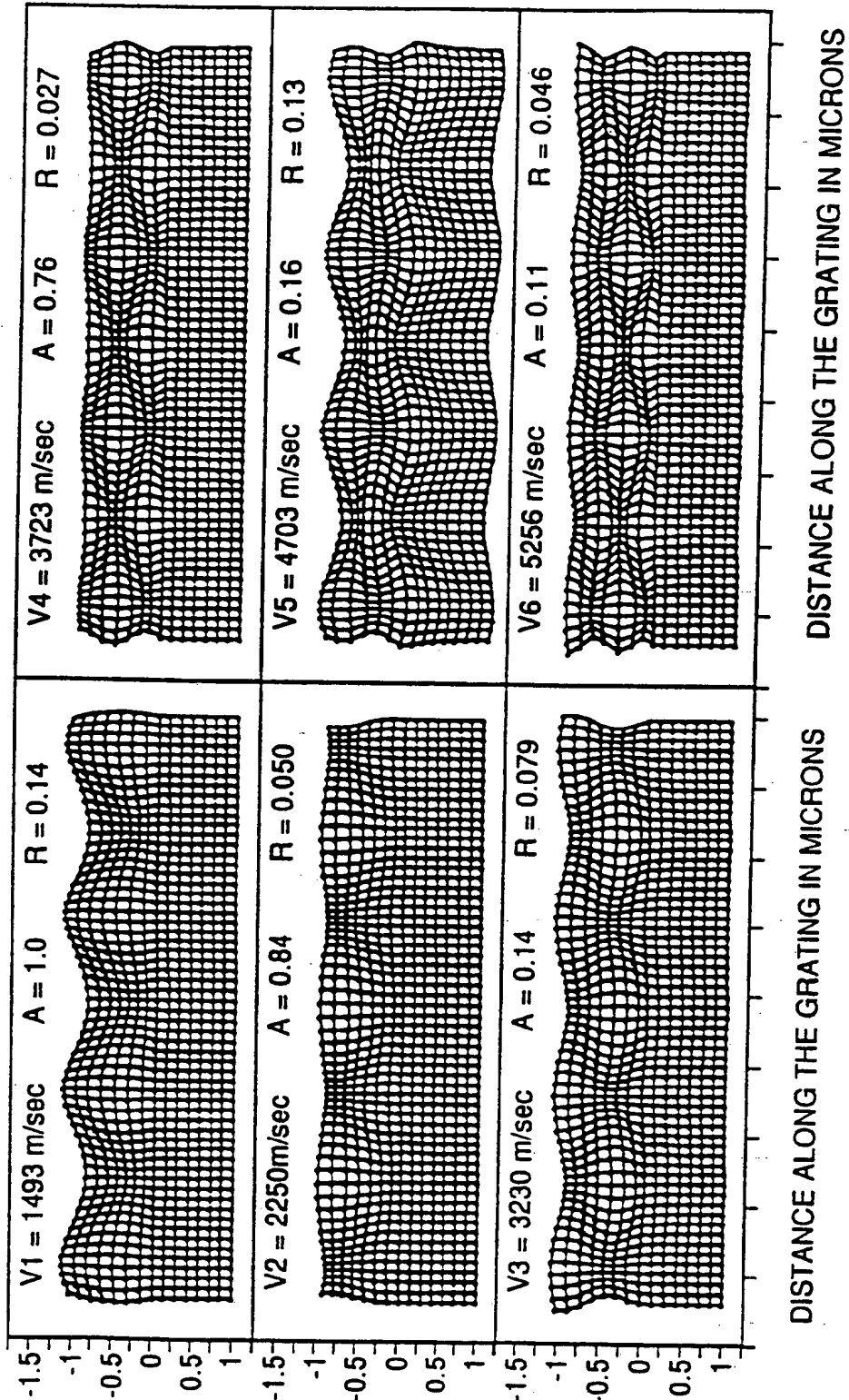


FIG. 9B



SUBSTITUTE SHEET

15/24



SUBSTITUTE SHEET

FIG 10

16/24

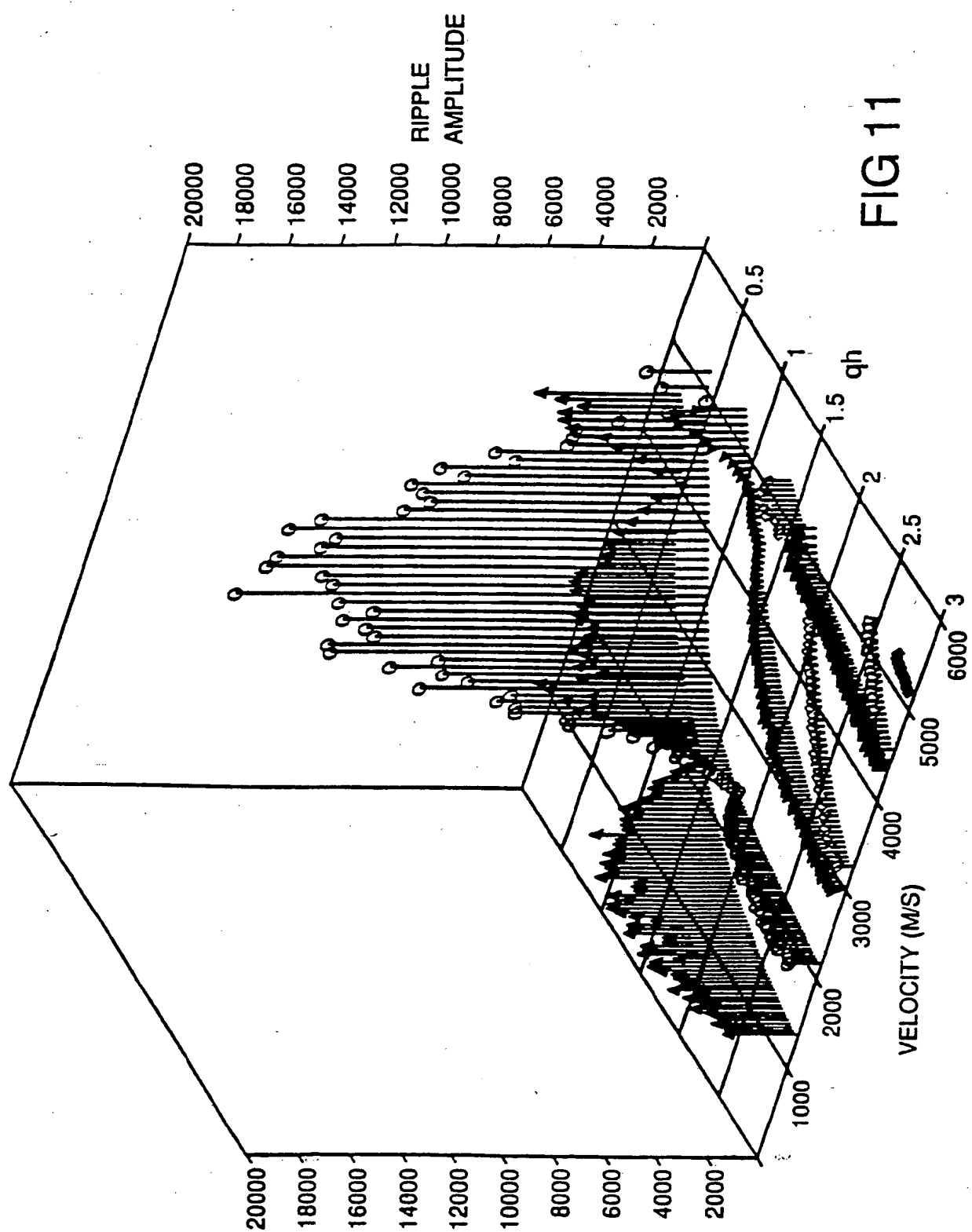


FIG 11

SUBSTITUTE SHEET

17/24

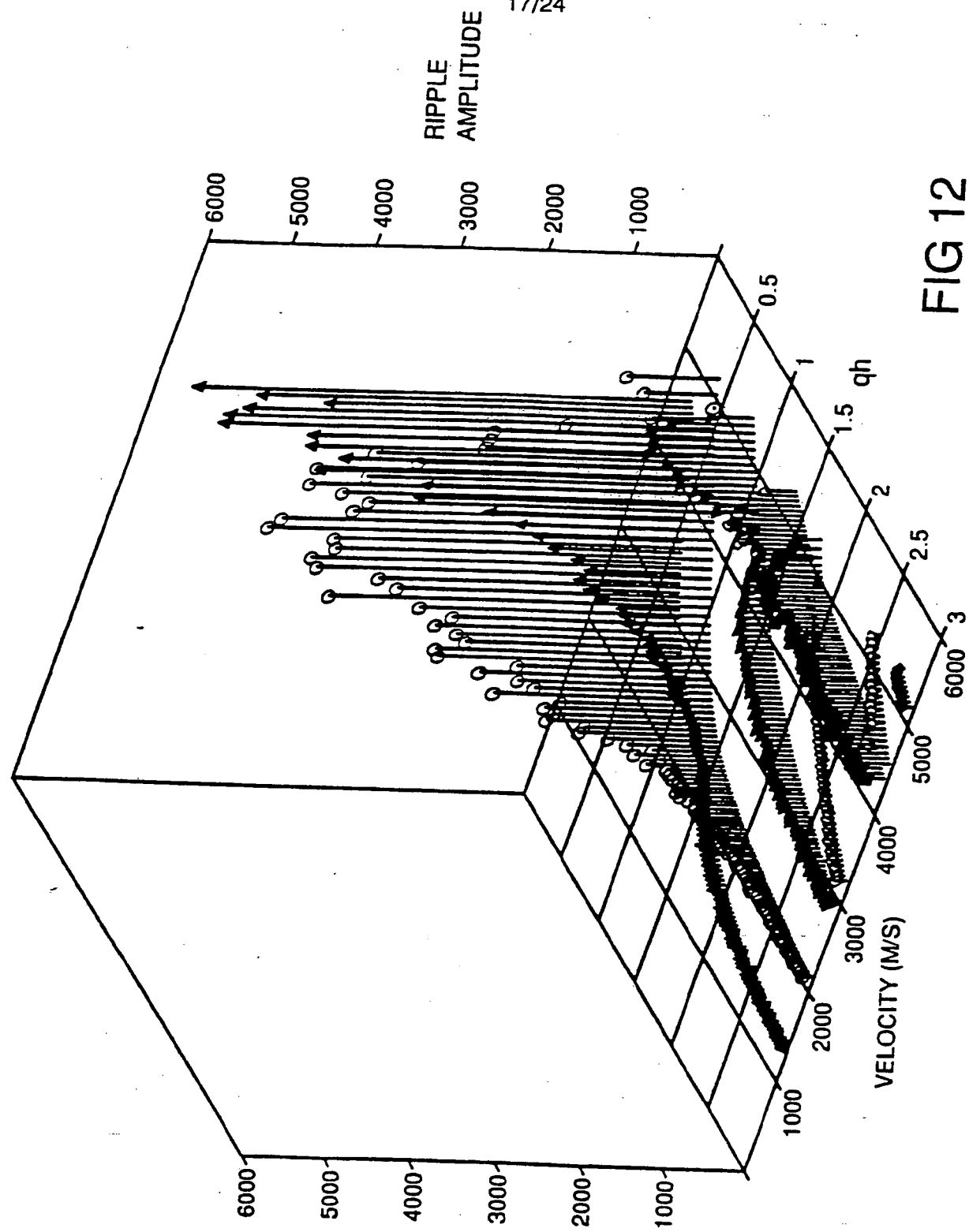
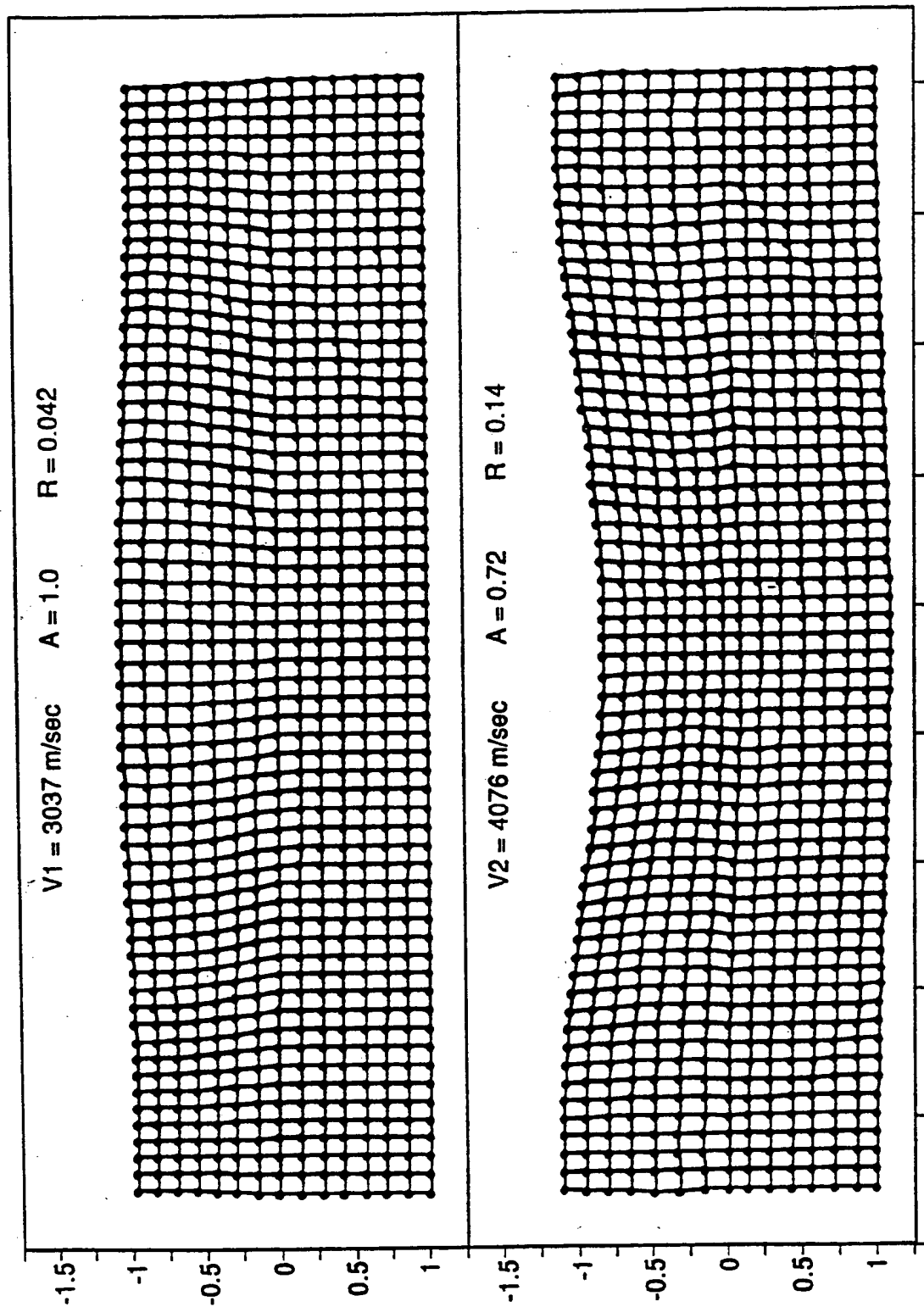


FIG 12

SUBSTITUTE SHEET

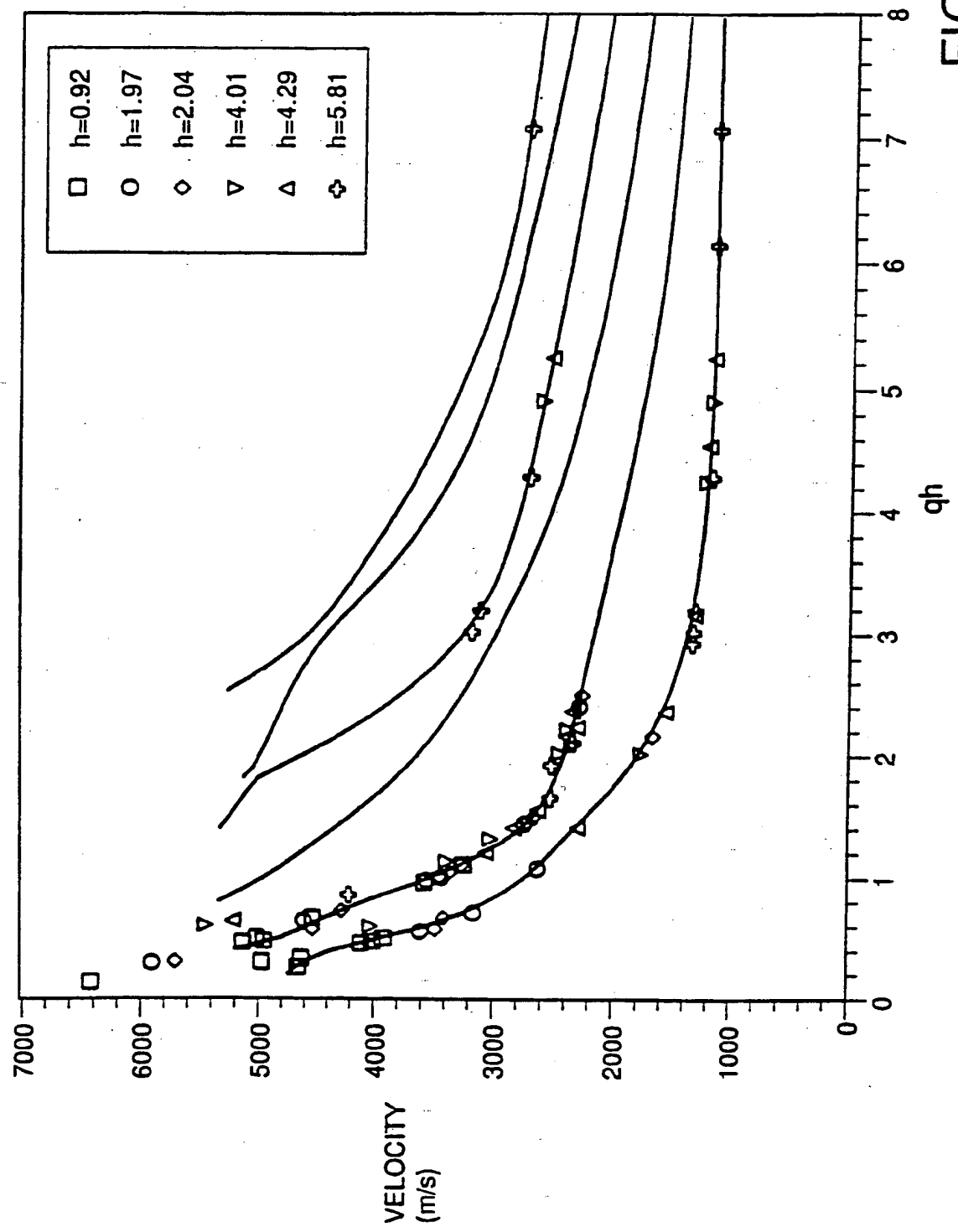
18/24



DISTANCE ALONG THE GRATING IN MICRONS

FIG 13

SUBSTITUTE SHEET



SUBSTITUTE SHEET

FIG 14

20/24

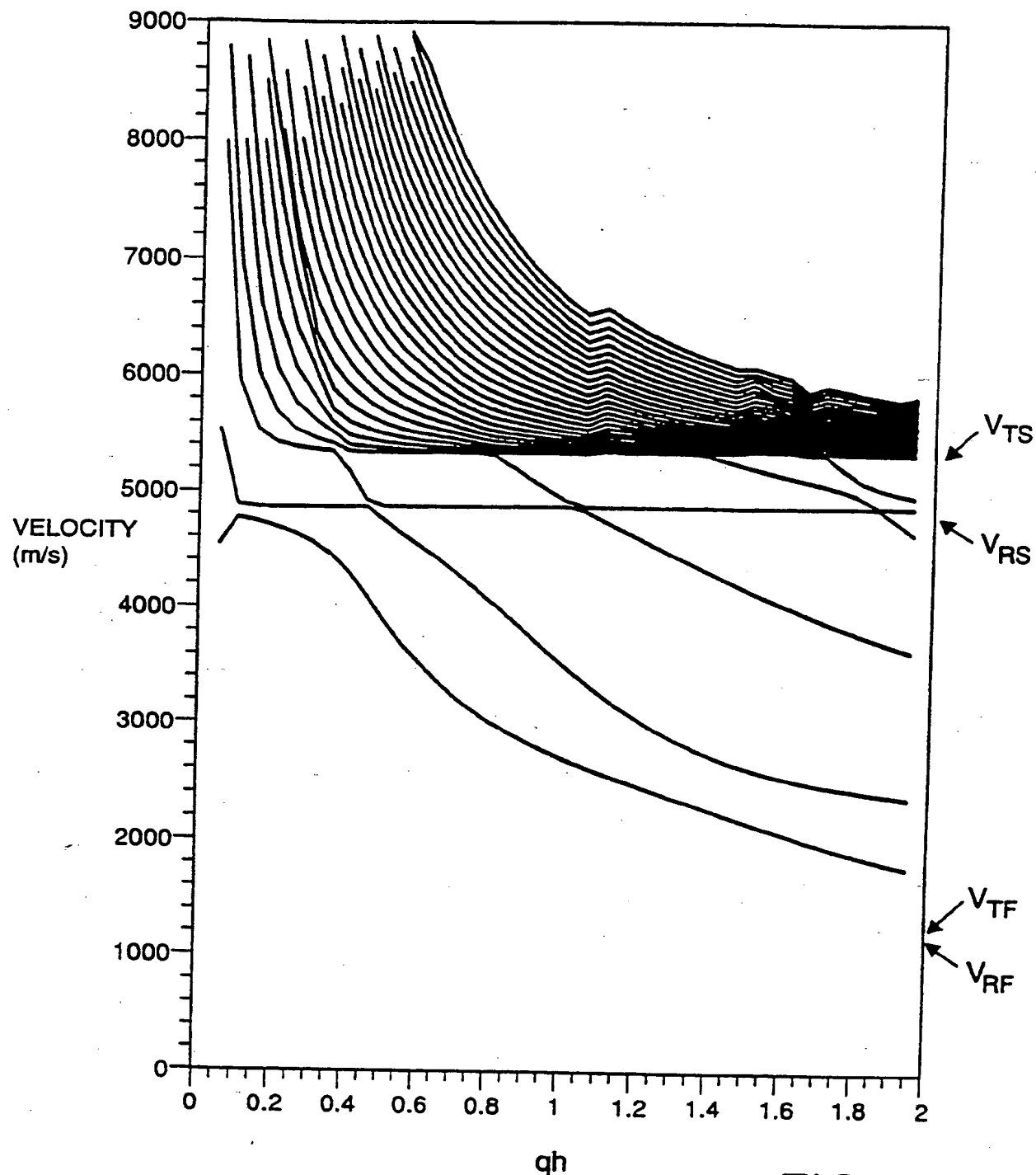
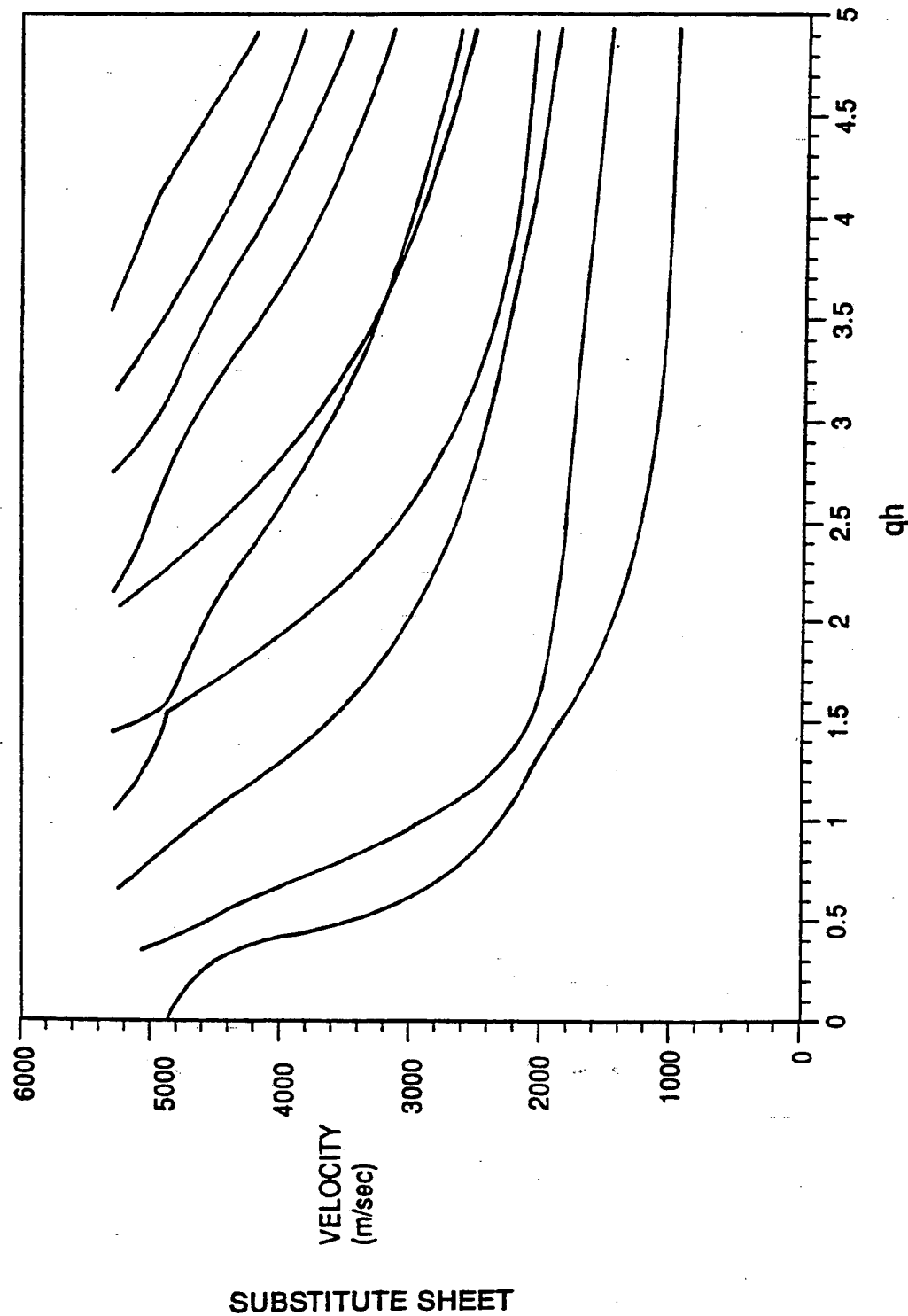


FIG 15

SUBSTITUTE SHEET

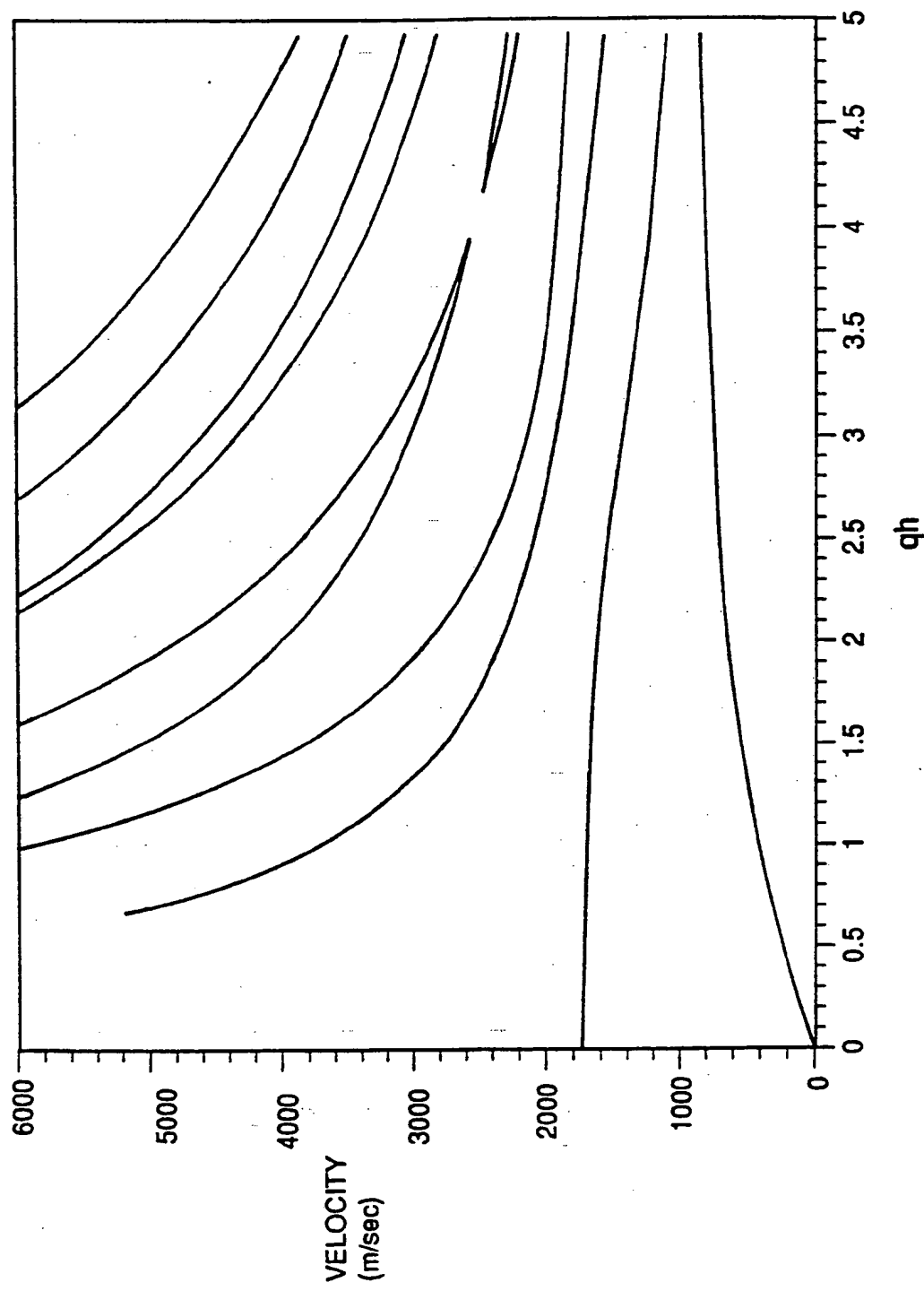
21/24

FIG 16



22/24

FIG 16a



SUBSTITUTE SHEET

23/24

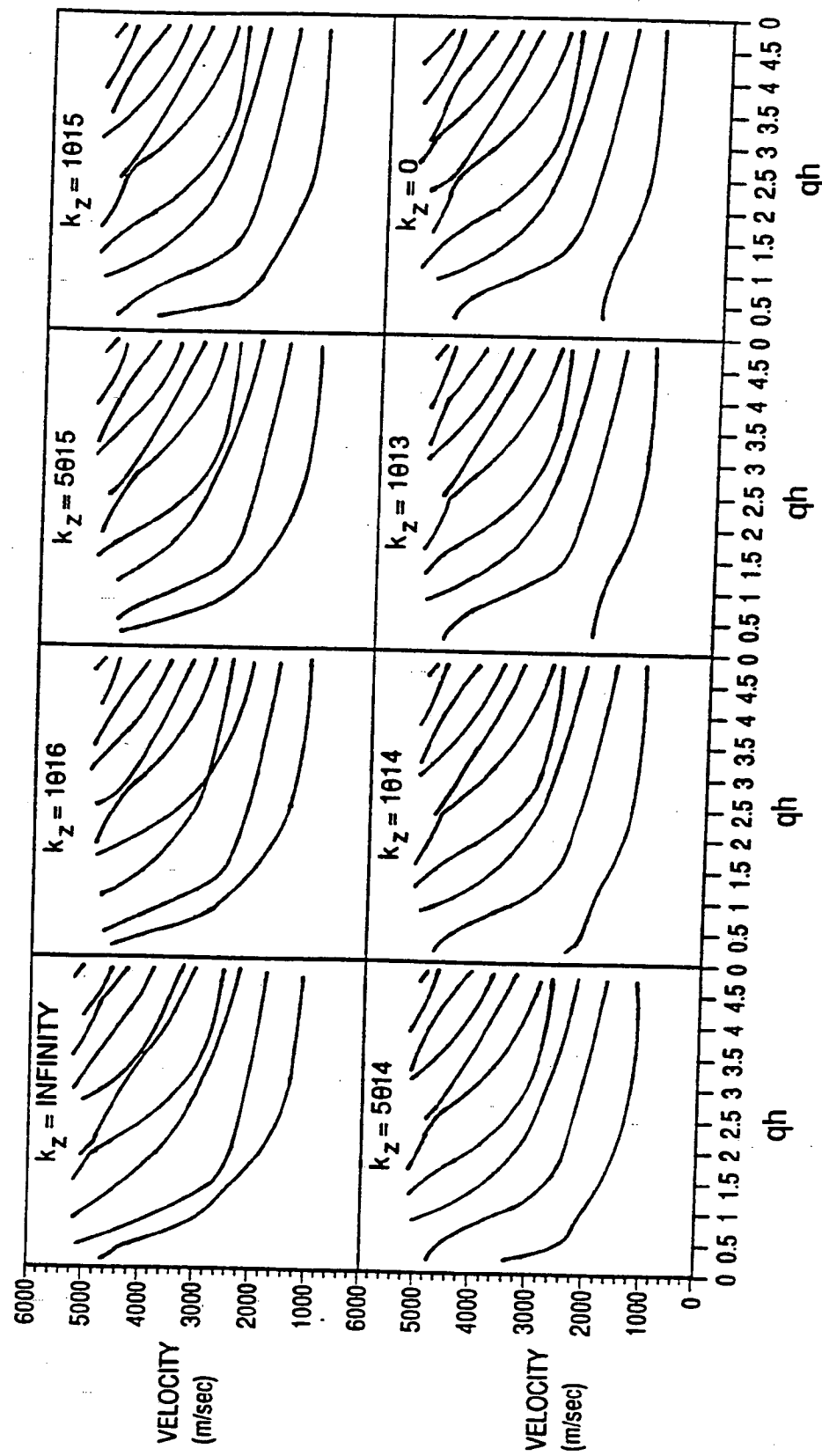


FIG 17

24/24

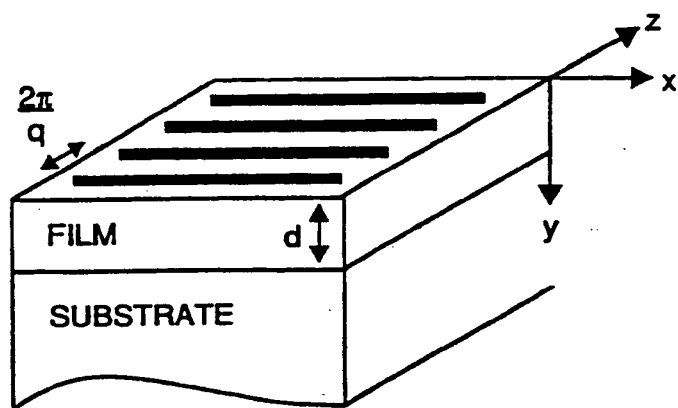


FIG 18

SUBSTITUTE SHEET

# INTERNATIONAL SEARCH REPORT

International application No.

PCT/US92/05679

## A. CLASSIFICATION OF SUBJECT MATTER

IPC(5) :G01J 3/30

US CL :356/318

According to International Patent Classification (IPC) or to both national classification and IPC

## B. FIELDS SEARCHED

Minimum documentation searched (classification system followed by classification symbols)

U.S. : 356/432T; 73/655

Documentation searched other than minimum documentation to the extent that such documents are included in the fields searched

Electronic data base consulted during the international search (name of data base and, where practicable, search terms used)

none

## C. DOCUMENTS CONSIDERED TO BE RELEVANT

Category*	Citation of document, with indication, where appropriate, of the relevant passages	Relevant to claim No.
X	Polymer July 1989, vol. 30, Burzynski et al., "Study of Anisotropy of Acoustic Wave Propagation in Stretched Poly (Vinylidene Di Fluoride) Film using the Picosecond Transient Grating Technique. See entire document.	1-52
X	Appl. Phys. Lett, 29 June 1987, vol. 50 Epinet, "Laser Induced Gratings in Nematic/Cholesteric Mixtures See entire document.	1-18,21-31,33-34,36-42,45-52
X	Chemical Physics Letters, 20 October 1989, vol. 162 Methetal, "Generation and Detection of Acoustic Waveguide Modes in Ultra thin Crystals using Transient Grating Technique "see entire document.	1-18,21-31,33-34,36-42,45-52
X	J. Appl. Phys. February 1982, vol. 53, Nelson et al, "Optical Generation of Tunable Ultrasonic Waves" See entire document.	1-18,21-31,33-34,36-42,45-52

Further documents are listed in the continuation of Box C.  See patent family annex.

* Special categories of cited documents:	"T"	later document published after the international filing date or priority date and not in conflict with the application but cited to understand the principle or theory underlying the invention
"A" document defining the general state of the art which is not considered to be part of particular relevance	"X"	document of particular relevance; the claimed invention cannot be considered novel or cannot be considered to involve an inventive step when the document is taken alone
"E" earlier document published on or after the international filing date	"Y"	document of particular relevance; the claimed invention cannot be considered to involve an inventive step when the document is combined with one or more other such documents, such combination being obvious to a person skilled in the art
"L" document which may throw doubts on priority claim(s) or which is cited to establish the publication date of another citation or other special reason (as specified)	"&"	document member of the same patent family
"O" document referring to an oral disclosure, use, exhibition or other means		
"P" document published prior to the international filing date but later than the priority date claimed		

Date of the actual completion of the international search

24 AUGUST 1992

Date of mailing of the international search report

5-11-1992

Name and mailing address of the ISA/  
Commissioner of Patents and Trademarks  
Box PCT  
Washington, D.C. 20231

Facsimile No. NOT APPLICABLE

Authorized officer

K. HANTIS

Telephone No. (703) 608-4801

Form PCT/ISA/210 (second sheet)(July 1992)\*

## INTERNATIONAL SEARCH REPORT

International application No.  
PCT/US92/05679

## C (Continuation). DOCUMENTS CONSIDERED TO BE RELEVANT

Category*	Citation of document, with indication, where appropriate, of the relevant passages	Relevant to claim No.
X	J. Appl. Phys. 01 April 1990, vol. 67, Meth et al, "Experimental and Theoretical Analysis of Transient Grating Generation and Detection of Acoustic Waveguide Modes in Ultrathin Solids," See entire document.	1-18,21-31,33-34,36-42,45-52
X	US,A, 4,522,510, (Rosenzweig et al.) 11 June 1985, See entire document.	1-6,9-18,20-22,25-27,28-31,33-42,45-52

Form PCT/ISA/210 (continuation of second sheet)(July 1992)★

The quality is considered a factor which relates the similarity or dissimilarity of the optical responses of the several samples to the generation of a stress wave or pulse by the pump beam.

- 5 This invention also pertains to the application of the pump and/or probe beams at different spatial locations on the sample with the intention of characterizing an intervening part of sample. The intervening part of the sample may be, by example, an interface, a crack, or a material in which  
10 signals cannot be directly generated, but which is desired to characterize.

The teaching of this invention furthermore pertains to methods and apparatus for exciting modes of one or two dimensional patterned objects for the purpose of  
15 characterizing their shapes, layer thickness, adhesion, and structural integrity. This aspect of the invention may be considered as a generalization of the foregoing features and advantages, and is directed to samples which are not thin films of uniform thickness and which may be large  
20 compared to their thickness. For these samples the analysis preferably includes the calculation of the stress, strain, electric fields due to the pump and probe light pulses, etc., as a function of two or three spatial coordinates rather than only the distance from the surface  
25 of the sample. While the time-step method described above may not be applicable to solving this problem, because it is applicable to one dimension, other numerical simulation methods may be applied to perform the calculation of how the stress changes with time. Also, the previously  
30 described simulations employ optical transfer matrices to calculate the electric field distribution of the pump light and the change in optical reflectivity (or other changes in the characteristics) of the probe light. However, the optical transfer matrix method is not applicable to

the arrival time of the echo. The function  $f(t)$  may be the shape of the echo measured on a reference sample having known physical characteristics or determined by simulation.

- 5 The echo time, or times, as determined are then used to yield film thicknesses or interface characteristics.

In view of the foregoing descriptions, it should thus be realized that the teaching of this invention also pertains to methods for deducing the physical characteristics of thin films or interfaces, in which the steps include the

- 10 sequential application of some or all of the above-described methods in order to determine the physical parameters of a complex sample having more than one layer or interface.

The teaching of this invention also pertains to methods for

- 15 deducing the sound velocity and refractive index of a film or substrate in which a stress wave is generated by a light pulse, and in which an oscillating response is observed in the detected probe beam as a function of delay, and measurements of the oscillation period are made

- 20 corresponding to at least two angles of incidence of the probe beam on the sample's surface. Measurements at several angles may be made sequentially or simultaneously. In this case the film may be partially absorbing, and could be a film which is underneath (i.e., on the substrate side

- 25 of) another partially-absorbing film or films.

Also encompassed by the teachings of this invention are methods of relating the quality of a sample to another reference sample prepared under a particular set of conditions, by comparing the observed temporal response of

- 30 the sample with that measured for the reference sample under similar conditions. The result of the comparison may or may not ascribe a cause for any observed differences to a specific physical or chemical property of either sample.

structures, to a stress pulse that is induced by the pump pulse, to simulations of the array of vibrating structures.

Further in this regard, the teaching of this invention also pertains to methods for deducing the physical characteristics of thin films patterned mechanically or by lithographic means into structures. Steps of the method include simulation of the mechanical vibrations of a single structure, calculation of the change in the probe beam after it impinges on the structure, and adjusting the physical characteristics of the simulated structure and interfaces in order to obtain a best fit to the observed response.

Further in accordance with the teaching of this invention, a picosecond ultrasonic system employs a method for deducing the physical characteristics of a sample, and uses an analysis of an acoustic echo or echoes based on either or both of the following two methods.

In a first method a characterization of the time of arrival of an echo is obtained by means of the location in time of one or more echo features, such as a point of maximum or minimum amplitude or inflection point.

In a second method a characterization of the time of arrival of the echo as seen in  $\Delta R(t)$  (or, by example,  $\Delta T(t)$ ,  $\Delta P(t)$ ,  $\Delta \phi(t)$ , and  $\Delta \delta(t)$ ) by convolution of the measured echo with a suitably chosen function  $f(t)$  of the time. Thus, the convolution

$$C(t_1) = \int \Delta R(t) f(t-t_1) dt \quad (12)$$

is calculated. The time  $t_1$  is then adjusted so as to maximize the result of the convolution, i.e. to maximize  $C$ . The resulting value of  $t_1$  is then used as an estimate of

- sample that includes, by example, a very thin film on a substrate, or a very thin film on a significantly thicker film. By example, a substrate may have a layer of a metal, such as aluminum, and an intervening layer comprised of a polymer. The measured response is then analyzed to determine the damping rate of the thickness vibration of the film. This damping rate is compared with a damping rate determined for a model based on classical acoustics in which the interface between the thin film and the substrate (or thicker film) is characterized by a coupling parameter ("adhesion strength") per unit area. This coupling parameter, which may be considered to be a spring constant parameter that is a linear property per unit area, is the strength of a spring per unit area which connects the surface of the thin film to the substrate, or to the thicker film. The adhesion strength is adjusted to give agreement between the simulation and the measured value of the damping, and is thus used as a measure of the quality of the interface.
- As was also indicated previously, the teaching of this invention furthermore pertains to a picosecond ultrasonic system in which a sample is comprised of an array of identical structures having dimensions much less than the pump and probe spot diameter. In this case each structure is simultaneously excited by the pump beam and then simultaneously examined by the probe beam. The response of each structure is simulated by the methods described above. The characteristics of the structures are then deduced by comparison of the simulation and the measured response.
- Relatedly, this invention also teaches methods for deducing the dimensions of substantially identical patterned structures arranged periodically, and for deducing the statistical distribution of sizes of such structures. This is accomplished by comparing the observed response of the

gives a change in the reflection coefficient of the probe light which can be calculated according to the methods described above. Let this change when the nth mode has unit amplitude be  $B_n$ . This change is linear in the 5 amplitude of the acoustic normal mode. Hence, the total change in the reflectivity of the probe light at time zero is

$$\Delta R(t=0) = \sum_n A_n B_n. \quad (10)$$

Fifth, let the frequency of the nth normal mode be  $f_n$ .  
10 Then the total change in reflectivity of the probe light at any later time t can be calculated as

$$\Delta R(t) = \sum_n A_n B_n \cos(2\pi f_n t). \quad (11)$$

This simulation method has the advantage that through the use of the formula just given the change in reflectivity at 15 any chosen time, or within any chosen time range, may be calculated without the need to consider the acoustic or optical processes occurring in the sample for all times intermediate between the application of the pump pulse and the time of interest. It is important to note that the 20 amplitudes  $A_n$  and the coefficients  $B_n$  need be calculated only once, and can then be used to find the response at any later time.

It should be further noted that the above description refers to the use of this method for the calculation of the 25 change in reflected intensity of the probe beam. However, completely analogous methods can be used to simulate the other responses of interest, i.e.  $\Delta T$ ,  $\Delta P$ ,  $\Delta \phi$ , and  $\Delta \theta$ .

As was indicated previously, the teaching of this invention is also directed to a picosecond ultrasonic system which 30 enables the measurement of a vibrational response of a

- very difficult and time-consuming because of the very large number of acoustic modes with very closely-spaced frequencies. However, for the purposes of creating an accurate simulation of the typical data on this type of sample it is not necessary to use the actual thickness of the substrate. Instead it is sufficient to consider the "substrate" to have a thickness much less than the real physical substrate. The thickness of this artificial substrate should be sufficiently large such that the time required for an acoustic wave to propagate through the substrate from the thin films deposited on the front surface of the substrate to the far side of the substrate and back again is longer than the total time span over which the data to be simulated extends. Thus, for example, if the data extends from zero time delay of the probe relative to the pump to a time delay of 1000 psecs, and the sound velocity  $v$  in the substrate is  $5 \times 10^5$  cm sec $^{-1}$ , then the artificial substrate can be taken to have a thickness of as little as 2.5 microns. If the thickness is at least this great no acoustic echoes can return from the back of the substrate during the time that measurements are made, and hence the difference in thickness between the artificial substrate and the actual substrate is irrelevant.
- Third, the initial stress distribution produced by the pump beam is decomposed into a sum over the normal modes just calculated. It is possible to choose a set of amplitudes for the normal modes such that when the contributions of each normal mode are added together, taking allowance for the amplitude of each mode, the initial stress distribution is accurately reproduced. The initial amplitude of the nth normal mode may be denoted as  $A_n$ .
- Fourth, each normal mode has a characteristic spatial stress pattern associated with it. This stress pattern

For both of these methods it is important to establish the autofocus conditions prior to making measurements of  $\Delta V_{\text{probe-refl}}$ , since C depends on the value of  $A_{\text{effective}}$ .

The teaching of this invention furthermore encompasses a picosecond ultrasonic system in which the results of measurements are compared with computer simulations of the measured response, as described above, but using a different method to perform the simulation. In this case the following steps may be employed.

5      10      First, the initial stress distribution in the structure is calculated using the method described above.

10      15      Second, the acoustical normal modes of the structure are calculated through solution of the equations of physical acoustics together with appropriate boundary conditions at the interfaces between the films, at the free surface of the sample, and at the free surface of the substrate. All normal modes up to certain maximum frequency  $f_{\text{max}}$  are calculated. The choice of this maximum frequency is related to the sharpness of the features, such as echoes, 20      that appear in the measured data. As an approximate rule, if it is desired to simulate data for a structure of interest which has a characteristic time-scale  $\tau$ , it is necessary to choose  $f_{\text{max}}$  such that the product of  $f_{\text{max}}$  and  $\tau$  is at least as large as unity. Thus, for example, if the 25      measured data contains an echo of width 1 psec, then to perform an accurate simulation it is desirable to calculate all normal modes up to the frequency 1000 GHz.

30      The substrate thickness is typically in the range around 200 microns, whereas often the total thickness of the thin films deposited onto the substrate is a micron or even less. A calculation of the normal modes of a sample consisting of films on a substrate of this thickness is

Eq. 6 could be expressed as

$$\Delta V_{\text{probe-refl}} = C V_{\text{probe-inc}} \Delta R_{\text{sim}}(t) V_{\text{pump-inc}} (1-R_{\text{pump}}) \quad (8)$$

where  $\Delta V_{\text{probe-refl}}$  is the output voltage from detector used to measure the change in the power of the reflected probe light (D1),  $V_{\text{pump-inc}}$  is the output voltage from the detector used to measure the incident pump light (D4), and  $V_{\text{probe-inc}}$  is the output voltage of the detector used to measure the incident probe light (D2). Thus, to provide an effective instrument it is sufficient to determine the constant C. This can be accomplished by either of the following two methods.

- (a) A first method measures the transient response  $\Delta V_{\text{probe-refl}}$  for a sample in which all of the quantities are known which enter into the calculation of the simulated reflectivity change  $\Delta R_{\text{sim}}(t)$  of the sample when it is illuminated with a pump pulse of unit energy per unit area of the sample. Next, the method measures  $V_{\text{probe-inc}}$  and  $V_{\text{pump-inc}}$ , then determines  $R_{\text{pump}}$  either by measurement or from the computer simulation. The method then finds the value of the constant C such that Eq. 8 is satisfied.
- (b) A second method measures the transient response  $\Delta V_{\text{probe-refl}}$  for a reference sample for which the transient optical response  $\Delta R(t)$ , when it is illuminated with a pump pulse of unit energy per unit area of the sample, has been measured using a system which has been previously calibrated, for example, by one or more of the methods described above. The method then measures  $V_{\text{probe-inc}}$  and  $V_{\text{pump-inc}}$ , determines  $R_{\text{pump}}$  by measurement, and then finds the value of the constant C such that the following equation is satisfied.
- $\Delta V_{\text{probe-refl}} = C V_{\text{probe-inc}} \Delta R(t) V_{\text{pump-inc}} (1-R_{\text{pump}}) \quad (9)$

To build a truly effective instrument it is essential that the effective area  $A_{\text{effective}}$  be stable throughout the course of a sequence of measurements. To ensure this, the system of this invention incorporates means for automatically focusing the pump and probe beams onto the surface of the sample so as to achieve a reproducible intensity variation of the two beams during every measurement. The automatic focusing system provides a mechanism for maintaining the system in a previously determined state in which the size and relative positions of the beams on the sample surface are appropriate for effective transient response measurements.

It should be noted that for any application in which the amplitude of an optical transient response is used to draw quantitative conclusions about a sample (for example, when the magnitude of a feature that arises from an acoustic echo is influenced by the condition of a buried interface) a calibration scheme such as described above must be a feature of the measurement system.

The preceding description of the method for the comparison of the computer simulation results and the system measurements supposes that the several detectors in the measurement system are calibrated. It is contemplated that such a system will use detectors operating in the linear range so that the output voltage  $V$  of each detector is proportional to the incident optical power  $P$ . For each detector there is thus a constant  $G$  such that  $V=GP$ . The preceding description assumes that the constant  $G$  is known for each and every detector. In the case that this information is not available, the individual calibration factors associated with each of the individual detectors measuring  $P_{\text{probe-inc}}$ ,  $P_{\text{pump-inc}}$ , and  $\Delta P_{\text{probe-refl}}$  may be combined with  $A_{\text{effective}}$  and  $f$  into a single overall system calibration constant  $C$ . Therefore in terms of a calibration factor  $C$ ,

the sample, i.e.,  $I_{\text{probe-inc}} (\frac{\text{--}}{\text{I}})$  and  $I_{\text{pump-inc}} (\frac{\text{--}}{\text{I}})$  as a function of position, and uses the results of these measurements to calculate  $A_{\text{effective}}$ . This is possible to accomplish but requires very careful measurements which may be difficult to accomplish in industrial environment.

- 5 (b) A second method measures the transient response  $\Delta P_{\text{probe-refl}}$  for a sample on a system S for which the area  $A_{\text{effective}}$  is known. This method then measures the response  $\Delta P_{\text{probe-refl}}$  of the same sample on the system S' for which  $A_{\text{effective}}$  is to be determined. The ratio of the responses on the two systems gives the inverse of the ratio of the effective areas for the two systems. This can be an effective method because the system S can be chosen to be a specially constructed system in which the areas illuminated by the pump and probe 10 beams are larger than would be desirable for an instrument with rapid measurement capability. Since the areas are large for this system it is simpler to measure the 15 intensity variations of the pump and probe beams over the surface of the sample, i.e.,  $I_{\text{probe-inc}} (\frac{\text{--}}{\text{I}})$  and  $I_{\text{pump-inc}} (\frac{\text{--}}{\text{I}})$  as 20 a function of position. This method is effective even if the quantities which enter into the calculation of the simulated reflectivity change  $\Delta R_{\text{sim}}(t)$  are not known.

- (c) A third method measures the transient response  $\Delta P_{\text{probe-refl}}$  for a sample in which all of the quantities are known which 25 enter into the calculation of the simulated reflectivity change  $\Delta R_{\text{sim}}(t)$  of the sample when it is illuminated with a pump pulse of unit energy per unit area of the sample. Then by comparison of the measured transient response  $\Delta P_{\text{probe-refl}}$  with the response predicted from the Eq. 6 the effective 30 area  $A_{\text{effective}}$  is determined.

where  $I_{\text{probe-inc}}$  ( $\frac{\wedge}{x}$ ) and  $I_{\text{pump-inc}}$  ( $\frac{\wedge}{x}$ ) are respectively the intensities of the probe and pump beams on the surface of the sample. One can consider  $A_{\text{effective}}$  to be an effective area of overlap of the pump and probe beams.

- 5      Analogous expressions can be derived for the change in optical transmission  $\Delta T(t)$ , the change in optical phase  $\Delta\phi(t)$ , the change in polarization  $\Delta P(t)$ , and the change  $\Delta\beta(t)$  in the angle of reflection of the probe light.

The following quantities are measured by the system:  $\Delta P_{\text{probe-refl}}$ ,  $P_{\text{probe-inc}}$ ,  $P_{\text{pump-inc}}$ ,  $R_{\text{pump}}$ ,  $R_{\text{probe}}$ . The computer simulation gives predicted values for  $AR_{\text{sim}}(t)$ ,  $R_{\text{pump}}$ , and  $R_{\text{probe}}$ . Thus the following comparisons can be made between the simulation and the system measurements in order to determine the characteristics of the sample.

- 15     (1) A comparison of the simulated and measured reflection coefficient  $R_{\text{pump}}$ .

(2) A comparison of the simulated and measured reflection coefficient  $R_{\text{probe}}$ .

- 20     (3) A comparison of the simulated and measured transient change  $\Delta P_{\text{probe-refl}}$  in the power of the reflected probe light.

To make a comparison of the simulated and measured change, it can be seen from the preceding equation (6) that it is necessary to know the value of  $A_{\text{effective}}$ . This can be accomplished by one or more of the following methods.

- 25     (a) A first method directly measures the intensity variations of the pump and probe beams over the surface of

$$\frac{P_{\text{pump-inc}}}{A_{\text{pump}}} \frac{(1-R_{\text{pump}})}{f} \quad (3)$$

where  $f$  is the repetition rate of the pump pulse train, and  $R_{\text{pump}}$  is the reflection coefficient for the pump beam. Thus, the change in optical reflectivity of the each probe light pulse will be

$$\Delta R_{\text{sim}}(t) \frac{P_{\text{pump-inc}}}{A_{\text{pump}}} \frac{(1-R_{\text{pump}})}{f} \quad (4)$$

5 and the change in power of the reflected probe beam will be

$$\Delta P_{\text{probe-refl}} = P_{\text{probe-inc}} \Delta R_{\text{sim}}(t) \frac{P_{\text{pump-inc}}}{A_{\text{pump}}} \frac{(1-R_{\text{pump}})}{f} \quad (5)$$

In a practical system the illumination of the sample does not, in fact, produce a uniform intensity of the incident pump beam. Moreover, the intensity of the probe light will also vary with position on the sample surface. To account 10 for these variations the equation for  $\Delta P_{\text{probe-refl}}$  is modified to read

$$\Delta P_{\text{probe-refl}} = P_{\text{probe-inc}} \Delta R_{\text{sim}}(t) \frac{P_{\text{pump-inc}}}{A_{\text{effective}}} \frac{(1-R_{\text{pump}})}{f} \quad (6)$$

where the effective area  $A_{\text{effective}}$  is defined by the relation

$$A_{\text{effective}} = \frac{\int I_{\text{pump-inc}}(\vec{r}) dA \int I_{\text{probe-inc}}(\vec{r}) dA}{\int I_{\text{pump-inc}}(\vec{r}) I_{\text{probe-inc}}(\vec{r}) (dA)} \quad (7)$$

to laterally patterned structures will be evident to workers skilled in the relevant art, when guided by the following teachings. Similarly, the following discussion will consider, again as a specific example, a particular 5 one of the transient optical responses, namely the change  $\Delta R(t)$  in optical reflectivity. The generalization of the discussion to a consideration of the other transient optical responses aforementioned should also become evident to workers skilled in the relevant art, when guided by the 10 following teachings.

In this example the computer simulations calculate the change in the optical reflectivity  $\Delta R_{\text{sim}}(t)$  of the sample when it is illuminated with a pump pulse of unit energy per unit area of the sample. The simulation also gives a value 15 for the static reflection coefficient of the pump and probe beams. The system measures the transient change  $\Delta P_{\text{probe-refl}}$  in the power of the reflected probe pulse as determined, for example, by photodiode D1 in Fig. 18. It also measures the static reflection coefficients of the pump and probe beams 20 from a ratio of the power in the incident and reflected beams. The incident probe power is measured by photodiode D2 in Fig. 18, the reflected probe power is measured by D1, the incident pump power is measured by D4, and the reflected pump power is measured by D3.

25 To relate the simulation results for the transient change in the optical reflectivity to the system measurement it is necessary to know: (a) the power of the pump and probe beams; (b) the intensity profiles of these beams; and (c) their overlap on the sample surface.

30 Let us suppose first that the pump beam is incident over an area  $A_{\text{pump}}$  and that within this area the pump intensity is uniform. Then for each applied pump pulse the pump energy absorbed per unit area is

layer of mass at the interface which affects the acoustic propagation. The contamination layer C may also lead to additional optical absorption at the interface. The additional optical absorption of the pump pulse will in 5 this case result in additional stress waves to be generated at the interface. The detection of these additional stress waves provides a means for detecting the presence of the contamination layer C. This method can be applied to advantage for detecting contamination on the surface of 10 optically transparent bulk materials.

A thirteenth adjustable parameter is related to dimensions other than thickness and geometrical shape. These parameters are generally not relevant to measurements on samples consisting solely of planar films. Instead, these 15 adjustable parameters enter into the characterization of samples of the type mentioned above with respect to laterally patterned structures and the like. These adjustable parameters apply as well to the characterization of an array of identical structures having dimensions much 20 less than the pump and probe spot diameter, as described below.

- A further adjustable parameter relates to the presence of and thickness of a region of intermixing between two adjacent layers.
- 25 An important aspect of this invention concerns the precise relation between the computer simulations and the transient optical responses measured by the system. The following discussion describes the essential aspects of this relation for the particular example of a sample containing a number 30 of planar films whose lateral extent is much greater than their thickness, and also greater than the linear dimensions of the region of the sample illuminated by the pump and probe pulses. A generalization of this discussion

electronic diffusivity of a particular film in the structure can be determined.

It should be appreciated that the seventh and eight adjustable parameters provide, separately or in conjunction  
5 with one another, a means for the determination of the electrical resistance of metallic films.

A ninth adjustable parameter involves the optical constants of the film(s) and/or substrate.

10 A tenth, related adjustable parameter is the derivatives of the optical constants with respect to stress or strain.

An eleventh adjustable parameter is the surface roughness. The surface roughness has the consequence that a stress pulse reflected at the surface of a sample is broadened.  
15 This broadening may be introduced into the simulation and adjusted until the simulation gives the best agreement with the measured data. In this way the surface roughness can be determined.

20 A twelfth adjustable parameter is interfacial contamination. If an interface between two materials A and B is contaminated by the presence of a thin layer of another material C, the presence of the layer C affects the reflection and transmission coefficients for stress waves incident on the interface. For two elastic media in perfect mechanical contact the reflection and transmission  
25 coefficients are given by well-known formulas from physical acoustics. The effect of interface adhesion strength on the coefficients is discussed below. The coefficients may also be affected by other effects which are unrelated to adhesion strength. For example, in addition to changing  
30 the strength of the coupling between A and B (i.e., the adhesion strength) the contamination layer C provides a

the average phase change of the pump and/or probe beams upon reflection; and/or the average polarization and optical phase of the incident and reflected pump and/or probe beams.

5 A fourth adjustable parameter is interface roughness. By example, the interface roughness parameter causes a broadening of a stress pulse which is transmitted across, or reflected at, the interface.

10 A fifth adjustable parameter is the interface adhesion strength, as will be described in further detail below.

A sixth adjustable parameter is the static stress. One suitable procedure by which this can be determined has been described previously in the context of measurements made at two or more temperatures of the sample.

15 A seventh adjustable parameter is the thermal diffusivity. The thermal diffusivity of the different films in the sample affects the shape and magnitude of the generated stress pulses. By treating the thermal diffusivity as an adjustable parameter, and selecting it to give the best 20 agreement between the simulation and the measured data, the thermal diffusivity of a particular film in the structure can be determined.

An eighth adjustable parameter is the electronic diffusivity. In some samples which contain metal films with 25 high electrical conductivity the diffusion of the conduction electrons before they lose the energy that they have received from the pump pulse has a large effect on the shape and magnitude of the stress pulses which are generated. By treating the electronic diffusivity as an 30 adjustable parameter, and adjusting it to give the best agreement between the simulation and the measured data, the

September 1988, H.T. Grahn et al., wherein reference is made to a simulation of a multilayer structure and a variation in layer thickness (as well as sound velocities). As was reported in this article, it was not possible to 5 find parameters such that the simulated response was in agreement with an experimentally observed  $\Delta R(t)$ . Reference may also be had, by example, to the following articles that were also coauthored by one of the inventors of this patent application: "Sound velocity and index of refraction of 10 AlAs measured by picosecond ultrasonics", Appl. Phys. Lett. 53 (21), 21 November 1988, pp. 2023-2024, H.T. Grahn et al.; "Elastic properties of silicon oxynitride films determined by picosecond acoustics", Appl. Phys. Lett. 53 (23), 5 December 1988, pp. 2281-2283, H.T. Grahn et al.; 15 and "Study of vibrational modes of gold nanostructures by picosecond ultrasonics", Appl. Phys. 73 (1), 1 January 1993, pp. 37-45, H.N. Lin et al.

A second adjustable parameter is the sound velocity. An example of a situation in which one may determine the sound 20 velocity has been described above. Thus, in this context what is taught is the determination of the parameters n, d, and v by comparison of the measured data with simulations, rather than by a measurement of the frequency  $f(\theta)$  as a function of the angle  $\theta$ .

25 A third adjustable parameter is the crystal orientation in a film. This can be achieved through measurement of the sound velocity, which is dependent on crystal orientation in all crystals, even those with cubic symmetry. In non-cubic crystals the crystal orientation of the film, or the 30 preferential orientation of crystalline grains, leads to anisotropic optical properties which can be detected via the measurements of the above described optical measures of the optical reflectivity by determining the incident and reflected average intensity of the pump and/or probe beams;

the distance along the direction normal to the surface of the sample. It is within the scope of this invention to extend the calculations to allow for the variation in the intensity of the pump and probe beams within the plane of 5 the surface of the sample. This approach is useful for the calculation of the change in the propagation angle of the reflected probe light  $\Delta\theta$ .

A series of such simulations are performed in which the assumed thicknesses of the films in the structure are 10 varied. By comparison of the results of the simulation with some or all of the measured quantities  $\Delta R$ ,  $\Delta T$ ,  $\Delta P$ ,  $\Delta\phi$  and  $\Delta\theta$  the thicknesses of the films are determined.

It is also within the scope of this invention to adjust the film thicknesses so as to be consistent with results of any 15 or all of: (a) measurements of the optical reflectivity through measurements of the incident and reflected average intensity of the pump and/or probe beams; (b) measurements of the average phase change of the pump and/or probe beams upon reflection; and (c) measurements of the average 20 polarization and optical phase of the incident and reflected pump and/or probe beams.

It is further within the scope of the teaching of this invention to include simulations which incorporate as 25 adjustable parameters at least one of the following for one or more films in order to find a best-fit to measured data.

A first adjustable parameter is the film thickness, so as to adjust the thicknesses obtained in accordance with the method described above.

In this regard reference can be had to an article entitled 30 "Time-resolved study of vibrations of  $\alpha$ -Ge:H/ $\alpha$ -Si: multilayers", Physical Review B, vol. 38, no. 9, 15

In some samples, particularly metal films of high electrical conductivity, a more detailed treatment of the diffusion of energy is required. The energy in the pump light pulse is initially input to the conduction electrons, 5 thereby raising their energy considerably above the Fermi level. These electrons have a very high diffusion coefficient and may spread a significant distance through the sample before losing their excess energy as heat to the lattice. Under these conditions the diffusion of the 10 energy is not adequately described by Fourier's law for classical heat conduction. Instead it is preferred to use a more microscopic approach, taking into account the diffusion rate of the electrons and the rate at which they lose energy.

15 (C) Calculation of the transient response measured by the probe

From the calculated strain distribution as a function of depth into the sample, the changes  $\Delta n$  and  $\Delta \kappa$  in the optical constants are calculated. This step requires knowledge of 20 the derivatives of the optical constants  $n$  and  $\kappa$  with respect to elastic strain.

From the calculated changes  $\Delta n$  and  $\Delta \kappa$  in the optical constants as a function of depth, and the unperturbed optical constants of the films, at least one of the 25 quantities  $\Delta R$ ,  $\Delta T$ ,  $\Delta P$ ,  $\Delta \phi$  and  $\Delta \beta$  is calculated and compared with the measured results. This calculation is most conveniently carried out through the use of optical transfer matrices.

The above description of the simulation steps A-C is 30 presented in terms of a one-dimensional model considering only the variation of the electric field of the probe light, the elastic stress, the elastic strain, etc., upon

passing through whatever films are deposited onto the substrate, is negligible. This condition holds for the majority of structures which are of current industrial interest.

- 5 When this condition is not satisfied, and light does reach the substrate, it is desirable to include in the simulation a thickness of the substrate sufficient to include the entire depth over which the pump or the probe light can significantly penetrate. This depth is typically some
- 10 number, e.g. five, of absorption lengths of the pump or probe light. This region of the substrate is then divided into bins of thickness as specified above. The last bin of the substrate is then treated according to the following boundary conditions.
- 15 First, at each time step the stress within the last bin of the substrate, and propagating towards the interior of the substrate, can be considered to be completely transferred into the remainder of the substrate so that no part of this stress is reflected. Second, the stress within the last
- 20 bin of the substrate, and propagating towards the film structure, is taken to be zero.

For some samples the above division of the simulation into the consideration of the calculation of the temperature rise and the propagation of the stress may not be applicable. It is noted that, as soon as energy is deposited into any part of the sample, a stress is set up and mechanical waves are launched into adjacent regions. If the diffusion of energy is sufficiently large and continues for a sufficient period of time then the changing

25 temperature and associated stress distribution in the sample will continue to generate new stress waves. However, the extension of the simulation to include this

30 effect is straightforward.

side of the boundary and still propagating in the same direction and partly into the original bin but propagating in the reverse direction. The fraction of the stress that is stepped across the interface and the fraction which 5 reverses direction are calculated from the laws of physical acoustics. At the top (free) surface of the structure the stress in the bin adjacent to the surface and propagating towards the surface remains in the same bin but has its direction reversed, i.e., it becomes a stress pulse 10 propagating into the interior of the structure rather than towards the top surface. By applying this procedure to all bins for a sufficient number of time steps  $\tau$ , the stress distribution can be calculated for as long a time as is required for comparison with the measured results. From 15 the calculated stress the strain is calculated by division by the appropriate elastic coefficient.

Samples that are of interest in chip fabrication typically have a number of thin films deposited on top of a semiconductor substrate. Presently, the total thickness of 20 these thin films is a few microns or less, whereas the substrate is typically approximately 200 microns thick. An important advantage of this "stepping method" is that it is not necessary to consider stress propagation throughout the entire substrate. Instead it is normally sufficient to 25 consider just one bin of the substrate together with "boundary conditions" specified as follows.

(1) At each time step  $\tau$  the stress within the single bin of the substrate and propagating towards the substrate can be considered to be completely transferred into the remainder 30 of the substrate so that no part of this stress is reflected. (2) The stress within the substrate bin and propagating towards the film structure is taken to be zero. This description of the treatment of the substrate holds if the amount of light that reaches the substrate, after

matrices. Next, from the calculated electric field distribution, the energy absorbed in the structure as a function of position is calculated. Next, the effect of thermal diffusion on the absorbed energy distribution is  
5 considered. Next, the temperature rise of each part of the sample is calculated. This temperature rise is the energy deposited per unit volume divided by the specific heat per unit volume. Next, the stress at all points in the sample is then calculated from the temperature rise by multiplying  
10 the temperature rise by the thermal expansion coefficient and the appropriate elastic modulus.

(B) Change in stress and strain with time

The change in stress and strain in the sample is next calculated as a function of time and position using the  
15 laws of physical acoustics. This calculation is effectively performed by means of a "stepping algorithm", which performs the following computations.

First, a time step  $\tau$  is chosen. For each film or layer that comprises the structure of interest a bin size  $b$  equal to  
20 the time  $\tau$  multiplied by the sound velocity in the film is then calculated. Each film is then divided into bins of this size or smaller. By example, smaller size bins can be employed at any film boundary. The time step  $\tau$  is chosen so that each film preferably contains a large number of  
25 bins. The results of the foregoing give the stress set up by the pump pulse in each bin of the structure. Next, the stress in each bin is decomposed into two components, one initially propagating towards the free surface of the sample and one away from it. Within a given film these two  
30 components are stepped forward from bin to bin in the appropriate direction. For a bin adjacent to the boundary between two films the stress propagating towards the boundary is stepped partly into the first bin on the other

- surface from one point to another. A second purpose is to generate bulk waves which travel through the sample from the pumped region to the probe spot. Other applications pertain to structures that are laterally patterned. In 5 this case the pump light may be directed so as to be absorbed in a "dot", i.e. a film which has a very small area. Stress waves generated in this dot then propagate to the region of the structure that is sensed by the probe pulse.
- 10 Also disclosed is a picosecond ultrasonic system in which the results of measurements are compared with computer simulations of the measured response or responses (1)-(5), for example. To perform the simulation the following steps are performed. Reference is also made to the flow chart of 15 Fig. 21.

(A) Initial stress distribution

The stress distribution in the sample produced as a result of the absorption of the pump pulse is calculated using known values for the optical absorption of the various 20 materials present in the sample, the specific heats of these materials, the thermal expansion coefficients, and the elastic constants. To calculate the stress distribution the effect of thermal diffusion may be taken into account. For a sample composed of several planar films 25 of different materials with material properties uniform throughout each film the following procedure is used.

From the optical constants and thicknesses of the films the electric field due to the pump light pulse at all points in the structure is calculated in terms of the amplitude, 30 angle of incidence, and polarization of the pump beam incident on the sample surface. This calculation is most readily performed through the use of optical transfer

scattered pump light. This embodiment is employed to advantage when the pump and probe sources have different wavelengths. The suppression of the pump light improves the signal to noise ratio when the sample surface is non-  
5 specular, and where the incident pump light is scattered at the sample surface.

The invention further provides a picosecond ultrasonic system that incorporates optical elements for delivering the probe beam to the sample, and which allows the  
10 location, shape and/or size of the probe spot on the sample to be kept substantially constant and free from changes due to the variation of the optical path length of the probe. This is a more general case than the above-mentioned use of an optical fiber for a similar purpose. Furthermore,  
15 "active" correction schemes can be employed in which the characteristics of the probe spot are sensed, and in which the characteristics of probe beam (e.g., profile and location) are adaptively corrected.

The invention further teaches a picosecond ultrasonic system that incorporates an optical guiding system in which the pump and probe beams are focused separately onto the sample. The pump and probe beams may be scanned laterally relative to each other. In particular, a guiding and focusing system can be employed in which the probe beam is  
20 guided through an optical fiber assembly with a tapered end which effects near field focusing into a spot which is smaller than the pump beam, and which may be scanned over small displacements relative while the pump beam is held substantially stationary. The use of a reduced tip fiber  
25 makes it possible to achieve spots for the pump and probe with dimensions as small as 1000 Å.  
30

It is thus possible to investigate the properties of a sample through the study of waves propagating across the

mechanical delay stage. This has the advantage that a mechanical stage is not required. In addition, the data can be acquired very quickly, provided that the signal-to-noise ratio is acceptable.

5 This invention further teaches a picosecond ultrasonic system that employs a multi-element delay stage. This has the advantage that the delay of the probe pulse is increased for a given distance moved by the mechanical stage. Thus, the distance travelled by the stage in order  
10 to produce a given delay of the probe pulse can be decreased.

Furthermore, the invention teaches the measurement of the transient optical properties of the sample using a probe pulse that is derived from an output pulse of the laser  
15 that is different from the output pulse used for the pump. This enables the production of a large effective delay for the probe, without requiring that a very long optical path difference be established in the system.

The invention also teaches a picosecond ultrasonic system  
20 which may include suitable additional optical sources, including additional lasers as well as white light sources. These sources may be directed to the sample by a guiding system which may include some elements in common with the pulsed pump and probe beam paths. These additional light  
25 sources may be used to effect ellipsometry or reflectometry, or to illuminate the sample for inspection purposes, or to raise the temperature at a particular location.

In one aspect the invention provides a picosecond  
30 ultrasonic system that incorporates the color filter F1 in the path of the probe beam after it has been reflected or transmitted at the sample for the purpose of suppressing

This invention further teaches a picosecond ultrasonic system which incorporates an optical fiber or fibers for any of the following purposes: (a) guiding the laser beam between different parts of the optical system; (b) guiding the pump and/or probe to the sample; (c) collecting the reflected or transmitted probe from the sample; and/or (d) maintaining a constant probe output profile and position for varying input conditions.

The picosecond ultrasonic system in accordance with this invention may incorporate light sources with any of the following features.

A first feature employs a pulsed laser with the output directed to an optical harmonic generator or generators, as in Figs. 19 and 20. The outputs of the harmonic generator 138 and/or the unmodified output of the laser are thus used for the pump and/or probe beams. This improves on conventional practice in that it allows for the rejection of the pump light at the detector of the probe beam so as to improve the signal to noise ratio. Also, for certain samples the most advantageous wavelength for the generating pump beam may be different from the optimum wavelength for the probe beam.

A second feature employs one or more of the polarizing beam splitters which are used to continuously vary the ratio of the pump and probe beams under computer control. The ratio can be controlled to optimize the signal to noise for a given sample. It may be advantageous to change the ratio to achieve the best performance for samples with particular characteristics.

This invention further teaches a picosecond ultrasonic system that incorporates different repetition rate lasers to effect a delay as an alternative approach to a

sound velocity, but only the change of the velocity with temperature. This is an important point, since to determine the absolute velocity it would be necessary to have a very precise value for the film thickness. To determine the 5 temperature-dependence of the sound velocity, on the other hand, requires only a measurement of the temperature-dependence of the acoustic transit time. To determine the temperature-dependence of the sound velocity from this quantity it is necessary only to apply a correction to 10 allow for the thermal expansion of the sample.

This invention further teaches a picosecond ultrasonic system which directly measures the derivative with respect to time delay between the pump and probe beams of some or all of the quantities listed above, i.e., (1) the small 15 modulated change  $\Delta R$  in the intensity of the reflected probe beam, (2) the change  $\Delta T$  in the intensity of the transmitted probe beam, (3) the change  $\Delta P$  in the polarization of the reflected probe beam, (4) the change  $\Delta\phi$  in the optical phase of the reflected probe beam, and/or (5) the change in 20 the angle of reflection  $\Delta\theta$  of the probe beam. To achieve the measurement of the derivative the probe pulse delay is varied periodically over a small range by means of an oscillating optical component in the pump or probe path. A frequency range of 10 Hz to 1 MHz is suitable for this 25 purpose.

One advantage of this method is as follows. In many applications one is interested in the time of arrival of acoustic echoes at certain points in the sample. These 30 acoustic echoes appear as sharp features in the measured reflectivity change  $\Delta R(t)$  as a function of time. These echoes can be enhanced relative to the background if the system directly measures the derivative of  $\Delta R$  (or the other quantities listed above) with respect to time, rather than  $\Delta R$  itself.

pump or probe beam is derived from the pulse rate of one or more of the pulsed lasers in the system. This overcomes a problem in the prior art, wherein the modulation is not synchronized with the repetition rate of the laser or 5 lasers. Thus, in each modulation cycle there can be a variation in the number of probe or pump pulses contained in one modulation cycle according to the instantaneous phase of the modulator relative to the timing of the laser pulses. This variation contributes to the noise of the 10 system, and is advantageously eliminated in the present invention.

This invention further teaches a picosecond ultrasonic system in which measurements for a particular sample are made at at least two temperatures for the purpose of 15 detecting the change in the sound velocity in one or more layers in response to the temperature change. The temperature change may be induced by a heat lamp directed at the surface of the sample, by a resistive heater in contact with the rear of the sample, by the average heating 20 of the sample by the pump light pulses, or by the use of another light source directed through some of the same optical elements used to guide the pump and/or probe beams onto the sample (or via some other optical system). The stress in one or more layers is determined by relating the 25 observed change in the sound velocity in one or more layers determined at two or more temperatures to the stress in the layer or layers.

As has been described, it has been established 30 experimentally that the temperature-dependence of the sound velocity depends on the static stress. This provides the basis for this aspect of the invention.

It is important to note that the application of this method does not require a measurement of the absolute value of the

The picosecond ultrasonic system in accordance with the teaching of this invention can also employ the simultaneous or sequential measurement of the ellipsometric parameters of the sample using signals corresponding to one or more  
5 suitable non-pulsed additional light sources (e.g., the He-Ne laser 136) whose optical path may or may not have some or all optical components in common with the means for directing the pulsed laser beams to and from the sample. This overcomes some of the difficulties of conventional  
10 systems in a manner similar to the methods described above.

An automatic adjustment of the position and orientation of the sample to achieve a desired overlap of the pump and probe beams on the sample surface can also be employed, in conjunction with the control of the spot size on the sample  
15 of one or both of the pump and probe lasers. This is accomplished, as described in reference to Figs. 16-20, with a means for detecting one or both beams after they impinge on the sample, and a means for adjusting the height and tilt of the sample with respect to the beams to achieve  
20 the desired focusing conditions. This approach is superior to the manual adjustment techniques taught by the prior art, in that an automatic adjustment scheme overcomes the difficulty of a slow and unreliable manual adjustment which is incompatible with the need to make rapid and accurate  
25 measurements in an industrial environment. Furthermore, the reproducability of measurements between samples is also improved.

It is also within the scope of this invention to provide a picosecond ultrasonics system using one or more modulators  
30 of the pump or probe beams in which the modulation drive signal for one or more of the modulators, and the pulse rate of one or more pulsed lasers, are derived from a common clock. In addition, it is also within the scope of the teaching of this invention that the modulation of the

change  $\Delta P$  in the polarization of the reflected probe pulse, the change  $\Delta\phi$  in optical phase of the reflected probe pulse, and the change in an angle of reflection  $\Delta\theta$  of the probe pulse. The measured transient responses are then  
5 associated with at least one characteristic of interest of the structure.

However, even when the measurement of  $\Delta P(t)$ ,  $\Delta\phi(t)$ , or  $\Delta\theta(t)$  does not show a response in which the feature of primary interest dominates, it may still be possible to  
10 effectively isolate the response of interest by a "differential method" (DM). That is, by taking a suitable linear combination of the different measured responses it may be possible to enhance the magnitude of the response of interest and reduce the size of the other competing  
15 response or responses.

The same type of DM procedure as just described can also be accomplished by making simultaneous or sequential measurements of one or more of the quantities  $\Delta R(t)$ , etc. at more than one wavelength of the pump and/or the probe,  
20 or angle of incidence of the pump and/or the probe, or polarization of the pump and/or the probe beams.

The same type of DM procedure can also be achieved for some samples by making measurements at more than one intensity of the pump and/or probe beams. The point is that the  
25 responses, such as the change in reflectivity  $\Delta R(t)$ , for example, may vary non-linearly with the intensity and/or the duration of the pump and/or probe pulses. Thus, again by taking suitable linear combinations of the responses measured at different intensities or pulse durations, it  
30 may be possible to enhance a portion of the response arising from one effect at the expense of competing effects.

referred to requires the identification of the different features that appear in the response  $\Delta R(t)$ . With the arrangement available in conventional systems the identification of the origin of the various features may be  
5 extremely difficult and/or time-consuming for a multi-layer structure. It is often necessary to make a guess that a particular feature arises from a stress pulse which originates at a particular location and has undergone a certain sequence of transmissions and reflections at  
10 different interfaces. In addition, it may be the case that a certain feature of interest, such as the arrival of a stress pulse at one particular interface, gives a response which happens to be dominated or masked by a larger response from another stress pulse reaching a different  
15 part of the structure at approximately the same time. The present invention overcomes these difficulties as follows.

As mentioned above, in the prior art the primary measured quantity for most samples of current technical interest is the change  $\Delta R(t)$  in optical reflectivity. If the response  
20  $\Delta R(t)$  is difficult to analyze, then it is also difficult to deduce the required information about the structure, for example the thicknesses of the different films. This difficulty may be overcome by measurements of  $\Delta P$ ,  $\Delta\phi$ , or  $\Delta\theta$ . For example, a particularly important feature may  
25 appear as a very small response in  $\Delta R(t)$ , but may make a dominant response in  $\Delta P(t)$ ,  $\Delta\phi(t)$ , or  $\Delta\theta(t)$ .

In accordance with an aspect of this invention the non-destructive system and method is enabled to also simultaneously measure at least two transient responses of  
30 the structure to the pump pulse. The simultaneously measured transient responses comprise at least two of a measurement of the modulated change  $\Delta R$  in an intensity of a reflected portion of a probe pulse, the change  $\Delta T$  in an intensity of a transmitted portion of the probe pulse, the

thickness to be deduced from a single measurement of the frequency  $f$ .

The foregoing example has been described in terms of a measurement of  $\Delta R(t)$ ; clearly the same technique may be  
5 applied to the other transient quantities.

For many samples of current interest in the semiconductor circuit fabrication industry it is not practical to measure the change  $\Delta T$  in the transmission of the probe light pulse. The films are normally deposited onto silicon substrates of  
10 thickness around 0.02 cm. Unless light of wavelength of one micron or greater is used, the light will be heavily absorbed in the substrate making the measurement of the transmission very difficult. For such samples conventional methods are thus essentially limited to the use of the  
15 measurement of the change  $\Delta R$  in the optical reflectivity induced by the pump pulse. Many samples of interest include a series of films deposited sequentially onto the substrate. This type of structure can be referred to as a "stack". When stress pulses are generated in a stack a  
20 very complicated response (for example, the result of a measurement of  $\Delta R(t)$ ) may be obtained. This complex response results from the generation of stress pulses in various different parts of the structure, the propagation of these pulses with partial transmission and partial  
25 reflection across the interfaces into other films, and the change in the intensity reflection coefficient of the structure due to the strain-induced change in the optical properties of each film. To determine the thickness of a number of the films in a stack requires the determination  
30 of the times at which stress pulses originating at known places in the structure are reflected or transmitted at the various interfaces. From these times, and using assumed velocities for the different films, the thicknesses of the films can be found. The determination of the times just

in the sample and the normal to the surface. Hence a measurement of the frequency of this oscillation can be used to determine the product  $nv$ , but not  $n$  and  $v$  separately. This oscillation will suffer an abrupt change 5 in phase when the stress pulse reaches the free surface of the sample at time  $\tau$ , and is then reflected back. By a measurement of  $\tau$ , one can thus determine the quantity  $d/v$ , where  $d$  is the film thickness. These two measurements and their analysis may be obtained using conventional systems, 10 but do not lead to definite values for the three quantities of interest  $n$ ,  $v$ , and  $d$ . The present invention overcomes this difficulty as follows.

If measurements are made of the frequency  $f$  as a function of the angle of incidence  $\theta$  of the probe light outside the 15 sample the measured  $f(\theta)$  can be analyzed to give both  $n$  and  $v$ . This is because the relation between  $\alpha$  and  $\theta$  involves only  $n$  and not  $v$ . Then the measurement of the time  $\tau$ , can be used to determine  $d$ .

Second, using measurements of the intensity of the 20 reflected pump or probe light, the phase change or the relative intensities of the different polarization components of the pump and/or probe light can also be used in many circumstances to deduce the refractive index and/or the thickness of the transparent film. For example, the 25 thickness or optical constants of one or more layers in a sample may be determined from the measured quantities according to the principles of optical reflectometry or ellipsometry. In this case the picosecond light pulses available in the system of this invention can be used to 30 make such reflectometry or ellipsometry measurements, and extra light sources may not be needed. The pulsed nature of the lasers is not relevant to these measurements. The determination of the optical constants and/or film thicknesses then enables the sound velocity and/or the

One function of the system is to determine the thickness of the films making up the sample, the mechanical properties of the films (sound velocities and densities), and the characteristics of the interfaces (adhesion, roughness, and 5 other interfacial characteristics).

The system in accordance with the various embodiments of this invention thus enables a combination of measurements of the type listed above so as to enable the determination of properties of the sample that are not obtainable through 10 the use of conventional systems.

By example, consider a sample in which the upper-most film is transparent. In such a sample the pump pulse will not be absorbed in this film, but will instead be absorbed in the next underlying film, assuming that this film is not 15 also transparent. There will, however, normally be a contribution to the change  $\Delta R$  in reflectivity of the probe pulse from the uppermost transparent film. A stress wave will be generated in the underlying optically-absorbing film and will propagate into the transparent film. This 20 will cause a local change  $\Delta n$  in the refractive index  $n$  of the transparent film, and the location of this change in the refractive index will propagate towards the free surface of the transparent film with a speed equal to the sound velocity  $v$  in the film. Probe light which is 25 reflected at this change in  $n$  will interfere constructively or destructively with the probe light which is reflected at the other interfaces of the sample. As a consequence there will be a change  $\Delta R$  in the intensity of the reflected probe light, which change will amount to an oscillation of 30 frequency  $f$  given by

$$f = 2nv \cos \frac{\alpha}{\lambda}$$

where  $\lambda$  is the wavelength in free space of the probe light and  $\theta$  is the angle between the direction of the probe light

embodiments of this invention, it can be appreciated that this invention teaches, in one aspect, a picosecond ultrasonic system for the characterization of samples in which a short optical pulse (the pump beam) is directed to 5 an area of the surface of the sample, and then a second light pulse (the probe beam) is directed to the same or an adjacent area at a later time. The retroreflector 129 shown in all of the illustrated embodiments 16-20 can be employed to provide a desired temporal separation of the pump and 10 probe beams, as was described previously with regard to, by example, Fig. 9.

The system measures some or all of the following quantities: (1) the small modulated change  $\Delta R$  in the intensity of the reflected probe beam, (2) the change  $\Delta T$  in 15 the intensity of the transmitted probe beam, (3) the change  $\Delta P$  in the polarization of the reflected probe beam, (4) the change  $\Delta\phi$  in the optical phase of the reflected probe beam, and/or (5) the change in the angle of reflection  $\Delta\theta$  of the probe beam. These quantities (1)-(5) may all be considered 20 as transient responses of the sample which are induced by the pump pulse. These measurements can be made together with one or several of the following: (a) measurements of any or all of the quantities (1)-(5) just listed as a function of the incident angle of the pump or probe light, 25 (b) measurements of any of the quantities (1)-(5) as a function of more than one wavelength for the pump and/or probe light, (c) measurements of the optical reflectivity through measurements of the incident and reflected average intensity of the pump and/or probe beams; (d) measurements 30 of the average phase change of the pump and/or probe beams upon reflection; and/or (e) measurements of the average polarization and optical phase of the incident and reflected pump and/or probe beams. The quantities (c), (d) and (e) may be considered to be average or static responses 35 of the sample to the pump beam.

transmission for the probe beam and the He-Ne wavelengths, but very low transmission for the pump wavelength.

Finally, Fig. 20 illustrates a normal incidence, dual wavelength, combined ellipsometer embodiment of this invention. In Fig. 20 the probe beam impinges on PBS2 and is polarized along the direction which is passed by the PBS2. After the probe beam passes through WP3, a quarter wave plate, and reflects from the sample, it returns to PBS2 polarized along the direction which is highly reflected, and is then directed to a detector DO in detector block 130. DO measures the reflected probe beam intensity.

In greater detail, WP3 causes the incoming plane polarized probe beam to become circularly polarized. The handedness of the polarization is reversed on reflection from the sample, and on emerging from WP3 after reflection, the probe beam is linearly polarized orthogonal to its original polarization. BS4 reflects a small fraction of the reflected probe onto an Autofocus Detector AFD.

DM3, a dichroic mirror, combines the probe beam onto a common axis with the illuminator and the pump beam. DM3 is highly reflective for the probe wavelength, and is substantially transparent at most other wavelengths.

D1, a reflected He-Ne laser 136 detector, is used only for ellipsometric measurements.

It should be noted that, when contrasting Fig. 20 to Figs. 18 and 19, that the shutter 1 is relocated so as to intercept the incident laser beam prior to the harmonic splitter 138.

Based on the foregoing descriptions of a number of

embodiment of the picosecond ultrasonics system, specifically a single wavelength, normal pump, oblique probe, combined ellipsometer embodiment. As before, only those elements not described previously will be described  
5 below.

Shutter 1 and shutter 2 are computer controlled shutters, and allow the system to use a He-Ne laser 136 in the ellipsometer mode, instead of the pulsed probe beam. For acoustics measurements shutter 1 is open and shutter 2 is  
10 closed. For ellipsometer measurements shutter 1 is closed and shutter 2 is opened. The HeNe laser 136 is a low power CW laser, and has been found to yield superior ellipsometer performance for some films.

Fig. 19 is a dual wavelength embodiment of the system  
15 illustrated in Fig. 18. In this embodiment the beamsplitter 126 is replaced by a harmonic splitter, an optical harmonic generator that generates one or more optical harmonics of the incident unsplit incident laser beam. This is accomplished by means of lenses L7, L8 and a nonlinear  
20 optical material (DX) that is suitable for generating the second harmonic from the incident laser beam. The pump beam is shown transmitted by the dichroic mirror (DM 138a) to the AOM1, while the probe beam is reflected to the retroreflector. The reverse situation is also possible.  
25 The shorter wavelength may be transmitted, and the longer wavelength may be reflected, or vice versa. In the simplest case the pump beam is the second harmonic of the probe beam (i.e., the pump beam has one half the wavelength of the probe beam).  
  
30 It should be noted that in this embodiment the AOM2 is eliminated since rejection of the pump beam is effected by means of color filter F1, which is simpler and more cost effective than heterodyning. F1 is a filter having high

laser, which is disadvantageous under normal conditions, since the bandwidth of the pulsed laser is much greater than that of a CW laser of a type normally employed for ellipsometry measurements.

- 5 When acoustics measurements are being made, the rotation compensator 132 is oriented such that the probe beam is linearly polarized orthogonal to the pump beam.

The analyzer 134 may be embodied as a fixed polarizer, and also forms a portion of the ellipsometer mode of the  
10 system. When the system is used for acoustics measurements the polarizer 134 is oriented to block the pump polarization. When used in the ellipsometer mode, the polarizer 134 is oriented so as to block light polarized at 45 degrees relative to the plane of the incident and  
15 reflected probe beam.

Finally, the embodiment of Fig. 17 further includes a dichroic mirror (DM2), which is highly reflective for light in a narrow band near the pump wavelength, and is substantially transparent for other wavelengths.

- 20 It should be noted in Fig. 17 that BS4 is moved to sample the pump beam in conjunction with BS3, and to reflect a portion of the pump to D3 and to a second PSD (PSD2). PSD2 (pump PSD) is employed in combination with the processor, computer controlled stage 122 (tilt and z-axis), and PSD1 (Probe PSD) to automatically focus the pump and probe beams onto the sample to achieve a desired focusing condition.  
25 Also, a lens L1 is employed as a pump, video, and optical heating focussing objective, while an optional lens L6 is used to focus the sampled light from BS5 onto the video camera 124.

Reference is now made to Fig. 18 for illustrating a further

measures a signal proportional to the intensity of the incident probe). Similarly, additional reflectometry data can be obtained from the pump beam using detectors D3 and D4. The analysis of the reflectometry data from either or 5 both beams may be used to characterize the sample. The use of two beams is useful for improving resolution, and for resolving any ambiguities in the solution of the relevant equations.

A third beamsplitter BS3 is used to direct a small fraction 10 of the pump beam onto detector D4, which measures a signal proportional to the incident pump intensity. A fourth beamsplitter BS4 is positioned so as to direct a small fraction of the pump beam onto detector D3, which measures a signal proportional to the reflected pump intensity.

15 Fig. 17 illustrates a normal pump beam, oblique probe beam embodiment of this invention. Components labelled as in Fig. 16 function in a similar manner, unless indicated differently below. In Fig. 17 there is provided the above-mentioned rotation compensator 132, embodied as a linear 20 quarter wave plate on a motorized rotational mount, and which forms a portion of an ellipsometer mode of the system. The plate is rotated in the probe beam at a rate of, by example, a few tens of Hz to continuously vary the optical phase of the probe beam incident on the sample. 25 The reflected light passes through an analyzer 134 and the intensity is measured and transferred to the processor many times during each rotation. The signals are analyzed according to known types of ellipsometry methods to determine the characteristics of the sample (transparent or 30 semitransparent films). This allows the (pulsed) probe beam to be used to carry out ellipsometry measurements.

In accordance with an aspect of this invention the ellipsometry measurements are carried out using a pulsed

unmodulated part of the probe and reference beam. This allows the difference signal (the modulated part of the probe) alone to be amplified and passed to the electronics.

The beamsplitter BS2 is used to sample the intensity of the  
5 incident probe beam in combination with detector D2. The linear polarizer 132 is employed to block scattered pump light polarization, and to pass the probe beam. Lenses L2 and L3 are pump and probe beam focusing and collimating objectives respectively. The beamsplitter BS1 is used to  
10 direct a small part of pump and probe beams onto a first Position Sensitive Detector (PSD1) that is used for autofocusing, in conjunction with the processor and movements of the sample stage 122. The PSD1 is employed in combination with the processor and the computer-controlled  
15 stage 122 (tilt and z-axis) to automatically focus the pump and probe beams onto the sample to achieve a desired focusing condition.

The detector D1 may be used in common with acoustics, ellipsometry and reflectometry embodiments of this  
20 invention. However, the resultant signal processing is different for each application. For acoustics, the DC component of the signal is suppressed such as by subtracting reference beam input D5, or part of it as needed, to cancel the unmodulated part of D1, or by  
25 electrically filtering the output of D1 so as to suppress frequencies other than that of the modulation. The small modulated part of the signal is then amplified and stored. For ellipsometry, there is no small modulated part, rather the entire signal is sampled many times during each  
30 rotation of the rotation compensator (see Fig. 17), and the resulting waveform is analyzed to yield the ellipsometric parameters. For reflectometry, the change in the intensity of the entire unmodulated probe beam due to the sample is determined by using the D1 and D2 output signals (D2

effected by having a motorized mount rotate WP1 under computer control.

A first acousto-optic modulator (AOM1) chops the pump beam at a frequency of about 1MHz. A second acousto-optic 5 modulator (AOM2) chops the probe beam at a frequency that differs by a small amount from that of the pump modulator AOM1. The use of AOM2 is optional in the system illustrated in Fig. 16. As will be discussed below, the AOMs may be synchronized to a common clock source, and may further be 10 synchronized to the pulse repetition rate (PRR) of the laser that generates the pump and probe beams.

A spatial filter 128 is used to preserve at its output a substantially invariant probe beam profile, diameter, and propagation direction for an input probe beam which may 15 vary due to the action of the mechanical delay line shown as the retroreflector 129. The spatial filter 128 includes a pair of apertures A1 and A2, and a pair of lenses L4 and L5. An alternative embodiment of the spatial filter incorporates an optical fiber, as described above.

20 WP2 is a second adjustable half wave plate which functions in a similar manner, with PBS2, to the WP1/PBS1 of the beamsplitter 126. With WP2 the intent is to vary the ratio of the part of the probe beam impinging on the sample to that of the portion of the beam used as a reference (input 25 to D5 of the detector 130. WP2 may be motor controlled in order to achieve a ratio of approximately unity. The electrical signals produced by the beams are subtracted, leaving only the modulated part of the probe to be amplified and processed. PSD2 is used in conjunction with 30 WP2 to achieve any desired ratio of the intensities of the probe beam and reference beam. The processor may adjust this ratio by making a rotation of WP2 prior to a measurement in order to achieve a nulling of the

freedom stage that is adjustable in height (z-axis), position (x and y-axes), and tilt ( $\theta$ ), and allows motor controlled positioning of a portion of the sample relative to the pump and probe beams. The z-axis is used to 5 translate the sample vertically into the focus region of the pump and probe, the x and y-axes translate the sample parallel to the focal plane, and the tilt axes adjust the orientation of the stage 122 to establish a desired angle of incidence for the probe beam. This is achieved via 10 detectors PDS1 and PDS2 and the local processor, as described below.

In an alternative embodiment, the optical head may be moved relative to a stationary, tiltable stage 122' (not shown). This is particularly important for scanning large objects 15 (such as 300mm diameter wafers, or mechanical structures, etc.). In this embodiment the pump beam, probe beam, and video are delivered to the translatable head via optical fibers or fiber bundles.

BS5 is a broad band beam splitter that directs video and a 20 small amount of laser light to the video camera 124. The camera 124 and local processor can be used to automatically position the pump and probe beams on a measurement site.

The pump-probe beam splitter 126 splits an incident laser beam pulse (preferably of picosecond or shorter duration) 25 into pump and probe beams, and includes a rotatable half-wave plate (WP1) that rotates the polarization of the unsplit beam. WP1 is used in combination with polarizing beam splitter PBS1 to effect a continuously variable split between pump and probe power. This split may be controlled 30 by the computer by means of a motor to achieve an optimal signal to noise ratio for a particular sample. The appropriate split depend on factors such as the reflectivity and roughness of the sample. Adjustment is

(such as a piezoelectric actuator) which is caused to oscillate rapidly ( $f_2$ ) (i.e. from 10 to  $10^6$  Hz) along the probe beam axis, thus executing a large number of oscillations (i.e., greater than 10) for each successive 5 delay position of the delay mechanism. The signal measured in such a system may be related to the derivative of the signal versus delay by a simple proportionality constant, provided that the amplitude of the oscillations corresponds to a range of delays which are small compared to the 10 minimum temporal extent of observed ultrasonic features in an undifferentiated response. In this embodiment it is also possible to detect at the difference frequency ( $f_1-f_2$  or  $f_1+f_2$ ), where  $f_1$  is the frequency induced by the AOM in the pump beam path (e.g., 1 MHz), and  $f_2$  is the frequency 15 induced by the delay modulator in the probe beam path.

Reference is now made to Fig. 16 for illustrating an embodiment of this invention which is referred to as a parallel, oblique embodiment.

This embodiment includes an optical/heat source 120, which 20 functions as a variable high density illuminator, and which provides illumination for a video camera 124 and a sample heat source for temperature-dependent measurements under computer control. An alternative heating method employs a resistive heater embedded in the stage sample stage 122. 25 The advantage of the optical heater is that it makes possible rapid sequential measurements at two different temperatures, as will be described below. The video camera 124 provides a displayed image for an operator, and facilitates the set-up of the measurement system. 30 Appropriate pattern recognition software can also be used for this purpose, thereby minimizing or eliminating operator involvement.

The sample stage 122 is preferably a multiple-degree of

invention to use the derivative of the signal versus time to determine the properties of a sample, rather than the signal itself. The purpose is to remove some of the background signal, associated with the cooling of the film,  
5 from the data. The derivative of the signal can also be compared with the derivative of a simulation to extract parameters.

In one embodiment of the algorithm used to determine unknown quantities from the observed reflectivity or  
10 transmission of the sample, the temporal features associated with the propagation of stress within the sample are compared with a simulation which includes only the ultrasonic response. Other features, in particular the slowly varying background associated with diffusion of heat  
15 within the sample, are ignored in such comparisons, or may be included in the fitting process by introducing one or several fitting parameters of a slowly varying function (e.g. an exponential, or a low order polynomial). For some materials the slowly varying background may have a much  
20 greater amplitude than the features associated with ultrasonic response of the sample. In order to improve the accuracy and speed of the fitting process in such situations, it may be convenient to numerically compute the derivative of the response with respect to delay time. A  
25 comparison may then be made between the derivative so determined and the derivative of the simulated response, and the values of the unknowns varied until a best fit is obtained.

An alternative method is to measure the derivative of the  
30 sample response directly, avoiding the step of numerical differentiation. This method provides superior signal to noise in comparison to the numerical procedure. In one embodiment of this derivative measurement scheme the retroreflector 46 in the probe path is placed on a mount

An important feature of this procedure is that simulation parameters so determined should simultaneously fit the response corresponding to the stress wave propagating in the metal. In the above procedure it is assumed that the  
5 detector 60 and processor 66 are so calibrated as to give the true reflectivity of the sample as a function of time. An alternative three step procedure which does not require the detector 60 and processor 66 to be so calibrated is as follows. In step (1) a stress pulse is generated in the  
10 material. Part of this stress wave enters the transparent layer and propagates to the free surface, then reflects from this surface, then propagates through the transparent layer, and then part of this stress reenters the metal film. The stress pulse reflecting from the free surface has the opposite sign to the incident stress pulse, but  
15 identical amplitude. The fraction of the stress pulse incident from the glass layer on the metal film which reenters the metal film may be calculated from the acoustic impedances (i.e. the product of the sound velocity and density) of the glass and metal (as described in Tauc et al.). While it propagates through the glass layer the stress wave gives rise to oscillations as described previously with regard to Figs. 15a-15d. In step (2)  $\partial n/\partial \eta$  for the glass and  $\partial n/\partial \eta$  and  $\partial \kappa/\partial \eta$  for the metal are allowed  
20 to be freely varied in the simulated response in order to achieve a best fit to the observed response. The values  $\partial n/\partial \eta$  and  $\partial \kappa/\partial \eta$  so obtained may be scaled by the ratio of the true value of  $\partial n/\partial \eta$  for the glass to the fitted value. Therefore, in Step (3) the true value of  $\partial n/\partial \eta$  for the  
25 glass is determined (this may be obtained by a number of methods, other than picosecond ultrasonics, that are applicable to transparent materials), and the fitted  $\partial n/\partial \eta$  and  $\partial \kappa/\partial \eta$  for the metal are scaled to obtain their true values.

35 It is also within the scope of the teaching of this

process of determining  $\partial n / \partial \eta$  and  $\partial \kappa / \partial \eta$  involves two steps which may be described in relation to Fig. 15d (which shows the case in which the material of interest is a thin metal film disposed on top of a substrate which may be silicon).

5     In step (1) a stress pulse is generated in the material. Part of this stress wave enters the transparent layer and propagates to the free surface, then reflects from this surface, then propagates through the transparent layer, and then part of this stress reenters the metal film. The

10    stress pulse reflecting from the free surface has the opposite sign to the incident stress pulse, but identical amplitude. The fraction of the stress pulse incident from the glass layer on the metal film which reenters the metal film may be calculated from the acoustic impedances (i.e.

15    the product of the sound velocity and density) of the glass and metal (as described in Tauc et al.). While the stress wave propagates through the glass layer it gives rise to oscillations as described previously with regard to Figs. 15a-15d. The amplitude of these oscillations may be used

20    20 to compute the quantity  $\partial n / \partial \eta$  for the glass (which in general will have a different value than the value corresponding to the metal) either analytically or by comparison with simulations of the oscillations:  $\partial \kappa / \partial \eta = 0$  for the glass. In step (2) the quantities  $\partial n / \partial \eta$  and  $\partial \kappa / \partial \eta$

25    25 for the metal layer are determined by carrying out a simulation of the reflectivity change which occurs in response to the stress reentering this layer, and by adjusting  $\partial n / \partial \eta$  and  $\partial \kappa / \partial \eta$  in order to achieve a best fit to the observed response for times during which the effects of

30    30 the stress wave on the reflected probe intensity may be observed. In these simulations the acoustic impedances and sound velocities of the glass and metal film are assumed to be known in advance. In addition, the optical constants  $n$  and  $\kappa$  for one or both materials at the pump and probe beam wavelengths may be used as inputs to the simulations, or alternatively may be used as further adjustable parameters.

accordingly.

- The teaching of this invention also includes methods and apparatus for measuring the change in the optical constants of a material with strain. In this technique the system is  
5 used to determine the quantities  $\partial n/\partial \eta$  and  $\partial \kappa/\partial \eta$  in a particular sample geometry. Samples have a film of glass, or another transparent material deposited on top of a thin film of opaque or semi-opaque material (the material of interest may be a metal). The optical constants of both  
10 materials are known. The quantities  $\partial n/\partial \eta$  and  $\partial \kappa/\partial \eta$  are also known for the transparent material, and are deduced for the second material by comparing acoustic data with simulations in which  $\partial n/\partial \eta$  and  $\partial \kappa/\partial \eta$  for the second material are varied.
- 15 To be able to carry out simulations which enable a quantitative comparison with data of the magnitude of the change in the reflectivity or transmissivity of a sample in which a stress pulse is generated, it is necessary to know in advance by how much the optical constant  $n$  and  $\kappa$  for the  
20 subject materials change in response to stress  $\sigma$ . It is preferable in some embodiments to carry out simulations in terms of the strain  $\eta$ , which may be related to the stress in a simple way. In terms of the strain, the foregoing is equivalent to the statement that the quantities  $\partial n/\partial \eta$  and  
25  $\partial \kappa/\partial \eta$  must be known. It is a feature of this invention that the methods and apparatus described herein may be used to determine these quantities. In one technique,  $\partial n/\partial \eta$  and  $\partial \kappa/\partial \eta$  may be found for a material by depositing on top of an optically smooth specimen of this material a layer of  
30 transparent material such as a glass (e.g. LP-CVD TEOS, or PE-CVD BPSG) having a thickness of at least several hundred Angstroms, and less than 100 microns. The underlying specimen of material for which  $\partial n/\partial \eta$  and  $\partial \kappa/\partial \eta$  are to be determined may be a thin film, or a thick substrate. The

semitransparent or transparent samples, or by producing a best fit to picosecond ultrasonic data by varying a sound velocity parameter in a simulation of one or more layers.

The temperature may be changed in the following ways: by a  
5 resistive heater embedded in the sample stage 50; by an  
inductive heater; radiatively (i.e. an intense lamp); by  
varying the pump beam intensity such that the mean  
temperature of the sample is above the ambient; or by  
introducing a continuous wave heating laser onto the  
10 measurement spot FS through a common or separate objective.

The temperature change may be measured in the following ways: by optical pyrometry; by a calculation of the deposited heating energy (which requires measurement of the incident and reflect radiation) and then using the values  
15 of the optical and thermal constants of the sample needed to determine the equilibrium temperature in the measurement region; with a thermocouple (in contact with the sample 51); or using the Mirage Effect. In the Mirage Effect the change in the refractive index in the air above the heated  
20 spot is measured via the deflection of a laser beam incident at a glancing angle, and the temperature is deduced from the refractive index change necessary to produce an observed beam deflection (see, for example, T.R. Anthony et al., Physical Review B, vol. 42, 1104 (1990)).

25 Calibration of the system of this invention can be accomplished in several manners. By example, films comprised of several different metals can be deposited on silicon wafers at different temperatures. In these samples, the stress can be independently estimated by calculation  
30 from differential expansion and from measurements of film-induced curvature. The calculated values are then compared with results obtained from the use of the system of this invention, and calibration factors are determined

- Measurements on several materials have shown how the temperature dependence  $\partial v_s / \partial T$  of the sound velocity is affected by stress. This quantity can be readily measured by the picosecond ultrasonic methods of this invention and
- 5 can be used to give the stress of the film, without the requirement of knowing the film's precise thickness. The technique has many advantages and is applicable even for very thin films, multilayers ( $\sim 100 \text{ \AA}$ ), and for submicron lateral dimensions.
- 10 Further in accordance with this invention, the sound velocity in a film is measured at two temperatures in the film. The difference between the two sound velocities depends in a predictable way on the stress within the film, whether the stress is externally imposed or "built-in".
- 15 This provides a method for stress measurement on a lateral scale of the spot size  $F_S$ , which may have a diameter of one micron or less. The temperature of the sample 51 can be changed via a resistively heated stage, an arc lamp, a CW laser focused onto the measurement spot, or by modulating
- 20 the pump power. The sound velocity can be measured by observing ultrasonic echoes, or oscillatory signals as disclosed in regard to Figs. 15a-15d, or the vibrational period of very thin films.

The rate of change of the sound velocity with temperature

25 depends on the stress in the film in a predictable way, as has been reported in the literature (Salama K. et al., Journal of Applied Physics vol. 51, page 1505 et seq. (1980); J. Cantrell, Ultrasonics International 1989 Conference Proceedings, pp. 977 et seq.).

- 30 Picosecond ultrasonics measurements of the sound velocity may be made in the following ways: echo time (as in Tauc et al.); ringing period; the oscillation period of oscillations caused by a travelling stress wave in

example, a delamination between the film 84 and an underlying film or substrate.

This technique is also sensitive to thin film processes that are intended to enhance adhesion between layers. One such technique is ion bombardment. It has been found by the inventors that the rate of damping of ultrasonic ringing of a film deposited on a substrate, and then implanted with high energy ions, is more slowly damped for low ion doses than for high ion doses. It is inferred that the adhesion is greater for samples with higher implant doses because the acoustic energy in the thin film is able to couple to the substrate more readily than in samples having lower implant doses or energies.

In summary, an ultrashort laser pulse ( $\tau_p \sim 0.1$  psec) is selectively absorbed in a thin film or in a more complex nanostructure. The absorption sets up a thermal stress which generates an ultrashort stress wave impulse. The propagating stress can affect the optical constants anywhere within the sample, causing a complex, but calculable, change in the reflectivity (or transmission, or polarization state, or optical phase) of the probe beam. Echoes are but one simple case of temporal features. Other, more complex temporal features may also be detected, such as those that correspond to ultrasonic vibrations in nanostructures and multilayer samples. These other temporal features may not correspond to a stress pulse returning to the surface. The only requirement for detection is that the stress generated by the pump is at a depth in the sample where it can interact with the probe beam.

A film or a multilayer deposited on a substrate at an elevated temperature is normally in a state of stress due to differential thermal expansion. Present techniques for evaluating the stress have severe practical limitations.

in a model of the sample structure (e.g. as a distinct film having certain physical properties, some of which may be of interest, and so may be left as fitting parameters).

In this regard it should be noted that Tas et al. reported  
5 detecting thin interfacial layers of  $CF_x$  between aluminum and silicon as a particular example of this effect for a situation in which the aluminum films were very thin (G. Tas et al., Appl. Phys. Lett. 61(15), 12 October 1992, pp. 1787-1789). Tas et al. did not observe echoes, but rather  
10 the ringing of the aluminum films. Moreover the result was for a very narrow class of structures in which the metal films were deposited on top of highly uniform, ultrathin layers of very soft material.

15 Interfacial layers producing much different effects can also be characterized with the technique of this invention. An important class of interfacial layers include layers which are formed at interfaces between two materials which have chemically reacted to form an intermediate compound. As an example, Ti and Al react to form  $TiAl_3$ ; Ti and Si  
20 react to form  $TiSi_2$ ; Co and Si react to form  $CoSi_2$ ; Pt and Si react to form  $PtSi$ . The thickness of interfacial layers so formed may be substantial. By example, in some of the above example pairings the materials may proceed until one or both of the original materials is completely consumed by  
25 the reaction.

Interfacial voids, cracks, and regions of poor adhesion may be detected similarly. Such defects usually give rise to acoustic reflections, such as but not limited to echoes, having larger amplitudes than would be seen for a perfect  
30 interface. The reason is that stress pulses exhibit no loss of amplitude when reflected from a perfectly free surface. As such, the presence of larger than expected probe signal amplitudes within the data can be indicative of, by

An important mechanism determining such distortion of echo shapes is dephasing at different parts of the stress front reaching a roughened interface (and reflecting toward the surface) at different times. By incorporating such 5 mechanisms into a simulation of a particular structure, it is possible to quantify the degree of interface roughness.

As employed herein the roughness of a surface or interlayer may be taken to be the RMS height and correlation length parallel to the surface or interlayer.

10 It should be noted that the same mechanism can cause echo broadening if it is the top surface (rather than a buried interface) which is rough. It is thus believed to be possible to distinguish between surface roughness-induced echo broadening and interface roughness-induced echo 15 broadening based, for example, on the symmetry of the echoes and a comparison with reference echo shapes and/or simulated echo shapes.

It should be noted that the use of echoes per se is but one exemplary technique for characterizing the sample 51. For 20 example, in some samples distinct echoes are not seen. However, the characterization of the sample can still be accomplished by comparing the reflected probe signal to reference data and/or simulations.

It is also within the scope of the teaching of this 25 invention to detect roughness, or to detect variations in film thickness over small lateral displacements, through the use of a small area optical generator and detector which are scanned relative to the sample surface.

Interfacial layers are another potential cause of echo 30 distortion. As in the preceding example, a preferred method to characterize such interfacial layers is to include them

temporally separated reflected probe beams 21b'.

In Fig. 15c the substrate 80 is assumed to at least weakly absorb the pump pulse, giving rise to the stress pulse in the substrate. By example, the substrate 80 may be  
5 comprised of silicon.

In Fig. 15d a buried film 84 absorbs the pump pulse and launches a stress pulse that propagates towards the surface of an overlying transparent film 84'. The resulting reflected probe pulses 21b' are similar to the case shown  
10 in Fig. 21b.

It should be noted that the teachings of this invention apply as well to very thin films that essentially vibrate when excited rather than supporting propagating stress or sound pulses.

15 In accordance with an interface characterization technique of this invention, amplitude information (i.e., the amplitude of the change in the reflected or transmitted probe beam intensity) is used to draw quantitative conclusions about the condition of buried interfaces or  
20 surfaces. The technique has superior sensitivity, compared to conventional ultrasonic techniques, to very subtle interfacial defects (contaminants, interlayers, roughness, bonding, etc.) because the wavelengths of the acoustic phonon comprising the pulse are much shorter than  
25 wavelengths which can be achieved by other methods. For example, in cases where distinct acoustic echoes are seen (e.g., for films thicker than few optical absorption lengths, and thin enough for an acoustic wave to return to the surface before the delay stage 44 runs out of delay  
30 travel), the echo amplitudes and widths can supply information about the smoothness of a buried interface from which it has reflected (see, for example, Fig. 15d).

of the sample 51 at two or more different angles of incidence.

An alternative technique for determining  $n$  and  $v$ , has been described by Grahn et al. (APL 53, no. 21 (21 Nov. 1988), 5 pp. 2023-2024, and APL. 53, no. 23, (5 Dec. 1988), pp. 2281-2283). However, the Grahn et al. technique depends on the use of an independently-determined thickness for the film.

10 Representative samples for which these techniques may be used are illustrated in Figs. 15a-15d.

In Fig. 15a a stress pulse is launched from the film layer 84 by the absorption of the pump beam energy, and propagates within the substrate 80 with a characteristic velocity  $v_s$ . The application of the probe beam pulse 21b 15 results in two reflections, one from the surface of the film 84 and another from the stress pulse. As the stress pulse continues to propagate away from the film layer 84, the part of the probe pulse reflected at the stress wave 20 has a changing phase shift relative to the probe pulse reflecting from the film's surface. One result is that constructive and destructive interference occurs between the probe pulse reflected from the surface and that reflected from stress wave, thereby giving a variation in the intensity of the probe pulse measured by the detectors 25 as the stress pulse propagates.

In Fig. 15b the pump pulse launches the stress pulse either by being applied to the film surface or to the lower surface of the non-absorbing substrate 80. For the latter case the pump pulse propagates through the substrate 80 and 30 is absorbed in the film 84, thereby generating the stress pulse. In either case the probe pulse is applied to the lower surface of the substrate 80, and gives rise to three

For a sample 51 with the property that the incident light penetrates at least one wavelength into a layer or layers into which a stress wave is launched, it is possible to use picosecond ultrasonics to independently measure the sound velocity and refractive index of said layer or layers with great precision. The sound velocity may also be used to determine the elastic modulus. Optical interference between probe light reflected from the surface of the sample and probe light reflected from the traveling stress wave gives rise to oscillations in the intensity of the reflected probe beam 21b' as a function of delay. The period of these oscillations may be measured very precisely. For a material having an index of refraction  $n$  and sound velocity  $v$ , the period of the oscillations is given by:

$$\tau = \frac{\lambda_0}{2nv_s \cos\theta} \quad (2)$$

where  $\lambda_0$  is the optical wavelength in free space and  $\theta$  is the angle between the direction normal to the surface of the sample 51 and the direction of light propagation in the sample. Typically one knows  $\theta$  and  $\lambda_0$  in advance. Thus, from the observed oscillation period, one can deduce the product  $nv$ , with high precision. The value of  $v$ , independent of  $n$  can be found by measuring  $\tau$  at a second angle (which yields a value for  $n$ ), or by using a published value for  $n$ . In addition, from the sound velocity, the elastic modulus  $c_{11} = \rho v^2$  of the film may be determined (using a previously determined value of  $\rho$ ).

In accordance with an aspect of this invention measurements at two angles are simultaneously made by detecting parts of the probe beam 21b impinging on the sample 51 within a single focused beam, which then reflects to two or more closely spaced detectors. It is also within the scope of the invention to controllably tilt the sample stage 50, and to thus cause the probe beam 21b to impinge on the surface

the modulation signal, the pulse rate signal is applied to a counter which changes the state of the modulator 40 after  $n$  laser pulses are counted. The modulation rate is then  $1/2n$  times the laser pulse rate. In such a synchronous scheme the number of pump pulses impinging on the sample 51 in any period of the modulator 40 is always the same. This eliminates a potential source of noise in the modulated probe beam 21b which might arise in an asynchronous system under conditions in which the laser energy contained within a single cycle of the modulator 40 varies from period to period of the modulation.

A major source of noise is scattered pump light which can reach the probe beam detector (a) despite having a nominally orthogonal polarization (polarizers are not perfect, and also the sample 51 may tend to depolarize the light). As was described above, one technique to suppress this source of noise is to use pump and probe beams of different color, so that the pump color may be blocked by means of a filter before the probe detector.

Another method is to modulate the probe beam 21b at a frequency different from the pump beam modulation frequency. By example, if the pump modulation frequency is  $f_1$ , and the probe modulation frequency is  $f_2$ , then the part of the probe beam modulated by the pump beam at the sample 51 will have a component at the frequency  $f_1 - f_2$ . This signal may be passed through a synchronous demodulator or low pass filter designed to reject  $f_1$  and  $f_2$  and pass only their difference frequency. Thus, any pump light scattered by the sample 51 onto the probe detector (a), which would otherwise appear as noise in the data, is suppressed. To minimize the introduction of ubiquitous  $1/f$  noise the difference frequency is preferably not below a few hundred kHz. Exemplary frequencies are  $f_1 = 1$  MHz and  $f_2 = 500$  kHz.

coupling effects between the vias. In either case the probe beam signal can be compared to a signal obtained from a reference "known good" structure, or to a simulation of the structure, or from a combination of reference data and simulations. Any deviation in the probe signal from the reference and/or simulated signal may indicate that the sample differs in some way from what was expected.

Fig. 14 shows that for samples considered in the ultrasonic technique, a multilayer thin film 84a, 84b may be substituted for a simple film 84. Such multilayer films may be formed intentionally by sequential depositions, or unintentionally because the substrate 80 may have been ineffectively cleaned prior to succeeding layer depositions, or by the (intentional or unintentional) chemical reaction between two or more layers (for example, following heat treatment). Such layers may give rise to ultrasonic echoes having complicated shapes and temporal characteristics. It is possible to determine the thicknesses and interface characteristics for thin film structures containing, by example, five or more sublayers. This is preferably accomplished by comparing the reflectivity or transmission data with simulations of the ultrasonics and detection physics to obtain a best fit set of unknowns with the obtained data.

In the system configurations which use the AOM 40 to modulate the pump beam 21a, there may be no relationship between the modulation rate and the repetition rate of the laser 12. As a result, the laser pulse train and modulation cycle are asynchronous. It is possible to make this a synchronous system by deriving the modulation rate from the pulse repetition rate. The pulse repetition rate may be obtained from the laser 12 by means of an optical detector which senses the emitted pulses, or by using the drive signal from an actively mode-locked laser. To derive

deposited before the tungsten). The structure may be evaluated by generating the stress wave in the substrate 80 (not applicable if the substrate, as in the above tungsten example, is glass) and detecting it in the embedded 5 structure 84; or by generating the stress wave in the structure 84 and detecting the stress wave in the structure 84 and detecting the stress wave in the substrate 80.

It should be realized that, in the three dimensional 10 structures illustrated in Figs. 12 and 13, the pump beam can also be employed to excite the normal modes in the structure, which can in turn affect the transmitted or reflected probe beam.

When applying the probe beam 21b to the structure 84 it may 15 be advantageous to use a near-field focussing arrangement, such as the tapered optical fiber shown in Fig. 7. In this case the pump beam FS can be significantly larger than the probe beam FS, thereby enabling the selective probing of small scale structures.

20 This capability for spatial imaging can be exploited to perform measurements of static stress with lateral spatial resolution to 100 nm scale and below.

It is also within the scope of this invention to apply a pump beam FS and a probe beam FS to simultaneously probe a 25 plurality of patterned structures (e.g., a two-dimensional array of tungsten vias 0.5  $\mu\text{m}$  in diameter and 1.0  $\mu\text{m}$  apart that are formed in a substrate). In this case each tungsten via may be considered a separate, independent oscillator, each of which contributes to the reflected or transmitted 30 probe beam signal. For closer spacings between elements, a "superlattice"-type of vibrational mode can be excited, wherein the reflected or transmitted probe signal includes

- probe spot size on the sample. The probe beam 21b may then be scanned by x-axis and y-axis piezoelectric actuators 102a and 102b on a very small spatial scale (similar to a Scanning Tunneling Microscope) with the pump beam location 5 fixed. This embodiment may be used to map structures patterned in two or more dimensions on a length scale smaller than can be achieved using conventional lithography. Therefore, it can be used to map the smallest structures found in integrated circuits.
- 10 The probe beam 21b can be an expanded beam that is focused onto the fiber 102 by a lens 104, and the reflected probe beam 21b' is directed through the fiber 102 and is diverted by a splitter 106 to a filter 108 and then to the detector 60.
- 15 Fig. 12 shows an interface 82 between a patterned structure 84 on top of the substrate 80, and is useful in explaining the use of this invention when characterizing three dimensional structures as opposed to planar structures. The patterned structure may be evaluated by generating a 20 stress wave in the substrate 80 and detecting the stress wave in the structure 84; or by generating the stress wave in the structure 84 and detecting the stress wave in the structure 84; or by generating the stress wave in the structure 84 and detecting the stress wave in the substrate 25 80.

Fig. 13 shows an interface 82 surrounding a structure 84 formed within a patterned recess within a surface of substrate 80. An example of this three dimensional configuration is a tungsten via formed in a hole in a glass 30 layer by (i) depositing the glass on a substrate, (ii) patterning and etching the hole, (iii) depositing a film of tungsten and (iv) polishing the tungsten layer until the glass is exposed (adhesion promoting layers may be

directed at normal incidence onto the sample 51 through objective 98. The probe beam polarization is rotated by means of a half wave plate 38 and is then passed through a polarizer 42 oriented to be orthogonal to the pump beam 5 polarization. This retarder/polarizer combination is also used as a variable attenuator for the probe beam 21b. The probe beam 21b is then sent to the variable delay stage 44, and is focused onto the sample 51 through the same normal incidence objective 98 as the probe beam 21a. The reflected 10 probe beam 21b' is directed to the detector 60 by a dichroic mirror 92 which passes the reflected pump beam 21a, thereby effectively filtering out any reflected probe light. A filter 94 which passes only the probe beam wavelength is placed before the detector 60. The detector 15 60 is followed by the tuned filter 62, lockin amplifier 64, and processor 66, as in Fig. 2.

Fig. 7 illustrates an embodiment of this invention wherein the pump beam 21a and the probe beam 21b are directed to the sample 51 by means of tapered optical fibers 100 and 20 102, respectively, to achieve near-field focusing and FS sizes of order 100nm. The probe beam 21b is shown having normal incidence, and may have a different wavelength than the pump beam 21a. In this embodiment a terminal portion 25 of the pump and/or probe beam delivery fiber 100, 102 is reduced in diameter, such as by stretching the fiber, so as to provide a focussed spot FS having a diameter that is less than the normal range of optical focussing. This enables the pump and/or probe optical pulse to be repeatably delivered to a very small region of the sample's 30 surface (e.g., to a spot having a diameter  $\leq$  one micrometer), regardless of any changes that are occurring in the optical path length of the pump and/or probe beam.

The pump beam 21a need not be brought in through a fiber, and in one mode of operation may be much larger than the

chosen as to block high spatial Fourier components of the beam may be used. A lens may be used to focus the beam onto the first aperture, and a second lens may be used to collimate the beam emerging from the second aperture. In 5 a system employing any of the above techniques it is preferred to monitor the intensity of the delayed (or advanced) beam either before or after it impinges on the sample, to properly normalize the final signal.

Referring now to Fig. 5, there is illustrated a deflection 10 through an angle  $\theta$  of the probe beam 21b by a non-uniform expansion of a region wherein a propagating stress wave exists (i.e. a bulge 86 in the film 84). The bulge 86 is caused at least in part by a stress wave which may also have a non-uniform profile across the spot. The deflection 15 can be detected by a position sensitive detector such as a split cell 60'. Movement of the reflected probe beam 21b' can also come about in the absence of the bulge 86 in transparent and semi-transparent samples due to a stress induced change in the refractive index. In this case the 20 beam is displaced by a small amount parallel to the direction along which it would normally deflect. This displacement can also be detected by a position sensitive detector. Fig. 5 also illustrates the lengthening of the path through the sample as a result of the surface 25 displacement (uniform or non-uniform).

Fig. 6 illustrates a configuration which is based on Figs. 1, 2 and 3, and is a preferred implementation of a "normal incidence, dual wavelength" system. The source 10' (Fig. 1b) is frequency doubled using the nonlinear crystal 24, 30 such as BBO, KTP or LBO. The pump and probe beams are separated by the dichroic mirror 26 such that the doubled wavelength is passed to become the probe beam 21b, and the undoubled part is reflected to become the pump beam 21a. The pump beam 21a is modulated by modulator 90 and is

successive pulses such that the effects of a pump pulse arriving at the sample more than one pulse interval before the probe may be detected.

The shape and position of the focused probe spot FS on the 5 surface of the sample 51 may vary systematically, depending on the position of the delay stage 44 (i.e. the time delay). For example, the system 1 may exhibit a lack of parallelism between the probe path in Fig. 2 and the delay stage axis due to misalignment, or as a result of a flaw in 10 the stage mechanism. This causes a translation of the probe beam across the focusing lens, and for a lens exhibiting typical aberrations, can introduce a corresponding lateral translation of the probe beam 21b relative to the pump beam 21a on the surface of the sample 15 51, as a function of delay.

In addition, since all laser beams exhibit some degree of divergence, varying the path length of one of the beams changes its diameter at the focusing lens, and this causes a corresponding change in the diameter of the focused spot 20 (FS) on the sample 51. The result of all such effects may be to introduce a spurious dependence of the signal upon delay time. One method to eliminate such dependencies is shown in Fig. 8, in which a length of optical fiber 114 is introduced to the path of the delayed probe beam (or 25 advanced pump beam). The fiber 114 serves as a spatial filter, preserving a constant spot position, size and profile throughout a range of input beam conditions. By incorporating such a device into the probe beam path it is possible to preserve a very stable overlap of the pump and 30 probe beams on the focus spot FS over a wide range of delay stage positions. Other types of spatial filters may also be used to achieve the same effect; for example, any small aperture (typically smaller than the beam size) such as a pinhole or narrow slit, followed by a second aperture so

quality, depending on the properties of the sample (e.g. the amount of surface roughness), and the source (e.g. pump and probe beams having different colors, versus pump and probe beams having the same color).

- 5 Alternative focusing geometries are also illustrated in Fig. 3, and include:
- (Fig. 3a) pump and probe beams oblique to the sample plane (i.e., the surface of wafer 70) and not parallel or coaxial to each other;
- 10 (Fig. 3b) pump and probe beams substantially normal to the sample plane and parallel, focused through a common lens 98 (as in Fig. 6);
- (Fig. 3c) pump and probe beams parallel and lying in a plane orthogonal to the plane of incidence, focused through common lenses 48 and 52;
- 15 (Fig. 3e) (i) pump beam normal and probe beam oblique, focused independently; or (ii) probe normal and pump oblique; and
- (Fig. 3f) pump beam and probe beam both normal to the sample plane and coaxial, focused through a common lens 74.

The variable delay between the pump and probe beams may be implemented as shown in Fig. 2 by means of the computer controlled delay stage 44 in the probe beam path. Alternatively, a similar delay stage may be inserted within the pump beam path to "advance" the pump beam pulses in time relative to the probe pulses. An extremely long delay may be implemented as shown in Fig. 9 by placing more than one retroreflector 46 on the single translation stage 44. In this embodiment a plurality of the beam steering mirrors 110a are employed to direct the probe beam 21b to individual ones of the retroreflectors 46, thereby significantly increasing the probe beam path length relative to the pump beam path length. It is possible to implement a delay which is longer than the time between

ratio may be improved by placing color filters and/or polarizers between the sample 51 and detector 60 to prevent light scattered from other parts of the system from impinging one or more detectors (as an example, to prevent  
5 pump light scattered from the sample 51 from impinging on reflected probe intensity detector (a)). The signal quality may be further improved by passing the modulated probe intensity output (i) from the detector 60 through the synchronous demodulator 64 (such as a lockin amplifier, or  
10 signal averager) located before the processor 66. The signal quality may be further improved for samples 51 tending to scatter the pump beam 21a into the probe detector by introducing a second intensity modulator into the probe beam path between the source 10 and the sample  
15 51. The second intensity modulator has a modulation frequency differing from the pump beam modulation frequency by an amount such that the difference frequency is greater than the input bandwidth of the synchronous demodulator 62. The detector output (i) corresponding to the reflected  
20 probe intensity may then be synchronously demodulated at the difference frequency, while the components of (i) at the modulation frequencies are rejected.

The pump and probe beams may be focused, as in Fig. 2, onto the sample through the common lens 48. This arrangement is simple to practice but is not optimal for all cases, since the pump beam 21a need be scattered through only a small angle by a non-ideal sample to impinge on the reflected probe detector (a), thereby introducing noise to the measurement of the modulated probe intensity. The common lens approach also has the weakness of achieving non-optimal spot overlap, which may be improved by using separate lenses, or coaxial beams. The common lens approach is represented in Fig. 3d in plan view from a location along a normal to the sample, here a semiconductor wafer  
30 70. Other focusing geometries may give improved signal

change in the sample's reflectivity  $R$  (i.e.  $\Delta R/R$ ), and normalizes this change by the intensity of the incident pump beam.

In the apparatus of this invention the detector input  
5 designated as (a) contains a modulated component which carries the stress information in addition to a large unmodulated reflected probe component  $21b'$ . Input (b) is proportional to the unmodulated portion of the probe signal  $21b$ . The output (i) is a voltage proportional to only the  
10 modulated part of the probe signal, which is determined by electronically removing the unmodulated component from the input (a). This output goes to a bandpass filter and preamplifier 62, then to a synchronous demodulator 64 (e.g. a lockin amplifier), and finally to the processor 66 where  
15 it is digitized and stored. The inputs (a) and (b) are also used to determine the reflectivity of the sample corresponding to the probe beam  $21b$ , and similarly inputs (d) and (c) are used to determine the reflectivity of the sample corresponding to the pump beam  $21a$ . These  
20 quantities may be used to validate the optical simulation of the structure, or in some cases to deduce layer properties such as thickness in accordance with known optical reflectometry principles. In addition, inputs (a) and (d) are used by the processor 66 to normalize the  
25 reflectivity change output (i). The energy deposited in the sample 51 by the pump beam  $21a$  may be determined by comparing the incident and reflected pump and probe beam intensities ( $21a'$ ,  $21b'$ ).

Portions of the pump and probe beams may also be directed  
30 via beam splitter 54 onto one or more position sensitive detectors (autofocus detector 58) whose output may be used by the processor 66, in conjunction with the sample translation stage 50, to effect an optimum focus of the pump and probe beams on the sample 51. The signal to noise

linearly polarized beam from laser 12 passes through the half-wave plate 16, which is used to rotate its polarization. The polarized beam is then split into pump and probe beams by a dielectric beam splitter 34. The 5 ratio of pump to probe may be varied by rotating the incoming polarization. The lower beam is the pump beam 21a, and the upper beam is the probe beam 21b. The pump beam 21a passes through a half-wave plate/polarizer combination 38 which rotates its polarization to be 10 orthogonal to that of the probe beam 21b, and which also suppresses any light not polarized along this orthogonal axis.

The pump and probe beams 21a and 21b are emitted by the source, and the intensity of the pump beam is modulated at 15 a rate of about 1MHz by an acousto-optic modulator (AOM) 40, or by a photoelastic modulator followed by a polarizer, or by other intensity modulation means. The probe beam path length is varied by translating a retroreflector 46 mounted on a computer-controlled delay stage 44, via a 20 steering mirror combination 110a. Both beams are then focused by lens 48 onto the sample 51 mounted on a translatable sample stage 50, and are detected by a photodetector 60. In this embodiment the inputs to the detector 60 include portions of the input pump and probe 25 beams (inputs c and b, respectively, via beam splitters 49a and 49b, respectively); and also include portions of the reflected pump beam 21a' and reflected probe beam 21b' (inputs d and a, respectively). Outputs from the detector 60 include signals proportional to the incident pump beam 30 intensity (e); incident probe beam intensity (f); reflected pump beam intensity (g); reflected probe beam intensity (h); and probe modulation intensity (i), i.e. only the modulated part of the reflected probe intensity. These detector outputs are fed into a processor 66. The 35 processor 66 calculates from the inputs the fractional

averager (SA). A measurement of, by example,  $\Delta R(t)$  may be performed by applying a signal corresponding to the reflected probe intensity from the output of the detector 60 to the input of the fast signal averager (SA), and by 5 triggering sample acquisitions at times corresponding to the pulsing of the probe laser 13. A large number (e.g., thousands) of measurements may be averaged in order to effect a desired signal to noise ratio. It should be noted in regard to this invention that the delay stage and 10 modulator described previously in regard to Fig. 2 may be omitted. It should also be appreciated that any "jitter" in the pulsing of the two lasers may have the effect of averaging the signals corresponding to closely spaced delay times, and that this effect may somewhat attenuate the high 15 frequency components of the measurement.

Although the pump and probe lasers are depicted in Fig. 1c separately, they may have one or more optical elements in common, including the gain medium. Other permutations of pump and probe color, polarization and pulse rate suggested 20 by the above description may be used to achieve an improvement in signal quality, depending on the properties of the materials to be investigated.

Examples of the pulsed lasers suitable for use in the 25 system 1 include an Argon ion pumped solid state mode-locked laser, such as Coherent Inc. Inova (Argon) and Mira (Ti:sapphire); a diode laser pumped solid state mode locked laser, such as a continuous wave diode pumped frequency doubled YAG and modelocked Ti:sapphire laser; and a direct 30 diode pumped mode-locked solid state laser.

Referring to the embodiment of Fig. 2, a further embodiment of an optical source 10''' provides both the pump and probe beams 21a and 21b, respectively, in a manner similar to the embodiment of Fig. 1a. In the Fig. 2 arrangement the

by means of a half-wave plate 32. The dichroic mirror 26 may be chosen to pass the fundamental frequency of the laser 12 and reflect the second harmonic, giving a probe beam at the fundamental and a pump beam at the second harmonic. Alternatively, the dichroic mirror 26 may be chosen to pass the second harmonic and reflect the fundamental, giving the probe beam 21b at the second harmonic and the pump beam 21a at the fundamental, as shown in Fig. 1b.

Another embodiment of an optical source 10'' is shown in Fig. 1c, in which the pump and probe beams are produced by two different lasers 12 and 13. In one embodiment, these may be identical pulsed lasers, in which case the upper beam is passed through the half-wave plate 16 to rotate its polarization relative to that of the lower beam by 90 degrees. Alternatively, the lasers 12 and 13 may emit dissimilar wavelengths (two "colors"). Alternatively, the probe laser 13 may emit a continuous (i.e. non-pulsed) beam. Alternatively, the pump laser 12 may emit pulses with a repetition period of  $\tau_A$  and the probe laser 13 may emit pulses with a repetition period  $\tau_B$ , as shown in Fig. 4a. Such a scheme may be used to effect a continuously variable delay between the pump and probe pulses without the use of a mechanical delay stage 44 of a type depicted in Fig. 2.

Referring now to Fig. 4b, in this alternative technique the delay between pairs of A and B pulses increases by a time  $\tau_B - \tau_A$  from one repetition to the next. By example,  $\tau_B - \tau_A$  may be 0.1 psec on average, and the repetition rate of the pump laser 12 may be 100 MHz. This gives a time between simultaneous arrivals of the pump and probe pulses of one millisecond (i.e., the scan time). This embodiment further includes suitable frequency locking electronics (FLE), mirrors, a lens, a suitable detector 60, and a fast signal

physical properties of the sample 51 which may be determined in this way include properties which may affect the time dependence of ultrasonic signals, and/or their amplitudes. These are (among others) layer thicknesses, 5 sound velocities, interfacial roughness, interfacial adhesion strength, thermal diffusivities, stress, strain, optical constants, surface roughness, and interfacial contaminants.

Figs. 1a-1c illustrate various embodiments of optical 10 sources that are suitable for practicing this invention, while Fig. 2 is a block diagram of an optical generation and detection system for performing non-destructive picosecond time-scale thin film and interface characterizations, referred to hereinafter as system 1.

15 A first embodiment of an optical source 10 is shown in Fig. 1a, in which the beam from a laser 12 is reflected from a mirror 14 and passes through a polarization rotating device, such as a half-wave plate 16, to a polarizing beam splitter 18. The beams emerging from the polarizing beam 20 splitter 18 are orthogonally polarized, and the ratio of their intensities may be varied through a wide range by adjusting the orientation of the half-wave plate 16. One beam forms the pump beam 21a, while the probe beam 21b reflects from a mirror 20.

25 An alternative embodiment of an optical source 10' shown in Fig. 1b includes a frequency doubling crystal 24, such as BBO or LBO, onto which the laser light is focused by a lens 22 positioned between it and the laser 12. The coaxial 30 beams of light emerging from the frequency doubling crystal 24 are separated by means of a dichroic mirror 26 into the pump and probe beams, each of which is then collimated by lenses 28 and 30. The polarization of the pump beam 21a is rotated to be perpendicular to that of the probe beam 21b

(penetration depth) for the pump or probe light in the structure.

- A method for finding any number of unknowns is to compute a simulated optical response for a particular set of parameters, and then to adjust the values of the parameters as needed to achieve a best-fit to the measured result. Presently preferred methods for carrying out this modelling and simulation are described in detail below with reference to Fig. 21.
- 10 The basic equations for the vibrational part of the simulations are taken from well-known continuum elasticity theory. The basic equations for the optical part of the simulation are the Fresnel equations. As an illustration in one dimension (i.e. for a sample 51 with a stress wave propagating with velocity  $v$ , along a direction  $z$  normal to the surface), the quantity to be computed in the simulation can be written as follows:
- $$\Delta R(t) = \int_0^{\infty} f(z) \eta_{33}(z, t) dz \quad (1)$$
- 20 In this equation  $f(z)$  is the change in the reflectivity with strain associated with stress  $\eta_{33}(z, t)$  at depth  $z$ .  $\Delta R(t)$  is the strain induced change in the optical reflectivity of the sample at a time  $t$ . Similar equations can be written for changes in the transmission or in the polarization state of the probe beam 21b. The function  $f(z)$  25 includes the effect of strain on the optical constants within the sample 51, as well as the effect of displacement of the surface or internal interfaces (i.e. a time-dependent change in the thickness of one or more layers) due to the presence of a stress wave.
- 30 In accordance with an aspect of this invention, the

For a sufficiently thick opaque film disposed on a substrate the pump light will be absorbed in a surface layer of thickness small compared to the film thickness. The absorption in the surface layer generates a stress pulse which propagates back and forth in the film, giving rise to a series of equally-separated features ("echoes") in the responses measured by the probe beam. The thickness of a simple film that is thick enough to have distinct echoes can be determined from the echo time, as described by Tauc et al. For a thinner film, the echoes become so closely spaced that they degenerate into vibrational thickness modes of the film, appearing as damped oscillations in the data, and the thickness can be deduced from the vibration period. For intermediate thickness films, or for films composed of multiple layers, the data may be too complicated to analyze so simply. In such cases it is preferred to construct a theoretical model for the vibrating structure in which there may be one or more adjustable unknowns (e.g. film thicknesses, densities, sound velocities). The theoretical model is used to simulate the vibrations of the structure over a suitable time interval (in discrete time steps), and to calculate the corresponding change in the optical reflectivity of the sample (or transmission, or polarization state, or optical phase of the transmitted or reflected beams caused by the stress induced change in the optical constants of the sample, or by stress induced displacements of the surface or of interfaces within the structure). The duration of the time steps are preferably selected to be small compared to a time required for an acoustic wave to propagate through a thinnest layer of the structure (e.g., 0.1 psec to 200 psec). By example, the duration of each time step can be established at less than one half (e.g., one tenth) of the propagation time through the thinnest layer. Also by example, the duration of each time step can be selected to be small compared to a shortest absorption length.

By way of introduction, the arrangement of the pump and probe beam according to this invention is illustrated in Fig. 10. A test sample 51 is shown comprised of a film 84 disposed on substrate 80. An interface 82 is formed between 5 the film 84 and the substrate 80. By example, the substrate 80 may be comprised of a semiconductor such as silicon and may form a portion of a semiconductor wafer, and the film 84 may be an overlying layer of oxide, polymer, metal, or another semiconductor. In another exemplary embodiment the 10 sample may be a SOI wafer comprised of a silicon substrate, a thin layer of silicon oxide, and an overlying (typically thin) layer of silicon, as is shown in Fig. 11. To test the sample 51 the pump beam 21a is directed onto a position on the film 84 (referred to as a focal spot FS1) to generate 15 a stress wave in the sample due to the absorption of energy in the film 84 or substrate 80. The pump beam 21a is incident on the sample 51 at an angle  $\theta_1$ , offset from normal. The unabsorbed portion of the pump beam is reflected as the reflected pump beam 21a'. The probe beam 20 21b may be directed to the same spot (FS1) on the sample at an angle  $\theta_2$ , to intercept the stress pulse generated by the pump beam 21a. In other embodiments of the invention the probe beam 21b can be directed to another location (FS2). A portion of the probe beam 21b reflects from the film 84 25 as the reflected probe beam 21b'. Any portion of the probe beam 21b that is transmitted through the sample is referred to as the transmitted probe beam 21b''. The actual values of angles  $\theta_1$  and  $\theta_2$  can be selected from a wide range of angles. The intensities of the reflected and transmitted 30 pump and probe beams depend on the optical constants of the film 84 and substrate 80 and on the thicknesses of the films.

Fig. 10 also illustrates probing at points (FS2) at a distance from the pump beam FS1, which applies to the 35 ultrasonic and all other applications disclosed herein.

simulation method in accordance with an aspect of this invention.

DETAILED DESCRIPTION OF THE INVENTION

The disclosure of the above-referenced U.S. Patent No. 5 4,710,030 (Tauc et al.) is incorporated by reference herein in its entirety.

The teaching of this invention is embodied by an optical generator and detector of a stress wave within a sample. In this system a first non-destructive pulsed beam of electromagnetic radiation is directed upon a sample containing at least one film and possibly also an interface between similar or dissimilar materials. The first pulsed beam of electromagnetic radiation, referred to herein as a pump beam 21a, produces a propagating stress wave within 10 the sample. A second non-destructive pulsed beam of electromagnetic radiation, referred to herein as a probe beam 21b, is directed upon the sample such that at least one of the polarization, optical phase, position, direction 15 and intensity of a reflected portion of the probe beam 21b' or a transmitted portion of the probe beam 21b'' is affected by a change in the optical constants of the materials comprising the sample, or by a change in the thickness of one or more layers or sublayers within a thin 20 film sample due to a propagating stress wave. Physical and chemical properties of the materials, and possibly also of 25 the interface, are measured by observing the changes in the reflected or transmitted probe beam intensity, direction, or state of polarization as revealed by the time dependence of the changes in beam intensity, direction or state of 30 polarization. The very short time scale is particularly important for achieving a high sensitivity to interfacial and other properties, and for measuring the properties of films having thicknesses less than several microns.

interfaces between the substrate and one of the thin film layers and between the thin film layers;

Figs. 15a-15d each illustrate an optically-induced stress wave, having a velocity  $v_s$ , that propagates in a material, and the reflection of a portion of the probe beam from the stress wave;

Fig. 16 is a block diagram of a first embodiment of a picosecond ultrasonic system in accordance with this invention, specifically, a parallel, oblique beam embodiment;

Fig. 17 is a block diagram of a second embodiment of a picosecond ultrasonic system in accordance with this invention, specifically, a normal pump, oblique probe embodiment;

15 Fig. 18 is a block diagram of a third, presently preferred embodiment of a picosecond ultrasonic system in accordance with this invention, specifically, a single wavelength, normal pump, oblique probe, combined ellipsometer embodiment;

20 Fig. 19 is a block diagram of a fourth embodiment of a picosecond ultrasonic system in accordance with this invention, specifically, a dual wavelength, normal pump, oblique probe, combined ellipsometer embodiment;

25 Fig. 20 is a block diagram of a fifth embodiment of a picosecond ultrasonic system in accordance with this invention, specifically, a dual wavelength, normal incidence pump and probe, combined ellipsometer embodiment; and

Fig. 21 is a logic flow diagram that illustrates a

Fig. 8 illustrates a further embodiment of this invention wherein a length of fiber optic is employed to compensate for a change in probe beam profile as a function of delay between the pump and probe beam pulses;

5 Fig. 9 illustrates an embodiment of a delay stage used for setting a delay between the pump and probe beam pulses;

10 Fig. 10 is a cross-sectional, enlarged view of the sample having the substrate, thin film layer, and the interface between the substrate and the thin film layer, and that further illustrates the impingement of the probe beam within a focussed spot (FS1) of the pump beam, and the impingement of the probe beam at a second FS (FS2) that is displaced from FS1;

15 Fig. 11 is an enlarged, cross-sectional view of a silicon-on-insulator (SOI) sample that is amenable to characterization in accordance with this invention;

20 Fig. 12 is a cross-sectional, enlarged view of the sample having the substrate, a localized thin film structure disposed on a surface of the substrate, and the interface between the substrate and the thin film structure, and that further illustrates various methods to apply the pump and probe beams;

25 Fig. 13 is a cross-sectional, enlarged view of the sample having the substrate, a localized thin film structure disposed within a surface of the substrate, and the interface between the substrate and the thin film structure, and that further illustrates various methods to apply the pump and probe beams;

30 Fig. 14 is a cross-sectional, enlarged view of a sample having a substrate, a plurality of thin film layers, and

BRIEF DESCRIPTION OF THE DRAWINGS

The above set forth and other features of the invention are made more apparent in the ensuing Detailed Description of the Invention when read in conjunction with the attached

5 Drawings, wherein:

Figs. 1a-1c depict embodiments of optical sources for use with the system of this invention;

Fig. 2 is a block diagram of an embodiment of a sample characterization system in accordance with this invention;

10 Figs. 3a-3f each depict an embodiment of a pump beam/probe beam delivery technique to a surface of a sample;

Fig. 4a is a diagram that illustrates a variability in a temporal offset between pump and probe beam pulses;

15 Fig. 4b is block diagram that illustrates an embodiment of electro-optical components responsive to the delay between the pump and probe pulses, as shown in Fig. 4a;

20 Fig. 5 is a cross-sectional, enlarged view of a sample having a substrate, a thin film layer, and an interface between the substrate and the thin film layer, and that further illustrates a stress-induced deformation in the thin film wherein constructive and destructive probe beam interference occurs;

Fig. 6 illustrates a second embodiment of the interface characterization system in accordance with this invention;

25 Fig. 7 illustrates a fiber optic-based pump and probe beam delivery and focussing system in accordance with an embodiment of this invention;

may incorporate a small lens at its output. A similar focussing fiber can be used to gather reflected probe light and direct it to an optical detector. A fiber may also be used to modify the beam profile, or as a spatial filter to effect a constant beam profile under widely varying input beam conditions.

This invention advantageously provides a non-destructive system and method for measuring at least one transient response of a structure to a pump pulse of optical radiation, the measured transient response or responses including at least one of a measurement of a modulated change  $\Delta R$  in an intensity of a reflected portion of a probe pulse, a change  $\Delta T$  in an intensity of a transmitted portion of the probe pulse, a change  $\Delta P$  in a polarization of the reflected probe pulse, a change  $\Delta\phi$  in an optical phase of the reflected probe pulse, and a change in an angle of reflection  $\Delta\theta$  of the probe pulse, each of which may be considered as a change in a characteristic of a reflected or transmitted portion of the probe pulse. The measured transient response or responses are then associated with at least one characteristic of interest of the structure.

In a presently preferred embodiment the system provides for automatically focusing the pump and probe pulses to achieve predetermined focusing conditions, and the application of at least one calibration factor to the at least one transient response. This embodiment is especially useful when employed with time-evolved simulations and models of a structure of interest, which is a further aspect of this invention.

- optically opaque substrate, at the pump wavelength, the pump and probe beams may both impinge from the film side, or the pump may impinge from the film side and the probe may impinge from the substrate side. For a sample with a
- 5 transparent substrate, both beams may impinge from the film side, or from the substrate side, or from opposite sides of the sample. The optical and thermal properties are such that the pump pulse changes the temperature within at least one film with respect to the substrate. The temperature
- 10 within one or more of the thin films disposed on the substrate may be uniform, and may be equal in several films. The films may have thicknesses ranging from 1 Å to 100 microns. At least one film in the sample and/or the substrate has the property that when a stress wave is
- 15 present it causes a change in the intensity, optical phase, polarization state, position, or direction of the probe beam at the detector. The probe beam source may provide a continuous radiation beam, and the pump beam source may provide at least one discrete pump pulse having a duration
- 20 of 0.01 to 100 psec and an average power of 10µW to 1 kW. Alternatively the probe beam source may provide probe beam pulses having a duration of 0.01 to 100 psec, the pump beam and probe beam may impinge at the same location on the sample, and the mechanisms for directing and guiding may
- 25 include a common lens system for focusing the pump beam and the probe beam onto the sample. The position of impingement of the probe beam may be shifted spatially relative to that of the pump beam, and the probe beam may be transmitted or reflected by the sample.
- 30 One or more fiber optic elements may be incorporated within the system. Such fibers may be used to guide one or more beams within the system for reducing the size of the system, and/or to achieve a desired optical effect such as focussing of one or more beams onto the surface of the
- 35 sample. To achieve focussing, the fiber may be tapered, or

- that generates a plurality of short duration pulses, and the system further includes a beam splitter for directing a first portion of the source beam to form the pump beam, having the plurality of pulses, and directing a second portion to form the probe beam, also having the plurality of pulses. The source beam has a single direction of polarization and the system further includes means for rotating the polarization of the probe beam and a device, disposed between a sample and the optical detector, for transmitting only radiation having the rotated direction of polarization. The system may further include a temperature detector and a chopper for modulating the pump beam at a predetermined frequency. The system can further include a mechanism for establishing a predetermined time delay between the impingement of a pulse of the pump beam and a pulse of the probe beam upon the sample. The system can further include circuitry for averaging the output of the optical detector for a plurality of pulse detections while the delay between impingements remains set at the predetermined time delay. The delay setting mechanism may sequentially change the predetermined time delay and the circuitry for averaging may successively average the output of the optical detector during each successive predetermined time delay setting.
- By example, the pump beam may receive 1% to 99% of the source beam, and the source beam may have an average power of  $10\mu\text{W}$  to 10kW. The source beam may include wavelengths from 100 Angstroms to 100 microns, and the radiation pulses of the source beam may have a duration of 0.01 psec to 100 psec.

The sample may include a substrate and at least one thin film to be examined disposed on the substrate such that interfaces exist where the films meet, and/or where the film and the substrate meet. For a sample with an

properties. In the system of this invention incident light is absorbed in a thin film or in a structure made up of several thin films; and the change in optical transmission or reflection is measured and analyzed. The change in reflection or transmission is used to give information about the ultrasonic waves that are produced in the structure. The information that is obtained from the use of the measurement methods and apparatus of this invention can include: (a) a determination of the thickness of thin films with a speed and accuracy that is improved compared to earlier methods; (b) a determination of the thermal, elastic, electrical, and optical properties of thin films; (c) a determination of the stress in thin films; and (d) a characterization of the properties of interfaces, including the presence of roughness and defects.

The invention features a radiation source for providing a pump beam and a detection system for non-destructively measuring the properties of one or more interfaces within a sample. The radiation source provides the pump beam so as to have short duration radiation pulses having an intensity and at least one wavelength selected to non-destructively induce a propagating stress wave in the sample, a radiation source for providing a probe beam, a mechanism for directing the pump beam to the sample to generate the stress wave within the sample, and a mechanism for guiding the probe beam to a location at the sample to intercept the stress wave. A suitable optical detector is provided that is responsive to a reflected or transmitted portion of the probe beam for detecting a change in the optical constants of the material induced by the stress wave.

In one embodiment, the optical detector measures the intensity of the reflected or transmitted probe beam. The pump and probe beam may be derived from the same source

structure.

It is one still further object of this invention to provide an ultrafast optical system and technique wherein optical fibers are used to advantage for directing and/or focussing 5 at least one of an incident pump beam, and incident probe beam, or a reflected or transmitted probe beam.

It is another object of this invention to provide a non-destructive system and method for simultaneously measuring 10 at least two transient responses of a structure to a pump pulse, the measured transient responses comprising at least two of a measurement of a modulated change  $\Delta R$  in an intensity of a reflected portion of a probe pulse, a change  $\Delta T$  in an intensity of a transmitted portion of the probe pulse, a change  $\Delta P$  in a polarization of the reflected probe 15 pulse, a change  $\Delta\phi$  in an optical phase of the reflected probe pulse, and a change in an angle of reflection  $\Delta\theta$  of the probe pulse.

It is one further object of this invention to provide a non-destructive system and method for determining a 20 characteristic of a sample that includes an automatic control over the focussing of pump and probe beams at the sample so as to provide a reproducible intensity variation of the beams during each measurement.

#### SUMMARY OF THE INVENTION

25 The foregoing and other problems are overcome and the objects of the invention are realized by methods and apparatus in accordance with embodiments of this invention.

This invention relates to a system for the characterization 30 of thin films and interfaces between thin films through measurements of their mechanical, optical, and thermal

It is still another object of this invention to provide an improved ultrafast optical technique for determining the elastic modulus, sound velocity, and refractive index of a thin film.

5 It is a still further object of this invention to provide an improved ultrafast optical technique for characterizing an interface between two materials, such as an interface between a substrate and an overlying thin film.

10 It is another object of this invention to provide an ultrafast optical technique for determining a derivative of a transient response of a sample to a pump pulse, and for correlating the derivative with a characteristic of interest, such as the static stress within the sample.

15 It is another object of this invention to provide an ultrafast optical technique for varying a temperature of the sample and, while varying the temperature, for determining a derivative of the acoustic velocity within the sample and for subsequently correlating the derivative of the acoustic velocity with the static stress within the  
20 sample.

It is another object of this invention to provide an ultrafast optical technique for determining an electrical resistivity of a sample.

25 It is a further object of this invention to provide simulation methods for modelling a time-evolved effect of a stress pulse generated within a sample of interest, and to then employ the model to characterize the sample.

30 It is a further object of this invention to provide an ultrafast optical technique for measuring a characteristic of interest in a patterned, periodic, multilayered

intercepts the stress pulse.

In one embodiment a distance between a mirror and a corner cube is varied to vary the delay between the impingement of the pump beam and the probe beam on the sample. In a 5 further embodiment an opto-acoustically inactive film is studied by using an overlying film comprised of an opto-acoustically active medium, such as arsenic telluride. In another embodiment the quality of the bonding between a film and the substrate can be determined from a measurement 10 of the reflection coefficient of the stress pulse at the boundary, and comparing the measured value to a theoretical value.

The methods and apparatus of Tauc et al. are not limited to simple films, but can be extended to obtaining information 15 about layer thicknesses and interfaces in superlattices, multilayer thin-film structures, and other inhomogeneous films. Tauc et al. also provide for scanning the pump and probe beams over an area of the sample, as small as 1 micron by 1 micron, and plotting the change in intensity of 20 the reflected or transmitted probe beam.

While well-suited for use in many measurement applications, it is an object of this invention to extend and enhance the teachings of Tauc et al.

OBJECTS OF THE INVENTION:

25 It is thus an object of this invention to provide an improved optical generator and detector of stress pulses.

It is a further object of this invention to provide an improved ultrafast optical technique for measuring stress in a thin film.

See Downer, M.C.; Fork, R.L.; and Shank, C.V., "Imaging with Femtosecond Optical Pulses", Ultrafast Phenomena IV, Ed. D.H. Auston and K. B. Eisenthal (Springer-Verlag, N.Y. 1984), pp. 106-110.

- 5 Other systems measure thickness, composition or concentration of material by measuring absorption of suitably-chosen wavelengths of radiation. This method is generally applicable only if the film is on a transparent substrate.
- 10 In a nondestructive ultrasonic technique described in U.S. Patent 4,710,030 (Tauc et al.), a very high frequency sound pulse is generated and detected by means of an ultrafast laser pulse. The sound pulse is used to probe an interface. The ultrasonic frequencies used in this
- 15 technique typically are less than 1 THz, and the corresponding sonic wavelengths in typical materials are greater than several hundred Angstroms. It is equivalent to refer to the high frequency ultrasonic pulses generated in this technique as coherent longitudinal acoustic phonons.
- 20 In more detail, Tauc et al. teach the use of pump and probe beams having durations of 0.01 to 100 psec. These beams may impinge at the same location on a sample's surface, or the point of impingement of the probe beam may be shifted relative to the point of impingement of the pump beam. In
- 25 one embodiment the film being measured can be translated in relation to the pump and probe beams. The probe beam may be transmitted or reflected by the sample. In a method taught by Tauc et al. the pump pulse has at least one wavelength for non-destructively generating a stress pulse in the sample. The probe pulse is guided to the sample to intercept the stress pulse, and the method further detects a change in optical constants induced by the stress pulse by measuring an intensity of the probe beam after it

be obtained. This method cannot be used if the film lacks a sharp, distinct edge, or is too soft in consistency to accurately support the stylus.

Another non-destructive method, based on Rutherford Scattering, measures the energy of backscattered helium ions. The lateral resolution of this method is poor.

Yet another technique uses resistance measurements to determine film thickness. For a material of known resistivity, the film thickness is determined by measuring the electrical resistance of the film. For films less than 1000 Angstroms, however, this method is of limited accuracy because the resistivity may be non-uniformly dependent on the film thickness.

In yet another technique, the change in the direction of a reflected light beam off a surface is studied when a stress pulse arrives at the surface. In a particular application, stress pulses are generated by a piezoelectric transducer on one side of a film to be studied. A laser beam focused onto the other side detects the stress pulses after they traverse the sample. This method is useful for film thicknesses greater than 10 microns.

A film may also be examined by striking a surface of the film with an intense optical pump beam to disrupt the film's surface. Rather than observe propagation of stress pulses, however, this method observes destructive excitation of the surface. The disruption, such as thermal melting, is observed by illuminating the site of impingement of the pump beam with an optical probe beam and measuring changes in intensity of the probe beam. The probe beam's intensity is altered by such destructive, disruptive effects as boiling of the film's surface, ejection of molten material, and subsequent cooling of the surface.

amplitudes are converted to a computer-generated photograph of the sample surface. Sample features below the surface are observed by raising the sample to bring the focal point beneath the surface. The lateral and vertical resolution 5 of the acoustic microscope are approximately equal.

Resolution is greatest for the acoustic microscope when a very short wavelength is passed through the coupling liquid. This requires a liquid with a low sound velocity, such as liquid helium. An acoustic microscope using liquid 10 helium can resolve surface features as small as 500 Angstroms, but only when the sample is cooled to 0.1 K.

Several additional techniques, not involving generation and detection of stress pulses, are available for measuring film thickness. Ellipsometers direct elliptically 15 polarized light at a film sample and analyze the polarization state of the reflected light to determine film thickness with an accuracy of 3-10 Angstroms. The elliptically polarized light is resolved into two components having separate polarization orientations and a 20 relative phase shift. Changes in polarization state, beam amplitudes, and phase of the two polarization components are observed after reflection.

The ellipsometer technique employs films which are reasonably transparent. Typically, at least 10% of the 25 polarized radiation must pass through the film. The thickness of metal sample films thus cannot exceed a few hundred Angstroms.

Another technique uses a small stylus to mechanically measure film thickness. The stylus is moved across the 30 surface of a substrate and, upon reaching the edge of a sample film, measures the difference in height between the substrate and the film. Accuracies of 10-100 Angstroms can

WO 97/27466

2

optical and mechanical devices which employ thin films. In one nondestructive technique a radio frequency pulse is applied to a piezoelectric transducer mounted on a substrate between the transducer and the film to be studied. A stress pulse propagates through the substrate toward the film. At the boundary between the substrate and the film, part of the pulse is reflected back to the transducer. The remainder enters the film and is partially reflected at the opposite side to return through the substrate to the transducer. The pulses are converted into electrical signals, amplified electronically, and displayed on an oscilloscope. The time delay between the two pulses indicates the film thickness, if the sound velocity in the film is known, or indicates the sound velocity, if the film thickness is known. Relative amplitudes of the pulses provide information on the attenuation in the film or the quality of the bond between the film and the substrate.

The minimum thickness of films which can be measured and the sensitivity to film interface conditions using conventional ultrasonics is limited by the pulse length. The duration of the stress pulse is normally at least 0.1  $\mu$ sec corresponding to a spatial length of at least  $3 \times 10^2$  cm for an acoustic velocity of  $3 \times 10^5$  cm/sec. Unless the film is thicker than the length of the acoustic pulse, the pulses returning to the transducer will overlap in time. Even if pulses as short in duration as 0.001  $\mu$ sec are used, the film thickness must be at least a few microns.

Another technique, acoustic microscopy, projects sound through a rod having a spherical lens at its tip. The tip is immersed in a liquid covering the film. Sound propagates through the liquid, reflects off the surface of the sample, and returns through the rod to the transducer. The amplitude of the signal returning to the transducer is measured while the sample is moved horizontally. The

**IMPROVED OPTICAL STRESS GENERATOR AND DETECTOR**

**CLAIM OF PRIORITY FROM A COPENDING PROVISIONAL PATENT**

**APPLICATION:**

Priority is herewith claimed under 35 U.S.C. §119(e) from copending Provisional Patent Application having application number 60/010,543, filed on January 23, 1996 in the names of Humphrey Maris and Robert Stoner, and entitled "Improved Optical Stress Generator and Detector". This Provisional Patent Application is incorporated by reference herein in its entirety.

**STATEMENT OF GOVERNMENT RIGHTS:**

This invention was made with government support under grant/contract number DEFG02-ER45267 awarded by the Department of Energy. The government has certain rights in the invention.

**FIELD OF THE INVENTION:**

This invention relates to a system for measuring the properties of thin films, and more particularly to a system which optically induces stress pulses in a film and which optically measures the stress pulses propagating within the film.

**BACKGROUND OF THE INVENTION:**

Presently, the nondestructive evaluation of thin films and interfaces is of interest to manufacturers of electrical,

**FOR THE PURPOSES OF INFORMATION ONLY**

Codes used to identify States party to the PCT on the front pages of pamphlets publishing international applications under the PCT.

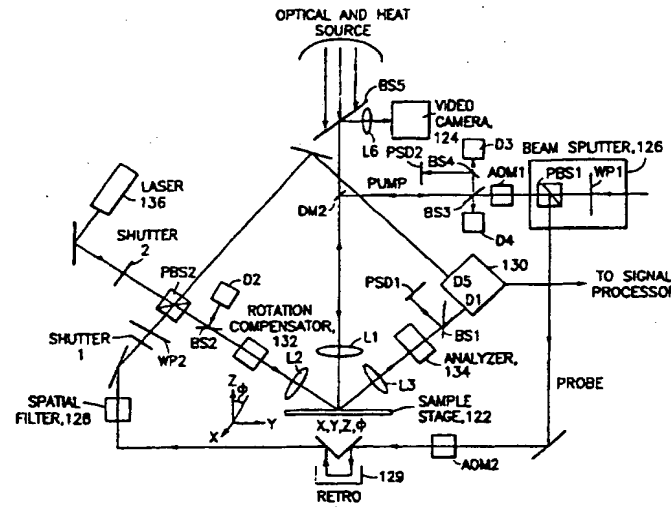
AM	Armenia	GB	United Kingdom	MW	Malawi
AT	Austria	GE	Georgia	MX	Mexico
AU	Australia	GN	Guinea	NE	Niger
BB	Barbados	GR	Greece	NL	Netherlands
BE	Belgium	HU	Hungary	NO	Norway
BF	Burkina Faso	IE	Ireland	NZ	New Zealand
BG	Bulgaria	IT	Italy	PL	Poland
BJ	Benin	JP	Japan	PT	Portugal
BR	Brazil	KE	Kenya	RO	Romania
BY	Belarus	KG	Kyrgyzstan	RU	Russian Federation
CA	Canada	KP	Democratic People's Republic of Korea	SD	Sudan
CF	Central African Republic	KR	Republic of Korea	SE	Sweden
CG	Congo	KZ	Kazakhstan	SG	Singapore
CH	Switzerland	LJ	Liechtenstein	SI	Slovenia
CI	Côte d'Ivoire	LK	Sri Lanka	SK	Slovakia
CM	Cameroon	LR	Liberia	SN	Senegal
CN	China	LT	Lithuania	SZ	Swaziland
CS	Czechoslovakia	LU	Luxembourg	TD	Chad
CZ	Czech Republic	LV	Latvia	TG	Togo
DE	Germany	MC	Monaco	TJ	Tajikistan
DK	Denmark	MD	Republic of Moldova	TT	Trinidad and Tobago
EE	Estonia	MG	Madagascar	UA	Ukraine
ES	Spain	ML	Mali	UG	Uganda
FI	Finland	MN	Mongolia	US	United States of America
FR	France	MR	Mauritania	UZ	Uzbekistan
GA	Gabon			VN	Viet Nam



## INTERNATIONAL APPLICATION PUBLISHED UNDER THE PATENT COOPERATION TREATY (PCT)

(51) International Patent Classification <sup>6</sup> : <b>G01N 21/00, 29/04</b>		A1	(11) International Publication Number: <b>WO 97/27466</b> (43) International Publication Date: <b>31 July 1997 (31.07.97)</b>
(21) International Application Number: <b>PCT/US96/20917</b> (22) International Filing Date: <b>31 December 1996 (31.12.96)</b>		(81) Designated States: DE, GB, IL, JP, KR, European patent (AT, BE, CH, DE, DK, ES, FI, FR, GB, GR, IE, IT, LU, MC, NL, PT, SE).	
(30) Priority Data: 60/010,543 23 January 1996 (23.01.96) US 08/689,287 6 August 1996 (06.08.96) US		<b>Published</b> <i>With international search report.</i>	
(71) Applicant: BROWN UNIVERSITY RESEARCH FOUNDATION [US/US]; 42 Charlesfield Street, Providence, RI 02912 (US). (72) Inventors: MARIS, Humphrey, J.; 9 Echo Drive, Barrington, RI 02806 (US). STONER, Robert, J.; 52 Crooked Lane, Duxbury, MA 02332 (US). (74) Agent: GREEN, Clarence, A.; Perman & Green, 425 Post Road, Fairfield, CT 06430 (US).			

## (54) Title: IMPROVED OPTICAL STRESS GENERATOR AND DETECTOR



## (57) Abstract

A system for the characterization of thin films and interfaces between thin films through measurements of their mechanical and thermal properties. In the system light, from laser (136) is absorbed in a thin film or in a structure made up of several thin films, and the change in optical transmission or reflection is measured and analyzed using analyser (134). The change in reflection or transmission is used to give information about the ultrasonic waves that are produced in the structure. The information that is obtained from the use of the measurement methods and apparatus of this invention can include: (a) a determination of the thickness of thin films with a speed and accuracy that is improved compared to earlier methods; (b) a determination of the thermal, elastic, and optical properties of thin films; (c) a determination of the stress in thin films; and (d) a characterization of the properties of interfaces, including the presence of roughness and defects.

patterned structures because, again, it is essentially a one dimensional method. Thus, another more suitable numerical method is used instead.

5 The teaching of this invention also includes methods and apparatus for exciting stress pulses in one part of a thin film or multilayer in order to detect a change in another part of the thin film, such as a presence of a chemical reaction, intermixing, or alloying at one or more interfaces within the sample.

10 Relatedly, the teaching of this invention also encompasses the characterization of interfacial chemical reactions between two or more layers, or between a layer and interface, and the correlation of the acoustical and optical measurements with reactant species. This includes  
15 the characterization of the structural phase, and one or more of the thickness and sound velocity of the layers in the sample, including any new layers formed by the chemical reaction.

20 The teachings of this invention also pertain to the characterization of ion implant dose, energy, species, or any other ion implant parameters for an ion implant made through a film for the purpose of, by example, altering its adhesion to a substrate or an underlying layer. This characterization is carried out in accordance with any of  
25 the above-described techniques, in which the adhesion may be deduced from the temporal characteristics of the observed probe response, or by a simple comparison with a reference response for a sample prepared under like conditions.

30 Finally, this invention teaches a method for deducing the derivative of the index of refraction  $n$  or extinction coefficient  $\kappa$  of a material with respect to stress or

strain by making measurements of the reflectivity change in the material caused by a stress pulse, of which a computable fraction has also been detected in a second material whose derivatives of index of refraction and  
5 extinction coefficient with respect to stress or strain are known or may be determined separately.

It should thus be apparent that while the invention has been particularly shown and described with respect to a number of embodiments thereof, the teachings of this  
10 invention are not to be construed to be limited to only these disclosed embodiments. That is, changes in form and details may be made to these disclosed embodiments without departing from the scope and spirit of the invention. The teaching of this invention should thus be afforded a scope  
15 that is commensurate with the scope of the claims which follow.

CLAIMS

What is claimed is:

1. A method for characterizing a structure, comprising the steps of:

applying first electromagnetic radiation to the structure for creating propagating stress pulses within the structure;

applying second electromagnetic radiation to the structure at a plurality of different incidence angles so as to intercept the propagating stress pulses;

sensing a reflection or transmission of the second electromagnetic radiation from the structure at the plurality of incidence angles;

associating a change in the reflection of the second electromagnetic radiation over time with a value of an optical characteristic of the structure, and determining in accordance with the value of the optical characteristic the velocities of the propagating stress pulses; and

optionally determining the elastic modulus of the structure in accordance with the determined velocities of the propagating stress pulses.

2. A method for characterizing a three dimensional sample comprised of a substrate and possibly one or more films deposited on said substrate together with at least one structure that is disposed upon or embedded within the substrate or one or more of the films, comprising the steps of:

simulating a mechanical response of the sample, at a plurality of discrete time steps, to the application of pulses of first electromagnetic radiation;

applying pulses of the first electromagnetic radiation to the sample for creating propagating stress pulses within the sample;

applying second electromagnetic radiation to the sample so as to intercept the propagating stress pulses;

sensing from a reflection of the second electromagnetic radiation from the sample at least one of a time-varying change in intensity, position, direction, polarization state, and optical phase of the second electromagnetic radiation; and

associating the sensed time-varying change with a property of interest of the sample in accordance with the simulated response of the sample.

3. A method as set forth in claim 2, wherein the property of interest includes a dimension that is other than a thickness of the at least one film.

4. A method for characterizing a structure, comprising the steps of:

simulating at predetermined time step increments, in accordance with one or more characteristics of the structure, a mechanical response of a simulated structure over an interval of time to an application of a first pulse of optical radiation by at least the steps of,

determining an initial stress distribution within the simulated structure;

determining a change over the interval of time in the stress and strain distribution in the simulated structure following an application of the first pulse of optical radiation, and

determining the transient optical response of the simulated structure by application of a second pulse of optical radiation within the interval of time;

applying the first pulse of optical radiation to the structure;

applying, during the interval of time, the second pulse of optical radiation to the structure;

comparing a measured transient response of the structure to the determined transient response for the simulated structure;

adjusting a value of the one or more characteristics of the simulated structure so as to bring the determined transient response into agreement with the measured transient response; and

associating the adjusted value of the one or more characteristics with a value of one or more actual characteristics of the structure.

5. A method as set forth in claim 4, wherein the structure further comprises at least one layer disposed over a substrate, and wherein the step of determining an initial stress distribution within the simulated structure includes the steps of:

from optical constants and a thickness of the at least

one layer, calculating an electric field, due to the first optical pulse, in the simulated structure in terms of an amplitude, angle of incidence, and polarization of the first pulse on a surface of the structure;

from the calculated electric field distribution, calculating an amount of energy absorbed in the simulated structure as a function of position;

determining an effect of thermal diffusion on the absorbed energy distribution;

calculating a temperature rise as a function of position within the simulated structure; and

calculating a stress within the simulated structure from the calculated temperature rise.

6. A method as set forth in claim 4, wherein the step of determining a change in stress and strain in the simulated structure includes the steps of:

selecting a time step  $\tau$ ;

for each layer of the simulated structure, calculating a bin size  $b$  equal to the time step  $\tau$  multiplied by the sound velocity in the layer; and

dividing each layer into bins of the calculated bin size or bins smaller than the calculated bin size.

7. A method as set forth in claim 6, wherein the step of determining a change in stress and strain in the simulated structure further includes the steps of:

decomposing the stress in each bin into two components, one component initially propagating towards a free surface of the simulated structure and one component propagating away from the free surface of the simulated structure;

within each layer, stepping the two components forward from bin to bin in the appropriate direction, wherein for a bin adjacent to a boundary between two layers the stress propagating towards the boundary is stepped partly into the first bin on the other side of the boundary;

repeating the foregoing steps for a sufficient number of time steps ; to determine the stress distribution for a period at least equal the interval of time; and

calculating the strain from the determined stress by division by an appropriate elastic coefficient.

8. A method as set forth in claim 4, wherein the structure further comprises at least one layer disposed over a substrate, and wherein the step of determining a transient response of the simulated structure to an application of a second pulse of optical radiation within the interval of time includes the steps of:

calculating changes  $\Delta n$  and  $\Delta k$  in optical constants of each layer from calculated strain distribution as a function of depth into the simulated structure; and

from the calculated changes  $\Delta n$  and  $\Delta k$  in the optical constants as a function of depth, and from unperturbed optical constants of the at least one layer, calculating at least one of the quantities  $\Delta R$ ,  $\Delta T$ ,  $\Delta P$ ,  $\Delta\phi$  and  $\Delta\beta$ .

9. A method as set forth in claim 8, wherein the step of comparing a measured transient response of the structure to the determined transient response compares the at least one of the calculated quantities  $\Delta R$ ,  $\Delta T$ ,  $\Delta P$ ,  $\Delta\phi$  and  $\Delta\beta$  with a measured result.

10. A method as set forth in claim 4, wherein said plurality of discrete time steps are selected to be small compared to a time required for an acoustic wave to propagate through a thinnest layer that comprises the structure.

11. A non-destructive system for characterizing a sample, comprising:

means for generating an optical pump pulse and for focussing the pump pulse relative to a surface of the sample;

means for generating an optical probe pulse and for focussing the probe pulse relative to the surface of the sample;

means for measuring at least one transient response of the structure to the pump pulse by detecting a change in a reflected or transmitted portion of the probe pulse; and

detector means for automatically adjusting the focus of at least one of the pump and probe pulses in response to reflected portions of at least one of the pump and probe pulses.

12. A non-destructive system for characterizing a sample as set forth in claim 11, wherein said means for generating an optical pump pulse generates a train of pump

pulses which are applied to a single location on the surface of the sample.

13. A non-destructive system for characterizing a sample as set forth in claim 11, wherein the pump pulse induces a stress pulse in the sample that propagates normal to the surface.

14. A non-destructive system for characterizing a sample, comprising:

means for generating an optical pump pulse and for directing the pump pulse to an area of the surface of the sample;

means for generating an optical probe pulse and for directing the probe pulse to a same or different area of the surface of the sample so as to arrive after the pump pulse;

means for measuring at least one transient response of the structure to the pump pulse by detecting a change in a reflected or transmitted portion of the probe pulse; and

means for determining an electrical resistivity of at least a portion of the sample in accordance with the measured transient response.

15. A non-destructive system for characterizing a sample, comprising:

means for generating an optical pump pulse and for directing the pump pulse to an area of the surface of the sample;

means for generating an optical probe pulse and for directing the probe pulse to a same or different area of the surface of the sample so as to arrive after the pump pulse;

means for measuring at least one transient response of the structure to the pump pulse by detecting a change in a characteristic of a reflected or transmitted portion of the probe pulse;

means for varying a temperature of at least a portion of the structure during the operation of the measuring means; and

means for determining, from the measured transient response, a derivative of a velocity of an acoustic wave within the structure with respect to temperature, and for associating the determined derivative of the velocity with a static stress within the structure.

16. A method for operating a non-destructive system for characterizing a sample, comprising the steps of:

generating an optical pump pulse and directing the pump pulse to an area of the surface of the sample;

generating an optical probe pulse and directing the probe pulse to a same or different area of the surface of the sample so as to arrive after the pump pulse;

measuring at least one transient response of the structure to the pump pulse by detecting a change in a characteristic of a reflected or transmitted portion of the probe pulse; and

determining an electrical resistivity of a portion of

the sample in accordance with the measured transient response.

17. A method for operating a non-destructive system for characterizing a sample, comprising the steps of:

generating an optical pump pulse and directing the pump pulse to an area of the surface of the sample;

generating an optical probe pulse and directing the probe pulse to a same or different area of the surface of the sample so as to arrive after the pump pulse;

measuring at least one transient response of the structure to the pump pulse by detecting a change in a characteristic of a reflected or transmitted portion of the probe pulse;

varying a temperature of at least a portion of the structure during the step of measuring; and

determining, from the measured transient response, a derivative of a velocity of an acoustic wave within the structure with respect to temperature, and associating the determined derivative of the velocity with a static stress within the structure.

18. A non-destructive system for characterizing a sample, comprising:

means for generating a sequence of optical pump pulses at a frequency  $f$ , and for directing the sequence of pump pulses to an area of the surface of the sample;

means for generating a sequence of optical probe

100

pulses at a frequency  $f_2$  and for directing the sequence of probe pulses to a same or different area of the surface of the sample, wherein  $f_1$  is not equal to  $f_2$  for continuously varying a delay between the generation of a pump pulse and the generation of a probe pulse; and

means for measuring, at a rate given by one of  $(f_1-f_2)$  or  $(f_1+f_2)$ , at least one transient response of the structure to the sequence of pump pulses by detecting a change in a characteristic of a reflected or transmitted portion of the sequence of probe pulses.

19. A non-destructive system for characterizing a sample, comprising:

means for generating a sequence of optical pump pulses and for directing the sequence of pump pulses to an area of the surface of the sample;

means for generating a sequence of optical probe pulses, wherein a delay between individual ones of the probe pulses, with respect to an individual one of the pump pulses, is modulated at a frequency  $f$  and for directing the sequence of probe pulses to a same or different area of the surface of the sample; and

means for measuring, at a rate given by  $f$ , at least one transient response of the structure to the sequence of pump pulses by detecting a change in a characteristic of a reflected or transmitted portion of the sequence of probe pulses.

20. A non-destructive system for characterizing a sample, comprising:

means for generating a sequence of optical pump pulses that are intensity modulated at a frequency  $f_1$ , and for directing the sequence of pump pulses to an area of the surface of the sample;

means for generating a sequence of optical probe pulses, wherein a delay between individual ones of the probe pulses, with respect to an individual one of the pump pulses, is modulated at a frequency  $f_2$ , and for directing the sequence of probe pulses to a same or different area of the surface of the sample, wherein  $f_1$  is not equal to  $f_2$ ; and

means for measuring, at a rate given by one of  $(f_1-f_2)$  or  $(f_1+f_2)$ , at least one transient response of the structure to the sequence of pump pulses by detecting a change in a characteristic of a reflected or transmitted portion of the sequence of probe pulses.

21. A non-destructive system for characterizing a sample, comprising:

means for generating an optical pump pulse having a first wavelength and for directing the pump pulse to an area of the surface of the sample;

means for generating an optical probe pulse from the optical pump pulse and for directing the probe pulse to a same or different area of the surface of the sample so as to arrive after the pump pulse, the optical probe pulse being generated to have a second wavelength that is a harmonic of the first wavelength; and

means for measuring at least one transient response of the structure to the pump pulse by detecting a change

in a characteristic of the reflected or transmitted portion of the probe pulse.

22. A non-destructive system for characterizing a sample, comprising:

means for generating an optical pump pulse and an optical probe pulse from an input pulse having a first wavelength, wherein the pump pulse has a wavelength that is a harmonic of the first wavelength and the probe pulse has a wavelength that is equal to the first wavelength;

means for directing the pump pulse to an area of the surface of the sample and for directing the probe pulse to a same or different area of the surface of the sample so as to arrive after the pump pulse; and

means for measuring at least one transient response of the structure to the pump pulse by detecting a change in a characteristic of the reflected or transmitted portion of the probe pulse.

23. A method for operating a non-destructive system for characterizing a sample, comprising the steps of:

generating an optical pump pulse and directing the pump pulse to an area of the surface of the sample;

generating an optical probe pulse and directing the probe pulse to a same or different area of the surface of the sample so as to arrive after the pump pulse;

measuring at least one transient response of the structure to the pump pulse by detecting a change in a reflected portion of the probe pulse; and

detecting at least one acoustic echo in the reflected portion of the probe pulse, the step of detecting including a step of determining a time of arrival of the acoustic echo by convolving the detected acoustic echo with a predetermined function.

24. A method for operating a non-destructive system for characterizing a sample, comprising the steps of:

generating an optical pump pulse and directing the pump pulse to an area of the surface of the sample;

for each generated optical pump pulse, generating an optical probe pulse and directing the probe pulse to the surface of the sample so as to arrive after the pump pulse, wherein some of the probe pulses are directed to the surface at a first angle relative to the surface, and others of the probe pulses are directed to the surface at a second angle relative to the surface; and

measuring at least one transient response of the structure to the pump pulses by detecting a change in a reflected portion of the probe pulses at each of the first and second angles.

25. A method for characterizing a structure comprised of a substrate and at least one layer that is an intentionally or a non-intentionally formed layer that is disposed over the substrate, comprising the steps of:

generating a reference data set of a transient optical response of the structure to an optical pump pulse, the reference data set being generated from at least one of (a) at least one reference sample or (b) a simulation of a mechanical motion of a simulated

structure at predetermined time step increments selected to have a duration of less than one half of a time required for an acoustic pulse to propagate through a thinnest layer of the structure;

applying a sequence of optical pump pulses and optical probe pulses to the structure;

comparing a measured transient response of the structure to the reference data set;

adjusting a value of the one or more characteristics of the structure so as to bring the reference data set into agreement with the measured transient response; and

associating the adjusted value of the one or more characteristics with a value of one or more actual characteristics of the structure.

26. A non-destructive system for characterizing a sample, comprising:

means for generating an optical pump pulse and for directing the pump pulse to an area of the surface of the sample;

means for generating an optical probe pulse and for directing the probe pulse to a same or different area of the surface of the sample so as to arrive after the pump pulse, wherein the pump pulse has the same wavelength as the probe pulse or a wavelength that is different than the wavelength of the probe pulse;

means for automatically controlling a focusing of the pump and probe pulses on the surface of the sample;

means for measuring at least one transient response of the structure to the pump pulse, the measured transient response comprising a measurement of at least one of a modulated change  $\Delta R$  in an intensity of a reflected portion of the probe pulse, a change  $\Delta T$  in an intensity of a transmitted portion of the probe pulse, a change  $\Delta P$  in a polarization of the reflected probe pulse, a change  $\Delta\phi$  in an optical phase of the reflected probe pulse, and a change in an angle of reflection  $\Delta\theta$  of the probe pulse;

means for calibrating the measurement system for a determination of an amplitude of the transient optical response of the sample; and

means for associating an output of said means for measuring with at least one characteristic of interest of the structure.

27. A non-destructive system for characterizing a sample as set forth in claim 26, and further comprising means for measuring a derivative of the transient response as a function of at least one of an incident angle of the pump or probe pulses and as a function of a wavelength of at least one of the pump and probe pulses.

28. A non-destructive system for characterizing a sample as set forth in claim 26, and further comprising means for measuring at least one static response of the sample to the pump pulse, the static response measurement comprising at least one of a measurement of the optical reflectivity in accordance with an incident and a reflected average intensity of at least one of the pump and probe pulses, an average phase change of at least one of the pump and probe pulses upon reflection from the structure; and an average polarization and optical phase of at least one of

the incident and reflected pump and probe pulses.

29. A non-destructive system for characterizing a sample as set forth in claim 26, wherein said characteristic of interest includes a thickness of at least one layer of the sample, a mechanical property of the at least one layer, and a characteristic of an interface between the at least one layer and at least one of another layer or the substrate.

30. A non-destructive system for characterizing a sample as set forth in claim 26, and further comprising means for varying a location of said sample relative to at least one of said pump and probe pulses.

31. A non-destructive system for characterizing a sample as set forth in claim 26, and further comprising means for varying a temperature of said sample during an operation of said measuring means, and for measuring a derivative of a velocity of an acoustic wave in said sample with respect to temperature, and for correlating the measured derivative with a static stress within said sample.

32. A non-destructive system for characterizing a sample as set forth in claim 26, wherein said pump and probe pulses are applied along parallel optical paths to a focussing objective that is disposed for focussing said pump and probe pulses on said sample.

33. A non-destructive system for characterizing a sample as set forth in claim 26, wherein said pump and probe pulses are applied along parallel optical paths to a focussing objective that is disposed for focussing said pump and probe pulses on said sample, and are applied with one of a normal or oblique incidence angle to said sample.

34. A non-destructive system for characterizing a sample as set forth in claim 26, wherein one of said pump and probe pulses is applied to said surface of said sample with a normal incidence angle, and wherein the other one of said pump and probe pulses is applied to said surface of said sample with an oblique incidence angle.

35. A non-destructive system for characterizing a sample as set forth in claim 26, wherein said pump and probe pulses are derived from a single laser pulse.

36. A non-destructive system for characterizing a sample as set forth in claim 26, wherein said pump and probe pulses are each derived from a separate laser pulse.

37. A non-destructive system for characterizing a sample as set forth in claim 26, wherein said pump and probe pulses are derived from a single laser pulse, and further comprising means for converting a wavelength of said single laser pulse to a harmonic of the wavelength such that one of the pump and probe pulses has a wavelength that differs from the wavelength of the other pulse.

38. A non-destructive system for characterizing a sample as set forth in claim 26, and further comprising means for impressing an intensity modulation on at least one of said pump and probe pulses.

39. A non-destructive system for characterizing a sample as set forth in claim 38, wherein said means for impressing is synchronized to a pulse repetition rate of a laser that generates said pump or probe pulses.

40. A non-destructive system for characterizing a sample as set forth in claim 38, wherein said means for impressing impresses a first intensity modulation frequency

on said pump pulse and a second, different intensity modulation frequency on said probe pulse.

41. A non-destructive system for characterizing a sample as set forth in claim 26, and further comprising:

a continuous wave laser source for illuminating a portion of a surface of said sample with cw light; and

means, responsive to reflected cw light, for performing an ellipsometric measurement of said sample.

42. A non-destructive system for characterizing a sample as set forth in claim 26, and further comprising:

a light source for illuminating a portion of a surface of said sample; and

means for imaging said illuminated portion and for providing the image to one of an operator or a pattern recognition software.

43. A non-destructive system for characterizing a sample as set forth in claim 26, and further comprising a thermal source for illuminating a portion of a surface of said sample with thermal radiation for controllably varying a temperature of said sample during the operation of the system.

44. A non-destructive system for characterizing a sample as set forth in claim 26, wherein said measuring means directly measures a derivative of said at least one transient response of the sample with respect to a time delay between said pump pulse and said probe pulse.

45. A non-destructive system for characterizing a sample as set forth in claim 26, wherein one of the pump and probe pulses has a wavelength that differs from the wavelength of the other pulse, and further comprising a wavelength selective filter in an optical path of the probe pulse for passing the probe pulse while blocking any scattered portion of the pump pulse.

46. A non-destructive system for characterizing a sample as set forth in claim 26, and further comprising means for changing a spatial relationship between a location where the probe pulse is incident on the sample to a location wherein the pump pulse is incident on the sample.

47. A non-destructive system for characterizing a sample as set forth in claim 26, wherein said pump and probe pulses are derived from first and second pulsed laser sources, respectively, and wherein a pulse repetition rate of said first laser source differs from a pulse repetition rate of said second laser source.

48. A non-destructive system for characterizing a sample as set forth in claim 26, and further comprising means for automatically varying a ratio of pump pulse energy to probe pulse energy.

49. A non-destructive system for characterizing a sample as set forth in claim 26, and further comprising means for automatically maintaining a substantially constant location, shape and size of the probe pulse on the sample for a range of temporal offsets between the probe pulse and the pump pulse.

50. A non-destructive system for characterizing a sample as set forth in claim 26, and further comprising

means for focussing and translating said probe pulse on a surface of said sample independent of said pump pulse.

51. A non-destructive system for characterizing a sample as set forth in claim 50, wherein said focussing and translating means is comprised of a fiber optic having a tapered end diameter for performing near field focussing of said probe pulse, and means for translating said tapered end of said fiber optic relative to a focal spot of said pump pulse.

52. A non-destructive system for characterizing a sample as set forth in claim 50, wherein said focussing and translating means is comprised of a fiber optic having an end disposed for collecting reflected probe light, and means for translating said fiber optic relative to a surface of said sample.

53. A non-destructive system for characterizing a sample as set forth in claim 26, and further comprising a plurality of fiber optics each having an end disposed relative to a surface of said sample for directing said pump and probe pulses to said sample.

54. A non-destructive system for characterizing a sample as set forth in claim 53, and further comprising a further fiber optic having an end disposed relative to the surface for collecting reflected probe light.

55. A non-destructive system for characterizing a sample as set forth in claim 26, wherein said sample is comprised of a plurality of patterned sub-structures having dimensions less than a focal spot diameter of either said pump or probe pulses, and wherein a plurality of said sub-structures are simultaneously illuminated by said pump and probe pulses.

56. A non-destructive system for characterizing a sample as set forth in claim 26, wherein said sample is comprised of a plurality of sub-structures that are arranged periodically, and further comprising means for determining at least one characteristic of said sub-structures by comparing an optical response of said sub-structures to simulations of a vibrational response of said sub-structures to the pump pulse.

57. A non-destructive system for characterizing a sample as set forth in claim 26, and further comprising means for detecting a presence of at least one acoustic echo in the reflected portion of the probe pulse.

58. A non-destructive system for characterizing a sample as set forth in claim 57, wherein said detecting means determines a time of arrival of the acoustic echo by detecting a location in time of a feature of interest of the acoustic echo.

59. A non-destructive system for characterizing a sample as set forth in claim 57, wherein said detecting means determines a time of arrival of the acoustic echo by convolving the detected acoustic echo with a predetermined function.

60. A non-destructive system for characterizing a sample as set forth in claim 26, wherein said measuring means measures the transient response at at least two different angles of incidence of said probe pulse.

61. A non-destructive system for characterizing a sample as set forth in claim 26, wherein said sample is further comprised of one of a transparent layer and a partially absorbing layer.

62. A non-destructive system for characterizing a sample as set forth in claim 26, wherein said sample is further comprised of at least one first layer disposed beneath at least one second layer, and wherein at least said probe pulse passes through said at least one second layer to reach said at least one first layer.

63. A non-destructive system for characterizing a sample as set forth in claim 26, wherein said associating means comprises means for comparing an output of said measuring means with at least one of a simulation of the sample to an application of the pump and probe pulses or to a result of an application of the pump and probe pulses to a reference sample.

64. A non-destructive system for characterizing a sample as set forth in claim 26, wherein said pump pulse is applied at a first location on a surface of the sample, wherein said probe pulse is applied at a second location on the same or a different surface of the sample, and wherein said associating means determines a characteristic of interest for a portion of the sample that lies between the first and second locations.

65. A non-destructive system for characterizing a sample as set forth in claim 26, wherein said sample is patterned into at least one three-dimensional multilayered sub-structure, and wherein said associating means comprises means for comparing an output of said measuring means with a three-dimensional simulation of the at least one multilayered sub-structure to an application of the pump and probe pulses.

66. A non-destructive system for characterizing a sample as set forth in claim 26, wherein said characteristic of interest includes a characteristic of an

interlayer between at least one layer and at least one of another layer or the substrate.

67. A non-destructive system for characterizing a sample as set forth in claim 66, wherein said characteristic of the interlayer includes at least one of a thickness of the interlayer, a structural phase of the interlayer, and a chemical species that is located within the interlayer.

68. A non-destructive system for characterizing a sample as set forth in claim 26, wherein said characteristic of interest includes an adhesion property of at least one layer to another adjacent layer or to the substrate.

69. A non-destructive system for characterizing a sample as set forth in claim 26, wherein said characteristic of interest includes at least one of a derivative of an index of refraction or a derivative of an extinction coefficient with respect to stress or strain induced by the pump pulse.

70. A method for characterizing a structure comprised of a substrate and at least one layer disposed on the substrate, comprising the steps of:

simulating a response of a model of the structure to an application of a first pulse of optical radiation followed by a transient response of the structure to an application of a second pulse of optical radiation within an interval of time;

applying the first pulse of optical radiation to the structure;

applying, during the interval of time, the second pulse of optical radiation to the structure;

comparing a measured transient response of the structure to the determined transient response;

adjusting one or more characteristics of the model of the structure so as to bring the determined transient response into agreement with the measured transient response; and

associating the adjusted one or more characteristics with one or more actual characteristics of the structure, wherein

the step of adjusting adjusts at least one of a crystal orientation within the at least one layer, an interface roughness between the at least one layer and another layer or the substrate, a thermal diffusivity within the at least one layer, an electronic diffusivity within the at least one layer, optical constants within the at least one layer, derivatives of optical constants with respect to stress or strain within the at least one layer, and a surface roughness of the sample.

71. A method as set forth in claim 70, wherein the step of adjusting further adjusts a static stress within the at least one layer.

72. A method as set forth in claim 70, wherein the step of adjusting further adjusts a presence of or a thickness of a region of intermixing between two layers or a layer and the substrate.

73. A method for characterizing a structure comprised

of a substrate and at least one layer disposed on the substrate, comprising the steps of:

simulating a mechanical response of a model of the structure to an application of a first pulse of optical radiation by the steps of determining an initial stress distribution within the structure in response to the first pulse of optical radiation, calculating acoustical normal modes of the structure, decomposing the determined initial stress distribution into a sum over the calculated normal modes, and determining a change in a transient optical response of the structure, at a time of interest, to a second pulse of optical radiation by summing, for each calculated normal mode, a change in the transient optical response due to a spatial stress pattern associated with each normal mode;

applying the first pulse of optical radiation to the structure;

applying, at the time of interest, the second pulse of optical radiation to the structure;

comparing a measured transient optical response of the structure to the determined transient optical response;

adjusting one or more characteristics of the structure so as to bring the determined transient optical response into agreement with the measured transient optical response; and

associating the adjusted one or more characteristics with one or more actual characteristics of the structure.

74. A method for characterizing a structure comprised of a substrate and at least one layer disposed on the substrate, comprising the steps of:

simulating a vibrational response of the at least one layer to an application of a first pulse of optical radiation, the response being simulated in accordance with a spring constant parameter per unit area at an interface between the at least one layer and another layer or the substrate;

measuring the actual response of the at least one layer by applying the first pulse of optical radiation followed by an application of a second pulse of optical radiation, and sensing a vibration of the at least one layer by a change in a reflected portion of the second pulse of optical radiation;

comparing the measured response with the simulated response;

adjusting the spring constant parameter to bring the simulated response into agreement with the measured response; and

characterizing a strength of the interface from the adjusted spring constant parameter.

75. A method as set forth in claim 74, wherein the simulated vibrational response is a simulated damping rate.

76. A non-destructive method for characterizing a sample, comprising the steps of:

generating an optical pump pulse and directing the pump pulse to an area of the surface of the sample;

for each generated optical pump pulse, generating an optical probe pulse and directing the probe pulse to the surface of the sample so as to arrive after the pump pulse;

automatically focusing the pump and probe pulses to achieve predetermined focusing conditions;

measuring at least one transient response of the structure to the pump pulse, the measured transient responses comprising a measurement of at least one of a modulated change  $\Delta R$  in an intensity of a reflected portion of the probe pulse, a change  $\Delta T$  in an intensity of a transmitted portion of the probe pulse, a change  $\Delta P$  in a polarization of the reflected probe pulse, a change  $\Delta\phi$  in an optical phase of the reflected probe pulse, and a change in an angle of reflection  $\Delta\beta$  of the probe pulse;

applying at least one calibration factor to the at least one transient response;

associating an output of said means for measuring with at least one characteristic of interest of the structure;

adjusting a value of the one or more characteristics of the structure so as to bring a reference data set into agreement with the measured transient response; and

associating the adjusted value of the one or more characteristics with a value of one or more actual characteristics of the structure.

77. A method for characterizing a structure,

118.

comprising the steps of:

applying first electromagnetic radiation to the structure for creating propagating stress pulses within the structure;

applying second electromagnetic radiation to the structure at a predetermined incidence angle so as to intercept the propagating stress pulses;

sensing a reflection or transmission of the second electromagnetic radiation from the structure;

associating a change in the reflection of the second electromagnetic radiation over time with a value of an optical characteristic of the structure for determining a transient response of the structure;

determining an index of refraction of the structure using an ellipsometric technique; and

determining a velocity of sound in the structure in accordance with the predetermined angle and the determined transient response and index of refraction.

1/16

FIG. 1a

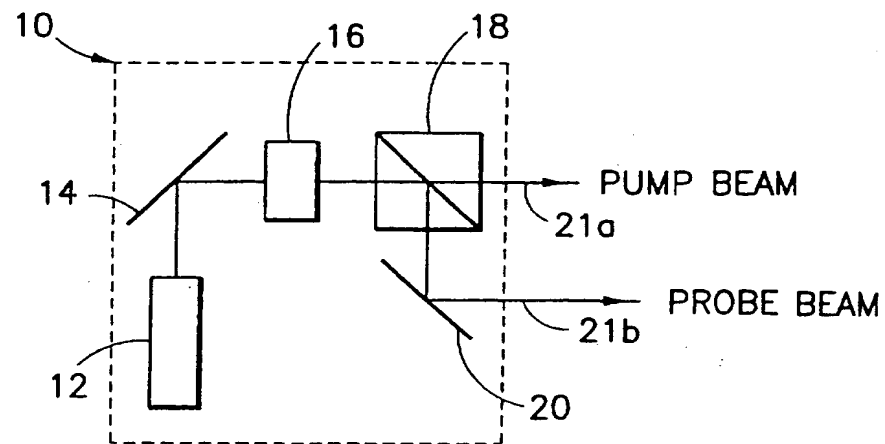


FIG. 1b

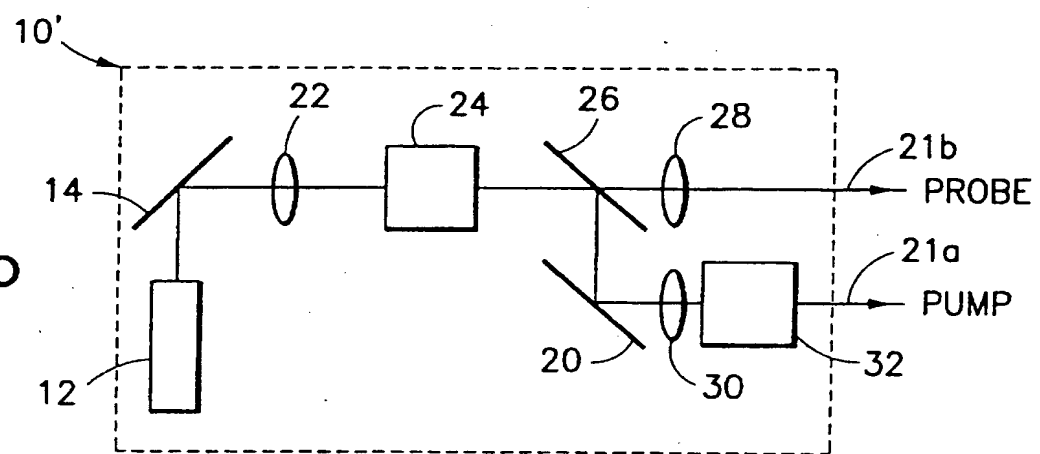
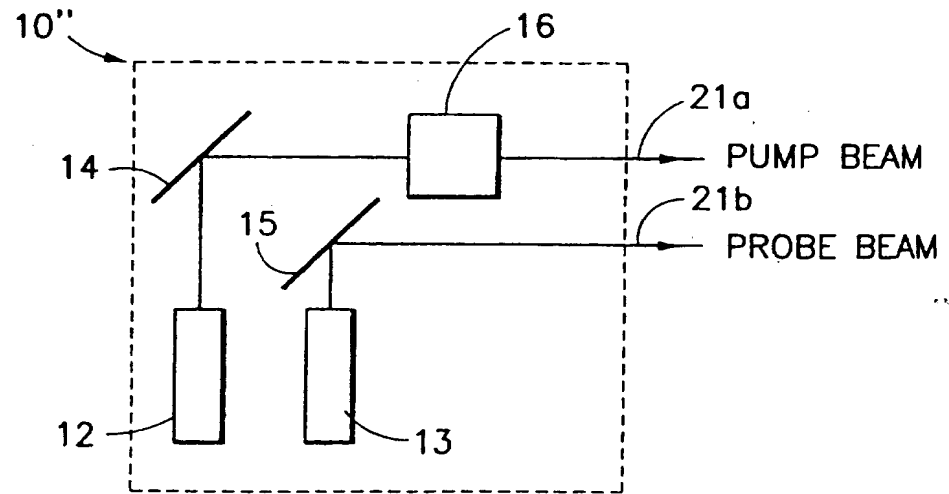


FIG. 1c



2/16

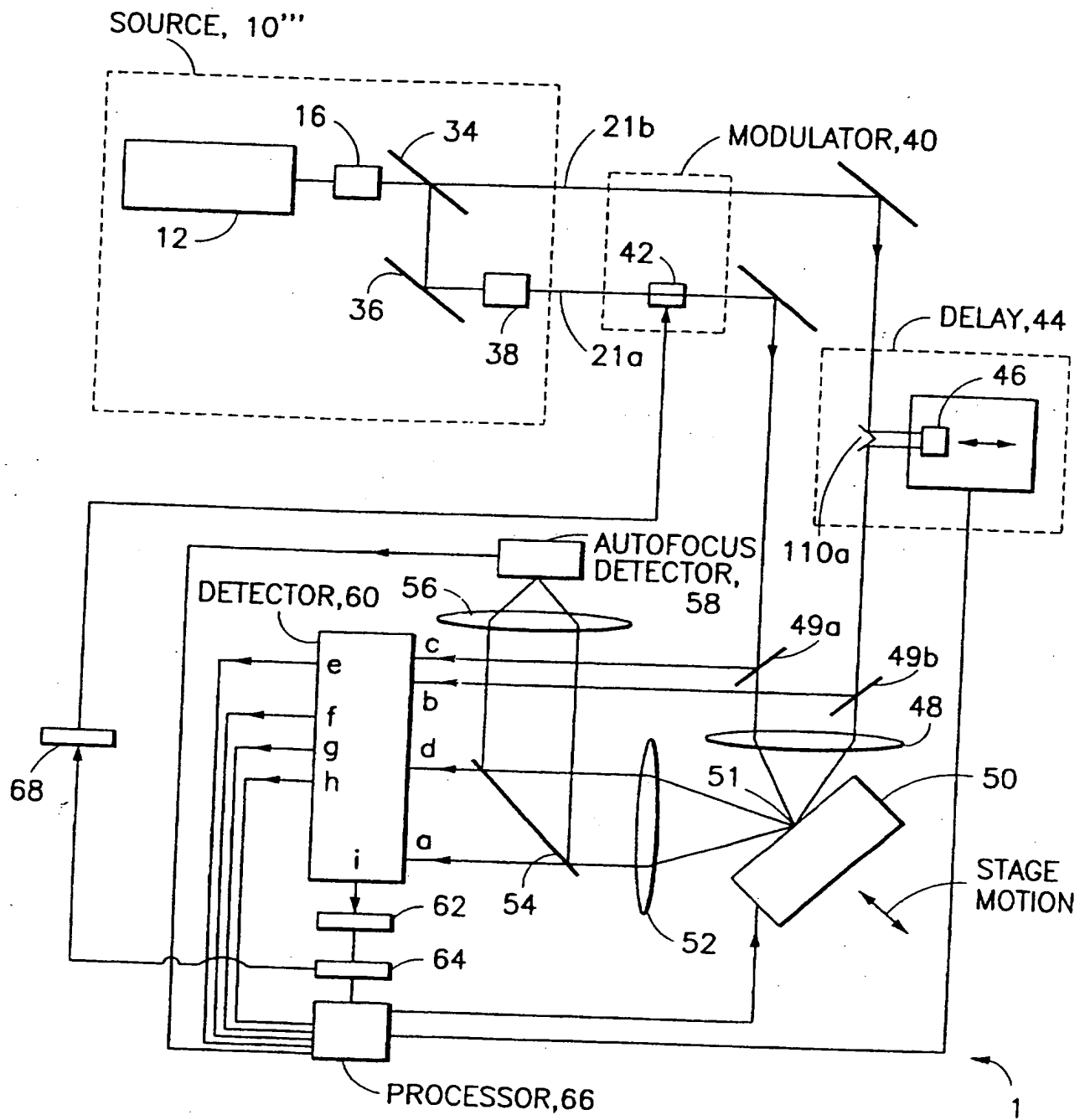


FIG. 2

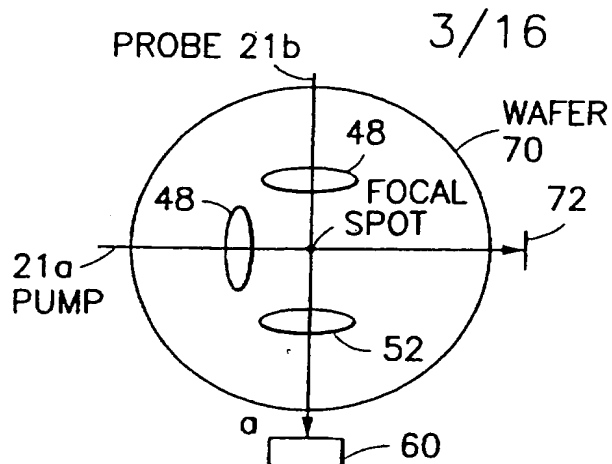


FIG. 3a

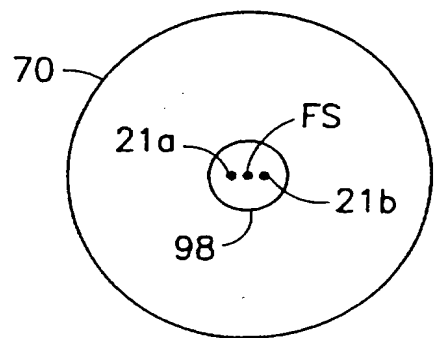


FIG. 3b

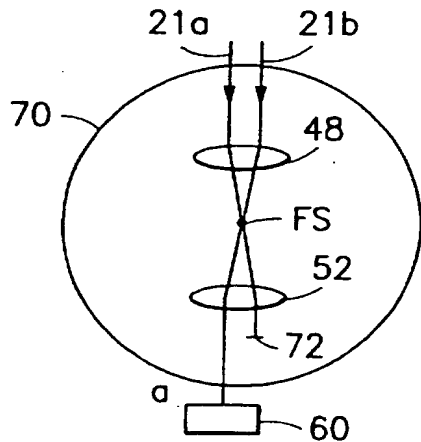


FIG. 3c

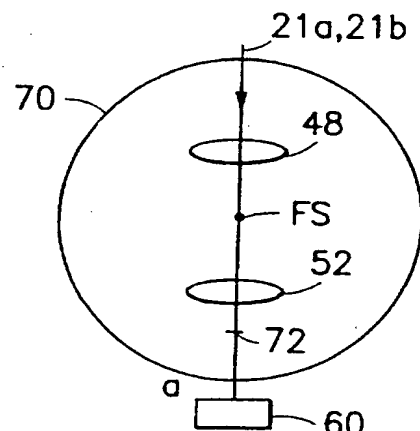


FIG. 3d

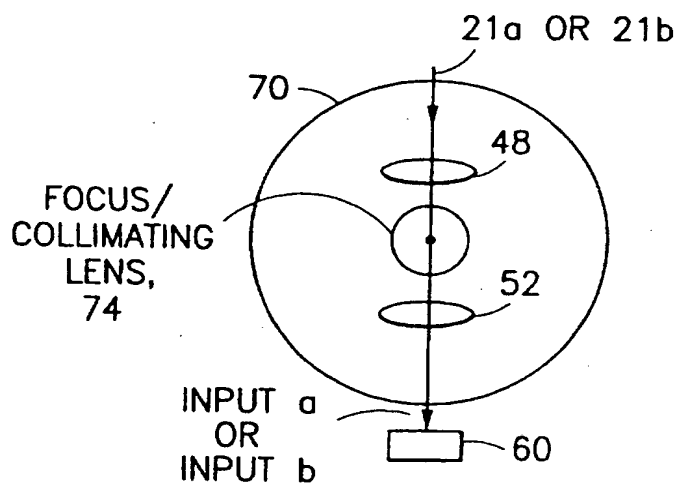


FIG. 3e

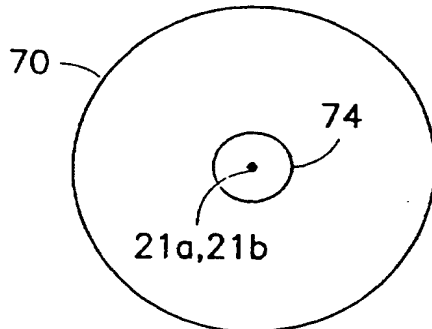


FIG. 3f

4/16

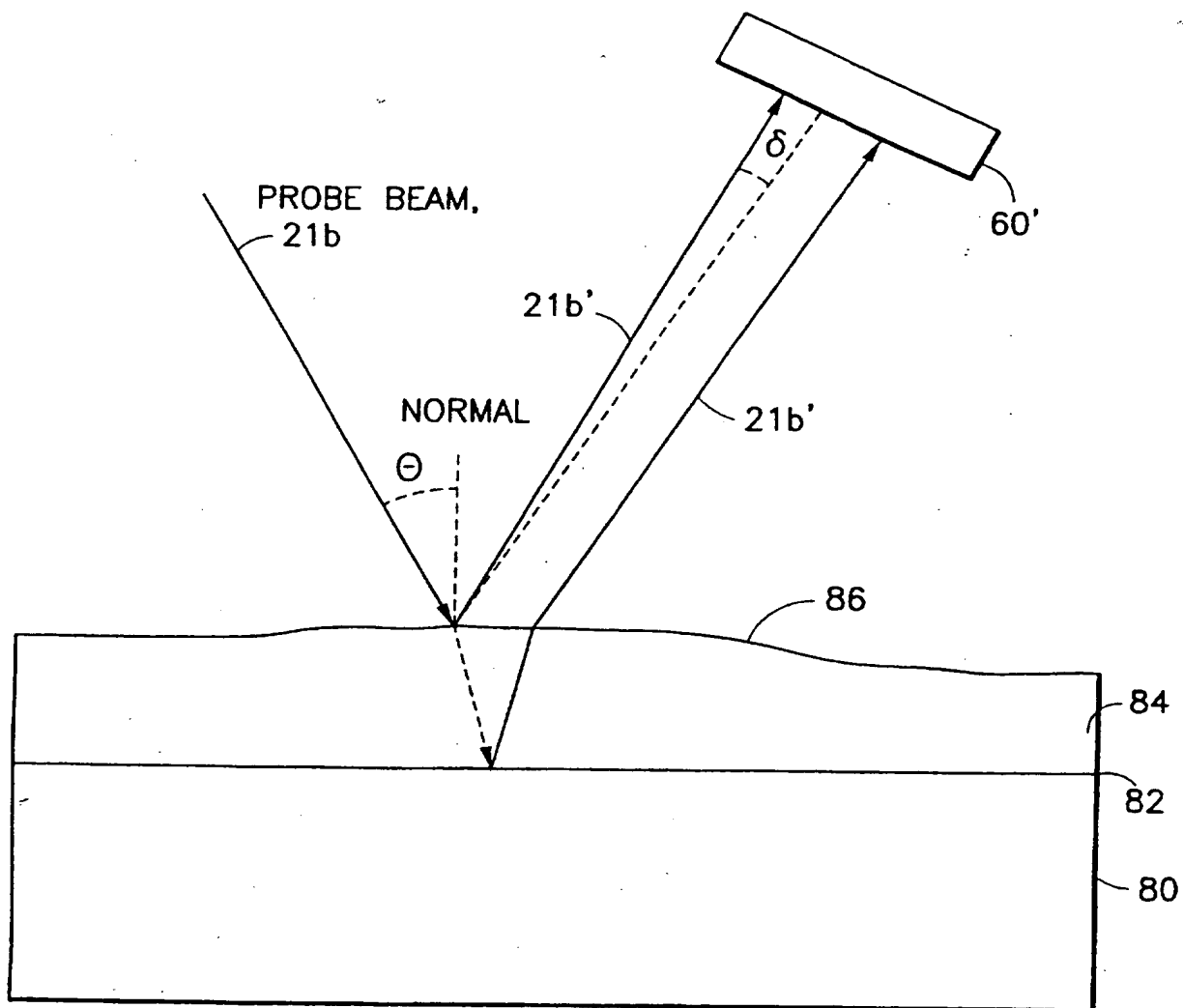


FIG. 5

5/16

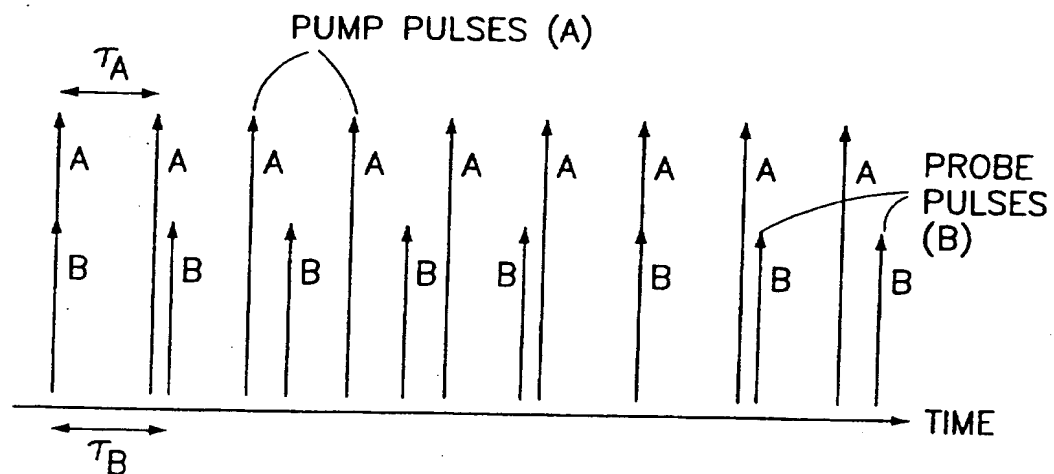


FIG. 4a

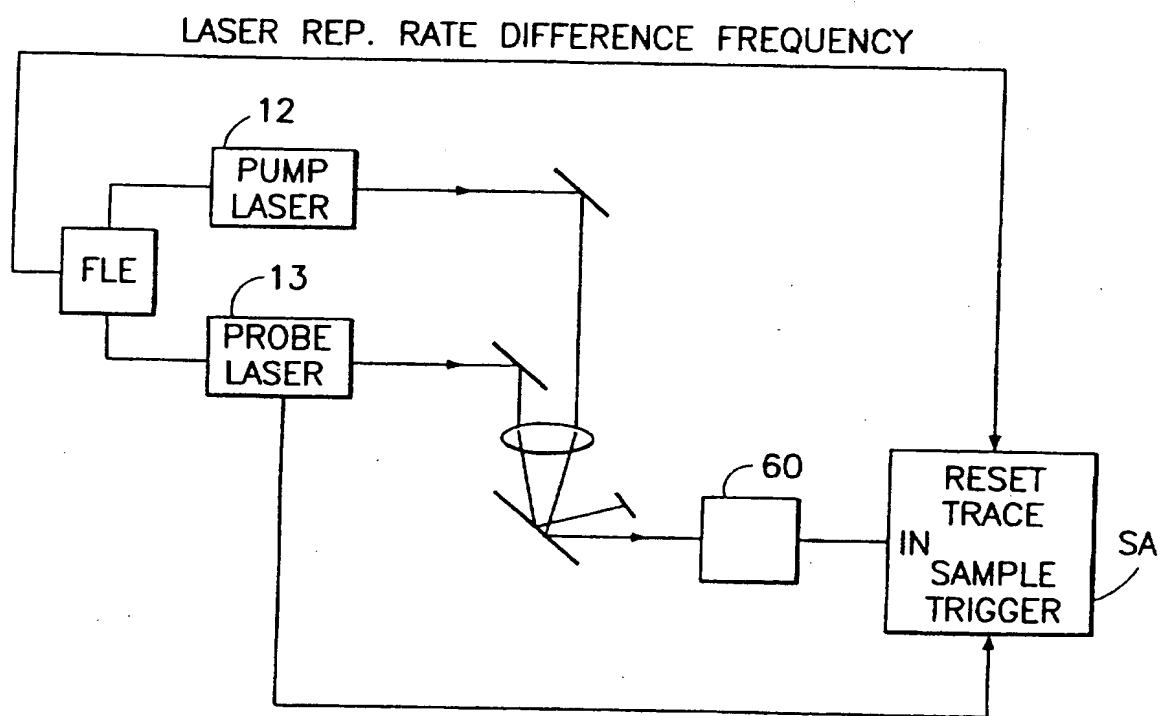
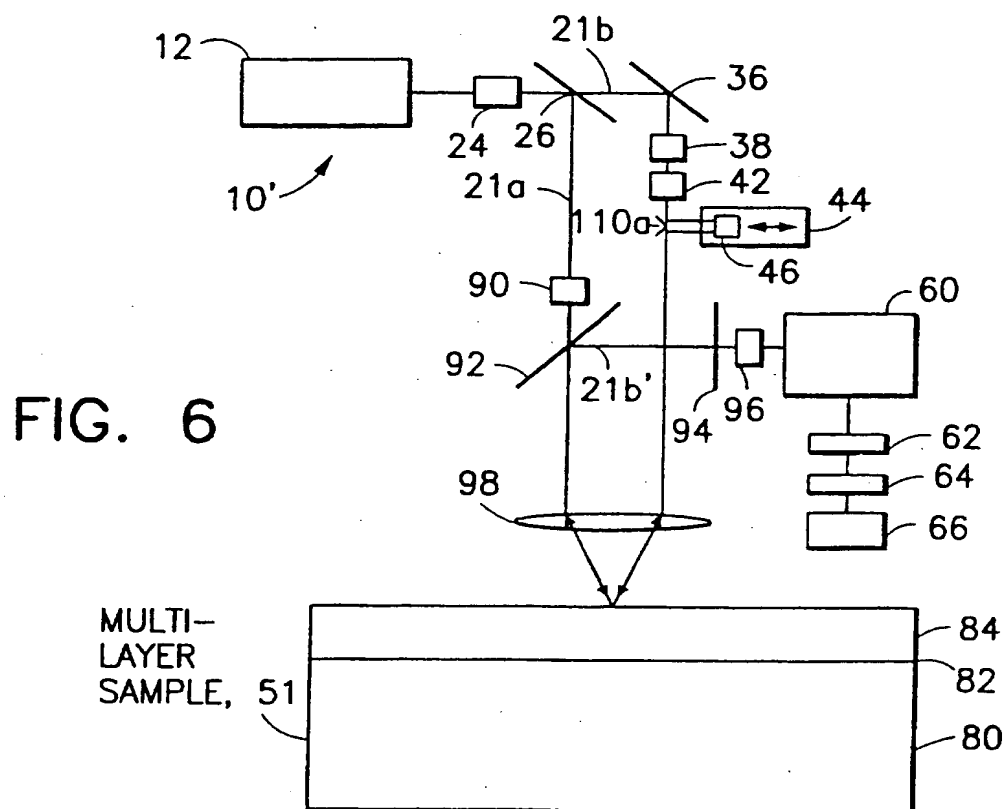
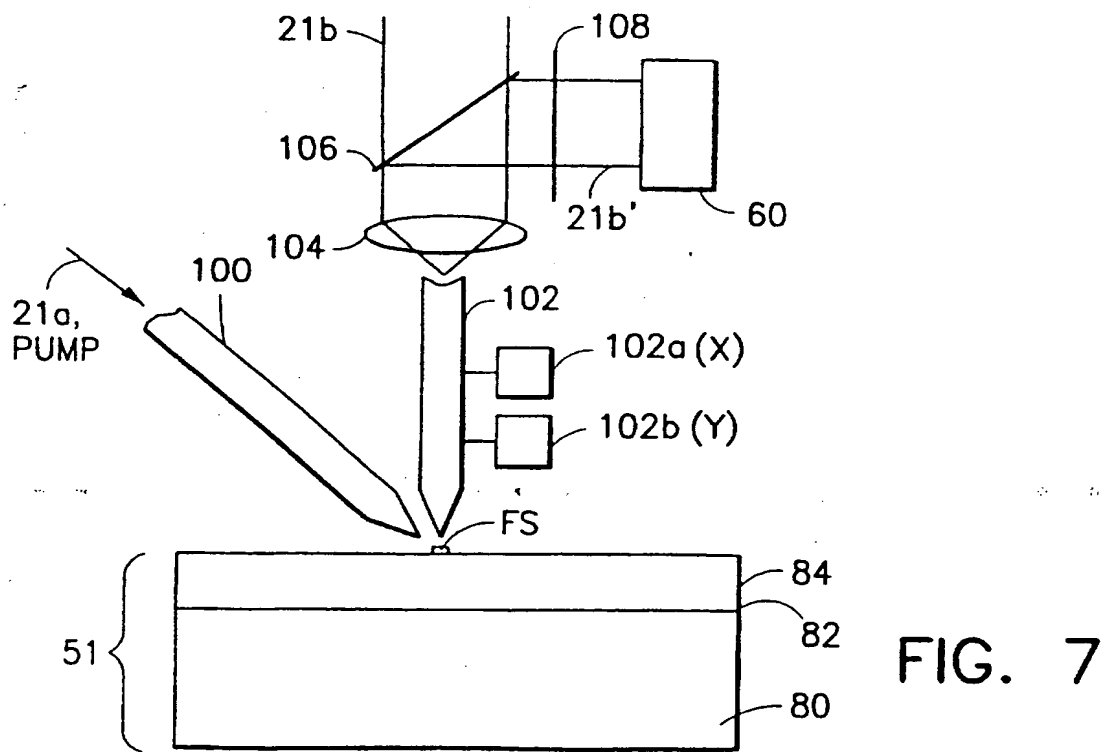


FIG. 4b

6/16

EXPANDED  
PROBE BEAM

7/16

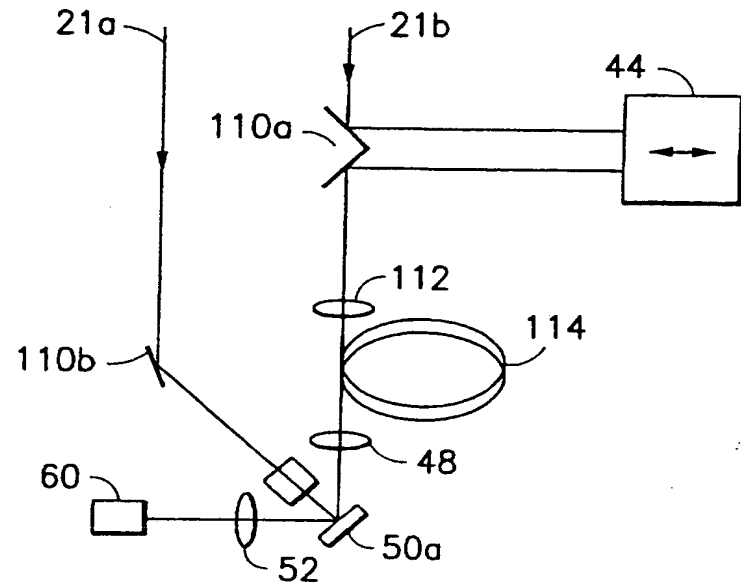


FIG. 8

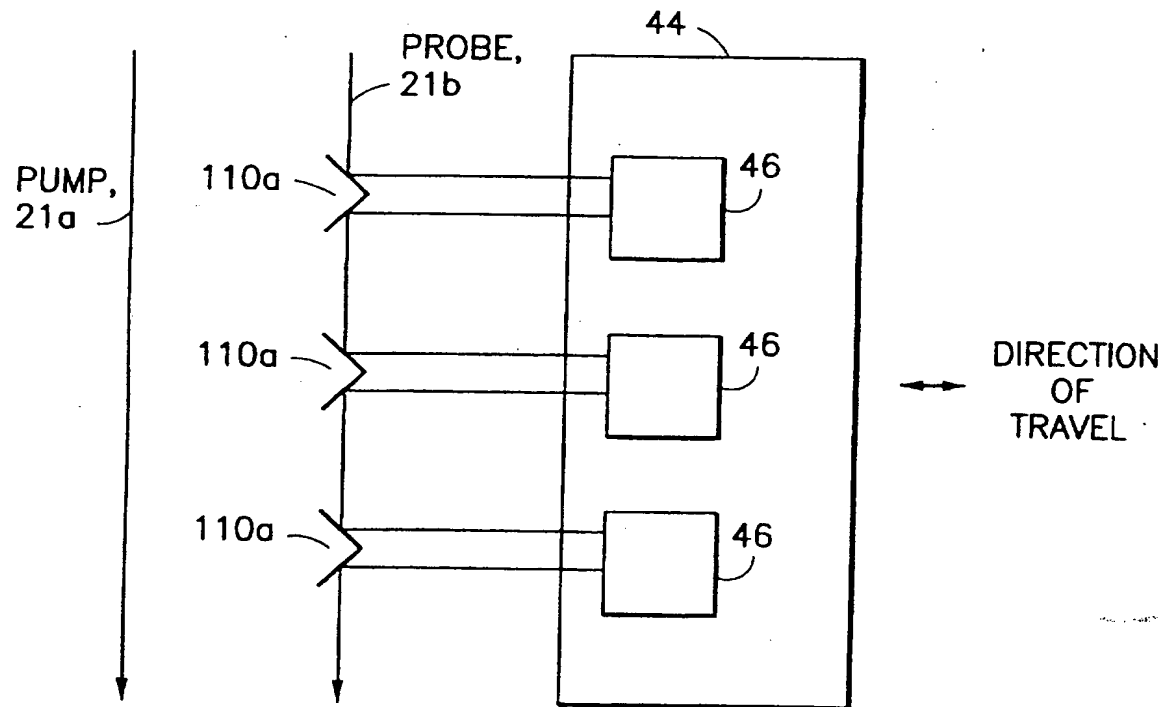


FIG. 9

8/16

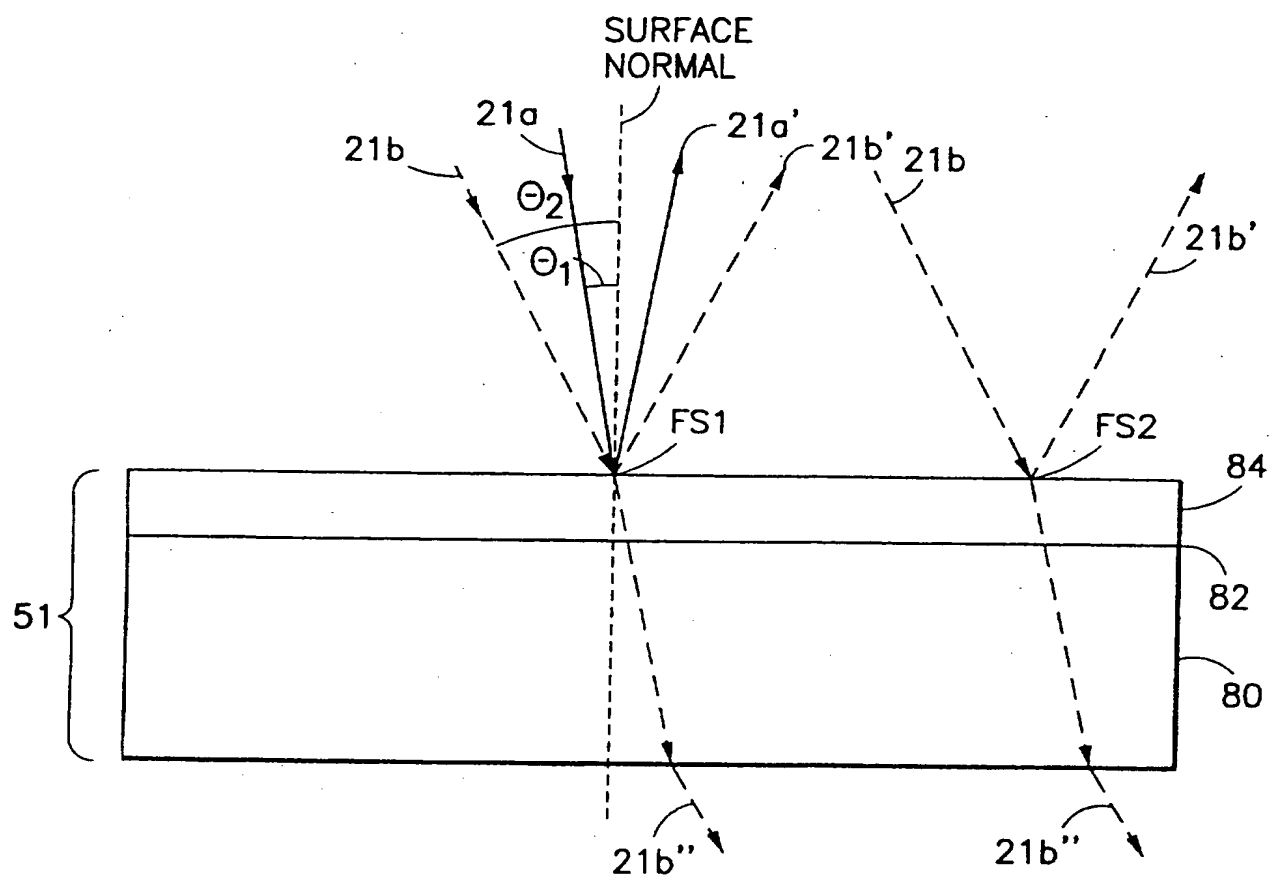


FIG. 10

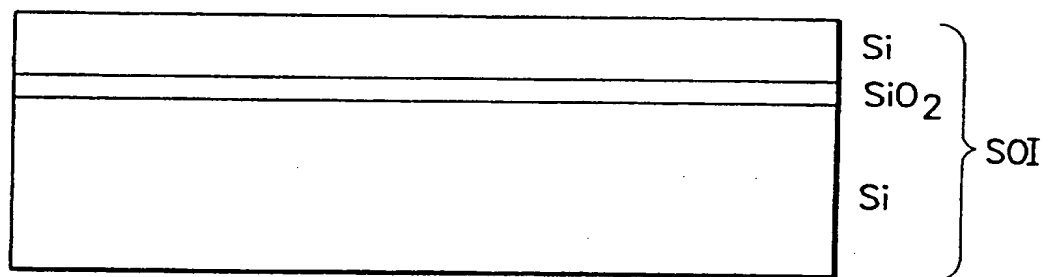


FIG. 11

9/16

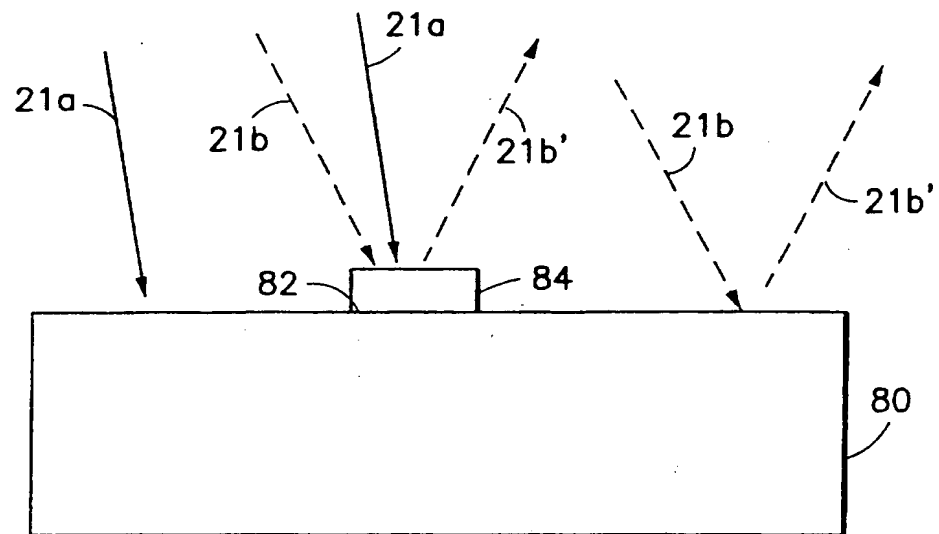


FIG. 12

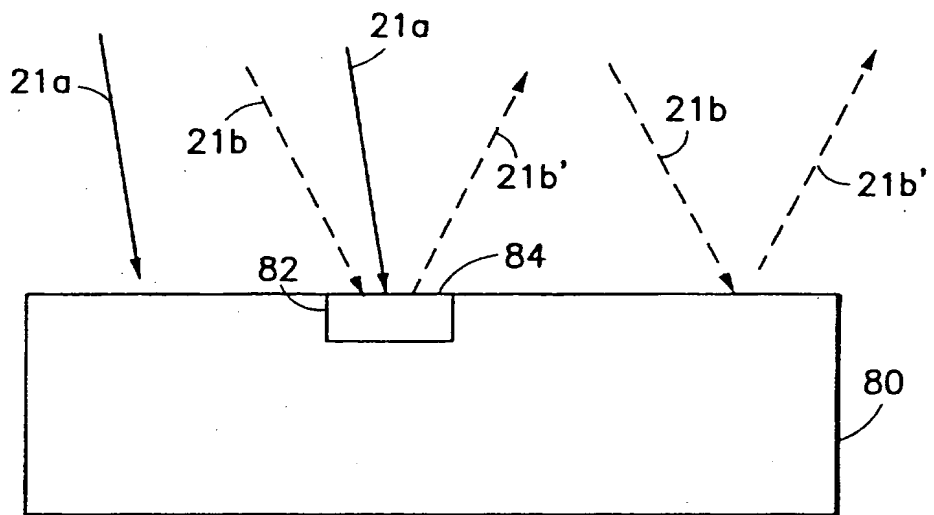


FIG. 13

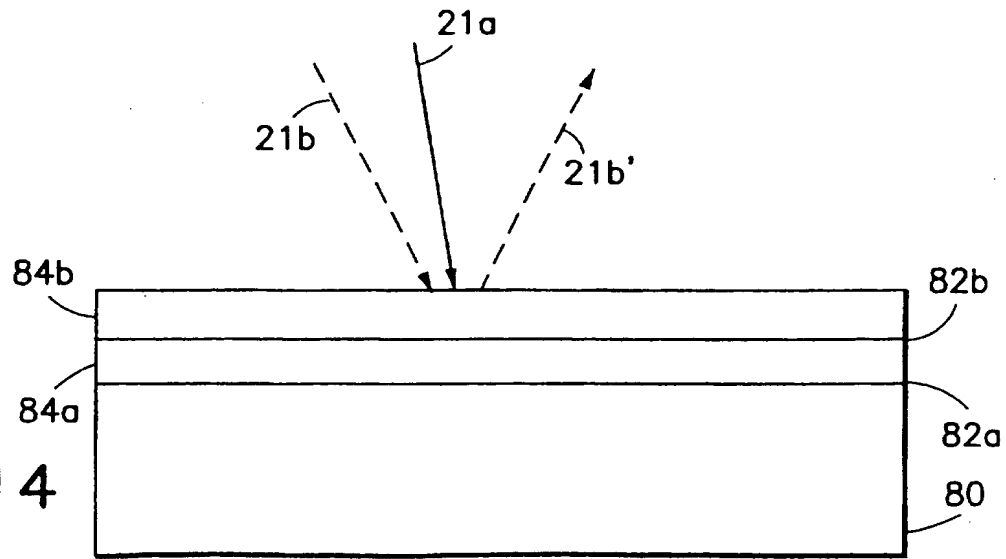


FIG. 14

10/16

FIG. 15b

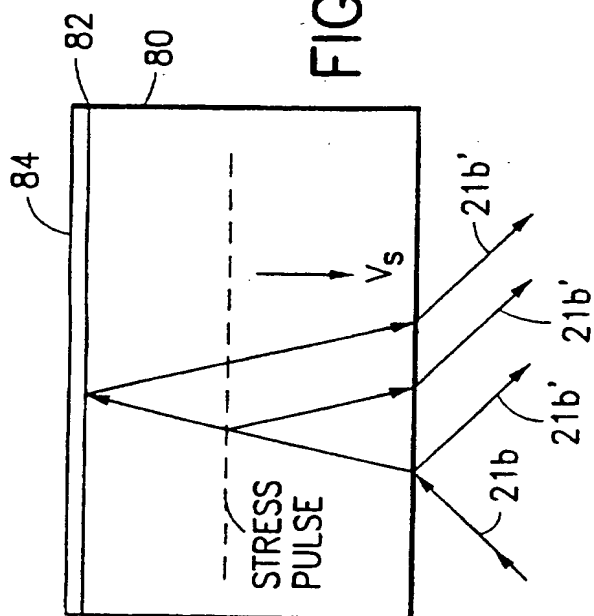


FIG. 15d

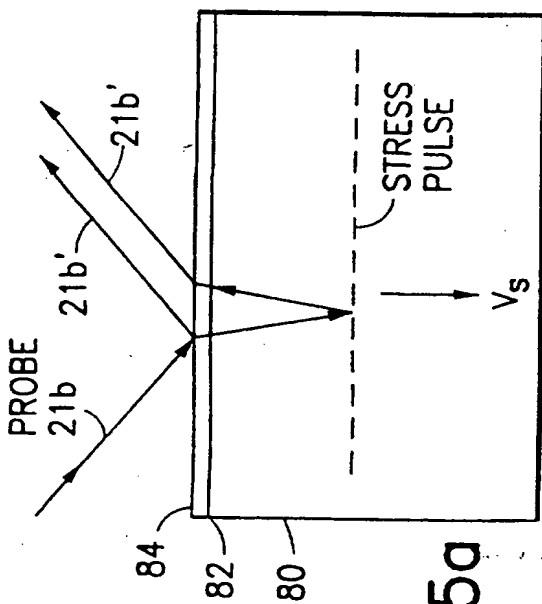
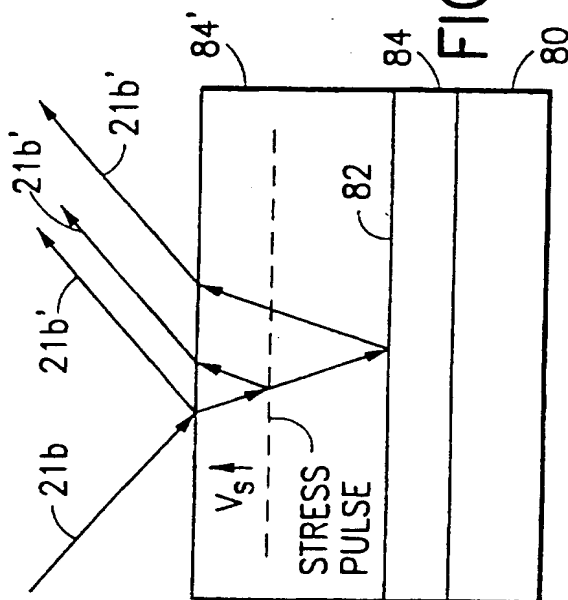


FIG. 15a

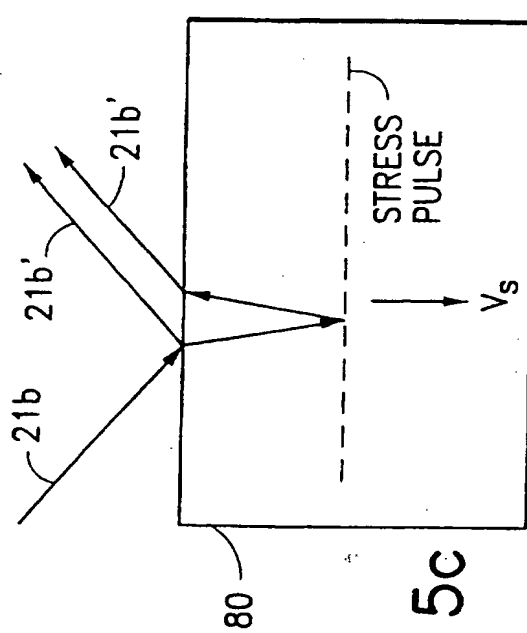
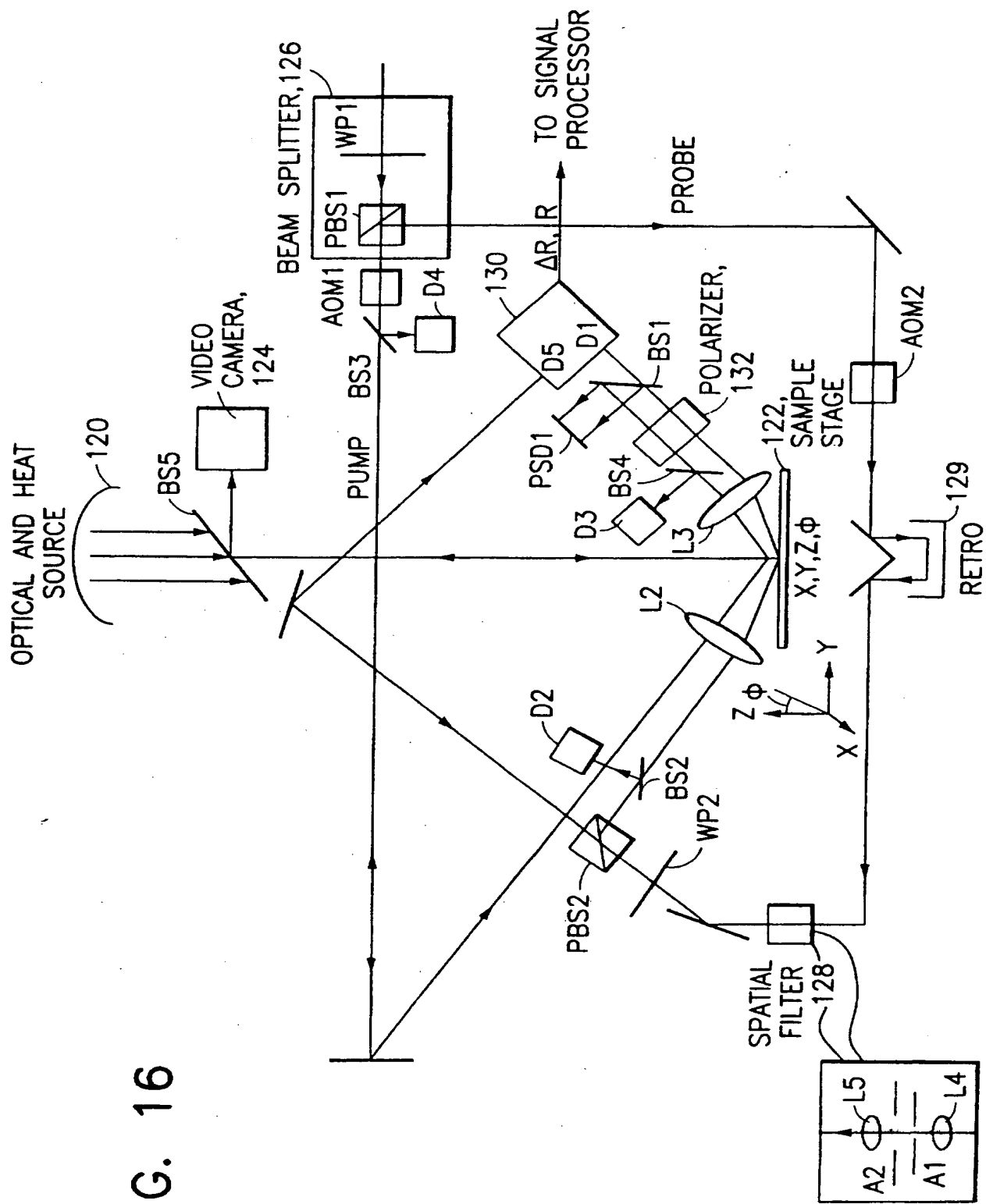


FIG. 15c

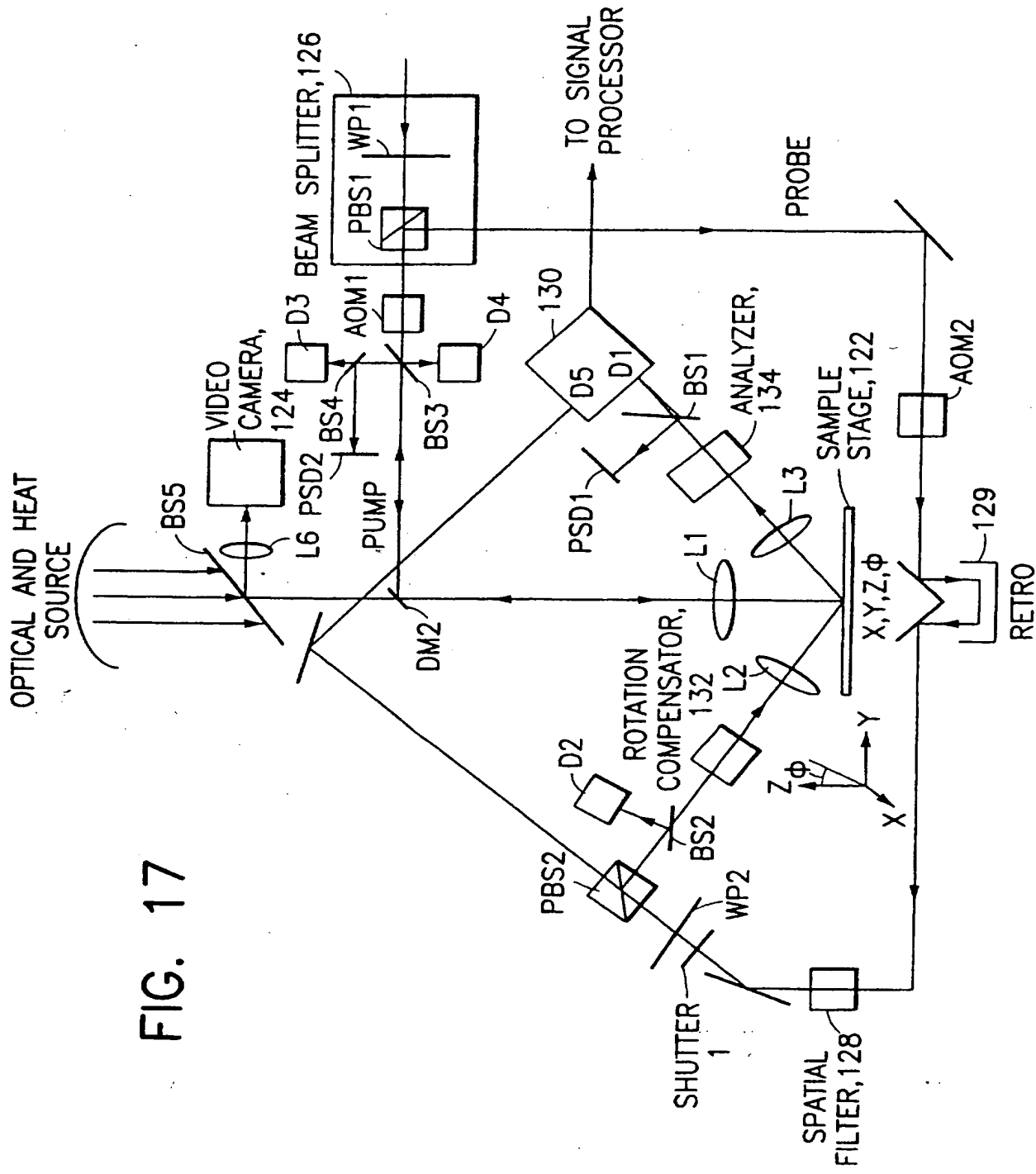
11 / 16

FIG. 16

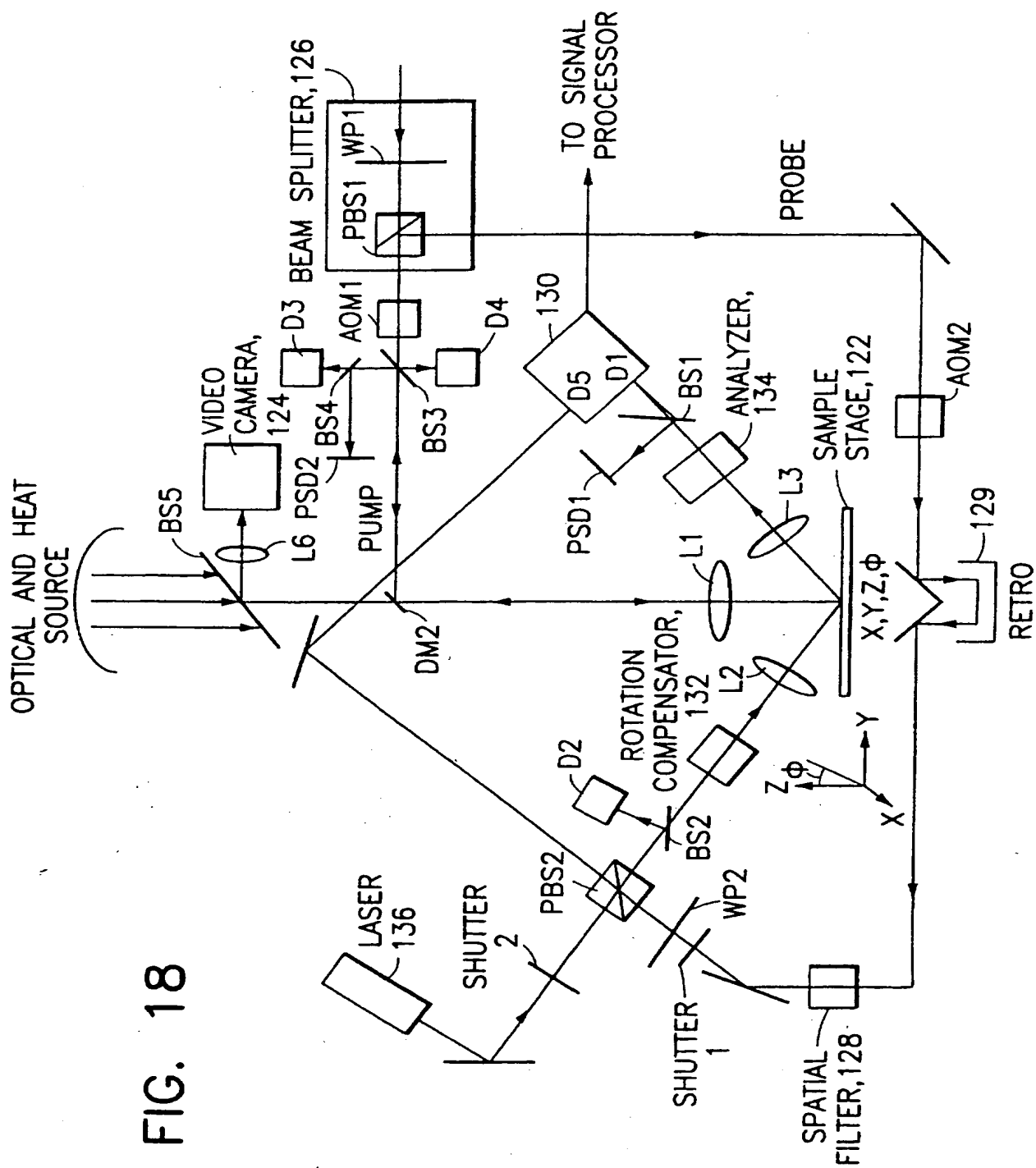


12/16

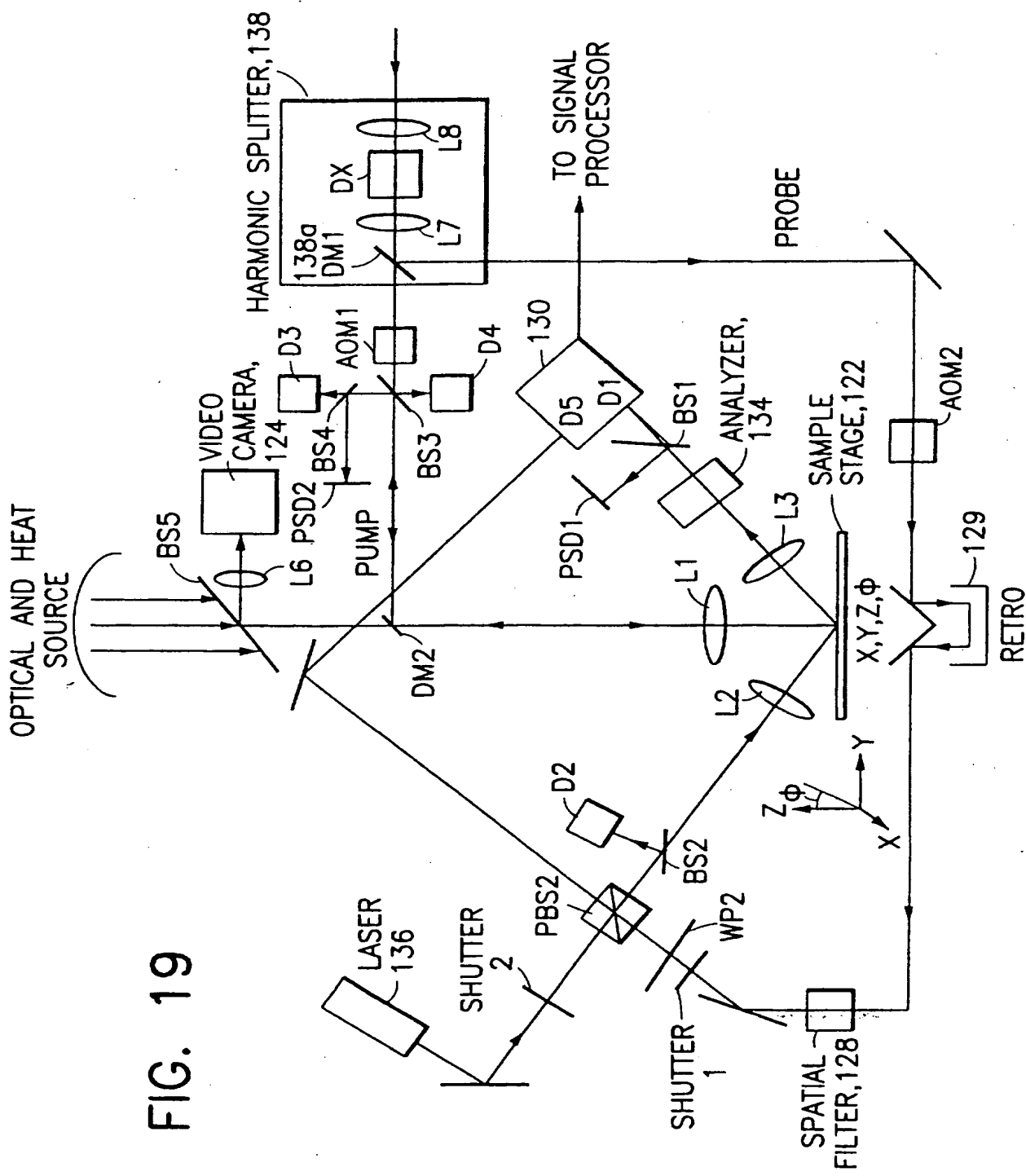
FIG. 17

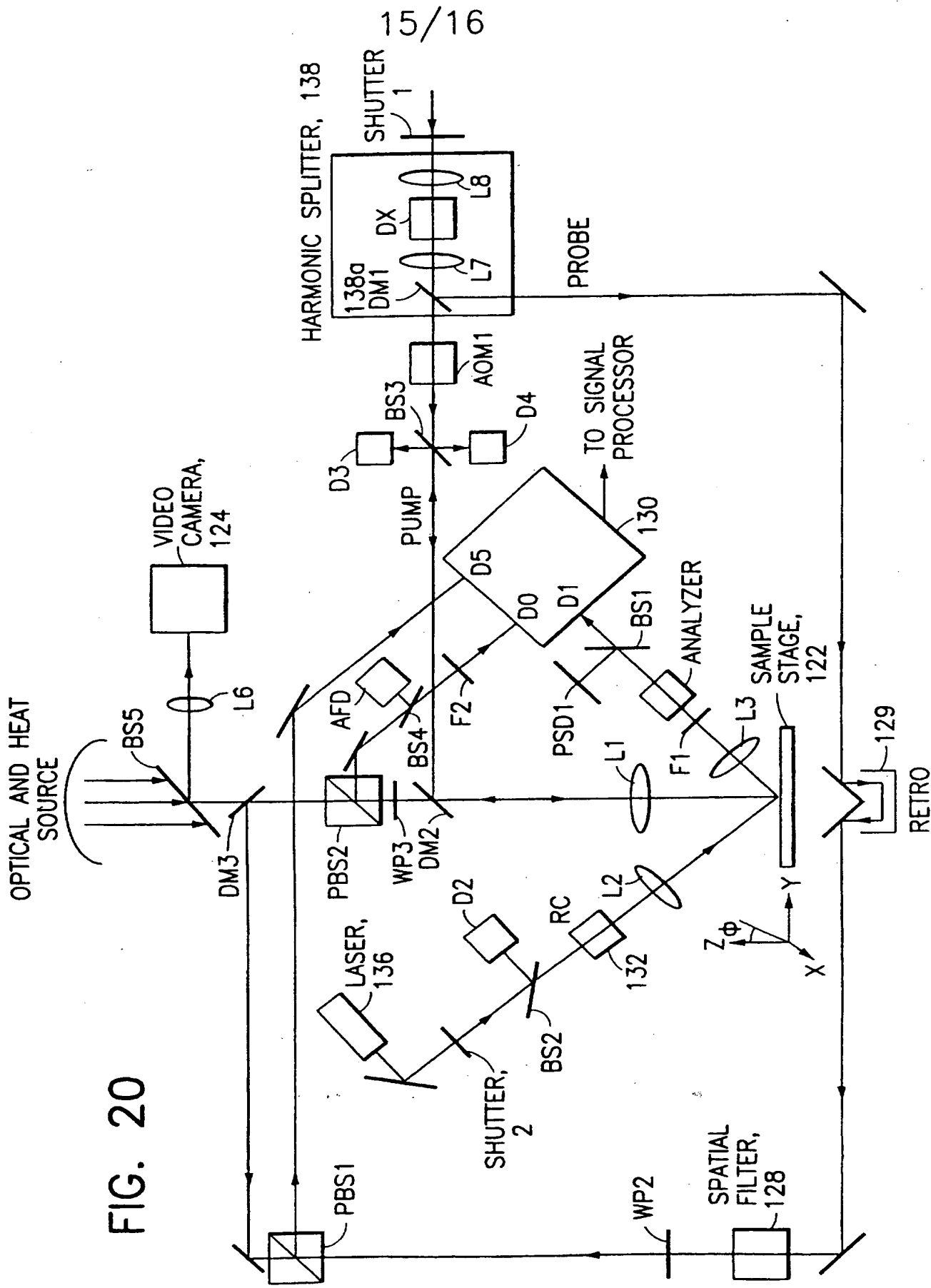


13/16



14/16





16/16

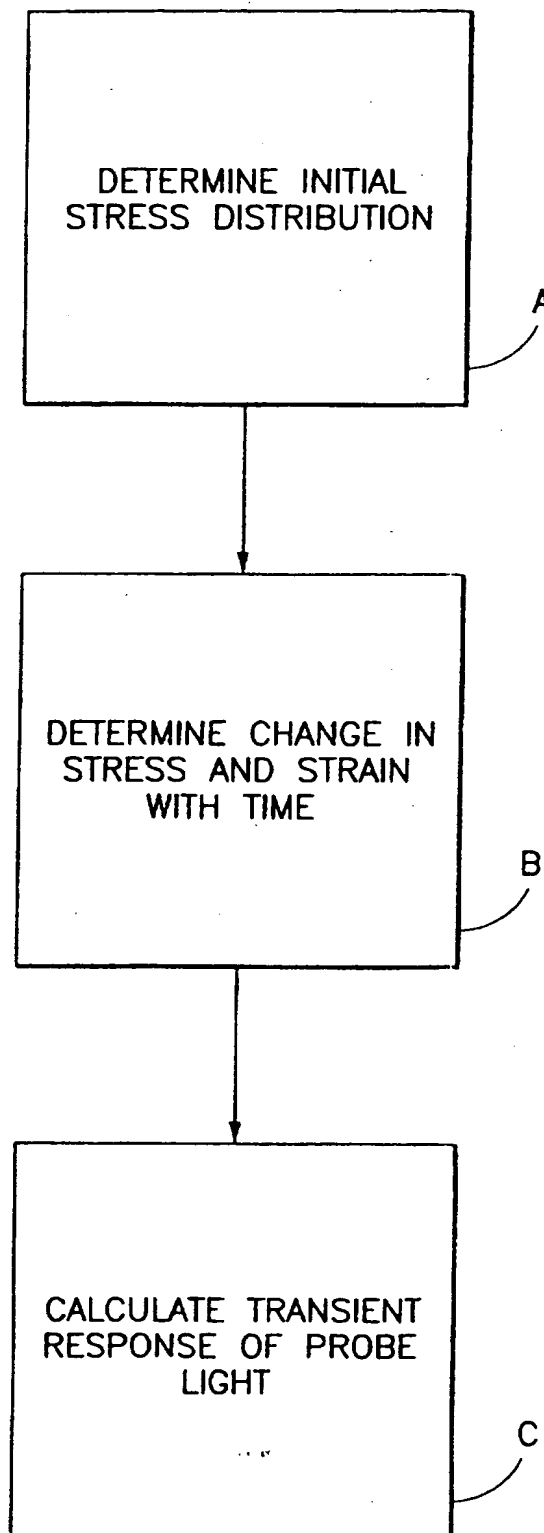


FIG. 21

## INTERNATIONAL SEARCH REPORT

International application No.

PCT/US96/20917

## A. CLASSIFICATION OF SUBJECT MATTER

IPC(6) : G01N 21/00; G01N 29/04  
 US CL : 356/432; 73/801

According to International Patent Classification (IPC) or to both national classification and IPC

## B. FIELDS SEARCHED

Minimum documentation searched (classification system followed by classification symbols)

U.S. : 356/432, 445; 73/800, 801, 150A

Documentation searched other than minimum documentation to the extent that such documents are included in the fields searched

Electronic data base consulted during the international search (name of data base and, where practicable, search terms used)

Please See Extra Sheet.

## C. DOCUMENTS CONSIDERED TO BE RELEVANT

Category*	Citation of document, with indication, where appropriate, of the relevant passages	Relevant to claim No.
A	US 3,950,987 A (SLEZINGER ET AL) 20 April 1976 (20/04/76), see entire document, especially column 6, lines 17-25 and column 9, lines 23-28.	1
X ---	US 4,710,030 A (TAUC ET AL) 01 December 1987 (01/12/87), see entire document, especially column 3, lines 62-68, column 4, lines 46-68, column 6, lines 18-21.	21-22, 24 ----
Y		4-10, 11-13, 15, 17, 18-20, 26, 73, 76
Y	US 5,042,952 A (OPSAI ET AL) 27 August 1991 (27/08/91), abstract, column 7, lines 29-32, column 9, lines 20-30.	14, 16

Further documents are listed in the continuation of Box C.  See patent family annex.

* Special categories of cited documents:	"T"	later document published after the international filing date or priority date and not in conflict with the application but cited to understand the principle or theory underlying the invention
"A" document defining the general state of the art which is not considered to be of particular relevance	"X"	document of particular relevance; the claimed invention cannot be considered novel or cannot be considered to involve an inventive step when the document is taken alone
"E" earlier document published on or after the international filing date	"Y"	document of particular relevance; the claimed invention cannot be considered to involve an inventive step when the document is combined with one or more other such documents, such combination being obvious to a person skilled in the art
"L" document which may throw doubts on priority claim(s) or which is cited to establish the publication date of another citation or other special reason (as specified)	"&"	document member of the same patent family
"O" document referring to an oral disclosure, use, exhibition or other means		
"P" document published prior to the international filing date but later than the priority date claimed		

Date of the actual completion of the international search

21 APRIL 1997

Date of mailing of the international search report

12 MAY 1997

Name and mailing address of the ISA/US  
Commissioner of Patents and Trademarks  
Box PCT  
Washington, D.C. 20231

Authorized officer

SANDRA V. SMITH *Sandra Smith*

Facsimile No. (703) 305-3230

Telephone No. (703) 305-7776

Form PCT/ISA/210 (second sheet)(July 1992)\*

## INTERNATIONAL SEARCH REPORT

International application No.

PCT/US96/20917

## C (Continuation). DOCUMENTS CONSIDERED TO BE RELEVANT

Category*	Citation of document, with indication, where appropriate, of the relevant passages	Relevant to claim No.
Y	US 5,083,869 A (NAKATA ET AL) 28 January 1992 (28/01/92), see abstract, column 4, lines 1-5.	11-13
Y	US 5,379,109 A (GASKILL ET AL) 03 January 1995 (03/01/95), column 3, lines 32-38, column 5, line 4.	15, 17
A, P	US 5,546,811 A (ROGERS ET AL) 20 August 1996 (20/08/96), see entire document.	15, 17, 23
Y, P	US 5,574,562 A (FISHMAN ET AL) 12 November 1996 (12/11/96), see abstract, column 2, lines 58-62, column 4, lines 26-50.	4-11, 17
Y, P	US 5,585,921 A (PEPPER ET AL) 17 December 1996 (17/12/96), see abstract, column 4, lines 38-42.	15, 17

# INTERNATIONAL SEARCH REPORT

International application No.

PCT/US96/20917

## Box I Observations where certain claims were found unsearchable (Continuation of item 1 of first sheet)

This international report has not been established in respect of certain claims under Article 17(2)(a) for the following reasons:

1.  Claims Nos.: because they relate to subject matter not required to be searched by this Authority, namely:
  
2.  Claims Nos.: because they relate to parts of the international application that do not comply with the prescribed requirements to such an extent that no meaningful international search can be carried out, specifically:
  
3.  Claims Nos.: because they are dependent claims and are not drafted in accordance with the second and third sentences of Rule 6.4(a).

## Box II Observations where unity of invention is lacking (Continuation of item 2 of first sheet)

This International Searching Authority found multiple inventions in this international application, as follows:

Please See Extra Sheet.

1.  As all required additional search fees were timely paid by the applicant, this international search report covers all searchable claims.
  
2.  As all searchable claims could be searched without effort justifying an additional fee, this Authority did not invite payment of any additional fee.
  
3.  As only some of the required additional search fees were timely paid by the applicant, this international search report covers only those claims for which fees were paid, specifically claims Nos.:-
  
4.  No required additional search fees were timely paid by the applicant. Consequently this international search report is restricted to the invention first mentioned in the claims; it is covered by claims Nos.:-

### Remark on Protest



The additional search fees were accompanied by the applicant's protest.



No protest accompanied the payment of additional search fees.

# INTERNATIONAL SEARCH REPORT

International application No.

PCT/US96/20917

## B. FIELDS SEARCHED

Electronic data bases consulted (Name of data base and where practicable terms used):

APS

search terms: pump, probe, stress, acoustic wave, electrical resistivity, strain, film, substrate, elastic modulus, temperature, spring, vibrational response

## BOX II. OBSERVATIONS WHERE UNITY OF INVENTION WAS LACKING

This ISA found multiple inventions as follows:

- I. CLAIMS 1, 11-13, 19, 21-22, 24,73 , DRAWN TO A GENERAL METHOD AND SYSTEM FOR MEASUREMENT OF A DESIRED FEATURE, CLASSIFIED IN 356, SUBCLASS 432.
- II. CLAIMS 2,3,4-10,25, 70-72, DRAWN TO A METHOD AND SYSTEM FOR SIMULATING A RESPONSE TO MEASURE A DESIRED FEATURE, CLASSIFIED IN CLASS 364, SUBCLASS 578.
- III. CLAIMS 14, 16, DRAWN TO A METHOD AND SYSTEM FOR MEASURING THE ELECTRICAL RESISTIVITY, CLASSIFIED IN CLASS 324, SUBCLASS 635.
- IV. CLAIMS 15, 17 DRAWN TO A METHOD AND SYSTEM FOR MEASURING THE ACOUSTIC WAVE VELOCITY, CLASSIFIED IN CLASS 73, SUBCLASS 597.
- V. CLAIMS 18, 20, DRAWN TO A METHOD OF USING A SUM AND DIFFERENCE OF DIFFERING FREQUENCIES TO MEASURE A DESIRED FEATURE, CLASSIFIED IN CLASS 356, SUBCLASS 432.
- VI. CLAIM 23, DRAWN TO A METHOD OF MEASURING AN ACOUSTIC ECHO, CLASSIFIED IN CLASS 73, SUBCLASS 587.
- VII. CLAIMS 74, 75, DRAWN TO A METHOD OF DETERMINING THE VIBRATIONAL RESPONSE/SPRING CONSTANT, CLASSIFIED IN CLASS 73, SUBCLASS 584.
- VIII. CLAIM 77, DRAWN TO A METHOD OF DETERMINING THE REFRACTIVE INDEX USING ELLIPSOMETRIC TECHNIQUES, CLASSIFIED IN CLASS 35644, SUBCLASS 73.
- IX. CLAIMS 26-55, 60-69, AND 76, DRAWN TO A METHOD OF AUTO-FOCUSING WITH MEANS MEASURING DERIVATIVE, CLASSIFIED IN CLASS 250, SUBCLASS 201.4.X. CLAIM 56, DRAWN TO A METHOD OF AUTO-FOCUSING WITH MULTILAYER SAMPLES AND MEASURING USING VIBRATIONAL SPECTRA, CLASSIFIED IN CLASS 73, SUBCLASS 800.LINKING CLAIM 31 WILL BE EXAMINED WITH EITHER GROUP 4, 9, OR 10.  
LINKING CLAIMS 57-59 WILL BE EXAMINED WITH EITHER GROUP 6, 9, OR 10.

THE INVENTIONS AS DEFINED BY THE GROUPED CLAIMS ABOVE, LACK A SPECIAL TECHNICAL FEATURE THAT IS COMMON TO ALL GROUPS; SIMULATION STEP OF GROUP II NOT PRESENTED IN THE OTHER GROUPS, STEP OF MEASURING THE ELECTRICAL RESISTIVITY, AS IN GROUP III, NOT PRESENTED IN ANY OF THE OTHER GROUPS,  
STEP OF MEASURING ACOUSTIC WAVE VELOCITY, AS IN GROUP IV, NOT PRESENTED IN ANY OF THE OTHER GROUPS,  
STEP OF USING THE SUM AND DIFFERENCE OF TWO FREQUENCIES, AS IN GROUP V, NOT PRESENTED IN ANY OF THE OTHER GROUPS,  
STEP OF MEASURING THE ACOUSTIC ECHO, AS IN GROUP VI, NOT PRESENTED IN ANY OF THE OTHER GROUPS,  
STEP OF DETERMINING THE VIBRATION RESPONSE/SPRING CONSTANT, AS IN GROUP VII, NOT PRESENTED IN ANY OF THE OTHER GROUPS,  
STEP OF DETERMINING THE REFRACTIVE INDEX USING ELLIPSOMETRIC TECHNIQUES, AS IN GROUP VIII, NOT PRESENTED IN ANY OF THE OTHER GROUPS,  
STEP OF AUTOPOCUSsing WITH MEANS MEASURING DERIVATIVES, AS IN GROUP IX, NOT PRESENTED IN ANY OF THE OTHER GROUPS,STEP OF MEASURING USING THE VIBRATIONAL SPECTRA, AS IN GROUP X, NOT PRESENTED IN ANY OF THE OTHER GROUPS,

XP 000630302

P.D. 01/02/96  
p. 663-675 = 13

D1

# Extrinsic optical-fiber ultrasound sensor using a thin polymer film as a low-finesse Fabry-Perot interferometer

P. C. Beard and T. N. Mills

Theoretical and experimental aspects of an extrinsic optical-fiber ultrasound sensor are described. The sensor is based on a thin transparent polymer film acting as a low-finesse Fabry-Perot cavity that is mounted at the end of a multimode optical fiber. Performance was found to be comparable with that of a piezoelectric polyvinylidene difluoride-membrane (PVDF) hydrophone with a sensitivity of 61 mV/MPa, an acoustic noise floor of 2.3 KPa over a 25-MHz bandwidth, and a frequency response to 25 MHz. The wideband-sensitive response and design flexibility of the concept suggests that it may find application as an alternative to piezoelectric devices for the detection and measurement of ultrasound.

*Key words:* Optical fiber, ultrasound, Fabry-Perot, polymer film. © 1996 Optical Society of America

## 1. Introduction

The detection of ultrasound is most commonly achieved by the use of piezoelectric devices. Transducers made from piezoceramics such as lead zirconate titanate (PZT) and lithium niobate ( $\text{LiNbO}_3$ ) can offer high sensitivity, but their poor acoustic-impedance match to liquids results in a very nonuniform frequency response, giving a poor representation of the detected signal. The piezoelectric polymer polyvinylidene difluoride (PVDF) has an acoustic impedance much closer to that of water, thus giving a more uniform frequency response, but it is not as sensitive as piezoceramic devices. Common to transducers fabricated from both types of material are a susceptibility to electromagnetic interference and signal distortion and a reduced sensitivity that is due to the electrical-loading effects of the transducer leads. In addition, the cost and fragility of piezoelectric-transducer elements limit their use for certain applications.

Various intrinsic and extrinsic optical-fiber ultrasound sensors have been suggested as an alternative to piezoelectric devices for applications in which a totally electrically passive sensor is required. Intrinsic ultrasound sensors, in which the fiber itself acts

as the transduction element, have tended to be either polarimetric<sup>1-6</sup> or interferometric<sup>7-10</sup> devices. Although intrinsic sensors have been demonstrated to be capable of detecting acoustic waves at ultrasonic frequencies, their sensitivity is relatively low compared with that of piezoelectric transducers. Their uniformity of frequency response is also poor because of the acoustic-impedance mismatch between the fused silica of the optical fiber and water.<sup>7</sup> A further limitation for applications in which a high degree of measurement accuracy is required arises from the fact that the active length of the fiber responds to the line integral of the acoustic field.<sup>3</sup> If the phase of the ultrasound field over the region intercepted by the fiber is not the same at all points along the fiber, the peak pressure of the field may be underestimated. In addition, active phase-control<sup>11</sup> and polarization-control<sup>12</sup> systems are often required to keep the sensor at its optimum operating point, adding to the cost and complexity of the system. For point measurements for which a probe-type configuration is required, intrinsic optical-fiber sensors are generally unsuitable because a length of fiber, typically close to 1 cm, must be placed in the ultrasound field. Extrinsic optical-fiber ultrasound sensors are more suitable in this respect. These sensors use the fiber simply to deliver light to and from an optical sensor at the end of the fiber, which interacts with the acoustic field. One scheme relies upon the interferometric detection of acoustically induced changes in the separation of two optical fibers in a silica tube.<sup>13</sup> Another that uses a fiber

The authors are with the Department of Medical Physics and Bioengineering, University College London, Shropshire House, 11-20 Capper Street, London WC1E 6JA, United Kingdom.

Received 1 August 1995.

0003-6935/96/040663-13\$06.00/0

© 1996 Optical Society of America

Micheleson interferometer<sup>14</sup> is essentially a fiber-optic version of a bulk optical scheme used for the primary calibration of ultrasonic hydrophones.<sup>15</sup> This scheme is based on the measurement of acoustically induced displacements of a thin membrane. High sensitivity has been reported, although a somewhat complex, active phase-bias-control system is required as both arms of the fiber interferometer are sensitive to ambient thermal and pressure fluctuations. Other extrinsic optical-fiber sensors have made use of beam-deflection techniques,<sup>16</sup> Raman-Nath diffraction,<sup>17</sup> and acoustically induced changes in the refractive index at a poly(methyl methacrylate)-water [(PMMA)-water] interface.<sup>18</sup> Most of these extrinsic noninterferometric optical-fiber techniques are of low sensitivity.

The extrinsic optical-fiber sensor described in this paper is based on the detection of acoustically induced changes in the thickness of a thin, clear, polymer film acting as a low-finesse Fabry-Perot interferometer<sup>19</sup> that is mounted at the end of an optical fiber. The use of a thin polymer film as the sensing element has a number of advantages. Because the polymer film itself is the interferometer and has a short path length, it exhibits a low sensitivity to environmental thermal and pressure fluctuations. Thus there is no need for complex polarization- and phase-bias-control systems. A film thickness of a few tens of micrometers gives a megahertz bandwidth and removes the need for a long-coherence source. The low Young's modulus (4–5 GPa) of many polymers as compared with that of a fused-silica (~70-GPa) fiber produce a high acoustic sensitivity. In addition, many polymers have an acoustic impedance close to that of water, resulting in a uniform frequency response. Furthermore, because the active area of the sensor is defined by the core diameter of the optical fiber, small active areas are possible. A small active area avoids the line-integral-response problem of intrinsic sensors and enables a high spatial resolution and a low directional sensitivity to be achieved. In this paper the theoretical aspects of the sensor's performance are considered. This is followed by a comparison of the experimentally measured performance with that of a PVDF-membrane hydrophone.

## 2. Principles of Operation

A schematic drawing of the system for the optical-fiber detection of ultrasound in water is depicted in Fig. 1. Light from a wavelength-tunable laser diode is launched into a multimode optical-fiber downlead. The sensing element, mounted at the end of the fiber, comprises a thin (typically a few tens of micrometers thick) transparent polymer film acting as a low-finesse Fabry-Perot interferometer. The optical reflection coefficients of the mirrors of the interferometer are defined by the Fresnel reflection coefficients arising from the refractive-index mismatches between the two sides of the film and the

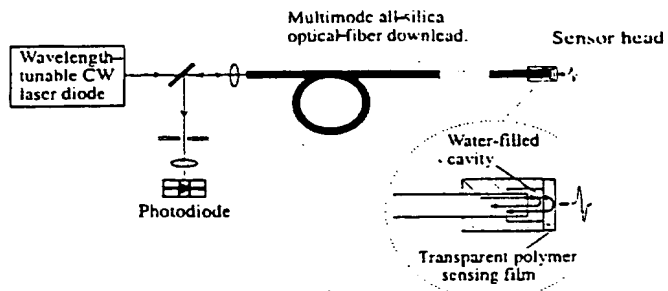


Fig. 1. Schematic diagram showing the optical-fiber detection of ultrasound.

surrounding media. This concept avoids the need for optically reflective coatings to be applied to the film. The stress that is due to an incident acoustic wave modulates the thickness of the film, and therefore the optical phase difference between the two reflections. A corresponding intensity modulation is produced, which is then transmitted back along the fiber for detection at a photodiode. For optimum sensitivity and linearity the sensor is operated and maintained at quadrature by adjustment of the wavelength of the laser diode. The space between the fiber tip and the sensing film is filled with water. With the assumption that the sensor is used to detect ultrasound in water, this water-filled cavity serves two purposes. First, the Fresnel reflection coefficients on either side of the film will be equal, giving an optimum fringe visibility of unity. Second, the water provides an acoustic-impedance match on the fiber side of the film, minimizing acoustic reflections that would otherwise degrade the sensor's uniformity of frequency response.

## 3. Theory

The theoretical aspects of the sensor's operation are considered first with an examination of the output of a low-finesse Fabry-Perot interferometer to obtain the phase sensitivity. Second, the acoustic sensitivity and the frequency response of the sensor are modeled by means of a consideration of the interaction of the sensing film with an acoustic field. Finally the interferometric and acoustic parameters are brought together to give the overall system sensitivity.

### A. Low-Finesse Fabry-Perot Interferometer Output

Figure 2 shows a polymer-film sensing element of refractive index  $n$  and thickness  $l$  in contact with two different media: on the left-hand side medium 1 of refractive index  $n_1$ , and on the right-hand side medium 2 of refractive index  $n_2$ . The Fresnel reflections coefficients arising from the refractive-index mismatches at the boundaries of the sensing film are assumed to be sufficiently low to permit the contribution of multiple reflections within the interferometer to be neglected. The analysis is therefore that of a two-beam interferometer. In the following subsec-

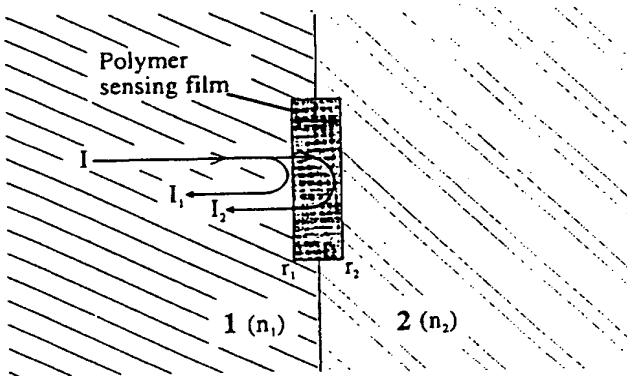


Fig. 2. Diagram of a polymer-sensing film acting as a low-finesse Fabry-Perot interferometer. 1 and 2 denote the media on the left- and right-hand sides, respectively.

tions, the case in which the interferometer is illuminated with light at normal incidence is examined, followed by a consideration of the effects of the illumination of the interferometer with the divergent output of an optical fiber.

### 1. Illumination of the Sensing Film at Normal Incidence

The resultant intensity  $I_0$  that is due to the superposition of reflections  $I_1$  and  $I_2$  from the two sides of the film as a result of light at normal incidence (Fig. 2) is

$$I_0 = I_1 + I_2 + 2\sqrt{I_1 I_2} \cos \Phi, \quad (1)$$

where  $\Phi$  is the total phase difference arising from the optical path-length difference between the two reflections. When an acoustic wave is incident on the sensing film,  $\Phi$  consists of two components: the untagged phase-bias term  $\phi$  that defines the working point of the interferometer and a time-varying signal term  $d\phi$  that arises from the acoustically induced change in thickness of the sensing film:

$$\Phi = \phi + d\phi. \quad (2)$$

Inserting Eq. (2) into Eq. (1) and expanding give

$$I_0 = I_1 + I_2 + 2\sqrt{I_1 I_2} \cos \phi \cos d\phi - \sin \phi \sin d\phi. \quad (3)$$

For optimum sensitivity and linearity it is desirable that we set the phase-bias term  $\phi$  at quadrature where  $\phi = (2m + 1)\pi/2$  (for integer  $m$ ) by tuning the wavelength of the laser source. At the first quadrature point,  $\phi = \pi/2$ , and for small  $d\phi$ , Eq. (3) reduces to

$$I_0 = I_1 + I_2 - 2\sqrt{I_1 I_2} d\phi. \quad (4)$$

Under these conditions, the output of the interferometer that is detected by the photodiode consists of an acoustically induced, time-varying, intensity-modu-

lated term  $dI_0$  that is linearly dependant on  $d\phi$  and a dc component  $I_{dc}$  by

$$dI_0 = -2\sqrt{I_1 I_2} d\phi, \quad (5)$$

$$I_{dc} = I_1 + I_2. \quad (6)$$

$I_1$  and  $I_2$  can be written in terms of the incident intensity  $I$  and the Fresnel reflection coefficients  $r_1$  and  $r_2$ , defined by the refractive-index mismatches at the boundaries of the sensing film by

$$I_1 = I r_1, \quad I_2 = I(1 - r_1)^2 r_2, \quad (7)$$

where

$$r_1 = \left( \frac{n - n_1}{n + n_1} \right)^2, \quad r_2 = \left( \frac{n - n_2}{n + n_2} \right)^2. \quad (8)$$

From Eqs. (5)–(7) the phase sensitivity of the interferometer, defined as the intensity modulation per unit phase shift,  $dI_0/d\phi$ , and the dc level  $I_{dc}$  can now be written as

$$\frac{dI_0}{d\phi} = -2I(1 - r_1)\sqrt{r_1 r_2}, \quad (9)$$

$$I_{dc} = I[r_1 + (1 - r_1)^2 r_2]. \quad (10)$$

It is desirable to maximize the phase sensitivity by a suitable choice of  $I$ ,  $r_1$ , and  $r_2$ , but it is important to note that these parameters also affect the dc component. This dc component is an undesirable element of the interferometer output, as it produces a large photocurrent with attendant shot noise that can dominate the noise characteristics of the photodiode. Furthermore, if the dc level is too high it will saturate the photodiode limiting the maximum phase sensitivity that can be achieved by an increase in  $I$ . For these reasons it is necessary to both minimize the dc level and maximize the phase sensitivity for optimum performance. This is achieved when values of  $r_1$  and  $r_2$  are chosen that give a fringe visibility of one. For low values of  $r_1$  and  $r_2$  ( $< 1\%$ ), such as those defined by the Fresnel reflection coefficients occurring at a polymer–water interface, this condition is met by setting  $r_1 = r_2$ . This condition can be readily achieved in practice if one ensures that water is in contact with both sides of the film. With the fringe visibility equal to one, the laser power can now be increased as much as possible before it reaches the saturation threshold of the photodiode. This increase enables the highest possible phase sensitivity to be obtained. When a polyethylene terephthalate (PET) sensing film ( $n = 1.6$ ) surrounded by water ( $n_1 = n_2 = 1.33$ ) is used,  $r_1 = r_2 = 0.00849$ , and for  $I = 3 \text{ mW}$  Eq. (9) yields  $dI_0/d\phi = 50.4 \mu\text{W}/\text{rad}$ . With the use of a typical silicon photodiode, this value of the phase sensitivity would enable phase shifts of the order of 10 mrad to be detected. Equation (10) gives

a value of  $I_{dc}$  of 50.4  $\mu\text{W}$ , which is well below the saturation threshold of such a photodiode.

## 2. Optical-Fiber Illumination of the Sensing Film

In a previous paper<sup>19</sup> it was noted that sensitivity decreased significantly when the sensing film was illuminated with the divergent output of an optical fiber. This decrease arises as a result of the increased optical path lengths taken by light at nonnormal angles of incidence.

Consider the case in which a collimated beam of light is normally incident upon the sensing film. All the light that is transmitted into and reflected back from the film travels the same optical path. Each point across the reflected optical field that is due to the interference between the reflections from the two sides of the sensing film is therefore associated with the same phase bias. Thus all the reflected-signal intensity-modulated light  $dI_0$  arriving at the photodiode is in phase. This is in contrast to the situation in which the sensor is illuminated with the divergent light emerging from the end of a large-diameter multimode optical fiber. The optical path length, and therefore the phase bias associated with the reflected light, is dependent on the angle of incidence, and this dependence can lead to conditions in which partial or complete cancellation of the signal occurs. Consider the case in which the light striking the film at normal incidence travels an optical path length  $2l$  and assume that this path length corresponds to the first quadrature point. A ray at an angle of incidence  $\theta$  takes an extra path length  $\Delta l$ :

$$\Delta l = 2l \left( \frac{1}{\cos \theta} - 1 \right). \quad (11)$$

The corresponding difference in the phase bias  $\phi_d$  as a result of this extra path length is

$$\phi_d = \frac{4\pi nl}{\lambda} \left( \frac{1}{\cos \theta} - 1 \right), \quad (12)$$

where  $\lambda$  is the wavelength of the laser source. As the angle of incidence is increased, the phase-bias difference  $\phi_d$  also increases until  $\phi_d = \pi$ . At this point the total optical path length corresponds to the next quadrature point and so the intensity-modulated signal is now in antiphase with the signal arising from the normally incident light. When imaged onto the same detector the two signals cancel. This signal-canceling effect not only reduces the phase sensitivity but also adds to the dc level. The solution is to ensure that the thickness of the interferometer and the maximum angle of divergence are such that the phase-bias difference  $\phi_d$ , as a result of the extra path length  $\Delta l$ , is less (ideally significantly less) than  $\pi$  rad. To meet this condition with a PET film ( $n = 1.6$ ), for example, and 850-nm light emerging from an optical fiber with a maximum half-angle divergence of  $5^\circ$ , the thickness

of the film as determined from Eq. (12) should be less than 35  $\mu\text{m}$ .

## B. Sensor-Acoustic-Field Interaction: Acoustic Sensitivity and Frequency Response

This subsection concerns the sensor-acoustic-field interactions and considers the phase modulation produced by an acoustic wave incident on the sensing film. The acoustic sensitivity, as a function of frequency, is considered by an examination of the thickness resonance modes arising from reflections of a normally incident acoustic wave within the sensing film only. The effects of radial resonance modes and acoustic perturbations produced by the structure holding the sensing film are not considered.

The strain that is due to a normally incident acoustic wave produces a change in the thickness of the polymer film  $dl$ , which then gives rise to a phase shift  $d\phi$  which, neglecting strain-induced changes in the refractive index, is

$$d\phi = \frac{4\pi n dl}{\lambda}, \quad (13)$$

where  $n$  is the refractive index of the polymer film and  $\lambda$  is the wavelength of the laser source. The changes in film thickness is given by

$$dl = \int_0^l \frac{P_T(x, t)}{E} dx, \quad (14)$$

where  $E$  is the Young's modulus of the polymer film.  $P_T(x, t)$  represents the spatial distribution of pressure across the thickness of the sensing film and is the sum of the component of the incident acoustic wave that is transmitted into the sensor film  $P_1$  and subsequent acoustic reflections  $P_2, P_3, \dots, P_n$  at the boundaries of the film. These reflections, shown schematically in Fig. 3, arise as a result of the differences in acoustic impedance between the polymer film and the surrounding media.

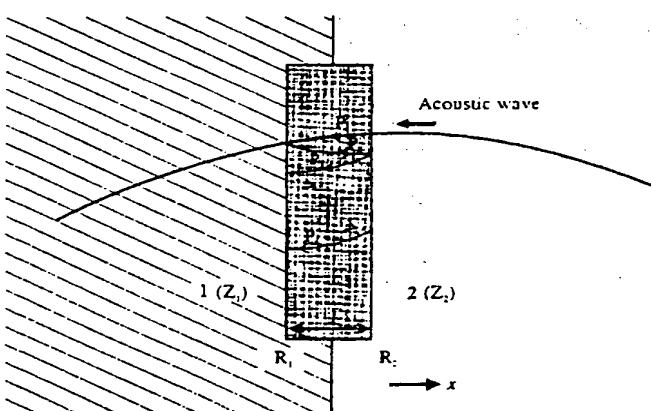


Fig. 3. Acoustic reflections within the sensing film. As in Fig. 2, the numerals denote media 1 and 2.

In general, for a sinusoidally varying incident acoustic wave of amplitude  $P_0$  and angular acoustic frequency  $\omega$  traveling in the negative  $x$  direction, the stress distribution across the film from the superposition of  $P_1$  and an odd number of subsequent reflections  $N$ , with the acoustic attenuation neglected, is

$$P_T = P_0 T \sum_{i=0}^{N-1} [R_1' R_2^i \sin(\omega t - k(2li - x)) + R_1'^{-1} R_2^i \sin(\omega t - k(2li + x))], \quad (15)$$

where  $T$  is the pressure-amplitude transmission coefficient resulting from the acoustic-impedance mismatch between the sensing film and surrounding media,  $R_1$  and  $R_2$  are the pressure-amplitude reflection coefficients at the two surfaces of the film, and

$$T = \frac{2Z}{Z + Z_2}, \quad R_1 = \frac{Z_1 - Z}{Z + Z_1}, \quad R_2 = \frac{Z_2 - Z}{Z + Z_2}, \quad (16)$$

where  $Z$  is the acoustic impedance of the polymer-sensing film and  $Z_1$  and  $Z_2$  are the acoustic impedances of the media on either side of the film. Substituting  $P_T$  into Eq. (14) and evaluating the integral give an expression of the form

$$dl = \frac{P_0 T}{Ek} \sum_{i=1}^{N-2} \psi_i \cos(\omega t + \xi_i). \quad (17)$$

This is the sum of  $N + 2$  sinusoids of the same frequency but different amplitudes and phases and can be written as

$$dl = \frac{P_0 T}{Ek} \psi \cos(\omega t + \xi), \quad (18)$$

where the amplitude  $\psi$  is

$$\psi = \left[ \left( \sum_{i=1}^{N+2} \psi_i \cos \xi_i \right)^2 + \left( \sum_{i=1}^{N+2} \psi_i \sin \xi_i \right)^2 \right]^{1/2}. \quad (19)$$

The thickness of the sensor film is therefore modulated at a frequency  $\omega$  and is of an amplitude

$$dl_0 = \frac{P_0 T}{Ek} \psi. \quad (20)$$

The pressure-amplitude reflection coefficient resulting from the acoustic-impedance mismatch between water (acoustic impedance of  $1.5 \times 10^6$  kg/m<sup>2</sup>s) and a polymer film such as PET (acoustic impedance of  $3.1 \times 10^6$  kg/m<sup>2</sup>s) is small at  $-0.35$ . For the purposes of modeling the frequency response of the sensor film it is sufficient to consider five reflections because, after this number of reflections, the amplitude is reduced by more than 2 orders of magnitude. After evaluation of Eq. (15) for  $N = 5$  and the integral

in Eq. (14), Eq. (19) yields

$$\begin{aligned} \psi_{[5]}^2 = & [(1 - R_1 + (R_1 - R_2 R_1 - 1) \cos kl \\ & + (R_2 R_1 - R_2 R_1^2) \cos 2kl \\ & + (R_2 R_1^2 - R_2^2 R_1^2) \cos 3kl \\ & + (R_2^2 R_1^2 - R_2^2 R_1^3) \cos 4kl + R_2^2 R_1^3 \cos 5kl]^2 \\ & + [(R_2 R_1 - R_1 - 1) \sin kl - (R_2 R_1 - R_2 R_1^2) \sin 2kl \\ & - (R_2 R_1^2 - R_2^2 R_1^2) \sin 3kl \\ & - (R_2^2 R_1^2 - R_2^2 R_1^3) \sin 4kl - R_2^2 R_1^3 \sin 5kl]^2. \end{aligned} \quad (21)$$

The acoustic sensitivity of the sensing film can be conveniently defined as the phase modulation per unit acoustic pressure  $d\phi_0/P_0$ . For  $N = 5$  this is

$$\frac{d\phi_0}{P_0} = \frac{4\pi n}{\lambda} \frac{T}{Ek} \psi_{[5]}. \quad (22)$$

Equation (22) can be used to predict the sensitivity and the frequency response for various sensor-film materials and different media in contact with the two sides of the film. Four different acoustic-loading configurations are considered below. The acoustic sensitivity as a function of acoustic frequency for each case is shown in Fig. 4 for a 50-μm-thick PET film that has the values  $E = 4.4$  GPa,  $c = 2200$  m/s, and  $n = 1.6$ .

### 1. Matched-Load Sensing Film

A matched load represents an ideal case in which the polymer film is surrounded by media of the same acoustic impedance ( $Z = Z_1 = Z_2$ ) so there are no acoustic reflections at the boundaries. Under these conditions  $R_1 = R_2 = 0$  and  $T = 1$ , and Eq. (21) reduces to

$$\psi_{[5]} = 2 \sin \left( \frac{kl}{2} \right). \quad (23)$$

Inserting Eq. (23) into Eq. (22) and using the relation  $k = 2\pi/\lambda_a$ , where  $\lambda_a$  is the acoustic wavelength, we find that the acoustic sensitivity is

$$\frac{d\phi_0}{P_0} = \frac{4n}{\lambda} \frac{\lambda_a}{E} \sin \left( \frac{\pi l}{\lambda_a} \right). \quad (24)$$

There are two frequency regimes of interest. First, there is the case in which the acoustic wavelength  $\lambda_a$  is much greater than the thickness  $l$  of the film, and second there is the case when  $\lambda_a$  approaches  $l$ . If  $\lambda_a$  is large compared with  $l$ , the pressure gradient across the sensor is effectively zero and Eq. (24) reduces to, for  $\lambda_a \gg l$ ,

$$\frac{d\phi_0}{P_0} = \frac{4\pi n}{\lambda} \frac{l}{E}. \quad (25)$$

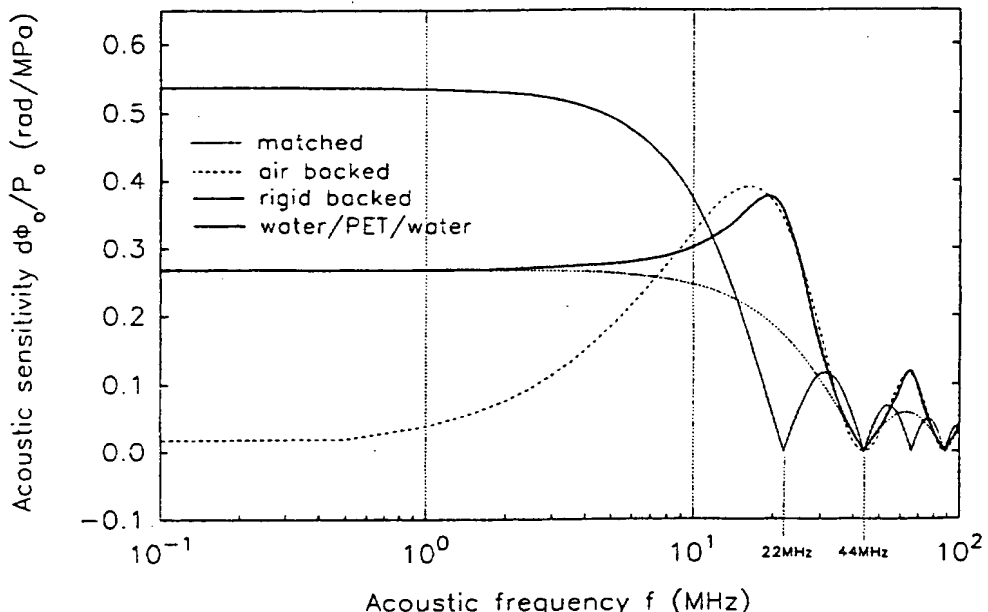


Fig. 4. Theoretical acoustic sensitivity as a function of the frequency response for different acoustic-loading configurations with a 50- $\mu\text{m}$ -thick PET sensing film. Parameters:  $E = 4.4 \text{ GPa}$ ,  $c = 2200 \text{ m/s}$ ,  $\lambda = 850 \text{ nm}$ , and  $Z = 3.1 \times 10^6 \text{ kg/m}^2 \text{s}$ .

Equation (25) shows that, at low frequencies and for a given laser wavelength and refractive index  $n$ ,  $d\phi_0/P_0$  is dependent on only the thickness and the Young's modulus of the sensor material. As the acoustic wavelength is reduced and approaches  $l$ , the spatial variation of the pressure field across the sensor becomes significant and  $d\phi_0/P_0$  decreases, becoming zero when  $\lambda_a = l$ . The first frequency at which  $d\phi_0/P_0$  is zero is given by

$$f_c = c/l, \quad (26)$$

where  $c$  is the speed of sound in the sensor material. Beyond  $f_c$  the value of  $d\phi_0/P_0$  varies rapidly with an increasing frequency and becomes zero for wavelengths equal to multiples of  $l$ . In the example shown in Fig. 4 this behavior is shown with  $f_c$  occurring at 44 MHz. This simple analysis provides an insight into the required acoustic properties of the sensing element. For the maximum acoustic sensitivity and frequency response, a material with both a low Young's modulus and a high speed of sound is required. A material with a very low Young's modulus will exhibit a high acoustic sensitivity for  $\lambda_a \gg l$ . If it also has a very low speed of sound then Eq. (12) shows that, for a high-frequency response,  $l$  must be small. This small value of  $l$  in turn reduces the acoustic sensitivity.

## 2. Rigid-Back Sensing Film

The sensing film is backed with a medium that has a very high acoustic impedance ( $Z_1 \gg Z$ ) and  $R_1 = 1$ . For algebraic simplicity the front-face reflection is neglected by setting the values  $R_2 = 0$  and  $T = 1$  and, from Eq. (21),  $\psi_{|S|}$  becomes

$$\psi_{|S|} = 2 \sin kl, \quad (27)$$

and the acoustic sensitivity is

$$\frac{d\phi_0}{P_0} = \frac{4n}{\lambda} \frac{\lambda_a}{E} \sin\left(\frac{2\pi l}{\lambda_a}\right). \quad (28)$$

In the low-frequency limit Eq. (28) reduces, for  $\lambda_a \gg l$ , to

$$\frac{d\phi_0}{P_0} = \frac{8\pi n}{\lambda} \frac{l}{E}. \quad (29)$$

This expression is a factor of 2 higher than the acoustic sensitivity of the matched-load configuration discussed in Subsection 3.B.1., although the cutoff frequency  $f_c$  has decreased by a factor of 2 and now occurs at

$$f_c = c/2l. \quad (30)$$

This change is shown in Fig. 4 occurring at 22 MHz.

## 3. Air-Backed Sensing Film

In this case the film is backed by air ( $Z_1 \ll Z$ ) so that  $R_1 = -1$ . To simplify Eq. (21) we again neglect the reflection from the front face of the sensing film by setting  $R_2 = 0$  and  $T = 1$ . Equation (21) becomes

$$\psi_{|S|} = 4 \sin^2 kl, \quad (31)$$

and from Eq. (22) the acoustic sensitivity is

$$\frac{d\phi_0}{P_0} = \frac{8n}{\lambda} \frac{\lambda_a}{E} \sin^2\left(\frac{\pi l}{\lambda_a}\right). \quad (32)$$

The nonuniform frequency-response characteristic of this configuration is shown clearly in Fig. 4, with

the acoustic sensitivity rising from zero to a maximum. Such a configuration gives a poor representation of the acoustic wave, particularly when sensing short pulses with a broadband frequency content.<sup>19</sup>

#### 4. Water-PET-Water Sensing Film

The closest practical configuration to the matched-load ideal described in Subsection 3.B.1. is to have water in contact with both sides of the PET sensing film. In this case  $Z_1 = Z_2 = 1.5 \times 10^5 \text{ kg/m}^2 \text{ s}$ , so that  $R_1 = R_2 = -0.35$ . The acoustic sensitivity is modeled by the use of the full form of Eq. (21). The prominent features of the frequency-response curve shown in Fig. 4 are the  $\lambda/2$  resonance at approximately 20 MHz and the cutoff frequency  $f_c$  at 44 MHz. In practice it can be expected that the effects of attenuation within the film (not considered in this model) would act to reduce the magnitude of the  $\lambda/2$  resonance. In the low-frequency regime where  $\lambda_a \gg l$  and when  $R_1 = R_2$ , Eq. (21) reduces to

$$\Psi_{[5]} = kl \sum_{i=0}^5 R_1^i = \frac{kl(1 - R_1^6)}{1 - R_1}, \quad (33)$$

which for small values of  $R_1$  further reduces to

$$\Psi_{[5]} = \frac{kl}{1 - R_1} = \frac{kl}{T}. \quad (34)$$

Substituting Eq. (34) into Eq. (22) gives

$$\frac{d\phi_0}{P_0} = \frac{4\pi n}{\lambda} \frac{l}{E}, \quad (35)$$

which is the same expression for the low-frequency acoustic sensitivity for the matched-load case given in Eq. (25). This behavior is shown clearly in Fig. 4, with the departure from the matched-load case beginning at approximately 2 MHz. The low-frequency acoustic sensitivity of the water-PET-water configuration is 0.27 rad/MPa.

#### C. Overall System Sensitivity

The essential point to be noted from Subsection 3.A. is that the phase sensitivity is limited by the maximum laser power that can be used before the dc level saturates the photodiode. To achieve the highest phase sensitivity we have established that (1) the dc level should be kept to a minimum by ensuring that the fringe visibility is equal to one, and (2) the interferometer thickness and the angle of divergence of the optical fiber should be kept to a minimum. Thus the thickness of the sensing element is not determined solely by considerations of the acoustic sensitivity and the frequency response, as might be expected. For example, if a low-frequency response is required, the film could be made quite thick to achieve a high acoustic sensitivity. This, however, would increase the signal-canceling problems arising from optical-fiber illumination of the sensing film and would degrade the overall sensitivity. The

trade-off is therefore between the requirements of phase sensitivity, acoustic sensitivity, and frequency response. When the very highest sensitivity is required for detecting small-amplitude signals, it is necessary to strive for both the highest possible acoustic and phase sensitivities. Under high-amplitude-signal conditions it is important to ensure that the acoustic sensitivity is not too high. If the signal-induced phase modulation becomes too large, the small-angle approximation cannot be invoked, resulting in a nonlinear response. In such circumstances it is the phase sensitivity that should be optimized for the maximum dynamic range.

Multiplying the phase sensitivity and the acoustic sensitivity brings together the interferometric and acoustic aspects of the sensor operation to give an expression for the overall system sensitivity in terms of the intensity per unit acoustic pressure. Multiplying Eq. (22) by Eq. (9) yields

$$\frac{dI_0}{P_0} = \frac{8\pi nl(1 - r_1)\sqrt{r_1r_2T}\Psi_{[5]}}{Ek\lambda}. \quad (36)$$

For a 50-μm PET sensing film surrounded by water with the use of the values 50.4 μW/rad for the phase sensitivity obtained in Subsection 3.A. and 0.27 rad/MPa for the acoustic sensitivity obtained in Subsection 3.B., Eq. (36) gives the system sensitivity at 13.6 μW/MPa.

#### 4. Experimental Procedure

The aim of the experimental work was to demonstrate the concept of the optical-fiber Fabry-Perot polymer-film ultrasound sensor. An experimental sensor head has been constructed and tested to evaluate the performance of a 50-μm PET film acting as the sensing element. Laser-generated thermoelastic waves were used as a source of wideband ultrasound, and the output of the sensor was compared with that of a PVDF-membrane hydrophone.

##### A. Experimental Sensor Head

The sensor head was designed so that the sensing film could be easily removed and replaced, the fiber-film separation varied, and different areas of the film interrogated for phase-bias control. The latter is necessary because, for the purpose of demonstrating the concept, a fixed-wavelength He-Ne laser was used rather than a tunable laser diode source. The sensor head, shown in Fig. 5, was

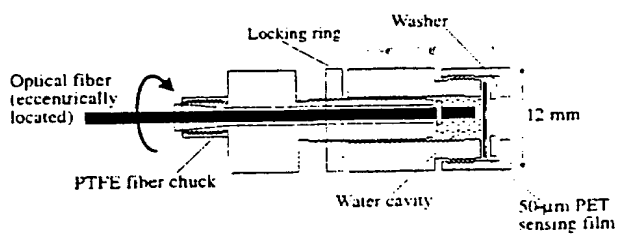


Fig. 5. Illustration of the experimental sensor head.

constructed from brass and is of an overall diameter of 12 mm. The sensing film used was 50- $\mu\text{m}$ -thick PET film. This thickness was chosen as an acceptable compromise between the requirements of acoustic sensitivity and of limiting the signal-canceling effects described in Section 3. The optical fiber is inserted through an eccentrically located hole in a polytetrafluoroethylene (PTFE) insert in the main screw, which permits it to be rotated without gripping the fiber. A plastic disk is bonded to the fiber a few millimeters from its distal end. Turning the screw advances the fiber toward the film, and a locking ring enables the screw to be locked at the appropriate fiber-film separation. The fiber is eccentrically located, so rotation of the screw results in the light emerging from the end of the fiber scanning a circle on the polymer film. Because a typical polymer film is not perfectly flat, the phase bias is different for each point on the film that is illuminated. Exploiting this fact provides a means of setting the interferometer at quadrature. First the main screw was rotated until it had passed through two consecutive points that produced a signal minimum. The screw was then turned back until the illuminated region of the film was at a point equidistant between the two points corresponding to the signal minima. At this point the interferometer was at quadrature, and the signal at a maximum. The experimental sensor head described above was designed primarily for evaluation purposes and is somewhat large for certain applications. A 1-mm-diameter sensor head with the same sensing element has been incorporated into a photoacoustic probe,<sup>20</sup> demonstrating the feasibility of a miniature-probe-type configuration.

#### B. Experimental Arrangement and Method

The experimental arrangement is shown in Fig. 6. Wideband ultrasonic thermoelastic waves were generated by the absorption of 20-ns optical pulses at 532 nm in Quink Solv-x ink, which was assumed to approximate a nonscattering absorber. The optical-beam diameter was 4 mm. The optical pulses, produced by a frequency-doubled Q-switched Nd:YAG laser, were directed onto the ink, which was placed in contact with the Perspex window in the bottom of the water bath. The resulting thermoelastic waves propagate vertically upward and are reflected from a glass block angled at 45° acting as an

acoustic reflector. A calibrated 25-MHz, 50- $\mu\text{m}$  bi-laminar PVDF-membrane hydrophone with an active diameter of 1 mm and which was immersed in the water bath was used as a reference hydrophone. This type of hydrophone is widely acknowledged as the gold standard in ultrasound measurements on account of its wideband, uniform frequency response, linearity and stability, and minimum perturbation to the acoustic field under measurement. The calibration of the hydrophone, carried out by the National Physical Laboratory, is over the range of 1–30 MHz in steps of 1 MHz. A 7-mW He-Ne laser operating at 633 nm was used to illuminate the sensor film by means of a 2-m length of 400- $\mu\text{m}$  all-silica optical fiber. The intensity-modulated signal reflected from the sensor film was transmitted back along the fiber and directed onto a 25-MHz silicon p.i.n. hybrid photodiode with an active diameter of 0.8 mm.

Experiments were carried out to measure the sensitivity, frequency response, linearity, and stability of the optical-fiber sensor. For the experiments in which linearity and stability were being measured, the sensor head was positioned directly behind the hydrophone in the water tank so that the same region in the acoustic field was measured simultaneously by both devices. For the sensitivity and frequency-response measurements, even the relatively small acoustic perturbation produced by the membrane hydrophone was unacceptable. We therefore obtained these measurements by immersing the optical-fiber sensor in the tank, taking a measurement, and then removing the sensor and replacing it with the hydrophone. To ensure that the same point in the ultrasound field was being measured by both the sensor and the hydrophone, the low-power, fixed-Q output of the Nd:YAG laser was used as an alignment beam. The position of the hydrophone or sensor was adjusted until the Fresnel reflection from the Perspex window was visible in the active area of the device. Fine adjustment was then carried out by steering the optical beam while thermoelastic waves were being generated in the liquid absorber until the output of the device under alignment was at a maximum. In addition, care was taken to ensure that the acoustic path length (approximately 6 cm) traveled by the thermoelastic wave was identical for both measurements. This was achieved to a high degree of accuracy by the adjustment of the position of each device so that the time from firing the Q-switched laser pulse to detection of the thermoelastic wave was the same. There is significant variation from pulse to pulse in the output of a Q-switched Nd:YAG laser, so the output from each device was averaged over 60 shots by means of the signal-averaging function of a 500-MHz digitizing oscilloscope.

#### C. Sensor Mode of Operation

In principle it is possible that the signal detected by the sensor is due to acoustically induced bulk move-

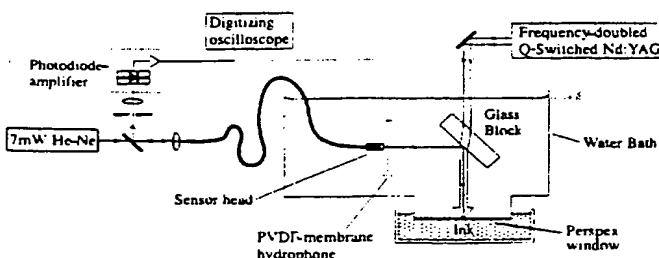


Fig. 6. Experimental arrangement for measuring the sensor performance.

ment or displacement of the sensing film. In this case it would be the Fresnel reflections from the cleaved distal end of the fiber and the front face of the film (the side closest to the end of the fiber) that would interfere. Verification that it was changes in the thickness of the sensing film that were being detected rather than its bulk displacement was achieved when the sensor was set up and aligned so that a clearly detectable acoustic signal could be observed. The back face of the film (the side furthest from the fiber) was then abraded with sandpaper, thus destroying the specular reflection from the back face. The only significant interference would then be between the reflections from the end of the optical fiber and the front face of the polymer film. Under these conditions no signal from an incident acoustic wave could be detected, verifying the thickness mode of operation of the sensor.

**D. PVDF-Membrane Hydrophone and Sensor Comparison**  
The signals measured by the optical-fiber sensor and the hydrophone are shown in Figs. 7. A measurement was made first with the optical sensor. The sensor was then removed and replaced with the membrane hydrophone as described in Subsection

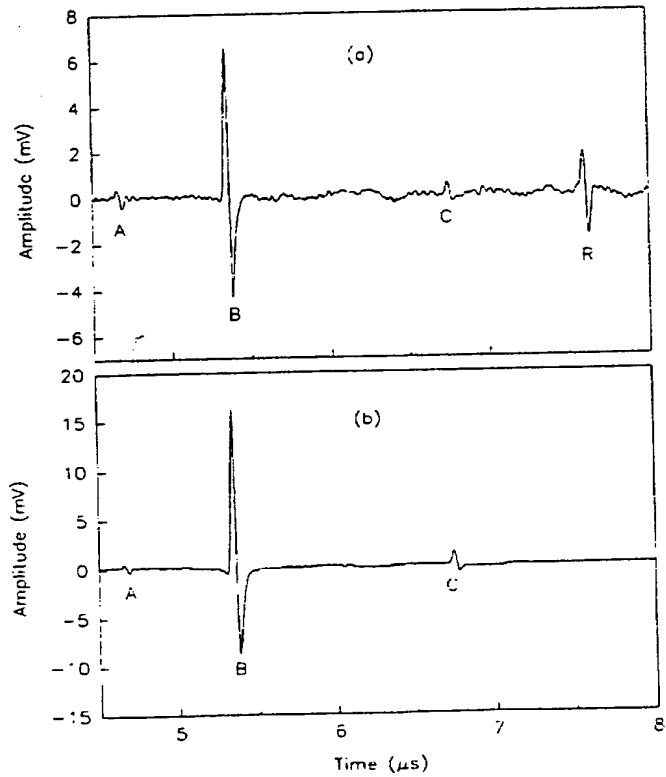


Fig. 7. Comparison of (a) the optical-fiber sensor output with (b) the 50- $\mu\text{m}$  PVDF-membrane hydrophone output in response to a thermoelastic wave of amplitude 0.1 MPa. Signal labels: A, thermoelastic wave generated in the Perspex window; B, thermoelastic wave generated in the ink absorber; C, reflection of signal A within the Perspex window; R, reflection of signal B from the tip of the optical fiber.

4.B. so that the same point in the acoustic field was measured with both devices. Signal averaging over 60 pulses was performed in each case. The first signal, A (see Figs. 7), is a small-amplitude thermoelastic wave generated at the boundary between the upper surface of the Perspex window and the surrounding water. The second signal B is the thermoelastic wave generated in the ink. Signal C is the reflection of signal A within the Perspex window. Signal R [Fig. 7(a)] is the reflection of the thermoelastic-wave signal B from the tip of the optical fiber (showing that the fiber-film separation is approximately 1.6 mm) and therefore appears on only the sensor output. These results indicate that the sensor exhibits a signal-to-noise ratio comparable with that of the membrane hydrophone. In addition, the shape of the wave measured by the sensor, as shown more clearly in the normalized, expanded view of signal B in Fig. 8, is in good agreement with that of the hydrophone, suggesting comparable frequency-response characteristics.

### 1. Sensitivity

The end-of-cable sensitivity of the membrane hydrophone is 150 mV/MPa at 10 MHz. By direct comparison of the peak positive pressures registered by each device as shown in Figs. 7, the sensitivity of the sensor is 61 mV/MPa. The sensitivity of the photodiode-amplifier combination is 10 mV/ $\mu\text{W}$ , so this value corresponds to a system sensitivity  $dI_0/P$  of 6.1  $\mu\text{W}/\text{MPa}$ . If we take into account that the laser power is 7 mW and the wavelength is 633 nm,  $dI_0/P$  is approximately a factor of 5 lower than the value predicted in Section 3 for normally incident light. The reason for this lower value is most likely due to the signal-canceling effects resulting from the divergent output of the optical fiber, which reduces and limits the phase sensitivity. The Fresnel reflections that fall on the photodiode from the front and the distal cleaved ends of the fiber further exacerbate this problem by adding to the dc level.

### 2. Noise

The noise floor of the membrane hydrophone is very low<sup>21</sup> (less than 0.5 KPa) and in these measurements is dominated by the noise associated with the oscilloscope. It is measured, in this example, over 60 averages at 0.050 mV (0.33 KPa) in a measurement bandwidth of 25 MHz. The corresponding measurement for the sensor, dominated by the photodiode-amplifier-combination noise, over the same measurement bandwidth is 0.14 mV (2.30 KPa). Thus in terms of the signal-noise ratio the sensor output is approximately a factor of 7 lower than the PVDF-membrane hydrophone.

### 3. Frequency Response

We obtained the frequency response by taking the Fourier transform  $B_s(f)$  of the normalized signal in Fig. 8 that was measured with the sensor. The Fourier transform of the corresponding signal as

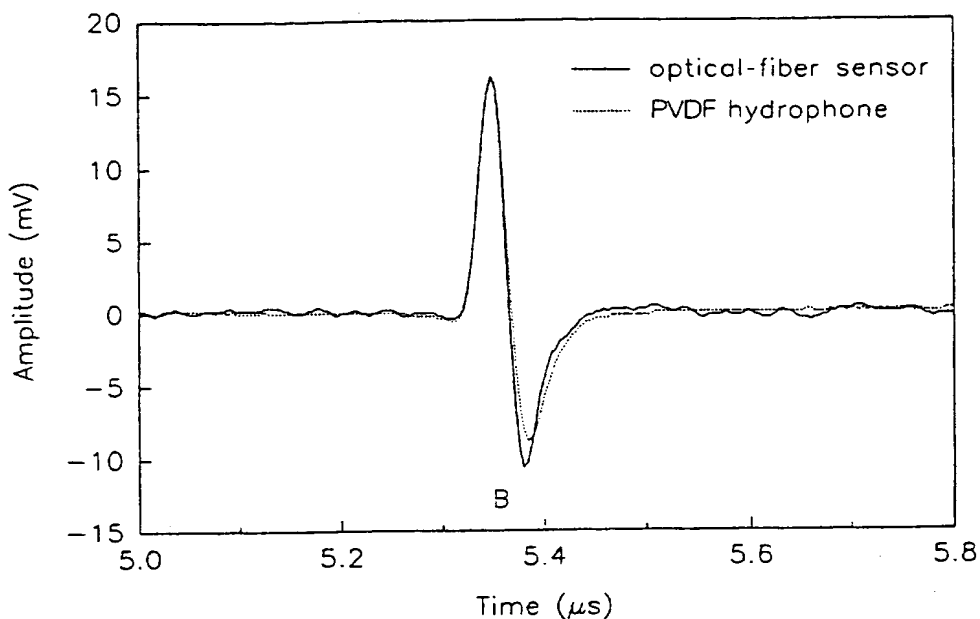


Fig. 8. Expanded view of signal B from Figs. 7 showing the comparison of the normalized optical-fiber sensor output with the PVDF-membrane hydrophone output.

measured with the hydrophone  $B_h(f)$  was then computed, and a correction was applied to take into account the frequency-response characteristics of the hydrophone, giving  $C_h(f)$ , as shown in Fig. 9.  $C_h(f)$  gives the distribution of frequency components arriving at the sensor head. Dividing  $B_s(f)$  by  $C_h(f)$  therefore gives the frequency response of the sensor, as shown in Fig. 10. The theoretical frequency response (given in Section 3) for the 50-μm PET film surrounded by water is also shown, along with the calibrated frequency response of the PVDF-membrane hydrophone. At low frequencies the correlation between theory and experiment is good. The half-wave resonance appears as expected at approxi-

mately 20 MHz, although its magnitude is a factor of 1.4 larger than expected. Although it was not terminated at  $50\ \Omega$ , the length of the coaxial cable (0.6 m) connecting the hybrid photodiode to the oscilloscope should not have produced a resonance close to this frequency. Further investigation showed that it was a peak in the frequency response of the photodiode-amplifier combination that coincided with the 20-MHz acoustic-thickness-mode resonance that was responsible for the apparent enhanced resonance, and, in the time domain, for the increased size of the rarefaction part of the signal as compared with the hydrophone output that is shown in Fig. 8. Careful choice of a detector with a uniform response and a matched electrical load would overcome this problem.

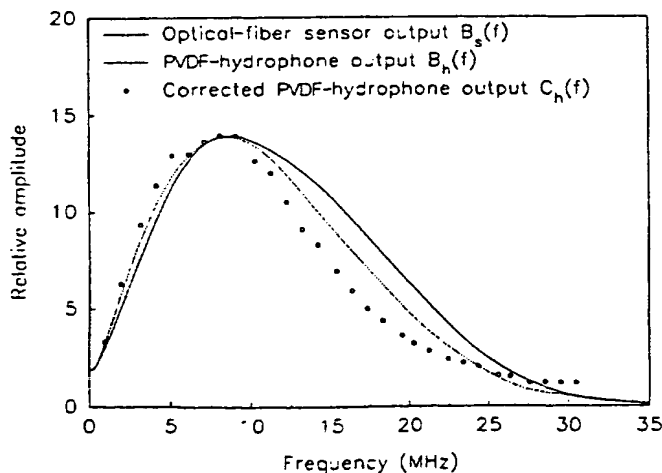


Fig. 9. Acoustic frequency spectra of the signals measured with the optical-fiber sensor and the PVDF-membrane hydrophone shown in Fig. 8.

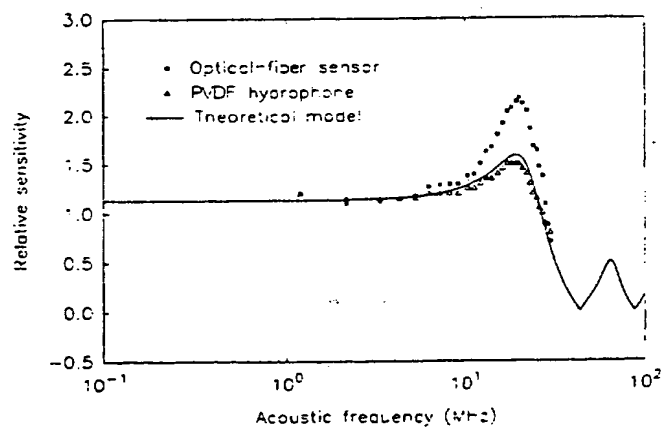


Fig. 10. Comparison of the optical-fiber-sensor frequency response with the theoretical model and the PVDF-membrane-hydrophone frequency-response values.

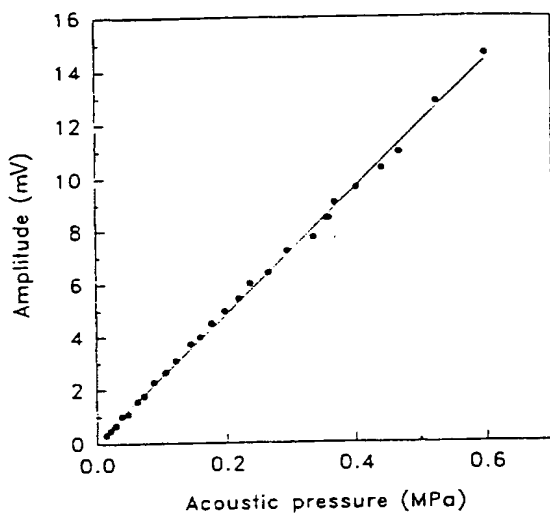


Fig. 11. Optical-fiber sensor output as a function of the acoustic pressure as measured with the PVDF-membrane hydrophone.

#### 4. Linearity

It is assumed that the PVDF-membrane hydrophone is linear to well beyond 0.6 MPa.<sup>21,22</sup> The sensor was placed directly behind the hydrophone, and the positions of both devices adjusted independently until the maximum signal detected by each was observed. Simultaneous readings from the sensor and the hydrophone were taken. This procedure was repeated over a range of acoustic pressures by variation of the energy of the optical pulses incident upon the ink absorber. The results, shown in Fig. 11, show an excellent linearity of response up to 0.5 MPa, limited by the maximum pulse energy of the Q-switched Nd:YAG laser. A dynamic range in excess of 30 dB was obtained. It should be noted that the acoustic pressures shown in Fig. 11 are those measured with the hydrophone. The true acoustic pressure arriving at the sensor head is somewhat lower as a result of the attenuation of the acoustic signal as it passes through the hydrophone.

#### 5. Stability

Adequate short- and long-term stabilities are essential for a practical measurement device. The usual source of sensitivity fluctuations in homodyne interferometric sensors is due to environmentally induced variations in the phase bias, particularly in the case of long-path interferometers. In the scheme presented here the thinness of the polymer film acting as the interferometer means that it is relatively insensitive to external perturbations that are likely to occur in the short term. The sensitivity over a period of 80 h is shown in Fig. 12. The experimental method was the same as that used for the linearity measurements. Figure 12 shows that the sensor is stable, within the uncertainty of the measurement, typically over a period of several hours, and over 80 hours the output does not fluctuate by more than 10%. This stability indicates a low sensitivity to ambient temperature and pressure fluctuations.

Other significant factors that may lead to changes in sensitivity are those influences that act on the optical-fiber download. Vibration produced when the fiber was rapidly and vigorously shaken had virtually no effect on the signal. The signal was, however, observed to decrease when the fiber was bent to a significant degree. Effectively the higher-order modes (which remain unfilled over a short length of the fiber) become filled when the fiber is bent, increasing the angle of divergence of the light emerging from the end of the fiber and thus bringing into effect the signal-canceling effects described in Subsection 3.A.2. This effect was reduced when the modes were scrambled and the input launch conditions adjusted so that all the propagation modes were filled, resulting in a constant angle of divergence. This improvement however is obtained at the expense of phase sensitivity.

#### E. Rigid-Backed Sensing Film

It would be useful to find some way to remove the reflection of the thermoelastic wave (signal R in Figs.

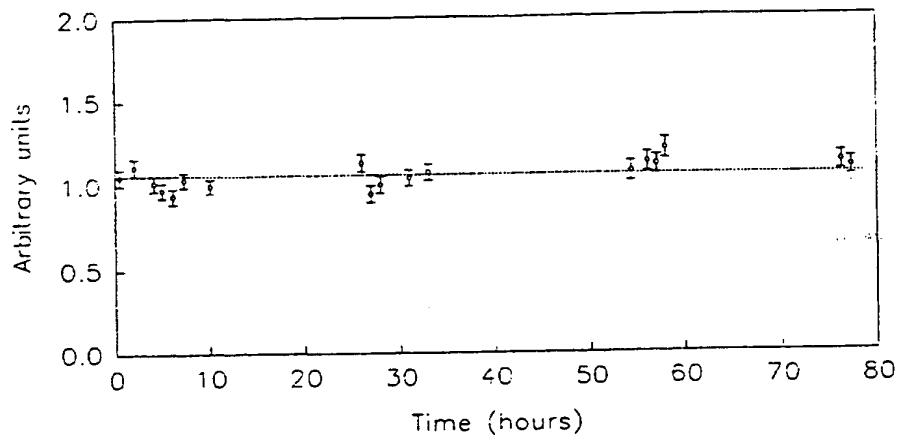


Fig. 12. Variation of optical-fiber sensor output with time.

7) from the tip of the fiber. This reflection may coincide with the arrival of a signal to be detected and can affect the low ( $<1$  MHz) frequency response of the sensor. A rigid backing offers a solution as it gives a high acoustic sensitivity and a uniform, although reduced, frequency response. It could conceivably be achieved by the attachment of a transparent material of relatively high acoustic impedance, such as glass, to the back of the sensing film. This solution, however, would destroy the fringe visibility because the Fresnel reflection coefficient between PET and glass is very low ( $1 \times 10^{-3}$ ). A novel approach has been found to overcome the reduction in fringe visibility if it is ensured that there is a gap between the film and the backing that, in acoustic terms, is of negligible thickness but is large enough to allow a thin layer of water to exist. The water layer maintains the fringe visibility at unity but allows the sensor to be effectively rigid backed. In practice this rigid backing was achieved by the use of the cleaved end of the fused-silica optical fiber as the backing material. The fiber was moved gradually closer toward the sensing film until the thermoelastic waves reflected from the tip of the fiber were superposed onto the initial wave incident on the sensor film. The effect of this superposition is to increase the acoustic sensitivity by a factor of 2, as shown in the theoretical model shown in Fig. 4. This result is verified in Figs. 13, which show the

output of the sensor before and after the fiber is brought close to the sensing film. Some broadening of the second half of the pulse is apparent in Fig. 13(b) because of the reduced frequency response of the rigid-backed configuration.

## 5. Conclusions

An extrinsic optical-fiber sensor has been described and demonstrated, showing that a thin polymer film acting as a Fabry-Perot interferometer can be used for the detection of ultrasound. High sensitivity and a flat, wideband frequency response have been demonstrated to be in good agreement with a theoretical model. The sensor was found to exhibit a performance comparable with that of a PVDF-membrane hydrophone.

It is considered that for practical use two aspects require further attention. First, a tunable laser diode would be needed to set the phase bias to quadrature on start up and to maintain the bias for high stability. Second, reducing the sensitivity to bends in the fiber without lowering the phase sensitivity is required. Reduced bend sensitivity has been demonstrated by the use of mode scrambling, but it reduces the ratio of the phase sensitivity to the dc level. This ratio could be increased if the distal end of the fiber were mode stripped to reduce the angle of divergence. Such a measure would significantly reduce the light emerging from the end of the fiber. A higher laser power would be needed to compensate the reduction in emergent light, or alternatively more efficient use of the light could be made by the application of optically reflective coatings to the two sides of the sensing film.

A particular advantage with this technology is that there are a wide range of optically clear polymer films of varying acoustic properties that could be used as the sensing film. This availability enables the properties of the sensing film to be chosen in accordance with the requirements of a specific application. For example, if a very flat frequency response is required, a polymer that has an acoustic impedance even closer to water than that of PET could be chosen to minimize the thickness resonance. If a high acoustic sensitivity is required, a material with a low Young's modulus can be selected. In addition, because polymer films of the order of a few micrometers thick are readily available, potential bandwidths of several hundred megahertz are possible. Furthermore, because the active area of the sensor is defined by the spot size illuminating the sensing film, very small active diameters (a few tens of micrometers) can be obtained by the use of small-diameter fibers. For example, a 50- $\mu\text{m}$ -diameter fiber could easily be employed, giving an excellent spatial resolution and a low directional sensitivity. This potential for high performance makes it particularly suitable for the measurement of the output of medical ultrasound equipment. For such measurements, an inexpensive sensor is required that gives an accurate temporal and spatial representation of

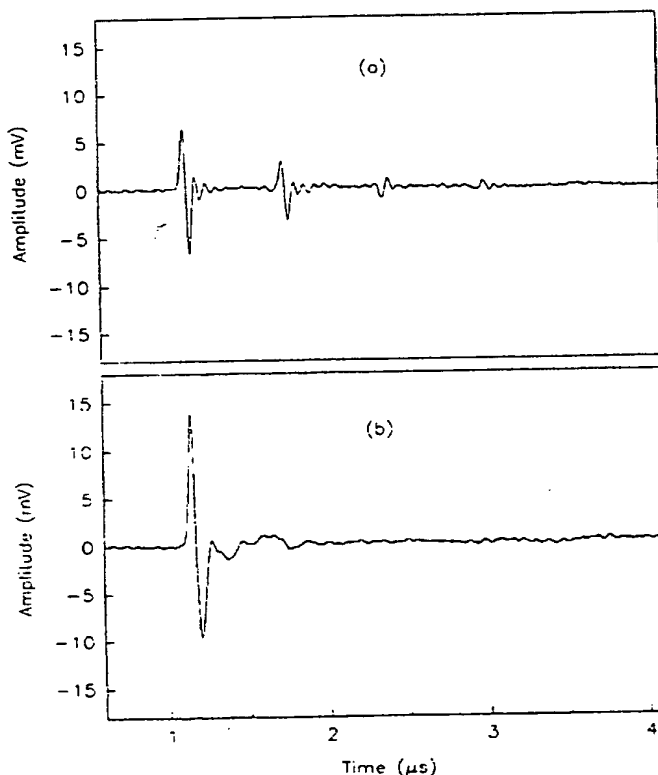


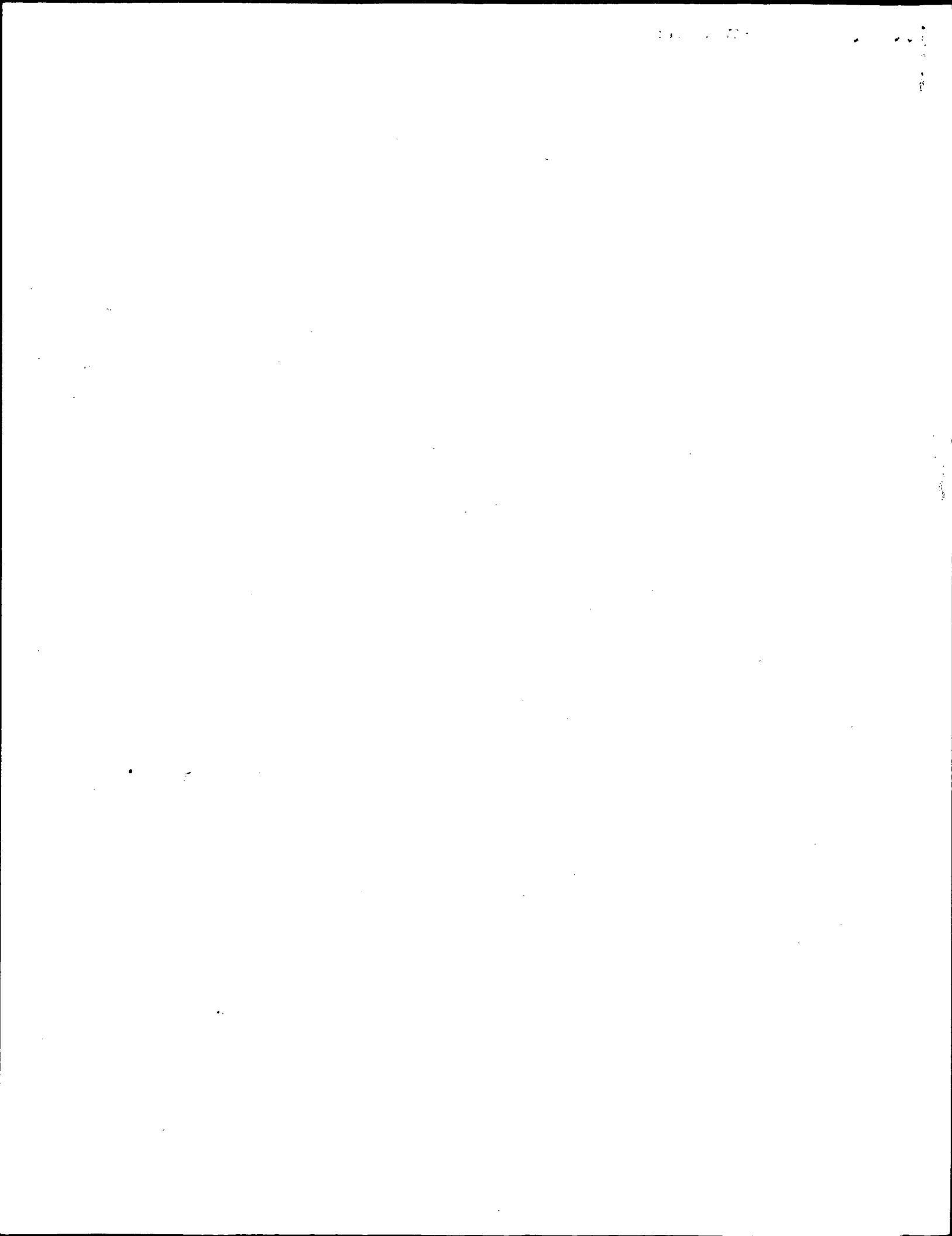
Fig. 13. (a) Water-backed configuration showing multiple reflections between the sensing film and the fiber tip, and (b) superposition of the same reflections in a rigid-backed configuration.

the ultrasound field under measurement. Application may also be found in situations in which high levels of electromagnetic interference preclude the use of conventional piezoelectric devices and limited access requires an inexpensive, miniature, flexible probe.

This work has been supported by the British Heart Foundation and the Medical Research Council.

#### References and Note

1. R. P. De Paula, L. Flax, J. H. Cole, and J. A. Bucaro, "Single mode fiber ultrasonic sensor," *IEEE J. Quantum Electron.* **QE-18**, 680-683 (1982).
2. H. L. W. Chan, K. S. Chiang, D. C. Price, J. L. Gardner, and J. Brinch, "Use of a fiber-optic hydrophone in measuring acoustic parameters of high power hyperthermia transducers," *Phys. Med. Biol.* **34**, 1609-1622 (1989).
3. H. L. W. Chan, K. S. Chiang, D. C. Price, and J. L. Gardner, "The characterisation of high frequency ultrasonic fields using a polarimetric optical fiber sensor," *J. Appl. Phys.* **66**, 1565-1570 (1989).
4. K. S. Chiang, H. L. W. Chan, and J. L. Gardner, "Detection of high frequency ultrasound with a polarisation maintaining fiber," *J. Lightwave Technol.* **8**, 1221-1227 (1990).
5. L. Liu and R. M. Measures, "Detection of high-frequency elastic waves with embedded ordinary single mode fibers," in *Fiber Optics and Laser Sensors IX*, R. P. De Paula and E. Udd, eds., *Proc. Soc. Photo-Opt. Instrum. Eng.* **1584**, 226-232 (1991).
6. N. Narendram, C. Zhou, S. Letcher, and A. Shukla, "Fiber-optic acoustic sensor for nondestructive evaluation," *Opt. Lasers Eng.* **22**, 137-148 (1995).
7. R. P. De Paula, J. H. Cole, and J. A. Bucaro, "Broad-band ultrasonic sensor based on induced optical phase shifts in single mode fibers," *J. Lightwave Technol.* **LT-1**, 390-393 (1983).
8. N. Lagakos, A. Dandridge, J. H. Cole, A. B. Tveten, and J. A. Bucaro, "Ultrasonic acoustic sensing," in *Automotive Displays and Industrial Illumination*, B. Chang and T. M. Lemons, eds., *Proc. Soc. Photo-Opt. Instrum. Eng.* **798**, 94-101 (1987).
9. J. J. Alcoz, C. E. Lee, and H. F. Taylor, "Embedded fiber-optic Fabry-Perot ultrasound sensor," *IEEE Trans. Ultrason. Ferroelectr. Freq. Control* **37**, 302-305 (1990).
10. S. Knudsen and K. Blotekjae, "An ultrasonic fiber-optic hydrophone incorporating a push-pull Sagnac interferometer," *J. Lightwave Technol.* **12**, 1696-1700 (1994).
11. D. A. Jackson, R. Priest, A. Dandridge, and A. B. Tveten, "Elimination of drift in a single-mode optical fiber interferometer using a piezoelectrically stretched coiled fiber," *Appl. Opt.* **19**, 2926-2929 (1980).
12. See, for example, D. W. Stowe, D. R. Moore, and R. G. Priest, "Polarization fading in fiber interferometric sensors," *IEEE J. Quantum Electron.* **QE-18**, p. 1644 (1982).
13. T. A. Tran, W. V. Miller, K. A. Murphy, M. Vengsarkar, and R. O. Claus, "Stabilized extrinsic fiber-optic Fizeau sensor for surface acoustic wave detection," *J. Lightwave Technol.* **10**, 1499-1505 (1992).
14. D. P. Hand, S. Freeborn, P. Hodgson, T. A. Carolan, K. M. Quan, H. A. Mackenzie, and J. D. C. Jones, "Optical-fiber interferometry for photoacoustic spectroscopy in liquids," *Opt. Lett.* **20**, 213-215 (1995).
15. D. R. Bacon, "Primary calibration of ultrasonic hydrophones using optical interferometry," *IEEE Trans. Ultrason. Ferroelectr. Freq. Control* **35**, 152-161 (1988).
16. B. A. Williams and R. J. Dewhurst, "Differential fiber-optic sensing of laser generated ultrasound," *Electron. Lett.* **31**, 391-392 (1995).
17. Y. Wu, P. M. Shankar, P. A. Lewin, and D. P. Koller, "Fiber optic ultrasonic sensor using Raman-Nath light diffraction," *IEEE Trans. Ultrason. Ferroelectr. Freq. Control* **41**, 166-171 (1994).
18. B. Granz, R. Holzapfel, and G. Kohler, "Measurement of shockwaves in the focus of a lithotripter," *Proc. IEEE* **991-994** (1989).
19. P. C. Beard and T. N. Mills, "An optical fiber sensor for the detection of laser generated ultrasound in arterial tissues," in *Medical Sensors II and Fiber Optic Sensors*, A. V. Scheggi, F. Baldini, P. R. Coulet, and O. S. Wolfbeis, eds., *Proc. Soc. Photo-Opt. Instrum. Eng.* **2331**, 112-122 (1994).
20. P. C. Beard and T. N. Mills, "Evaluation of an optical fiber probe for in vivo measurement of the photoacoustic response of tissues," in *Advances in Fluorescence Sensing Technology II*, J. R. Lakowicz, eds., *Proc. Soc. Photo-Opt. Instrum. Eng.* **2388**, 446-457 (1995).
21. R. C. Preston, D. R. Bacon, A. J. Livett, and K. Rajendran, "PVDF membrane hydrophone performance properties and their relevance to the measurement of the acoustic output of medical ultrasound equipment," *J. Phys. E* **16**, 786-796 (1983).
22. P. A. Lewin, "Practical implementations and technology of measurement devices," in *Ultrasonic Exposimetry*, M. C. Ziskin and P. A. Lewin, eds. (CRC Press, Boca Raton, Fla., 1993), Chap. 7, pp. 195.



**Measurements:** The output from detector 1 using cyanoacrylate glue is shown in Fig. 3. Both linear (upper) and logarithmic (lower) time scales are shown. The detected signal evolves through six cycles ( $12\pi$ ) before it stabilises, i.e. before the glue is completely cured. The output from detector 2 shows a similar response (not shown), shifted in phase with respect to detector 1. By dissolving the cyanoacrylate with a few drops of dimethyl formamide, the reverse response could be observed with a duration of a few minutes.

The output from detector 1 using epoxy glue is shown in Fig. 4. The spike in the curve is due to a manual interrogation to ensure that the sensor was well adjusted. No induced birefringence could be measured during the full curing time of the epoxy.

**Discussion:** The measurements in Fig. 3 indicate that the cyanoacrylate glue induces birefringence in optical fibres when used for surface mounting as in Fig. 1. The birefringence is caused by stresses in the fibre core induced during the curing process, with a direction equivalent to that resulting from loading a weight on top of the fibre. The induced birefringence in the fibre is given by the difference in optical path length for the polarisations parallel ( $n_1$ ) and perpendicular ( $n_2$ ) to the plate:

$$\frac{2\pi L}{\lambda} (n_1 - n_2) = 12\pi \quad (1)$$

The birefringence is found to be  $B = n_1 - n_2 = 3.6 \times 10^{-3}$ . For comparison, the equivalent weight needed to induce the same birefringence may be found using the following formula [7]:

$$B = 4C \frac{f}{\pi r E} \quad (2)$$

where  $f$  is the force per unit length (N/m),  $r = 62.5 \mu\text{m}$  is the outer radius of the fibre, and  $E = 7.6 \times 10^{10} \text{ N/m}^2$  is Young's modulus for fused silica. The constant  $C$  is given as  $C = 0.5 \times n_o^3 (p_{12} - p_{11})(1 + v_r)$ , where  $n_o = 1.46$  is the average refractive index of the fibre,  $p_{11} = 0.113$  and  $p_{12} = 0.252$  are the components of the strain-optical tensor of the fibre material [8], and  $v_r = 0.17$  is the Poisson ratio for the fibre. Taking the measured value of  $B = 3.6 \times 10^{-3}$  and inserting numbers into eqn. 2 yields the force needed over 13 cm to produce the same birefringence as gluing with cyanoacrylate as  $F = f \times L = 69 \text{ N}$ . Thus, the cyanoacrylate glue induces a stress in the fibre core equivalent to applying a weight of 7kg on top of the 13cm fibre. This was confirmed experimentally by squeezing the fibre between two glass plates. The required weight to induce a polarimeter readout of  $12\pi$  was 7.8kg.

There are two reasons for the large difference between the cyanoacrylate and the epoxy. First, the cyanoacrylate shrinks more during the curing process than the epoxy; secondly, by inspection of Fig. 1, it is evident that any shrinking of the thin layer of cyanoacrylate glue will produce an anisotropic stress in the fibre. For the epoxy, the stresses will affect the fibre more uniformly due to the larger volume of epoxy surrounding the fibre. No attempt to distinguish between the two effects has been made.

For a polarimetric sensor consisting of a birefringent fibre, the added birefringence is unwanted. The glue induced birefringence will be superimposed on the internal birefringence of the fibre, which, for example, for bow-tie fibres has axes with arbitrary orientations with respect to the surface. The net sensor response will therefore be disturbed in an unpredictable manner.

For a Bragg grating, the induced birefringence will cause the reflected spectrum for the two polarisations to split. The shift between the two centre wavelengths for the two polarisations for a 1550 nm grating will be given by  $\Delta\lambda_s = 2(n_1 - n_2) \Lambda \approx 38 \text{ pm}$ . For a Bragg grating used as a strain sensor the typical strain-wavelength conversion factor is  $1.2 \text{ pm}/\mu\epsilon$  at 1550nm [1]. The cyanoacrylate thus causes an increased uncertainty in strain measurements of  $32 \mu\epsilon$ , which for many applications is unacceptable. Polarisation splitting of Bragg gratings glued using cyanoacrylate of this order and larger has been observed by the authors. In [9], a polarisation splitting of 60pm for a surface mounted Bragg grating using cyanoacrylate glue was reported. Here, the grating was mounted in a v-groove, which further enhances the glue induced stresses.

**Conclusions:** The birefringence introduced by two commonly used glues for surface mounting optical fibres was investigated. Cyanoacrylate glue was found to induce a birefringence in a standard singlemode optical fibre of  $3.6 \times 10^{-3}$ , which for many

sensor applications is unacceptable. A thick layer of epoxy glue induced no measurable birefringence. Hence, if an application requires low fibre birefringence, epoxy is a better choice than cyanoacrylate. Further, for measurements involving cyanoacrylate, the curing time for most commercially available glues is 24h or more.

© IEE 1997  
Electronics Letters Online No: 19970528

13 February 1997

H. Storøy (Faculty of Electrical Engineering and Computer Science, Norwegian University of Science and Technology, N-7034 Trondheim, Norway)

K. Johannessen (SINTEF Department of Electronics and Cybernetics, N-7034 Trondheim, Norway)

## References

- 1 MOREY, W.W., MELTZ, G., and GLENN, W.H.: 'Fibre optic Bragg grating sensors'. Proc. SPIE-Int. Soc. Opt. Eng., 1990, Vol. 1169, pp. 98-107
- 2 RASHLEIGH, S.C.: 'Polarimetric sensors: Exploiting the axial stress in high birefringence fibres'. Presented at First Int. Conf. optical fibre sensors, London, UK, 1983, Paper 4.1
- 3 MOREY, W.W., BALL, G.A., and SINGH, H.: 'Applications of fiber grating sensors'. Proc. SPIE-Int. Soc. Opt. Eng., 1996, 2839, pp. 2-7
- 4 HOGG, W.D., TURNER, R.D., and MEASURES, R.M.: 'Polarimetric fibre optic structural strain sensor characterisation'. Proc. SPIE-Int. Soc. Opt. Eng., 1989, 1170, pp. 542-549
- 5 NIELSEN, P.L.: 'Investigation of optical fibers as sensors for condition monitoring of composite materials'. Proc. SPIE-Int. Soc. Opt. Eng., 1991, 1588, pp. 229-240
- 6 SIRKIS, J.S., and HASLACH, H.W., Jr.: 'Interferometric strain measurement by arbitrarily configured, surface-mounted, optical fibers'. *J. Lightwave Technol.*, 1990, 8, pp. 1497-1503
- 7 RASHLEIGH, S.C.: 'Origins and control of polarisation effects in single-mode fibers'. *J. Lightwave Technol.*, 1983, 1, pp. 312-331
- 8 BERTHOLDS, A., and DÄNDLAKER, R.: 'Determination of the individual strain-optic coefficients in single-mode optical fibers'. *J. Lightwave Technol.*, 1983, 1, pp. 312-331

(PCT.202) 8030 Electronics Letters  
33(1997) 24 April, No. 9, Stevenage, Herts, GB

XP 000695342

## Miniature optical fibre ultrasonic hydrophone using a Fabry-Perot polymer film interferometer

P.C. Beard and T.N. Mills

P d. 24-04-1997

Indexing terms: Fibre optic sensors, Light interferometers, Hydrophones

An optical fibre hydrophone for the measurement and detection of ultrasound is described. The active sensing element consists of a low finesse Fabry-Perot polymer film interferometer bonded to the tip of an optical fibre, of 50μm core diameter and 0.25mm outer diameter. Sensitivity was found to be 114mV/MPa with an acoustic noise floor of 15kPa over a 25MHz bandwidth.

**Introduction:** Ultrasonic hydrophones such as those based on piezoelectric PVDF sensing elements are widely used for characterising ultrasound fields [1]. There can, however, be problems associated with the electrical nature of piezoelectric devices, including sensitivity to EMI and cable loading and resonance effects due to the connecting cable. Fragility, expense and the difficulties involved in fabricating small (<100μm) active element diameters for low directional sensitivity whilst retaining adequate acoustic sensitivity can also present limitations. We describe a miniature optical fibre hydrophone which, by its electrically passive nature, small active diameter and simplicity of fabrication, has the potential to overcome these disadvantages. The acoustically active element comprises a thin polymer film (~50μm) acting as a

low finesse Fabry-Perot interferometer [2] mounted at the tip of an optical fibre. An incident acoustic wave modulates the thickness of the film and hence the optical phase difference between the laser light reflected from the two sides of the film. This produces a corresponding intensity modulation of the light reflected from the film. For optimum sensitivity and linearity, the interferometer should be operated at a phase bias that corresponds to quadrature. An advantage of using a polymer film as an extrinsic interferometric acoustic sensing element, rather than the fibre itself [3, 4], is that the low Young's modulus of polymers enables high acoustic sensitivity to be achieved, even when using a sensing film of only a few tens of micrometres thick to obtain a wideband acoustic response at megahertz frequencies.

Theoretical and experimental aspects of this type of optical fibre ultrasound sensor have previously been reported using a large (12 mm) diameter sensor head containing a transparent water-backed sensing film [5]. In this Letter, a miniature (0.25mm) rigid-backed configuration in which the sensing film is bonded directly to the end of the optical fibre is described.

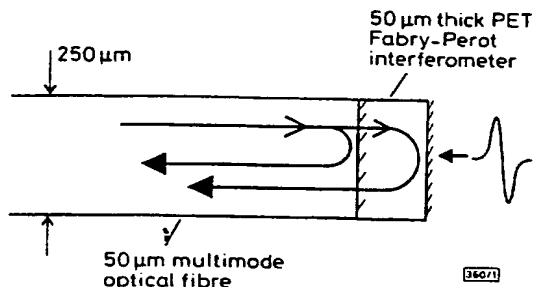


Fig. 1 Sensor head

**Experiment:** The sensor head used is shown schematically in Fig. 1. The optical fibre used was a 50 $\mu\text{m}$  core all-silica multimode fibre of numerical aperture 0.1 and outer diameter 0.25mm. The Fabry-Perot polymer sensing film bonded to the cleaved end of the fibre comprised a 0.25mm diameter disk of 50 $\mu\text{m}$  thick PET (polyethylene terephthalate) with a 40% optically reflective aluminium coating on one side and a 100% reflective coating on the other; the two coatings form the mirrors of the interferometer. The sensing film was interrogated using 633nm light from a 7mW He Ne laser and the reflected intensity modulation was transmitted back along the fibre for detection at a 25MHz photodiode with an integral transimpedance amplifier. In the absence of a tunable laser source, operation close to quadrature was obtained by a process of trial and error. A number of optical fibre hydrophones were fabricated using sections of PET sensing film cut from different parts of the same sheet. The slight variations in thickness over the area of the polymer film sheet produced a range of different phase biases and hence sensitivities. The optical fibre hydrophone that gave the highest sensitivity was assumed to have a thickness that resulted in a phase bias close to quadrature, and was used for these experiments. The short path length of the polymer film interferometer (100 $\mu\text{m}$ ) means that, once set at quadrature, the sensor is inherently insensitive to environmental thermal and pressure fluctuations giving good stability [5].

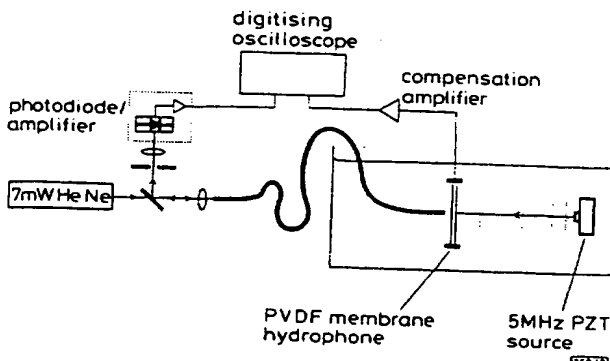


Fig. 2 Experimental arrangement

The optical fibre hydrophone was inserted into a water tank and positioned directly behind the active region of a calibrated, 50 $\mu\text{m}$  thick, 25MHz bilaminar PVDF membrane reference hydrophone of active diameter of 0.5mm (Fig. 2). A compensation amplifier was used to correct for any small variations in the frequency response of the membrane hydrophone, ensuring a uniform response (to within 1dB) up to 20MHz. Since this type of hydrophone provides minimum perturbation to the acoustic field under measurement, it was assumed not to affect the measurement of the optical fibre hydrophone. A pulsed 5MHz PZT transducer of 13mm diameter was used as the ultrasound source. The separation between the source and hydrophone was ~6cm. A 500MHz digitising oscilloscope was used to capture the waveforms from each device.

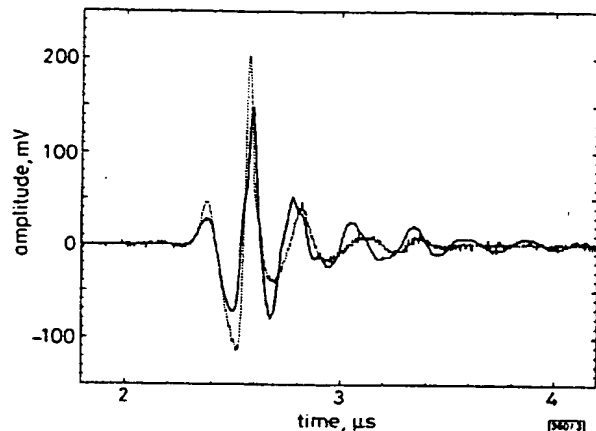


Fig. 3 Comparison between optical fibre hydrophone output and PVDF membrane hydrophone output in response to 1.3 MPa acoustic signal  
 — optical fibre hydrophone output  
 - - - PVDF membrane hydrophone output

**Results:** A comparison between the output of the optical fibre hydrophone and the PVDF membrane hydrophone system is shown in Fig. 3. The sensitivity of the optical fibre hydrophone is 114mV/MPa with an acoustic noise floor of < 15kPa over a 25MHz bandwidth. The corresponding sensitivity and acoustic noise floor of the PVDF membrane hydrophone system is 155mV/MPa and 40kPa, respectively. The sensitivity of the optical fibre hydrophone is almost a factor of 2 higher than that previously reported using a water-backed polymer sensing film [5]. This is because the rigid-backed configuration shown in Fig. 1 produces a higher acoustically-induced strain in the polymer film.

The temporal profiles of the two waveforms shown in Fig. 3 are in good agreement for the first two cycles of the signals. Thereafter, the signals begin to differ in relative amplitude and phase, indicating a non-uniformity in the frequency response of the optical fibre hydrophone. There are several possible reasons for this. (i) the thickness of the optical adhesive used to attach the sensing film to the tip of the fibre is sufficiently large that acoustic reflections from the cleaved end of the fibre are significantly time-delayed; (ii) the sensor is not operating solely in thickness mode and acoustic energy is being coupled into the radial direction causing radial resonance modes to be excited; (iii) diffraction around the tip of the fibre may also be responsible. Additionally, the discrepancy may be due to spatial variations in the acoustic field, the effect of which is related to the differing degrees of spatial integration produced by each device due to their large differences in active diameters.

A measure of the directional response of the optical fibre hydrophone was obtained by altering the angle of the optical fibre to the incident acoustic field and computing the FFT of the output waveforms for three angles. The amplitude component at the 5MHz transducer centre frequency fell by a factor of 1.8 when the fibre was orientated at 45° to the incident field and by a factor of 3.3 at 90°. Despite the large angular increments, this indicates that the optical fibre hydrophone has a sufficient degree of omnidirectionality to provide a useful output even when aligned orthogonally to the acoustic field. Its relatively low directional sensitivity is a consequence of its small active area which, to a first approximation, is defined by the 50 $\mu\text{m}$  diameter of the optical fibre output incident on the sensing film.

**Conclusion:** A miniature ultrasonic optical fibre hydrophone of small active area that has a sensitivity which is comparable to piezoelectric devices has been demonstrated. The frequency response of the system requires further investigation to determine whether the differences in the temporal output between the PVDF membrane hydrophone and the optical hydrophone are due to the experimental setup or are inherent in the design of latter. For practical use a tunable laser diode could be used to obtain quadrature on 'start-up' and maintain it thereafter. It is envisaged that this system has the potential for use in characterising the output of ultrasonic transducers and as a general purpose tool for the measurement and detection of ultrasound. A particular application is the *in vivo* safety-related exposure measurements of the output of diagnostic and therapeutic medical ultrasound equipment. Such an application would benefit from the small physical size, omnidirectionality, and electrical passivity that this technology has the potential to offer.

**Acknowledgements:** The authors would like to thank F. Duck of the Royal United Hospital Bath for his help in making the measurements described above and A. Coleman of St Thomas's Hospital, London for his assistance throughout this project. This work was originally funded by the MRC and is currently supported under the DTI/EPSCC LINK Photonics scheme in collaboration with Precision Acoustics Ltd, Dorchester, Dorset.

© IEE 1997

*Electronics Letters Online No: 19970545*

20 February 1997

P.C. Beard and T.N. Mills (University College London, Department of Medical Physics and Bioengineering, Shropshire House, 11-20 Capper Street, London WC1E 6JA, United Kingdom)

## References

- LEWIN, P.A.: 'Practical implementations and technology of measurement devices', in ZISKIN, M.C., and LEWIN, P.A. (Eds.): 'Ultrasonic exposimetry' (CRC Press, Boca Raton, USA, 1993), Chap. 7, pp. 189-197
- BEARD, P.C., and MILLS, T.N.: 'An optical fibre sensor for the detection of laser generated ultrasound in arterial tissues', *Proc. SPIE - Int. Soc. Opt. Eng.*, 1994, 2331, pp. 112-122
- ALCOZ, J.J., LEE, C.E., and TAYLOR, H.F.: 'Embedded fibre-optic Fabry-Perot ultrasound sensor', *IEEE Trans. Ultrason., Ferroelectr., Freq. Control*, 1990, 37, (4), pp. 302-305
- DORIGHI, J.F., KRISHNASWAMY, S., and ACHENBACH, J.D.: 'Stabilisation of an embedded fibre optic Fabry-Perot sensor for ultrasound detection', *IEEE Trans. Ultrason., Ferroelectr., Freq. Control*, 1995, 42, (5), pp. 820-824
- BEARD, P.C., and MILLS, T.N.: 'Extrinsic optical fibre ultrasound sensor using a thin polymer film as a low finesse Fabry-Perot interferometer', *Appl. Opt.*, 1996, 35, (4), pp. 663-675

## Optical add/drop multiplexer based on UV-written Bragg grating in a fused 100% coupler

F. Bakhti, P. Sansonetti, C. Sinet, L. Gasca, L. Martineau, S. Lacroix, X. Daxhelet and F. Gonthier

**Indexing terms:** Gratings in fibres, Optical couplers, Multiplexing

The authors report the first realisation of a simple and stable optical add/drop multiplexer based on a UV-written Bragg grating in the coupling region of a fused 100% coupler. Add/drop functions are demonstrated with a low insertion loss (<1dB).

**Introduction:** The photosensitivity occurring in germanium-doped silica under UV irradiation [1] allows the direct and simple realisation of grating filters in optical fibres, with low insertion loss and the potential for low cost. Among them the optical add/drop multiplexer (OADM) is a key component for future WDM networks. A solution based on gratings in a fibre Mach-Zehnder has been demonstrated [2-4]. However, these structures require several

UV-writing steps to properly balance the gratings and the phases in both arms. Other designs have been proposed based on grating writing in the coupling region [5, 6] of polished fibre couplers, but they do not represent a satisfactory solution to producing compact, stable, and low cost components.

We propose here a breakthrough in OADM technology. Using fused coupler technology, an OADM is developed which is based on a 100% coupler (launched light entirely exits in crossed ports) where a strong grating is UV-written in the coupling region. This novel lowloss component offers simple implementation, a compact device, as well as stable operation, since it is based on the interference between two modes in the same guiding region, compared to the Mach-Zehnder configuration where the two arms are separated.

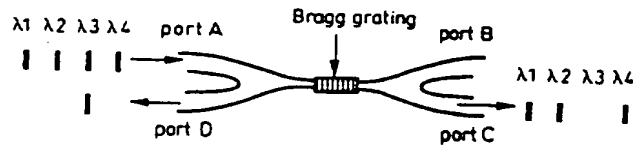


Fig. 1 Schematic diagram of OADM based on Bragg grating in fused 100% coupler

**Principle of operation:** A grating is UV-written in the middle of the coupling region of a 100% coupler (Fig. 1). Light launched in port A is dropped in port D when reflected by the grating, while it exits at port C if it is not.

**OADM implementation:** Because of the diameter reduction in the coupling region, the grating coupling efficiency is small when standard singlemode fibre is used. We thus fabricated a special fibre with an index profile close to that of standard fibre, but designed with a portion of the cladding made highly photosensitive, but still with a matched cladding configuration, for efficient coupling. 100% lossless couplers could then be manufactured [7] taking into account the lower softening temperature of this fibre, as well as dopant diffusion.

Extinction between the output ports of up to 25dB could be obtained. Couplers were then hydrogen soaked at 150 bar and ambient temperature for 3 days, the time necessary for hydrogen to diffuse into the whole coupling region.

Bragg gratings were then written in the coupling region of the fused couplers, using an excimer pumped dye laser with fluence 80mJ/cm<sup>2</sup>/pulse.

**Experimental results:** Resulting performances were measured using a tunable laser launched either in port A to study the drop properties, or in port B for the add properties. Two devices are reported.

A flat-top drop filter with a 1dB insertion loss, measured by cutback techniques, and 20dB transmitted channel extinction at the Bragg wavelength was achieved, resulting from a 8mm long grating written on one side of the coupling region of a 100% coupler (Fig. 2). This filter was not phase matched for the add function, but the result highlights the potential for high extinction bandpass filters, with a stable configuration.

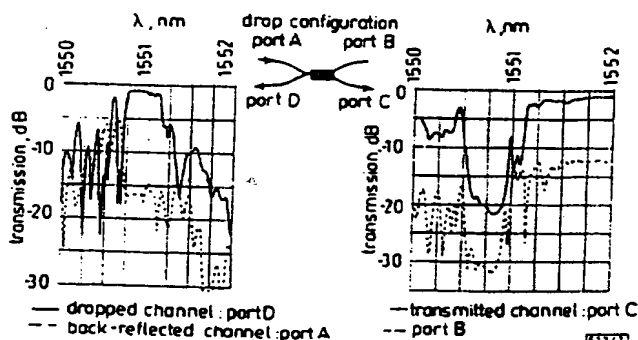
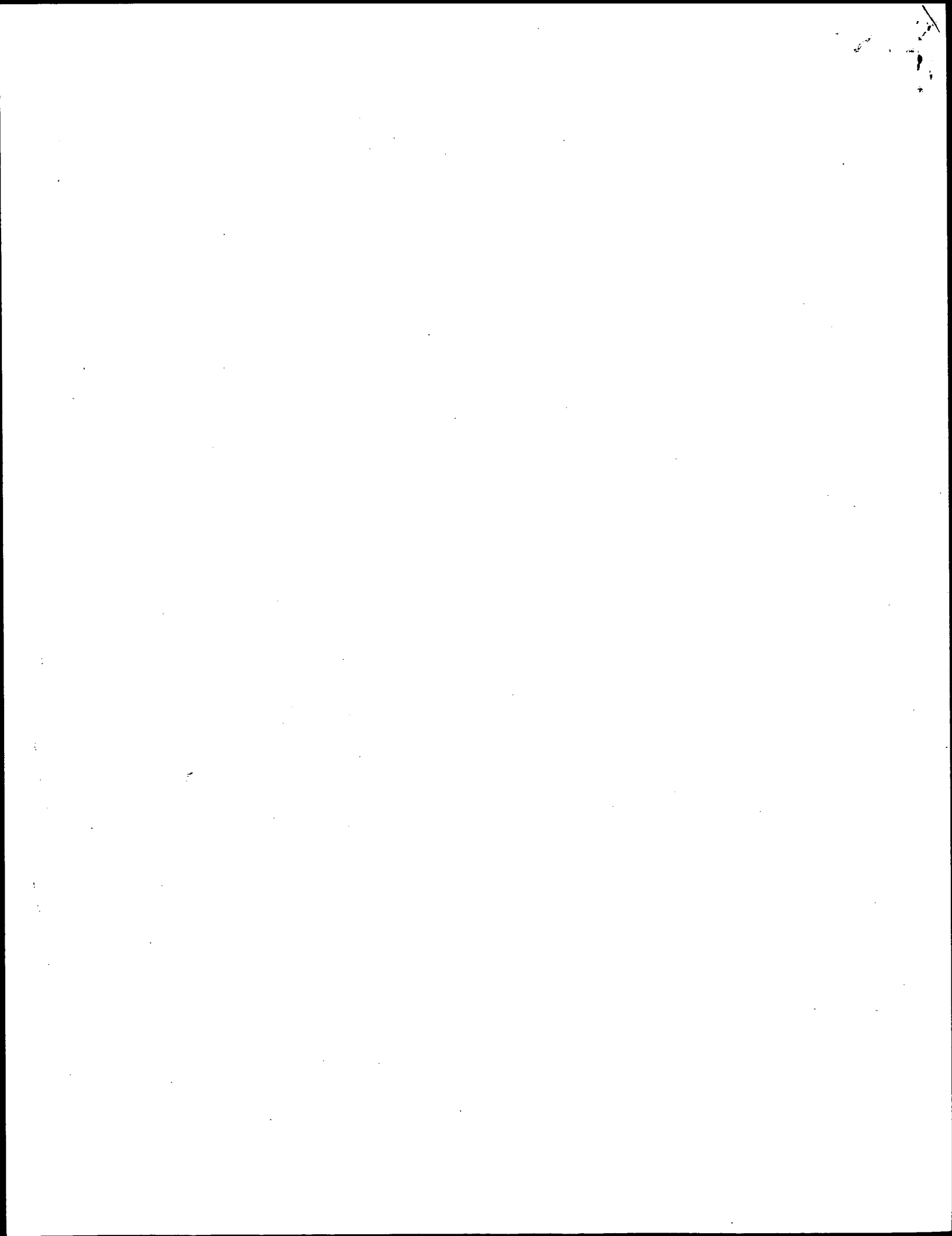


Fig. 2 Flat-top drop filter achieved by UV-writing 8 mm long grating in coupling region of 100% coupler

1dB insertion loss, 20dB extinction in transmitted channel C, 0.4nm - 1dB dropped bandwidth were obtained





## Fiber-optic multilayer hydrophone for ultrasonic measurement

V. Wilkens \*, Ch. Koch

Lab. 1.43, Physikalisch-Technische Bundesanstalt, PF 3345, D-38023 Braunschweig, Germany

Received 2 June 1998

---

### Abstract

An ultrasonic hydrophone is presented that comprises a fiber tip coated with a dielectric multilayer system. Two different layer designs are investigated with respect to their suitability for sensing and their reflectance slope which determines the sensitivity. The more advantageous Fabry–Perot stack was experimentally implemented, and first successful measurements are described. Low-intensity signals are detected with a high signal-to-noise ratio. The sensor can be used for acoustic pressure measurement with high temporal and spatial resolution in a wide power range. © 1999 Elsevier Science B.V. All rights reserved.

**Keywords:** Fiber-optic sensors; Ultrasonic pressure measurement; Multilayer interference filter

---

### 1. Introduction

Fiber tip sensors have proved to be useful for the detection of ultrasonic signals in fluids. In principle, they permit a high temporal and spatial resolution, and the measurement is not disturbed by electromagnetic influences. One possible method consists of using the cut end of a fiber placed in the acoustic field as a sensing element [1]. An incident pressure wave modulates the refractive index of the fluid in front of the fiber tip. The resulting variation of the optical reflectance of the interface between fiber and fluid can be measured by a simple optical detection system. This method offers a rather low sensitivity, which is, however, sufficient for the measurement of high-pressure fields as shock waves if high-power light sources are applied. The performance of the sensor can be improved by introducing optical interference processes, for instance by using a polymer film at the fiber tip as a low-finesse Fabry–Perot microinterferometer [2]. Another possibility is the use of evaporated dielectric multilayer coatings [3]. The advantages of such a dielectric layer or layer system are the small sensor thickness, which allows high acoustic frequencies to be detected, and the simple manufacturing process employing standard evaporation techniques. Hard coatings are obtained that withstand even high-energy pulses. In contrast to other optical arrangements for ultrasonic

measurement, in which the end face of the fiber forms the mirror in one arm of a Michelson interferometer [4,5], the reflectance detection setup requires much less optical and technical effort to obtain the acoustic pressure signal.

The simplest version of a fiber-optic hydrophone with dielectric coating consisting of only one high-index quarter-wave layer was already employed for shock wave measurements [3]. In this paper, the use of multilayer coatings is considered, that take advantage of multipass interference effects for detecting low-intensity ultrasonic signals with high signal-to-noise ratio. Two different layer systems are theoretically investigated: the mirror design and the Fabry–Perot or interference filter design. Since the latter provides higher sensitivity, it was experimentally realized and the performance was successfully tested in first measurements of ultrasonic pulses with the multilayer hydrophone.

### 2. Principle of operation and sensor design

Ultrasonic pressure measurement using the multilayer hydrophone is based on the elastic deformation of the layer system by an incident acoustic wave and the detection of the induced change in optical reflectance. A system of  $N$  non-absorbing layers on a fiber tip and assume normal incidence of the light with intensity  $I_{in}$  from the side of the fiber (Fig. 1) is considered. Polarization effects may be negligible. The reflected light

\* Corresponding author. Tel.: +49 531 592 1423; fax: +49 531 592 1015; e-mail: volker.wilkens@ptb.de

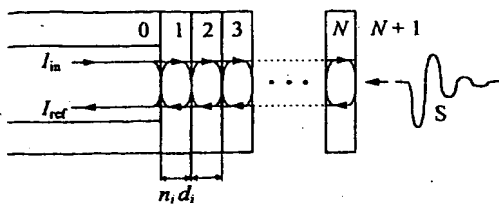


Fig. 1. Design of the fiber-optic multilayer hydrophone; 0: fiber tip, 1,..., N: dielectric layers, N+1: fluid, S: acoustic pressure signal.

intensity  $I_{\text{ref}}$  results from the interference of all reflected fields including multiple reflections. The intensity reflectance  $R$  of the multilayer system, defined by  $R = I_{\text{ref}}/I_{\text{in}}$ , is determined by the physical thicknesses  $d_i$  and the refractive indices  $n_i$  of all individual layers ( $i = 1, \dots, N$ ), the indices of the fiber  $n_0$  and the fluid  $n_{N+1}$  and the free-space optical wavelength  $\lambda$ . Three processes lead to a significant change in reflectance  $\Delta R$  of the multilayer sensor responding to a variation of the acoustic pressure  $\Delta p_i$  in the  $i$ th medium: the change in layer thicknesses ( $i = 1, \dots, N$ ) [3]

$$\Delta d_i = -\frac{\Delta p_i}{\rho_i v_i} d_i \quad (1)$$

the variation of the refractive indices of the layers and the fiber  $\Delta n_i$  ( $i = 0, 1, \dots, N$ ) [3,7]

$$\Delta n_i \approx \frac{0.3 \Delta p_i}{\rho_i v_i^2} \quad (2)$$

and the modulation of the refractive index of the fluid in front of the sensor [1]

$$\Delta n_{N+1} \approx 1.4 \times 10^{-4} \Delta p_{N+1} [\text{MPa}] \quad (3)$$

where  $\rho_i$  and  $v_i$  denote the density and the sound velocity of the  $i$ th medium. The dependence of the reflectance on the pressure signal can be assumed to be linear for a given layer design, since the variation of layer thicknesses is small compared with the optical wavelength in most practical cases.

To detect low-intensity ultrasonic signals with a high signal-to-noise ratio, a large reflectance slope

$$|D| = |\Delta R/\Delta p|$$

is necessary. This can basically be achieved by large layer thicknesses, because a thicker layer is deformed by the same pressure  $\Delta p$  to a larger amount  $\Delta d$  relative to  $\lambda$  (Eq. (1)), resulting in a larger change in the phases of the interfering optical waves. However, the overall thickness of the sensor must be small compared with the acoustic wavelength in the sensor to avoid the signal to be measured being blurred. Since the sensor should provide a large detection bandwidth, layer systems combining a small overall thickness with a high value of  $|D|$  are of interest. In the following, two different layer designs are investigated with respect to their maximum

### reflectance slope

$$D_{\max} = \max_{nd} \left\{ |\Delta R/\Delta p| \right\}.$$

There are two different methods to evaluate a multi-layer system and to determine the reflectance  $R$ : the matrix formalism and the recursion method [6]. In our calculations the second method is applied, which is easy to implement because of the successive character. In the first step the complex Fresnel coefficients of the two-interface system formed by the front and rear side of the first layer ( $i=1$ ) are calculated, taking all multiple reflections into account. Then this two-interface system can be considered as one interface described by two complex reflectivity and transmission coefficients, and in the next step this interface is analyzed together with the interface between the second and the third layer. This procedure is repeated until the whole layer system is evaluated [3].

The first design considered consists of alternating high- and low-index layers of equal optical thickness  $n_i d_i$ . This assembly is well known, for instance from its application as a high-reflecting mirror. In this case the optical thicknesses are adjusted to  $n_i d_i = \lambda/4$ , whereas in our application as a pressure sensing element the best performance, i.e. the highest  $|D| = |\Delta R/\Delta p|$  will be obtained if optical thicknesses are chosen between  $\lambda/4$  and  $3\lambda/8$ , depending on the total number of layers  $N$ . In Fig. 2 the reflectance in dependence on the layer thickness for the example of a 15-layer mirror system is shown.  $D_{\max}$  is found at that edge of the stop band which belongs to the thicker layer.

The second multilayer design taken into consideration is known as all-dielectric interference filter [8] or Fabry-Perot filter. A first-order interference filter consists of  $\lambda/4$  layers and a doubled layer in the middle of the stack. In this way two high-reflecting subsystems are obtained that are separated by a central  $\lambda/2$ -spacer layer. Spacer layers with multiples of  $\lambda/2$  as optical thickness

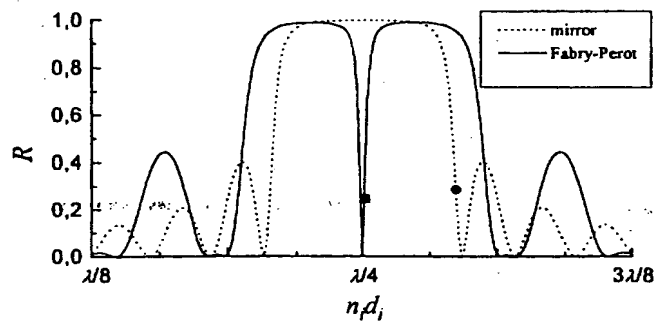


Fig. 2. Reflectance  $R$  of a 15-layer mirror and a 15-layer Fabry-Perot system (spacer:  $n_8 d_8 = 2n_1 d_1$ ) in dependence on the optical thickness  $n_i d_i$  of all layers;  $n_{\text{high}} = 2.3$ ,  $n_{\text{low}} = 1.48$ ,  $n_0 = 1.48$ ,  $n_{N+1} = 1.329$ ; points of maximum  $|D| = |\Delta R/\Delta p|$  for mirror (●) and Fabry-Perot sensor (■).

can also be used (higher-order interference filters). In comparison to the mirror system with the same number of layers, the reflectance curve  $R(n_i d_i)$  of a first-order interference filter design shows a broadened high-reflectance region with slightly reduced peak reflectance and an additional narrow transmission band (Fig. 2). For the Fabry–Perot sensor design the point of maximum  $|D| = |\Delta R/\Delta p|$  is located at the edge of this central transmission band.

A comparison of  $D_{\max}$  of the two layer designs investigated is shown in Fig. 3. The reflectance slope rises with increasing total layer number  $N$  of the sensor. A 15-layer Fabry–Perot system offers a value approximately 300 times higher than that of the uncoated fiber tip sensor ( $D_{\max} = 5.4 \times 10^{-6}/\text{MPa}$ ). For layer numbers  $N$  larger than 5, where the multi-interference process prevails over the effect of index modulation in the fluid, the Fabry–Perot system provides a larger reflectance slope than the mirror system for a given  $N$ . The higher the layer number, the larger the difference. Further calculations show that the use of higher-order Fabry–Perot systems do not yield better results. For instance, a spacer thickness of  $\lambda$  instead of  $\lambda/2$  for a second-order system leads to less improvement than the addition of another two  $\lambda/4$  layers to the mirror subsystems, which results in a similar overall thickness of the sensor. Thus, an increase in the finesse of the Fabry–Perot system due to higher reflectances of the mirror subsystems provides a larger improvement of  $D_{\max}$  than a simple increase in sensor thickness. It should be noted that for very large layer numbers, deviations from these theoretical results are expected, because light losses due to the beam divergence at the fiber tip and to scattering at inhomogeneities within the layers may not be ignored.

For the choice of the optimum design, the simplicity of the technical implementation is an important criterion. Since sample variations during the evaporation process are not completely avoidable, the effect of deviations of single layer thicknesses on the sensor

characteristics should be considered. The reflectance of the mirror subsystems at the high reflectance plateau is quite insensitive to small thickness deviations, and the finesse of the Fabry–Perot filter is therefore changed only to a very small extent, whereas thickness deviations in the mirror system used at the edge of the stop band show much larger effects. In Fig. 4(a) the change in  $D_{\max}$  caused by a deviation of +5% in the  $i$ th individual layer thickness is shown for both 15-layer systems in dependence on the number  $i$  of the modified layer. Obviously, also in view of the simplicity of manufacture, the Fabry–Perot system is the preferable design, because thickness errors cause lower deviations of  $D_{\max}$ .

A change in one layer thickness relative to the others has the second effect that  $D_{\max}$  is found at a slightly different thickness of all layers compared with the undisturbed design. In other words, to achieve the largest  $|D|$  of the modified system (shown in Fig. 4(b)) a different optical wavelength  $\lambda$  is necessary (Fig. 4(b)). In particular, the wavelength deviation  $\Delta\lambda$  is large for a thickness deviation of the spacer layer of the Fabry–Perot system, so special care must be taken when the spacer is deposited. The wavelength shift can be coped with to a certain degree if a tunable light source is used, for instance a temperature-tuned laser diode.

Fig. 4(a) shows that  $D_{\max}$  of the mirror system will slightly increase if the layers with  $i=6,\dots,11$  are thicker

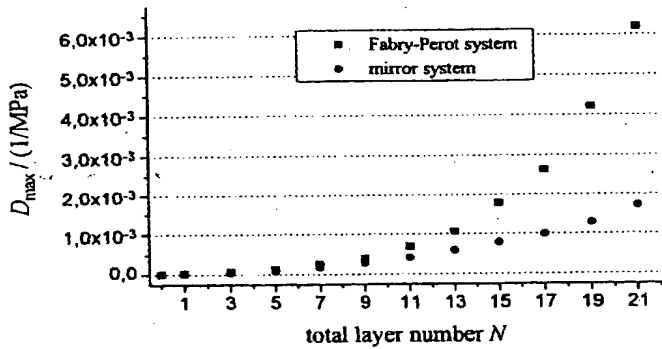


Fig. 3. Maximum reflectance slope  $D_{\max}$  vs. total layer number  $N$  of mirror and Fabry–Perot systems (refractive indices as in Fig. 2).

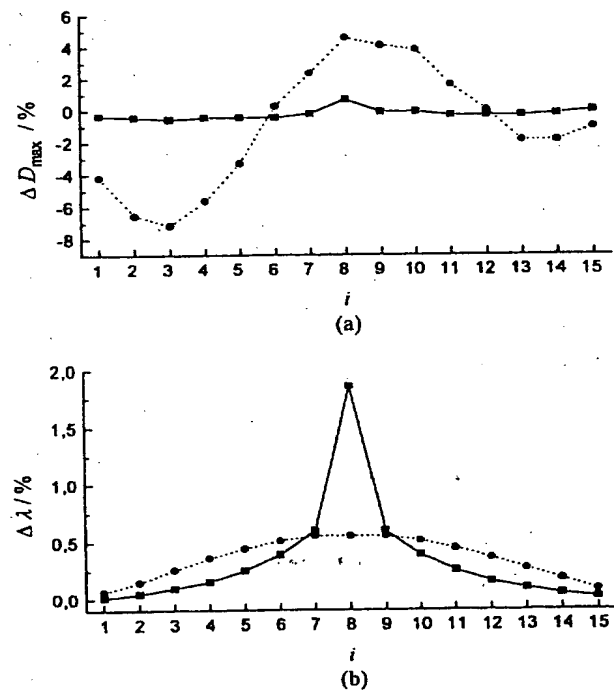


Fig. 4. Deviation of the maximum reflectance slope (a) and of the optimum wavelength (b) caused by a +5% deviation in the  $i$ th layer thickness for 15-layer mirror (dotted line) and Fabry–Perot system (solid line).

than the others. This may indicate that the performance of the system can be improved by refinement of the individual thicknesses, but the manufacture of such a multilayer coating is much more sophisticated. It can also be observed in Fig. 4(a) that the Fabry–Perot system can be improved to a very small extent if the integer ratio of 2 between mirror subsystem layers and spacer is dropped and a slightly thicker spacer is used. Thereby a system with exactly  $\lambda/4$  layers is built in order to achieve the highest possible reflectance of the mirror subsystems resulting in the highest finesse of the Fabry–Perot, and with a spacer thickness of slightly more than  $\lambda/2$  to set the system to the edge of the transmission band. In the system with the exactly doubled spacer, the high-reflecting layers were slightly thicker than  $\lambda/4$  at the point of maximum  $D$  (Fig. 2), and this common interference filter design may also be used, since the difference in  $D_{\max}$  is very small.

### 3. Experimental realization, results and discussion

For a first experimental implementation of a fiber-optic multilayer hydrophone, a 15-layer Fabry–Perot system (physical thickness of the whole sensor:  $\sim 1.4 \mu\text{m}$ ) was deposited on a cut fiber tip using the sputtering technique for a robust coating. Both, multimode and single-mode fibers were used. Standard deposition materials were evaporated: the high-index material was  $\text{Nb}_2\text{O}_5$  ( $n=2.3$ ), the low-index material  $\text{SiO}_2$  ( $n=1.48$ ). First, white light was coupled into the fiber and the spectral transmission of each sensor was measured by a grating spectrometer. The optical wavelength for acoustic sensor operation was determined at the transmission band edge in the spectrum obtained. For each sensor an individual operating wavelength was found because of systematic and random deviations in the evaporation process. The measured full-width-at-half-maximum value (FWHM) of the transmission band of approximately 8.5 nm indicating the finesse achieved for the Fabry–Perot system is in good agreement with the calculation.

The sensor was then put in the focal region of a focussing broadband transducer (K. Deutsch, 4 MHz, lens diameter: 20 mm, focal length: 30 mm), which was driven by a pulse generator (peak voltage: 350 V, repetition frequency: 300 Hz). The beam of a temperature-tuned laser diode ( $\lambda=636.5 \text{ nm}$ , output power: 5 mW) was coupled into the fiber and the reflected light was detected by a balanced photodetection system (Fig. 5). The induced photocurrent is transformed by a transimpedance amplifier into a signal voltage acquired by a digitizing oscilloscope.

Fig. 6 shows the result of a measurement using the multilayer hydrophone. By averaging of some pulses the signal-to-noise ratio (SNR) was improved (single pulse:

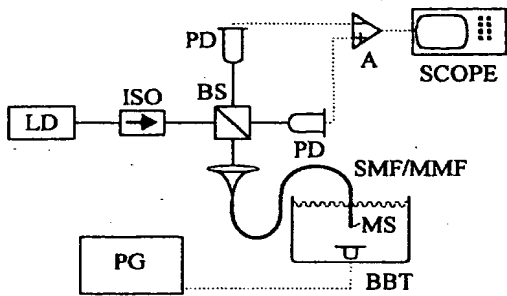


Fig. 5. Experimental setup for ultrasonic pressure measurement; LD: laser diode, ISO: optical isolator, BS: beam splitter, PD: photodiode, A: transimpedance amplifier, SMF/MMF: single-/multimode fiber, MS: multilayer sensor, BBT: broadband transducer, PG: pulse generator.

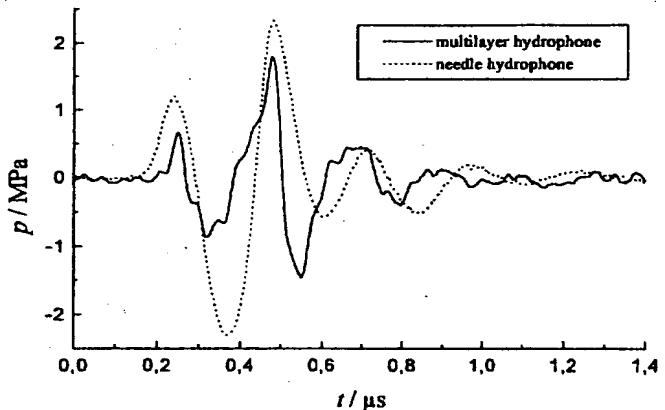


Fig. 6. Acoustic pressure  $p$  vs. time  $t$  measured with a multilayer hydrophone (30-pulse-averaged) and a PVDF needle hydrophone.

$\text{SNR} \approx 12 \text{ dB}$ , 30-pulse averaged signal:  $\text{SNR} \approx 29 \text{ dB}$ , detection bandwidth:  $\sim 25 \text{ MHz}$ ). The intensity noise is mainly caused by back-reflections into the laser diode due to insufficient optical isolation.

The multilayer hydrophone signal was scaled using the theoretically found reflectance slope of  $|D|=1.8 \times 10^{-3}/\text{MPa}$  (Fig. 3). The comparison of the signal amplitude with that obtained by a calibrated piezoelectric needle hydrophone (Fig. 6) shows fairly good agreement and confirms the reflectance slope of the multilayer hydrophone theoretically expected. The focal region of the ultrasonic transducer has a lateral FWHM of approximately 0.8 mm and the needle hydrophone has a sensing element 0.6 mm in diameter. Thus, the needle hydrophone signal was corrected by a factor of 1.19 to compensate the spatial integration [9].

Comparing the two time waveforms it can be seen that the multilayer hydrophone signal is modulated by additional oscillations ( $f \approx 23 \text{ MHz}$ ) induced by acoustical resonances of the fiber and acoustical diffraction phenomena at the sensor tip. Measurements with other fiber-optic hydrophone configurations also show such oscillations, but their exact origin is not yet completely

understood [9]. The frequency shift of the time waveform is caused by the non-uniform frequency characteristic of the sensor. Similar results were obtained in measurements with sensors using a low-finesse cavity at the fiber tip [2, 10]. The correct waveform can be calculated using the transfer function to be determined by a separate calibration procedure [9].

The multimode fiber sensor furnished similar results. The signal amplitude was a little smaller, perhaps because of increased losses due to the larger beam divergence at the end of the fiber, and the noise was reduced due to lower backscattering into the laser diode. The larger core diameter of the multimode fiber (multimode:  $\sim 50 \mu\text{m}$ , single-mode:  $\sim 3.5 \mu\text{m}$ ) leads to spatial averaging and therefore to a decreased spatial resolution of the sensor, while the optical alignment is easier.

#### 4. Conclusions

A fiber-optic multilayer hydrophone was presented. The principle of measurement is based on the deformation of the layer system by an incident wave and the detection of the induced change in optical reflectance. Two different multilayer systems were theoretically investigated for use as ultrasonic pressure sensors. The Fabry-Perot assembly shows some advantages concerning the sensitivity and the simplicity of the manufacturing process and was experimentally implemented. A first measurement of ultrasonic pulses with a multilayer hydrophone was presented for the frequency region of some MHz. A signal-to-noise ratio of about 29 dB was achieved in the measurement of low-intensity signals, and improvement should be possible by better isolation of the laser diode. Signal losses in the optical setup can

be reduced by the use of a polarizing beam splitter and a fiber-optic polarization controller.

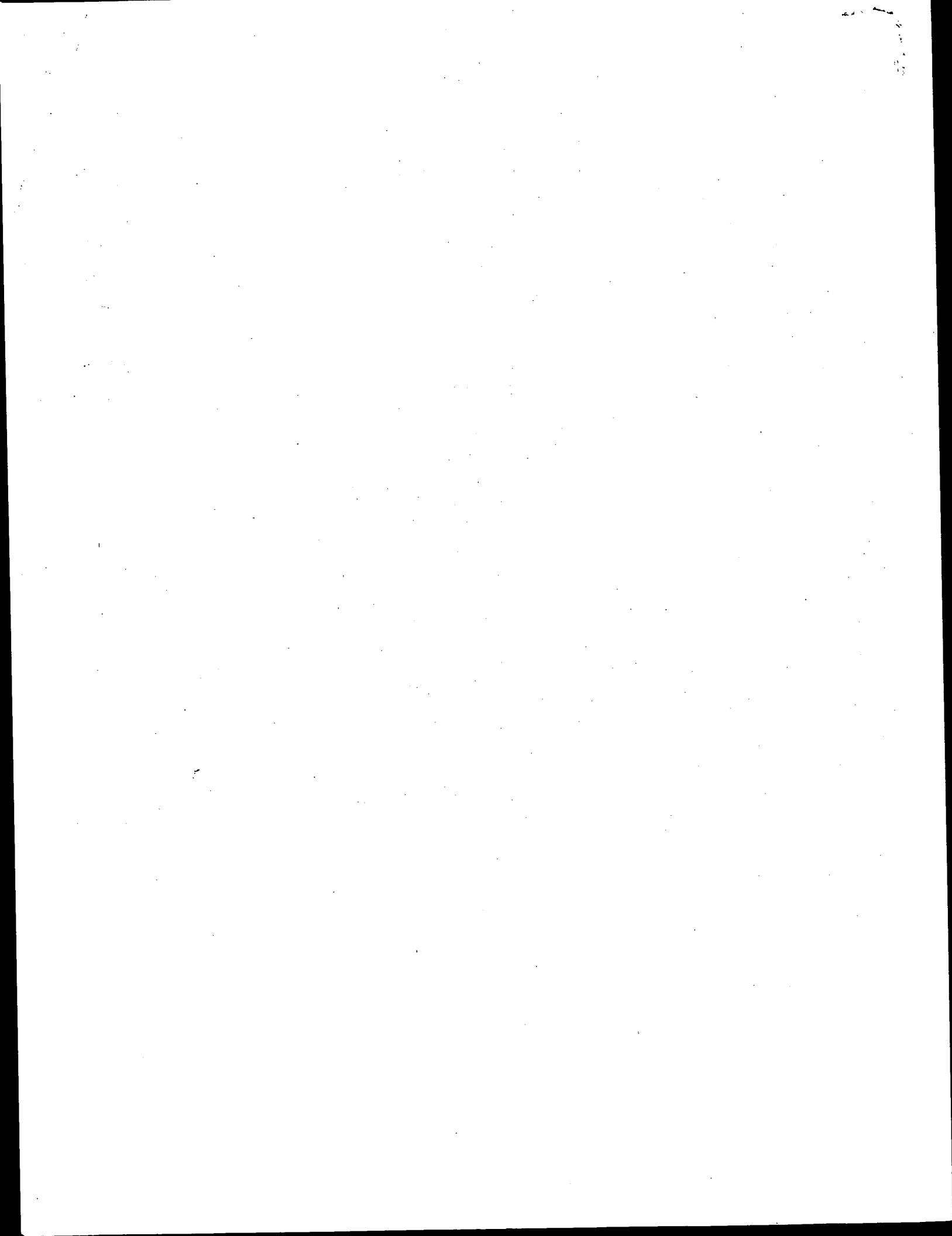
The multilayer hydrophone can be applied for solving many ultrasonic measurement problems in the whole power and frequency range. It has a high durability and combines high spatial and temporal resolution with high sensitivity. The small sensor dimensions provide an undisturbed measurement, for example in ultrasonic resonators. Shock wave characterization, measurement of high-power ultrasound with low frequencies for technical applications, low-intensity signals from diagnostic devices, or ultrasound fields with tens of MHz for the inspection of matter are potential fields of application for this new sensor type.

#### **Acknowledgement**

The authors wish to thank the Deutsche Forschungsgemeinschaft, DFG, for the financial support of this work.

## References

- [1] J. Staudenraus, W. Eisenmenger, Ultrasonics 31 (1993) 267.
  - [2] P.C. Beard, T.N. Mills, Electron. Lett. 33 (1997) 801.
  - [3] Ch. Koch, Ultrasonics 34 (1996) 687.
  - [4] W. Menssen, W. Molkenstruck, R. Reibold, Proc. Ultrasonics Int. 91 (1991) 347.
  - [5] Ch. Koch and R. Reibold, World Congress on Ultrasonics 95, Berlin, 1995, paper 4-16:00-7.
  - [6] H.A. Macleod, Thin Film Optical Filters, Adam Hilger Ltd, Bristol, 1986, Chapter 2.
  - [7] C.D. Butter, G.B. Hocker, Appl. Opt. 17 (1978) 2867.
  - [8] H.D. Polster, J. Opt. Soc. Am. 42 (1952) 21.
  - [9] Ch. Koch, G. Ludwig, W. Molkenstruck, Ultrasonics 35 (1997) 297.
  - [10] A.J. Coleman, E. Draguioti, R. Tiptaf, N. Shotri, J.E. Saunders, Ultras. Med. and Biol. 24 (1998) 143.



# Optical multilayer detection array for fast ultrasonic field mapping

XP-000973108

PD: 01-08-1999 (3)  
P: 1026-1028

V. Wilkens and Ch. Koch

Labor 1.43, Physikalisch-Technische Bundesanstalt, PF 3345, D-38023 Braunschweig, Germany

Received April 7, 1999

An optical multilayer detection array for ultrasonic measurements is presented. The probe comprises a dielectric interference filter structure that is evaporated onto a glass plate. An incident acoustic pressure signal deforms the layer system, and the induced modulation of the optical reflectance is determined by a simple optical detection scheme. The principle of measurement is demonstrated by a line scan through the focus of a broadband transducer and can be applied to rapid two-dimensional characterization of ultrasonic fields. The high temporal and spatial resolution of the measurements is combined with high sensitivity and durability of the probe, and, in contrast with fiber-tip multilayer hydrophones, the multilayer detection array provides signals that are not influenced by acoustic resonances and diffraction phenomena. © 1999 Optical Society of America

OCIS codes: 110.2970, 110.7170, 120.4640, 170.3880, 230.4170.

Successful use of optical dielectric multilayer structures evaporated onto fiber tips as ultrasonic sensors with high spatial and temporal resolution has been reported.<sup>1,2</sup> Acoustic pressure measurement is based on elastic deformation of the layer system by an incident sound wave and detection of the induced modulation of the optical reflectance. A serious disadvantage of fiber-optic sensors is the strong influence of acoustic resonances and diffraction phenomena on the obtained waveforms. This influence depends on the sensor size, which is of the same order of magnitude as the acoustic wavelength if ultrasound in water at ~10 MHz is being investigated. In this Letter, reducing the disturbance of the measured signal that is due to these effects by use of the concept of an enlarged acoustic probe is considered. A glass plate 30 mm in diameter is coated with a dielectric multilayer Fabry-Perot system. The reflectance modulation is determined by use of a free-field laser beam, and focusing offers high spatial resolution. The position and the spot size of the laser beam define a single element of a detection array, and one can investigate two-dimensional ultrasound pressure fields by shifting the spot. This optical scanning procedure can be performed comparatively fast because light beams are moved instead of mechanical elements that must be shifted when one is scanning with common single-element hydrophones.

Ultrasonic detection arrays that combine high spatial and temporal resolution are of interest not only for characterization of transducers but also for high-frequency ultrasound pulse-echo imaging systems.<sup>3</sup> With increasing ultrasound frequency, leading to higher image resolution, the array element spacing and, as a consequence, the element size must be reduced. Although some progress has been made, it seems to be difficult to manufacture piezoelectric arrays with element spacing in the micrometer range, wide bandwidths, and large apertures and simul-

taneously to ensure acoustic and electric isolation of the small elements.<sup>4</sup> Since optical measurement techniques avoid these problems, they are an interesting alternative to electrical systems, and the optical multilayer detection array in particular offers a simple solution.

The implemented multilayer system consists of 19 dielectric layers with alternating refractive indices of  $n = 2.3$  ( $\text{Nb}_2\text{O}_5$ ) and  $n = 1.48$  ( $\text{SiO}_2$ ) (Fig. 1). The Fabry-Perot or interference filter structure, which is a well-suited design for use as a pressure-sensing element,<sup>2</sup> comprises a central  $\lambda/2$  spacer layer and two highly reflecting subsystems, both of which consist of nine  $\lambda/4$  layers. By use of the sputtering technique, a robust coating is obtained that can be used

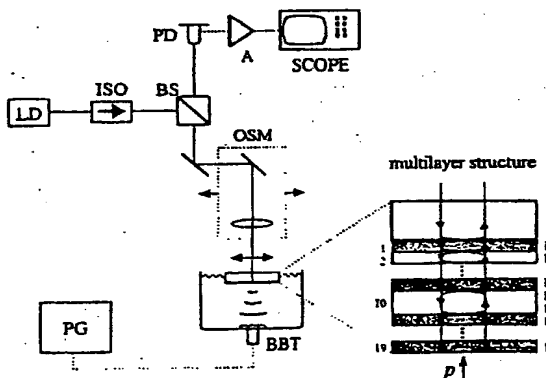


Fig. 1. Experimental setup for ultrasonic pressure measurement with a multilayer detection array and (inset) a magnified schematic of the multilayer structure: LD, laser diode; ISO, optical isolator; BS, beam splitter; PD, photodiode; A, transimpedance amplifier; SCOPE, oscilloscope; OSM, optical scanning mechanism; BBT, broadband transducer; PG, pulse generator; H's, high-index  $\lambda/4$  layers; L's, low-index  $\lambda/4$  layers.

in water without swelling of the layers. The overall thickness of the multilayer system has to be small compared with the acoustic wavelength of the signal to be measured. To obtain a large acoustic bandwidth one must reduce the thickness of the system to a few micrometers because, for instance, the wavelength in the sensor medium at a frequency of  $f = 100$  MHz is approximately  $56 \mu\text{m}$ . The 19-layer stack provides a thickness of  $d = 1.9 \mu\text{m}$ . The sensitivity of the assembly can be expressed in terms of the reflectance slope  $D = \Delta R / \Delta p$ , where  $\Delta R$  denotes the change in optical intensity-reflectance of the layer system that is caused by variation of the acoustic pressure  $\Delta p$  of an incident ultrasound wave.  $D$  can be calculated by use of multilayer theory, taking into account the pressure dependence of the individual layer thicknesses and refractive indices and the modulation of the refractive index in the water beneath the sensor. For the 19-layer system a theoretical value of  $D = 4.3 \times 10^{-3} / \text{MPa}$  is found for a laser wavelength at the edge of the central transmission band of the interference-filter system.<sup>2</sup> Covering the upper surface of the substrate of the detection array with glycerin suppresses optical standing waves in the glass plate, which is not antireflection coated. An important advantage of the multilayer detection array is its simple and moderate-priced manufacture. The deposition of the layer system can be directly controlled during the evaporation procedure by monitoring of, for instance, the reflectance. This common technique for producing optical multilayer structures such as interference filters, laser mirrors, or antireflection coatings is more difficult and expensive to apply in the case of fiber tips.

The experimental setup for ultrasonic field mapping with the multilayer detection array is shown in Fig. 1. The probe is placed on the surface of the fluid in the focal plane of a broadband transducer (K. Deutsch GmbH; 3–12 MHz; lens diameter 12 mm, focal length 50 mm) excited by a pulse generator (peak voltage 350 V, repetition rate 300 Hz). The beam of a temperature-tuned and optically isolated laser diode ( $\lambda = 672$  nm, output power 10 mW) passes a beam splitter and a mirror and is focused on the fixed multilayer system. The spot size and position define the single array element, and the detection array is emulated by shifting of the spot by use of, for instance, Bragg cells or high-speed mechanical scanners. For the first experiments the laser spot was positioned manually by translation of the mirror together with the focusing lens with a micrometer screw. In this way a line scan could be performed. The reflected light is detected by a photodiode, and the induced photocurrent is transformed by a transimpedance amplifier into a signal voltage that is acquired and stored by a digitizing oscilloscope.

The performance of the device is shown by a measurement at a single position in the center of the focal region of the transducer. In Fig. 2 the obtained time waveform of the ultrasonic pressure pulse is shown (20 pulse averaged). In addition, the pressure waveforms that are received by a calibrated piezoelectric membrane hydrophone (Marconi IP038; single pulse) and by a 19-layer fiber-optic hydrophone (20 pulses

averaged) are depicted. The pressure signals are calculated from the measured signal voltages by use of the theoretically found reflectance slope  $D$  for both of the optical detection systems and the calibration factor in the case of the membrane hydrophone. The spatial integration of the different-sized sensor elements is compensated for by correction factors.<sup>3</sup> Comparing the waveforms shows very good agreement between the multilayer detection array and the membrane hydrophone measurement, but the sensitivity of the multilayer detection array obviously is ~20% less than expected from the theory. This deviation may be caused by an error in the experimental determination of the laser wavelength for optimum operation of the multilayer system<sup>2</sup> or by an incorrect description of the elastic and elasto-optic properties of the sputtered-layer media.<sup>1</sup> The signal-to-noise ratio is ~32 dB for a single pulse and ~50 dB for the 20-pulse-averaged signal at a detection bandwidth of ~25 MHz, which leads to minimum detectable pressure amplitudes (signal-to-noise ratio, 1) of ~80 and ~10 kPa, respectively. The fiber-optic multilayer hydrophone signal (Fig. 2) shows characteristic deviations from the other waveforms that were obtained, i.e., a frequency shift and additional oscillations ( $f \approx 23$  MHz) caused by acoustic resonances and diffraction phenomena at the sensor tip. Significantly, these effects do not occur with the multilayer detection array because of the enlarged probe size. The finite thickness of the glass plate of ~2.4 mm leads to acoustic reflections that disturb the signal ~0.85  $\mu\text{s}$  after the leading edge of the pulse, and for longer undisturbed measurements a thicker glass plate has to be used.

The scanning operation mode of the multilayer detection array was demonstrated by performance of a line scan in the focal plane of the transducer as a first test. The laser spot was shifted in steps of 0.25 mm over a distance of 4.5 mm. At each position the time waveform was detected, and the results are depicted as a pseudo-three-dimensional plot in Fig. 3, which shows the lateral structure of the acoustic field in the focus region of the transducer. For the FWHM of the positive pressure peak a value of ~1.2 mm was obtained.

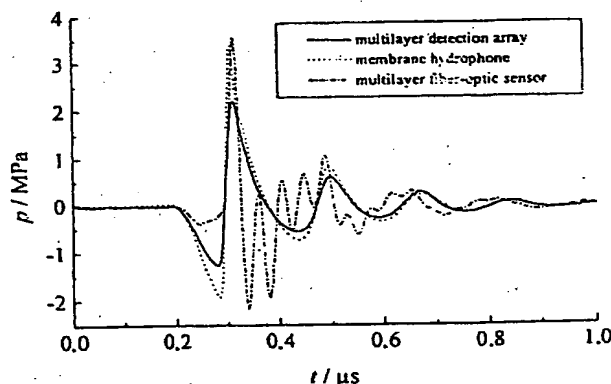


Fig. 2. Acoustic pressure  $p$  versus time  $t$ , measured with the multilayer detection array, a polyvinylidene fluoride membrane hydrophone, and a fiber-optic multilayer hydrophone.

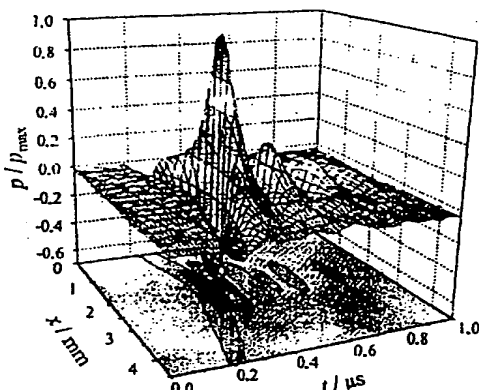


Fig. 3. Line scan in the focal plane of the transducer: normalized pressure signal  $p/p_{\max}$  versus time  $t$  at different positions  $x$ .

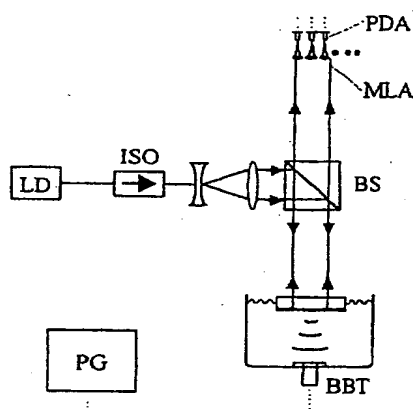


Fig. 4. Optical arrangement for the parallel acquisition of the spatial ultrasound pressure field: PDA, photodiode array; MLA, microlens array; other abbreviations as in Fig. 1.

Automation of the scanning mechanism, which contains only a few mechanical moving elements, or in the case of beam deflection with Bragg cells none, together with automatic data acquisition would permit rapid investigation of two-dimensional ultrasonic fields. Also, parallel evaluation at different sensor points can be realized with the multilayer detection array, which would lead directly to a one- or a two-dimensional image of the ultrasound field. The whole detection array is illuminated by a collimated laser beam from a high-power laser diode (Fig. 4). The single photodiode (Fig. 1) is replaced with an array of microlenses and photodiodes. Each lens defines one array element according to the imaging geometry. The photodiode signal can be fed into a multichannel data-storage system. Data acquisition is more sophisticated than in the scanning operation mode, but this technique would offer simultaneous two-dimensional characterization of

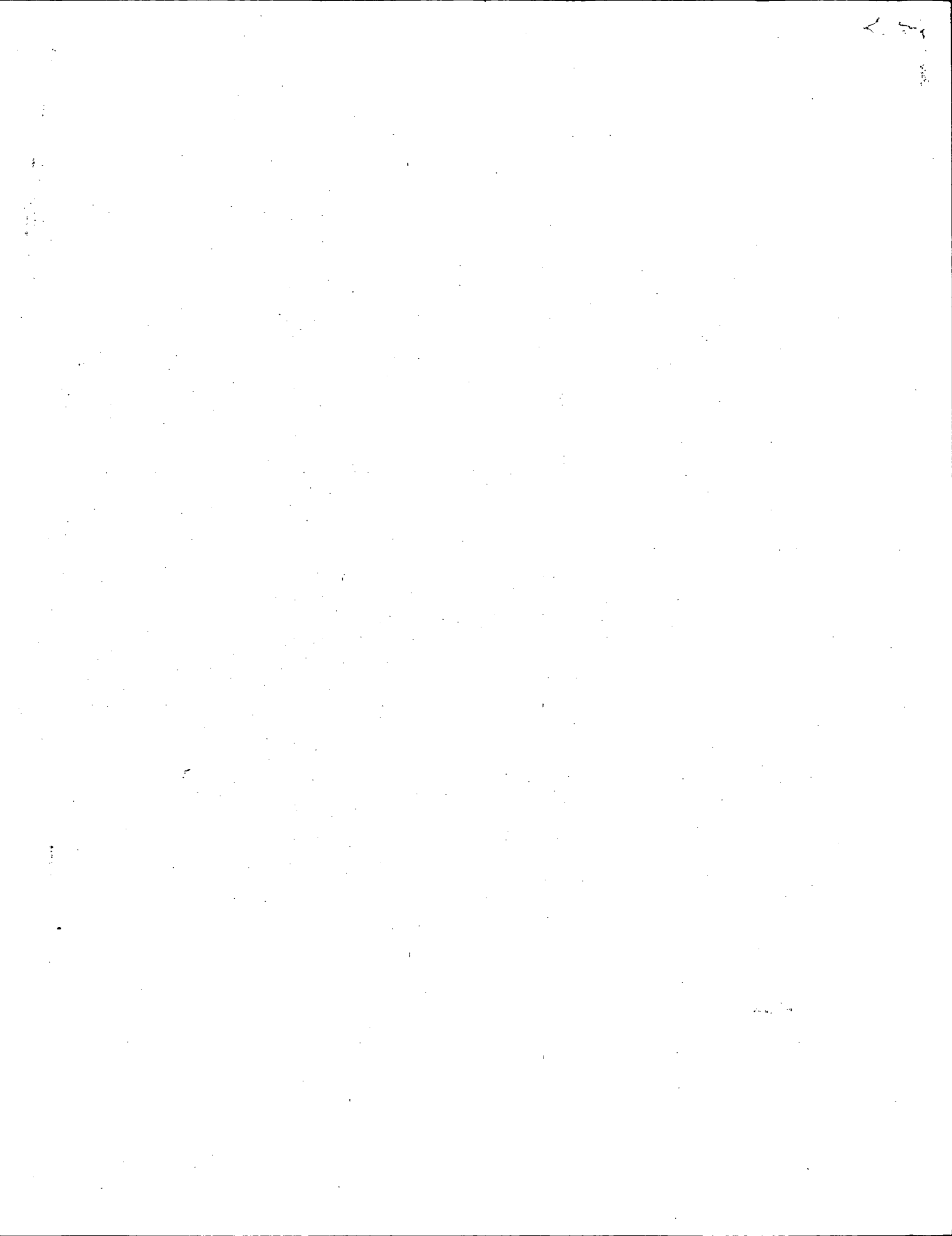
single-event ultrasonic fields. For the investigation of repetitive ultrasonic fields an alternative to the scanning operation and the photodiode array may be the use of a CCD camera together with a pulsed laser diode that again illuminates the whole multilayer detection array. The laser diode is triggered by a pulse generator that excites an ultrasonic transducer, and a CCD camera detects an image of the ultrasonic pressure distribution at the moment of laser illumination. By sweeping the delay time between the trigger pulse and the illuminating pulse from CCD frame to CCD frame, one can obtain a time signal if a sequence of acquisitions is evaluated. Problems may be caused by this setup because of the relatively high dc part of the light compared with the acoustically induced modulation of brightness, since the resolution of CCD sensors in combination with common image-processing electronics is not as high as that of photodiodes.

An optical multilayer detection array has been described that has the potential for fast two-dimensional measurements of ultrasonic pressure fields by optical scanning techniques. The operation of the system was demonstrated in a first measurement at a single position of the sound field, and the result was compared with the signal from a calibrated polyvinylidene fluoride membrane hydrophone. The obtained time waveforms of both systems showed very good agreement, whereas the pressure signal detected with a fiber-optic multilayer hydrophone showed characteristic deviations that were due to acoustic resonances and diffraction phenomena. A line scan was performed to demonstrate the operation mode of field mapping with the multilayer detection array. Different proposals were made to develop further an experimental setup that allows simultaneous data acquisition in one or two dimensions. Besides the characterization of ultrasonic transducers, the described technique can be applied, for instance, to nondestructive testing of inhomogeneous or porous materials by use of ultrasound transmission. High spatial resolution and wide bandwidth make the system suitable for ultrasound pulse-echo imaging systems at high frequency.

The authors thank the Deutsche Forschungsgemeinschaft for financial support of this work. V. Wilkens's e-mail address is volker.wilkens@ptb.de.

## References

1. Ch. Koch, *Ultrasonics* **34**, 687 (1996).
2. V. Wilkens and Ch. Koch, *Ultrasonics* **37**, 45 (1999).
3. J. D. Hamilton and M. O'Donnell, *IEEE Trans. Ultrason. Ferroelectr. Freq. Control* **45**, 216 (1998).
4. F. S. Foster, L. K. Ryan, and D. H. Turnbull, *IEEE Trans. Ultrason. Ferroelectr. Freq. Control* **38**, 446 (1991).
5. Ch. Koch, G. Ludwig, and W. Molkenstruck, *Ultrasonics* **35**, 297 (1997).





## Review Article

# A strategy for the development and standardisation of measurement methods for high power/cavitating ultrasonic fields: review of high power field measurement techniques

Mark Hodnett \*, Bajram Zeqiri

*Centre for Mechanical and Acoustical Metrology, National Physical Laboratory, Teddington, Middlesex TW11 0LW, UK*

Received 1 March 1997

**Abstract**

This review was compiled as part of a project to formulate a UK strategy for the development and standardisation of measurement methods for high power/cavitating ultrasonic fields. It reviews the scientific literature relating to various methods of measuring high power fields which have been developed for application in health care, sonochemistry and industrial ultrasonics, and compares these methods in terms of attributes such as spatial resolution, bandwidth and sensitivity. Crown Copyright © 1997 Published by Elsevier Science B.V.

**Keywords:** High power fields; Measurement; Cavitation; Hydrophones; Thermal probes

**1. Introduction**

This literature review of high power field measurement techniques was compiled as part of a six-month project for the UK Department of Trade and Industry entitled Study to Review Progress, Identify Measurement Methods and Address Implementation for Remote and Local Sensing Methods for the Measurement of High Power/Cavitating Ultrasonic Fields. The review was undertaken in April 1996 and was carried out by the National Physical Laboratory (NPL). The objective of this report was to review the state of technical progress in measuring high power ultrasonic fields as revealed in the open scientific literature. The findings have been fed into a final project report [1] which provides recommendations on an implementation strategy for future developments in this area.

**1.1. Background**

High power ultrasonic fields are used in a number of diverse application areas, which are described briefly in

Section 1.2. Measurement methods for these high power fields are important for reasons of safety, for example in monitoring output levels of ultrasonic lithotripters in medicine, and also in device and process monitoring, for example in ultrasonic cleaning. Currently, there are few well-documented, traceable measurement methods for high power ultrasonic fields.

Initially, the development of measurement techniques was driven by the medical applications of ultrasound, amid concerns over the safety of exposure levels from diagnostic and therapeutic equipment devices which generally operate at acoustic frequencies in the megahertz range [2]. Standard techniques have been established for the measurement of low power ultrasound, centred on the medical field [3–6]. Indeed, declaration of the levels of the acoustic output parameters of medical equipment is now in itself a requirement [7]. In the high power arena, this applies specifically to lithotripters. Thus, there is an explicit need for standardised measurement techniques suitable for measuring the acoustic parameters of high power ultrasound fields, using calibrated instrumentation.

Extension of the standards infrastructure to include high power fields requires an initial assessment of current techniques, and an evaluation of their suitability for

\* Corresponding author. Tel: (+44) 181 943 6365; Fax: (+44) 181 943 6161; e-mail: mark.hodnett@npl.co.uk

development as standard high power field characterisation methods. Reviews of measurement techniques aimed specifically at the medical field have been published [8,9], but there are comparatively few similar articles applicable to other applications [10].

Measurement of the output levels from medical devices is made easier by the fact that many systems operate in pulsed or toneburst modes. In interpreting measurements of medical fields, it can be assumed that free-field conditions apply. This is generally not the case for high power systems, which normally operate in continuous wave modes, and in which the environments are strongly reverberant. Increasingly, knowledge of the spatial dependence of these ultrasound fields is becoming more crucial. This is reflected not only in medical applications, where such concerns have been prevalent for some time, but also in applications such as ultrasonic cleaning, where some regions in a typical bath will clean better than others, and in sonochemistry, where knowledge of reaction locality will almost certainly lead to users and manufacturers being able to address the issue of scale-up on a more informed level.

### 1.2. Application areas

High power ultrasound is utilised in a broad range of applications, and the review of current field measurement techniques was undertaken in relation to these. Fig. 1 presents an overview of these applications.

Defining the term 'high power' is not trivial. It is

easiest to consider high power fields as those which utilise cavitation to produce some desired effect, in other words, in this review, we are concerned with measurement techniques that can, or could be enhanced to, measure acoustic parameters in cavitating fields. In water, the threshold of cavitation can be as low as 1 bar ( $10^5$  Pa) of excess pressure, a level well within the range of many ultrasound systems, although this threshold is dependent also on the frequency, the nature of excitation, and physical conditions such as temperature and dissolved gas content. Fig. 1 illustrates a range of applications that either use or can generate cavitation. It would appear that high power fields can range in pressures from 10 kPa to over 100 MPa, depending on the frequency and the number of cycles per pulse.

High power ultrasound fields can be extremely difficult to characterise, often because of the cavitation events occurring. Not only can the cavitation activity cause damage to the measuring sensor being used, but the bubble populations generated can also scatter the acoustic signal produced by the source under investigation. Furthermore, the oscillating bubbles present will produce their own acoustic signatures, and resolving these from the signal produced by the source can be a complex process. The monitoring of cavitation itself is addressed in an accompanying literature review carried out by the Institute of Sound and Vibration Research, Southampton, UK (ISVR) [11], and the techniques described will not be repeated here.

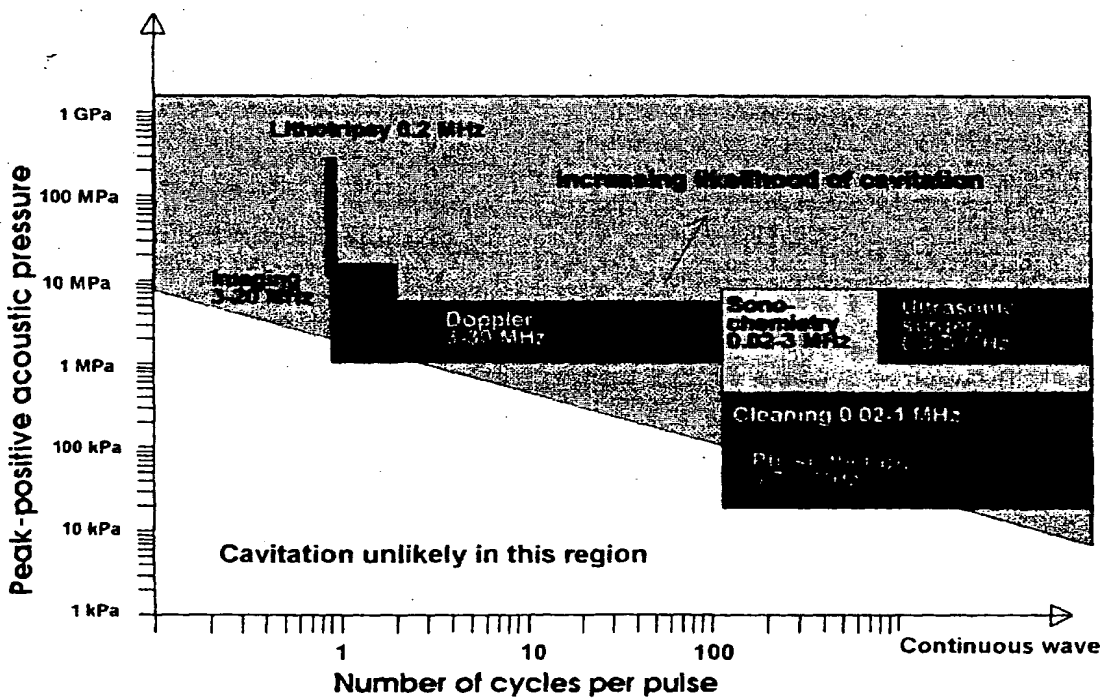


Fig. 1. Applications of high power ultrasound fields.

### 1.3. Important acoustic parameters

This review deals with those measurement techniques which have been applied to the characterisation of the acoustic field properties of high power cavitating ultrasonic fields. It will be clear that, for a number of reasons, the review has leaned heavily on the progress made in the area of medical ultrasonic field measurements. In this area, the high power cavitating fields encountered are those produced by extracorporeal shock-wave lithotripters along with some surgical devices and many of the techniques cited in the review have been drawn from these applications.

It is appropriate firstly to consider which specific acoustic field parameters are important in characterising a high power ultrasound system and in so doing we will ignore the influence of cavitation. Cavitation bubbles produced in the acoustic field will scatter the ultrasound and will themselves act as additional sources of sound, giving rise to a complex, time-dependent pressure distribution of the acoustic field. It is appropriate here to comment briefly on potential methods which may be of use in the suppression of cavitation, enabling quasi free-field characterisation of the field to be attempted. Viscous fluids or water of extremely high purity (thereby containing a low concentration of nucleation sites) could be used as propagation media of increased tensile strength. Alternatively, the application of high static pressures to the propagation medium may be used to increase its cavitation threshold. However they are made, such measurements undertaken in the absence of cavitation would provide information regarding the pressure distribution under specified test conditions, but these conditions (change of fluid, nucleation site concentration, application of increased pressure) may not relate simply to those experienced during a high power application.

Here, we will restrict ourselves to considering the acoustic properties of high power systems, such as ultrasonic cleaning baths or sonochemical reactors, which will normally produce a strongly reverberant environment. Ideally, we would wish to measure or monitor a quantity which is directly related to the process being facilitated by the ultrasound, so that the process may be manipulated or controlled in a precise fashion. In practice, this assumes a knowledge of the basic mechanisms surrounding the process and in most areas in which high power ultrasound is applied, this knowledge is still developing. In its absence, the most appropriate approach is to determine a range of acoustic field parameters which it is felt may influence or affect the process in question.

Principal amongst these must be the acoustic pressure generated in the field. Techniques used for determining pressure are given in Section 2 where the performance of various types of hydrophone is discussed.

Additionally, Section 2.1.5 provides examples of high power ultrasound systems to which hydrophones have been applied. Under nonlinear conditions the peak rarefactional pressure may differ from the peak compressional pressure, but here we will assume that the pressures generated in the propagation medium are sufficiently low for nonlinearities to be ignored. We can associate this pressure  $p$ , with a particle velocity,  $u$ . The acoustic intensity,  $I$ , which gives the average rate of energy flow through unit area normal to the propagation direction, is given by

$$I = \langle pu \rangle = \frac{1}{t} \int p u \, dt$$

where  $\langle \rangle$  signifies a time average and the limits of integration are taken over one acoustic cycle. The acoustic intensity is a vector quantity but in a plane progressive wave, where the pressure and particle velocity are in phase, the intensity is given by

$$I = \frac{p^2}{2\rho_0 c}$$

where  $\rho_0$  and  $c$  are the density and propagation velocity of ultrasound in the medium respectively. This relationship between pressure and intensity also holds in the transducer far field. In a reverberant field, typically encountered in ultrasonic cleaning and sonochemical applications, the pressure and intensity will vary strongly with position, due to the presence of standing waves set up within the enclosure. This standing wave pattern, and therefore the measurements of pressure or derived intensity, will be very sensitive to the effects of temperature and the liquid level of the cleaning bath. It is not clear whether a knowledge of the intensity vector is relevant in the characterisation of such systems. A more appropriate parameter for such systems may be the acoustic energy density. Comprised of both potential and kinetic energy contributions, the instantaneous acoustic energy density,  $\xi_i$ , is given by

$$\xi_i = \frac{\rho_0}{2} \left( u^2 + \frac{p^2}{\rho_0^2 c^2} \right)$$

The time-averaged energy-density,  $\xi$ , is derived by integrating this expression over one period of the wave. Again, assuming plane-wave conditions, the time-averaged energy density is given by  $\xi = p^2/(2\rho_0 c^2)$  or  $\xi = I/c$ . The discrete thermal probes dealt with in Section 4.1 respond to the time-averaged intensity flowing into the volume occupied by the thermal sensor and will therefore provide a measure of the energy density. This parameter will vary in space throughout the reverberant enclosure and a spatially averaged parameter, derived from a sampling of the acoustic field at a number of field points, may provide a more robust measure of

the acoustic energy being deposited in the tank. Such a device designed specifically for the characterisation of ultrasonic cleaning baths is described in Section 4.2.

For the reasons described above, the reverberant environment occurring in high power systems is very complex. The standing-wave pattern produced by an array of transducers in a cleaning bath, for example, can produce local variations in the acoustical parameters although frequency modulation is often used to smooth out the pressure distribution. Theoretical modelling of these systems is likely to be exceedingly complex for a number of reasons: the bubbles generated by cavitation will scatter the ultrasound, the water surface will distort under the influence of the acoustic radiation force and the vessel walls will undergo vibrations which are not solely piston-like but may include radial or surface-wave modes. Although it lies beyond the scope of the current project, the concepts used in airborne acoustics in the treatment of reverberation rooms may have some validity here. In particular, issues such as reverberation time, direct and reverberant sound fields may have some application. Additionally, the energy density may be determined from pressure measurements, provided that these are made in the far-field of the transducers, in a sufficient number of positions in the acoustic field.

## 2. Hydrophones

By definition, these are simply devices that measure acoustic pressure. Historically, hydrophone development was driven by the increasing need to be able to make quantitative assessments of the spatial and temporal characteristics of medical ultrasonic fields propagating into water. At the megahertz frequencies used in these applications, the need arose for broadband miniature sensors capable of accurate and reproducible measurements of such fields, fuelled by exposure concerns. Increasingly, however, the development of ever-more sophisticated diagnostic and therapeutic devices in the medical field has increased the demand for sensors of better spatial resolution, bandwidth and sensitivity, which are able to withstand increasingly hostile environments. This has led to the production of piezoelectric hydrophones with active elements as small as 40 µm and devices with membrane thicknesses of a few µm. The development of optical-based techniques for characterising ultrasonic fields has also increased, in the form of fibre-optic hydrophones, which can measure the acoustic pressure in a minimally perturbing manner. In this section, the various designs of hydrophones available will be discussed in detail, following a general description of the requirements of such a device when applied to high power field characterisation.

### 2.1. Piezoelectric hydrophones

Hydrophones of this type work according to the piezoelectric effect [12]: a change in the force on a material (in this case, due to the presence of an acoustic disturbance) produces a proportional change in the charge distribution within the material. In measurement practice, this charge is picked up by electrodes attached to surfaces of the piezoelectric element, and can then be amplified as a charge or as a voltage to produce a visual representation of the acoustic waveform, via a signal-processing oscilloscope. The implementation of this effect in the form of a device to assess the acoustic pressure in the field of an ultrasonic source is by no means straightforward. There are a number of important factors to consider in hydrophone design. The device should be non-perturbing: for example in a cleaning bath, we do not want to alter the standing wave pattern established. The errors due to spatial averaging which can occur when measuring medical fields of frequencies of a few megahertz are of less concern in most high power industrial applications, where devices operating at frequencies of 20 kHz produce ultrasound with a wavelength of approximately 7.5 cm. In addition, particularly for the measurement of medical fields, the device needs to have a uniform response over a wide frequency range, yet still be sensitive enough to produce a reasonable signal level that increases linearly with acoustic pressure. Further, it must be robust and rugged enough to withstand the sometimes hostile fields produced by high power ultrasonic equipment.

Robustness is perhaps the most relevant to high power ultrasound applications. By their very nature, many hydrophonic devices can be quite delicate and fragile as designs reach new levels of spatial resolution and non-invasiveness, with their susceptibility to cavitation damage around the active element being of concern. In part, this explains the comparative lack of literature available on the use of hydrophones in measuring the acoustic fields generated by high power ultrasound devices, with the exception of measurements made in the medical field, where concerns over safety have driven the development of accurate and robust devices (at the expense of performance, to a certain extent) which have been used in the characterisation of lithotripter fields.

#### 2.1.1. Needle devices

Piezoelectric ceramics have been widely used in the development of hydrophones, and most designs using materials of this type consist of a disc-shaped active element supported at the tip of a needle-like structure which is made from some acoustically absorbing material. The element and absorbing material are then housed in some form of supporting tube [13,14]. A schematic representation of such a device is shown in Fig. 2.

Needle-type ceramic probes can be fairly robust

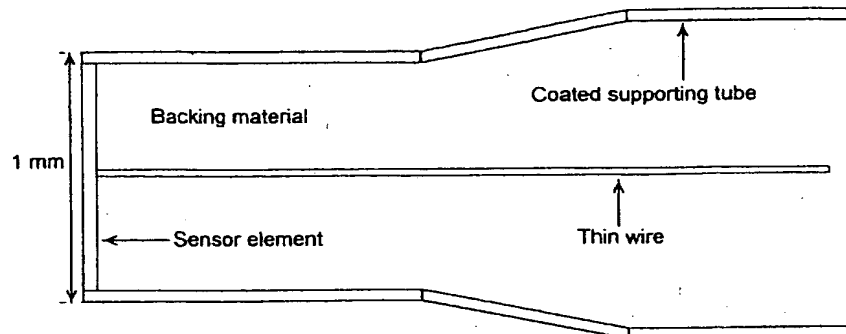


Fig. 2. Schematic representation of ceramic needle-type hydrophone.

devices, so are appropriate for the measurement of high power fields, and are usually of high sensitivity. However, they can suffer from unpredictable structure both in their frequency and directional responses due to radial resonance modes, reflections and mode conversions in the active element and backing material. The high characteristic acoustic impedance of ceramic materials (when compared to water) means that they perturb the field being measured. Typically, hydrophones of this type are constructed with active elements of diameter 0.4–0.6 mm, values which are much less than the wavelength at 40 kHz.

Closer characteristic acoustic impedance matching between the sensor element and water may be achieved through the use of the piezoelectric polymer polyvinylidene fluoride (PVDF). PVDF is also flexible and resistant to chemical attack. Using the type of construction employed in the ceramic needle probe, hydrophones have been designed using a PVDF active element [15,16]. Fig. 3 shows such a design. The problems of irregular frequency responses when using ceramic piezoelectric materials noted above are reduced when using PVDF, but radial resonances are still of concern. In addition, the contact between the active element and the

connecting thin wire can deteriorate over time, and like the ceramic needle-type hydrophone described earlier, this can lead to instability.

#### 2.1.2. Membrane devices

A further design of hydrophone has been produced, which has largely solved the problems encountered in using needle devices. This design is the membrane hydrophone [17], and it is now the accepted 'gold-standard' world-wide device for making absolute, traceable measurements of acoustic pressure distribution in medical ultrasonic fields. It comprises a large sheet of PVDF in the form of a thin film, with gold or chromium electrodes vacuum-deposited on the surface, stretched across an annular frame. Metal film leads are evaporated onto both sides of the membrane, and the small overlap region formed determines the active area of the device. The majority of device developments were carried out in the early 1980s [18,19]. Modern manufacturing techniques can produce devices with active elements of 40 µm diameter, with bandwidths up to 150 MHz. Fig. 4 depicts a typical coplanar design.

The characteristic acoustic impedance of PVDF is well matched to that of water and therefore, provided the membrane is thin, membrane hydrophones have the advantage of causing minimal disturbance to the acoustic field, especially as the ultrasonic beam generally passes through the aperture of the supporting ring. Also, the frequency response of membrane devices tends to be smooth in the megahertz frequency range. Membrane hydrophones find their use almost exclusively in the characterisation of medical fields below the threshold of cavitation, and are frequently used in degassed water to minimise the risk of cavitation occurring (for example, in physiotherapy fields). Some authors have used them in assessing the fields generated by lithotripters, fields in which peak-compressional pressures can reach in excess of 70 MPa [20]. PVDF would appear to be linear in its piezoelectric properties up to these levels [21]. However, when characterising lithotripter fields, membrane hydrophones may be susceptible to cavitation

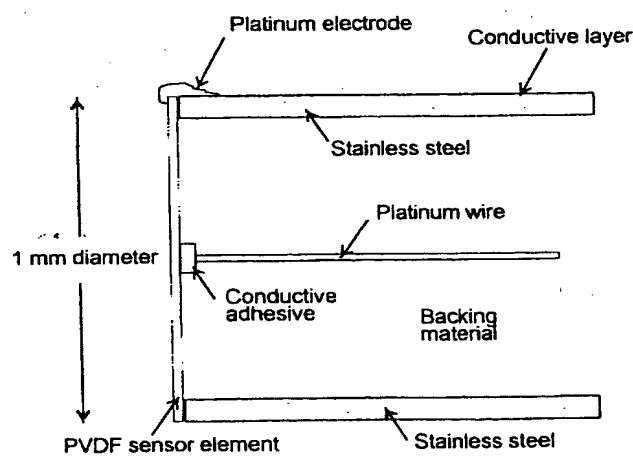


Fig. 3. Schematic construction of PVDF needle-type hydrophone.

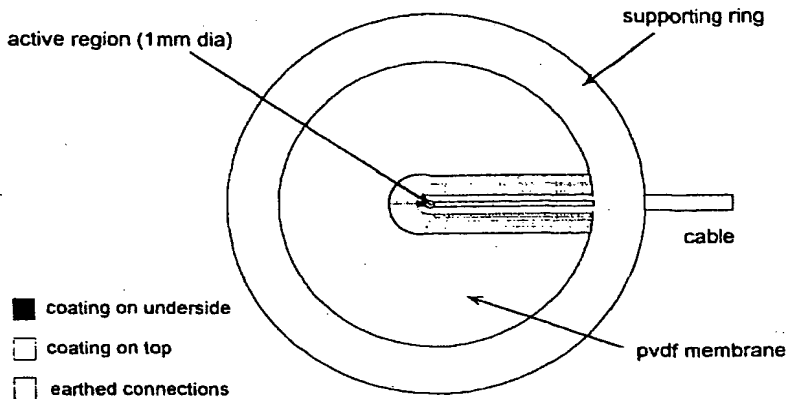


Fig. 4. Schematic diagram of a coplanar membrane hydrophone.

induced damage. The gold electrodes attached to the PVDF membrane can become locally eroded, even though the polymer itself is undamaged, and the sensitivity of the hydrophone can then decrease with continued exposure to lithotripter shock pulses. Bilaminar membrane hydrophones used in lithotripter measurements can suffer from delamination damage.

The application of membrane hydrophones to measurements of high power ultrasound fields has been limited to measurements of medical fields only, and even these have demonstrated problems with fragility [20]. Some needle-type probes have also been used in the characterisation of lithotripter fields [22], and generally this has been the limit of the extent of measurements using calibrated devices.

The need to make measurements of lithotripter field parameters, specifically of the peak-rarefactional pressure amplitude, coupled to the limitations shown when using conventional hydrophones has led to several variants on the conventional piezoelectric hydrophone theme [23,24]. Further, capacitance hydrophones have been applied to such fields [25]. An objective assessment of the desirable qualities of a piezoelectric hydrophone designed to measure lithotripter fields has been published, along with some results from a prototype device [26]. Two specific devices are covered in Sections 2.1.3 and 2.1.4 below.

#### 2.1.3. Liquid electrode hydrophone

Cathignol [23] has developed a membrane-style hydrophone applicable specifically to lithotripter measurements. The design is similar in some respects to a previously described hydrophone [27], but differs in that the electrodes are connected to the active element via an electrolyte rather than a dielectric liquid medium. A schematic cross-section of the device is shown in Fig. 5.

The device works by the piezoelectric effect, as described in Section 2.1. However, the effect of the charge distribution created by the impinging ultrasonic wave is transferred to the two metal electrodes via the

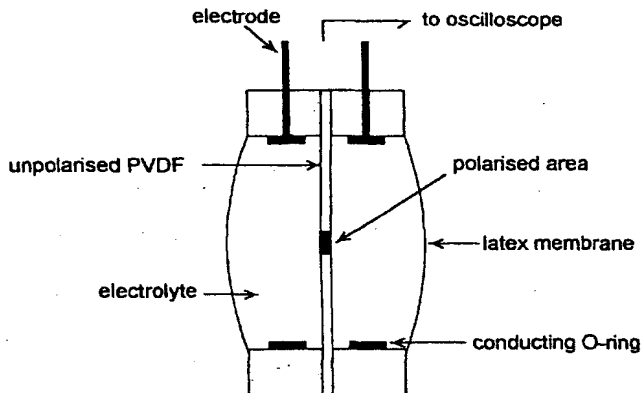


Fig. 5. Schematic diagram of liquid electrode hydrophone.

electrolyte, rather than exposing the fragile electrodes themselves to the hostile field directly. The author constructed the device from a PVDF film of thickness 9 µm, with an active element diameter of 1 mm. This was calibrated against a conventional membrane hydrophone and shown to have a sensitivity of 12 mV/MPa over a bandwidth of 20 MHz. More importantly, it was able to stand in excess of  $10^5$  shock pulses of 30 MPa pressure amplitude without any significant decrease in sensitivity. The device is not as sensitive as a conventional membrane hydrophone (a similar coplanar device with a 1 mm diameter active element would have a sensitivity of around 70 mV/MPa, a factor of 6 higher), and may not have the temporal response. It is undoubtedly useful, however, for the assessment of lithotripter fields. A miniature device based on a similar liquid electrode mode of operation has also been developed [28].

#### 2.1.4. Reflector-style hydrophone

Bedi and Selfridge [24] have published details of another hydrophone variant developed specifically for measuring the output from lithotripter fields. Rather than using a polymer, they have reverted to manufac-

ing the device with a ceramic piezoelectric (lead titanate) active element backed by a matched acoustic impedance. This has been shown to undergo no significant change in sensitivity after 5000 shocks of acoustic pressures in excess of 100 MPa. In addition, the device is able to faithfully reproduce rarefactional pressures. The effect of the matched impedance is to reflect the incoming wave, rather than be acoustically transparent, as is the case for membrane hydrophones. Potentially, this mechanism can be damaging to the device, because if the reflection occurs at a boundary with an acoustic impedance less than that of water, an incident compressional pulse will be inverted to a rarefactional pulse, instantly causing cavitation adjacent to the surface. The matching layer is hence designed to prevent this occurring. In comparison with a conventional calibrated membrane hydrophone (the sensitivity of which was determined at low power levels), excellent agreement was seen in the peak-compressional and peak rarefactional pressures indicated by the two devices. In addition, the ceramic design did not suffer from the characteristic resonances seen in the response of a conventional membrane hydrophone (associated with the thickness response of the active element and cable resonances). The use of a ceramic active element also meant that the device had a higher sensitivity than that of a conventional membrane device with a similar (1 mm) active element size.

#### *2.1.5. The application of hydrophones to the characterisation of high power systems*

The application of hydrophones used in the medical field to many high power applications may be limited by their bandwidth, with lower cut-off frequencies typically being at hundreds of kHz, outside the 20 kHz operating frequencies of many sonochemistry and cleaning applications. Recent work has produced two miniature ceramic devices that claim to overcome this barrier, and also be resistant to the extreme conditions produced by strongly cavitating fields [29]. The construction of these devices is similar to that shown in Fig. 2, comprising a lead zirconate titanate crystal supported on a cylindrical body. To reduce the influence of resonances on the device output, the active element was embedded in a silicone rubber and cork mixture, effectively decoupling the crystal from any tube wall vibrations. In addition, the active element was coated with a thin layer of polymer resin for protection. The hydrophone also includes an integral amplifier, producing a uniform gain over a frequency range from 10 kHz to over 100 kHz. In evaluation, the devices showed a flat frequency response up to 150 kHz, and sensitivities of a few mV/Pa. They appeared to produce a stable output over a 100 h period of testing in a strongly cavitating environment.

Perhaps more suitable for application to the measurement of acoustic parameters at lower frequencies are hydrophones commonly used in underwater applica-

tions. These generally consist of a piezoelectric ceramic active element mounted inside a specialised rubber surround, which serves to match the acoustic properties of the sensor to the water. Devices of this type usually approach uniformity in their directional response, as at low frequencies, the element dimensions tend to be less than one-tenth of the acoustic wavelength. In comparison to the membrane and needle devices described above, the bandwidth of underwater hydrophones extends to the tens of kHz range. Use of hydrophones of this type in measurements of high power devices has not been widely reported, although a recent paper described such a device being used for measurements on an ultrasonic surgical instrument [30].

Ultrasonic surgical instruments, used in dental descaling treatment, tissue fragmentation, phacoemulsification and other similar processes also fall into the category of 'intentionally cavitating' devices. There is still a degree of uncertainty over the mechanism by which they operate, be it through cavitation, a hammer action, or perhaps a combination of these and other effects. Instruments of this type are usually characterised in terms of the vibration amplitude of the tip [31–33], but the link between this and the action of the devices is still uncertain. A paper cited above [30] demonstrated some attempts to characterise the acoustic field produced by such a device using two hydrophones: one to measure the acoustic signal directly at frequencies below 100 kHz, and another to quantify the 'cavitation energy' over a wider bandwidth. Such acoustic emission techniques for monitoring cavitation can be found in the ISVR report [11].

#### *2.2. Fibre-optic hydrophones*

In making measurements of high power ultrasound fields, the ability of the device to withstand the extremes of conditions produced by the field is of concern. A means to overcome this difficulty is to measure the field parameters using a device with a replaceable tip. Also, with uncertainties over the degree of field perturbation caused by piezoelectric devices, and the difficulties associated with manufacturing sensors with small active elements and usable sensitivities, there exists a need to investigate alternative measurement techniques or devices. These problems can be overcome to some extent by using fibre-optic techniques.

The compressive and rarefactive regions in an ultrasonic wave result in local changes of the refractive index of the transmitting medium. Due to the speed of light being much greater than the speed of sound, these regions of pressure maxima and minima appear stationary to an incident light beam. The ultrasound behaves as a phase grating, and using a photodetector and lens (or optical fibre) arrangement, information about the acoustic beam can then be derived from the resultant

diffraction pattern [34–37]. The use of an optical fibre to measure an acoustic signal was first demonstrated by Bucaro et al. [38].

A comprehensive demonstration of this form of optical hydrophone is given by Wu et al. [39]. The device is based upon a two-fibre sensor, with the incident light beam being diffracted by the acoustic signal propagating at right angles to it. Using the principle of Raman–Nath light diffraction, the amplitude and phase information from the acoustic signal can be reconstructed from the light intensity levels produced by the receiving fibre, assuming the number of harmonic terms produced by the diffraction is restricted. The device showed good agreement with results obtained from a piezoelectric needle probe positioned at the same point in the field. The frequency response was reasonably flat over the range 1–15 MHz; however, this is limited only by the wavelength of the light beam used ( $0.6328\text{ }\mu\text{m}$ ), the bandwidth of the photodetector, the interaction region and the properties of this medium. The authors concluded that the device was suitable for measurements of both continuous wave and pulse signals, and has potentially a high spatial resolution, comparable to the core diameter of the optical fibre used.

In further studies using the same device [40], a range of spectral and spatial measurements of focused and unfocused transducers of frequencies up to 20 MHz were carried out, again showing reasonable agreement with data from a 0.5 mm diameter PVDF needle hydrophone. However, in both sets of studies, the system suffered from electrical noise, and the fibre optic sensor had a sensitivity some 20 dB lower than that of the PVDF probe.

A further development of optical sensor has been demonstrated by Huber et al., in their so-called laseroptic hydrophone [41]. In this case, light from a laserdiode is coupled to a quartz glass optical fibre of a  $50\text{ }\mu\text{m}$  core diameter, and the end placed into the acoustic propagation medium. Some of the emitted light is reflected back into the fibre, depending on the ratio of the refractive indices of the medium and the fibre. This reflected light can then be detected using a y-coupler and photodiode arrangement. The local density of the water, and hence its refractive index is increased in the compressional phase, thereby reducing the difference between the respective refractive indices, and the reflectivity. The reverse occurs in the rarefactional phase, producing a time-varying signal at the photodiode. The laseroptic probe was independently calibrated using a range of liquids of known refractive indices. Good agreement was seen between the laseroptic probe, a needle hydrophone and a capacitively coupled membrane hydrophone in the acoustic pressure values derived.

Interestingly, the laseroptic hydrophone appeared to provide information on cavitation occurring close to the end of the fibre, shown by the photodetector as sharp

peaks, due to the marked difference in the refractive indices of water and air. A proportional correlation was seen between the negative pressure amplitudes measured and the duration of the cavitation signal detected. It would seem, in this case, that the probe could be used to monitor simultaneously both acoustic pressure and cavitation. The device demonstrated would appear to provide useful information on the lithotripter fields measured. However, it still suffers from the lack of sensitivity prevalent in most optical techniques, again being 20 dB lower than the piezoelectric devices tested.

A version of the type of sensor demonstrated by Huber et al. was also developed by Staudenraus and Eisenmenger [42]. Using the same principles of an acoustic pressure change inducing a variation in the optical reflectance at the boundary between the fibre end and the medium, the authors constructed a more sophisticated variant, incorporating a noise detector, producing a clean waveform. The device was shown to have a bandwidth of 20 MHz, and a spatial resolution of 0.1 mm. Again, the authors tested various aspects of its performance against several different piezoelectric hydrophones: a PVDF needle probe, a PVDF membrane hydrophone and a capacitively coupled PVDF device [27]. The limitations in measuring rarefactional pressures with conventional PVDF hydrophones (due to the low cavitation threshold at the metallised surface) were seen in the comparison, with the fibre-optic probe providing the lowest values of peak rarefactional pressure ( $-15\text{ MPa}$ ) seen. The PVDF devices showed that the rarefactional pressure responses were truncated by cavitation, only reaching levels of around  $-7\text{ MPa}$ . The fibre-optic probe was again shown to be less sensitive than the PVDF devices. However, this problem was overcome somewhat by the application of a thin layer of optically clear silicone rubber over the end of the fibre, which produced a seven-fold increase in sensitivity. Recent measurements using a fibre-optic hydrophone of this type have shown an ability to measure peak rarefactional pressures as low as  $-25\text{ MPa}$  [43].

The principle of Fabry–Perot interferometry has been used in the development of a different type of fibre-optic probe [44]. The device described consists of a optical fibre which has a thin polymer film mounted at the end. The presence of an ultrasonic field induces changes in the thickness of this element, which are then picked up by an interrogating interferometer. Such a design has been shown to be of wide bandwidth and of excellent spatial resolution, with a sensitivity similar to a PVDF membrane hydrophone; indeed performance evaluation in comparison to membrane hydrophones has shown excellent agreement when used in lithotripter fields. The device has its main application in this area, being of sufficiently small dimensions to be used in vivo. It is thought that information on cavitation activity at

the focus of an extracorporeal shock wave lithotripter can also be obtained from the design.

An interesting method is again based on interferometry [45], in which the presence of an acoustic signal causes measurable changes in the refractive index. In this case, the authors investigated these refractive changes in a solid material, using optical fibres embedded in sample materials of polyethylene and graphite composite. Using a PZT transducer for their ultrasonic source, they were able to detect signals over a 100 kHz to 5 MHz bandwidth. The technique would perhaps have limited application in 'real systems', although it may be applicable to ultrasonic welding, where currently, acoustic measurements are rarely performed.

The use of optical techniques in the characterisation of high power ultrasonic fields has currently been limited to making measurements on medical devices. Fibre optic hydrophones can be calibrated against piezoelectric devices at low acoustic pressures to yield absolute information, and their use would seem to be gaining increasing recognition as a suitable means of evaluating high power field characteristics. Further, an optical technique could be used to monitor acoustic pressure and cavitation emissions simultaneously, with the required signal being achieved by signal filtering techniques. Sonoluminescence could even be monitored by fibre-optic probes, if the signal-to-noise ratio was adequate.

### 3. Optical interferometry

The use of optical techniques is not restricted solely to hydrophone probe-like devices. The local changes of particle position in a medium caused by the progression of an acoustic wave can cause a displacement of a surface or membrane, which can then be interrogated by an optical beam. Such a technique hence allows remote monitoring of field parameters. The displacement produced by continuous plane progressive waves of intensity  $100 \text{ mW cm}^{-2}$  at 5 MHz is around 1 nm, and greater displacements are seen at lower frequencies. Using a moving membrane or pellicle, a heterodyne interferometer can be used to assess the exact displacement, which is proportional to the acoustic pressure amplitude at that point (assuming plane wave propagation). This technique has been demonstrated by Royer et al. [46]. The method demonstrated involved the probing of a field using a reference beam and a probe beam, focused onto a gold reflecting coating on a thin pellicle immersed in water. The technique exhibited a bandwidth of 20 MHz, with a spatial resolution better than 0.1 mm, corresponding to a minimum detectable time-averaged acoustic energy of  $2 \mu\text{J m}^{-2}$ . An interferometer of this type has been adapted for use as a primary standard instrument for the calibration of hydrophones [47]. The Michelson interferometry prin-

ciple has also been extended recently to a fibre-optic based sensor [48].

Recent work directed specifically at the assessment of lithotripter fields has produced a variant of the Michelson interferometer with a long-path-difference geometry, to measure the velocity of a pellicle placed in the acoustic beam [49]. Again, this parameter can be used to derive the absolute acoustic pressure. Extracorporeal shockwave lithotripters can produce particle velocities in the range  $1\text{--}100 \text{ ms}^{-1}$ , and in the cited research, the velocity of an acoustically transparent but optically reflecting target located in the field of a shock-wave source was evaluated with an interrogating single-mode laser beam. Preliminary trials have shown that the system has a bandwidth of 100 MHz.

### 4. Thermal methods

As ultrasound propagates through a medium, its amplitude decays due to the attenuating nature of the medium. This is due to absorption and scattering effects. In a homogeneous material, where energy losses due to scattering may be considered negligible, the absorption is attributable to thermal conductivity, viscous effects and other molecular processes. This energy transfer results in a temperature rise in the medium, which can be used to provide information about the acoustic field. Two independent classes of measurement technique can be derived from this effect, one of bulk techniques, the other discrete.

#### 4.1. Discrete thermal methods – single element probes

Almost certainly, the first type of sensor that was developed and used to yield information on ultrasonic field distributions was based on a thermal detection method. The original theory and experimental evaluation of this type of probe was first carried out in the 1950s [50].

Simple and inexpensive in construction, discrete thermal probes are based on thermocouples or thermistors, usually encased in an acoustically absorbing material, preferably with a similar acoustic impedance to that of water. When placed in an ultrasonic field, temperature rises are produced in the surrounding material by the absorption of ultrasound, which causes a change in the electrical output of the thermal device. From the literature, the initial rate of temperature rise in the absorbing medium, during the first few tenths of a second after the insonating field is activated, is proportional to the acoustic intensity [51], assuming that the heat losses are small over this short time period. Fig. 6 illustrates a typical time response of a discrete thermal sensor.

As the temperature of the sensor rises, heat losses occur due to conduction, convection and radiation. An

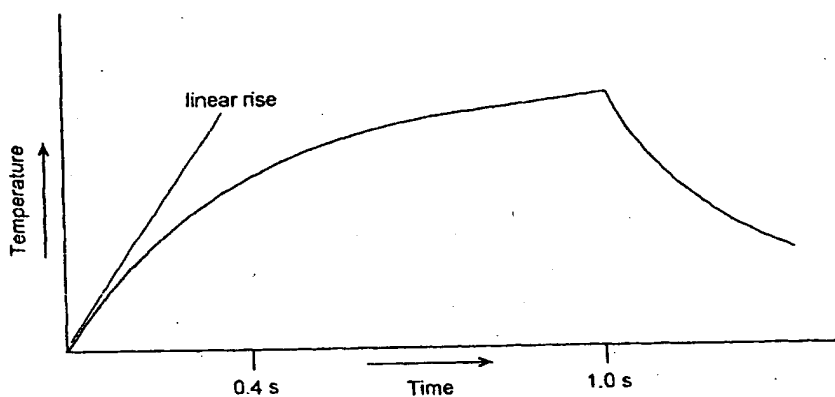


Fig. 6. Temporal response of a typical thermal probe.

equilibrium temperature is reached when the rate of heat loss is equal to the rate of energy absorption. This equilibrium temperature can also be a linear function of the ultrasonic intensity, provided the losses (including enhanced convection losses due to streaming caused by the ultrasonic beam) are proportional to the difference between the temperature of the probe and that of the water bath [51]. The physical construction of probes of this type is normally in the form of a cylindrical block of encapsulating material about the thermal device, or sometimes with the thermal element suspended via its connecting leads on a frame, allowing the acoustic beam to pass through the support in a similar fashion to that employed in hydrophone construction. Fig. 7 shows typical discrete thermistor designs.

Similar devices can be constructed using thermocouples, with the addition of an amplifier in the signal chain. In characterising a 980 kHz field, Fry and Fry [50] used a design similar to the suspended thermistor case in Fig. 7, but with two polyethylene diaphragms stretched over the supporting ring with the void between them filled with castor oil, which provided high absorption in the immediate vicinity of the uncoated thermocouple used. The rise in temperature observed in the

presence of ultrasound is thought to result from two phenomena: conversion of the acoustic energy in the field into heat by viscous forces acting between the thermocouple wire (or thermistor casing) and the embedding medium, and absorption of sound in the body of the embedding medium.

Thermal probes can be fabricated with an extremely small measurement volume and are hence well suited for performing measurements of local intensity. In practice, however, there is a trade-off between limiting the dimensions of the sensor and obtaining an observable temperature rise. It should be noted that thermocouple probes measure the relative acoustic intensity as a function of temperature: absolute intensity measurement requires prior calibration, or accurate knowledge of the acoustical and thermal properties of the absorbing medium. Studies have been undertaken to evaluate suitable absorbing materials and encapsulation configurations [52].

#### 4.1.1. Application of thermal probes to the characterisation of high power fields

Thermal probes are applicable to measuring high power fields in that their response is omnidirectional,

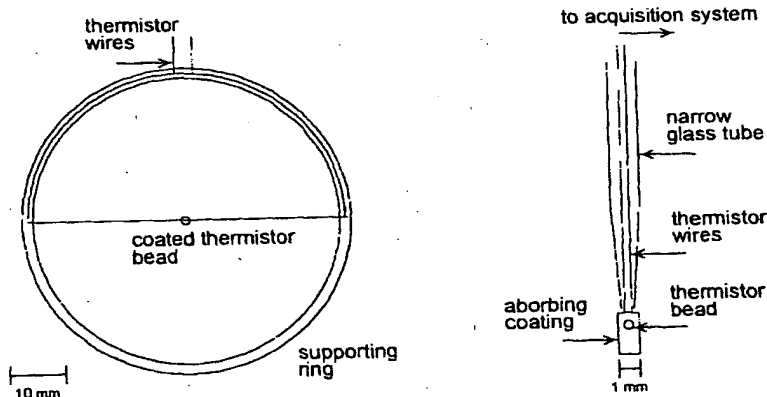


Fig. 7. Typical thermistor probe designs.

and they can often yield results of fine spatial detail; thermocouple devices may be made as small as 10 µm. However, reproducibility of probe manufacture can be a problem, particularly when using encapsulating materials, as any trapped air in the absorber will alter the acoustic properties of the material. In addition, the acoustic properties of the absorbing material are often frequency and temperature dependent. Ultrasonic fields at megahertz frequencies produce significant temperature rises, even in devices with thin rubber coatings, whereas materials which have sufficiently high attenuation coefficients at tens of kilohertz are less widely documented. Cavitating bubbles can attack the potting compound, altering the volume of the absorbing material around the thermal device, which affects the sensitivity, and perhaps more importantly, produces small motes in the surrounding liquid, which act as nucleation sites for cavitation. In using a thermal sensor, the ambient temperature must be monitored. Further, the response time of thermal sensors is comparatively slow, meaning that the temporal variation in pulsed fields cannot be resolved.

The temporal response of a thermal probe is also limited: in addition to the few hundred milliseconds over which the rate of temperature increase is linear with intensity, the device must be allowed to cool down between measurements over a period of several seconds. In procedural terms, this means switching off the applied signal, which in the case of performing field distribution measurements in an ultrasonic cleaning bath, for example, may have the effect of changing the standing wave patterns produced, as the time taken for the water surface in such a device to settle down after switching on can be considerably greater than the linear response time of a thermal sensor.

Recently, the literature has shown research groups revisiting this measurement technique, in conjunction with computer-controlled positioning and acquisition systems [53–55]. This recent work has moved towards the characterisation of fields produced by ultrasonic generators employed in sonochemistry applications, when previously, much of the research in the 1970s and early 1980s was orientated towards medical fields. This shows a growing awareness amongst research groups of the need for spatial information of the intensity distribution. Continued work in this area will enable optimum vessel geometries and insonification configurations to be determined and may ultimately establish a set of measurement techniques that will enable results from different research groups on similar chemical reactions to be intercompared.

The spatial distribution of the acoustic intensity in an ultrasonic field has been assessed using a thermal technique, and the results compared with spatial information on the extent of acoustic cavitation, assessed by foil erosion and chemical dosimetric techniques [10], the

Sarvazyan dye method (see below) [56], by a hydrophone [57], and by a chemiluminescent method [58]. The results seen in the latter case are of interest, as the authors discovered that the sites in the acoustic field where the highest number of OH<sup>·</sup> radicals were produced (illustrated by the level of chemiluminescence observed), which correspond to cavitation 'hot-spots', did not correspond to the positions at which the highest output levels were shown by the thermocouple probe output. They suggested that this provides evidence to indicate that a significant part of the ultrasonic energy delivered to a liquid volume is probably not used to induce sonochemical changes. This may also indicate that the presence of the thermocouple probe causes sufficient perturbation such that the regions of highest intensity are displaced from their true locations. However, the authors showed that the intensity distribution measured with the thermocouple probe agreed with conventional plane-piston transducer theory.

#### 4.2. Discrete thermal methods – multi-element probes

In the 1970s the IEC published a report which summarised the position on standardisation for establishing the output of an ultrasonic cleaning bath [59]. Part of the work involved an assessment of a multi-element thermal probe designed and produced in Germany which utilises many of the same principles described above, but which provides spatially averaged acoustic information, by employing an array of linked thermal sensors [60]. The instrument consists of 32 coated thermocouples, mounted on 'stalks' projecting from a central sphere. The outputs from the thermocouples are integrated, and the overall device output takes the form of a DC voltage. The dimensions of the device are such that it corresponds to half a wavelength in water at 20 kHz, which is equal to the separation of successive nodes or antinodes in a standing wave field. In this way, the authors predicted that the device would produce the same output, regardless of its location when positioned in a uniform standing wave field at 20 kHz, generally the most common frequency for cleaning tanks.

Each thermocouple element was coated in a form of Perspex which had been aerated to increase its acoustic absorption properties. Unfortunately, the apparent variation in probe output with dissolved gas content in the surrounding liquid led to it being rejected as the basis of a standard measurement technique by the IEC. However, a device of this type that produces a spatially averaged figure for the energy density in a cleaning bath is potentially useful as a routine monitor of cleaning bath output.

#### 4.3. Bulk thermal methods

In applications such as sonochemistry, a more global measure of the 'energy' entering a fluid volume is often

of use. This can be achieved by making calorimetric measurements, where the acoustic power delivered is assessed simply by measuring the temperature rise observed when a known volume of liquid of known heat capacity is sonificated for a known time. Care must be taken in reducing errors due to heat losses, and contributions to the temperature rise from acoustic source inefficiency. In a controlled environment, useful absolute power data can be obtained [61–66]. Ratoarinoro et al. [66] compared different power measurement techniques for both electrical input and acoustical output power with chemical yield for a given reactor, as a function of liquid height in the vessel, and concluded that the dissipated acoustic power density appeared to show the best correlation with reaction yield.

Some sonochemists make an estimate of the acoustic intensity in a vessel by simply dividing the power (derived from calorimetry or electrical power measurements) by the area of the radiating horn tip or bath surface [10]. While acceptable as a very rough means of comparing different sonicating devices, this is by no means an adequate way of quantifying the acoustic field, due to uncertainties in the effective area of the probe tip.

### 5. Radiation force methods

Targets placed in the path of an acoustic beam experience a unidirectional force, known as the radiation force. Characterisation methods based on the measurement of this force predate the use of piezoelectric hydrophones [67]. Such methods can be used to provide data on both spatially averaged and local intensities, depending on the size of the target relative to the ultrasonic beam dimensions. The radiation force experienced by the target per unit area is proportional to the ultrasonic intensity in the field. This manifests itself either by a measurable change in the target 'weight', in the case of a large target, observed on a balance; or by a linear displacement, seen for a small target and measured with a travelling microscope. A large target which covers the total effective beam area provides the total power, whereas a small target totally immersed in the field will provide local information on the time-averaged intensity.

This would appear to be a simple and inexpensive method, but is very limited in its applicability to typical high power fields. Radiation force devices are used for making power measurements in the megahertz frequency range, but the rapidly diverging fields produced by high power devices (for example, sonochemical processors) operating in the tens of kilohertz range would be difficult to characterise, unless the beams were collimated in some way. Also, consideration would need to be given to the propagation medium used, as cavitation bubbles will scatter the acoustic field.

The cavitation bubble activity produced by lithotripter fields is generally longer lasting than the acoustic pulse itself, and these events may also cause a measurable force on a target. This effect forms the basis of a measurement device recently reported in the literature [68]. The device consists of an electromagnetic velocity sensor linked via a short rigid rod to a stainless steel ball. This ball is placed underwater at the focus of a lithotripter, and the violent cavitation activity produced by an incident shock wave causes the ball and rod to move. The output voltage from the electromagnetic probe is measured on an oscilloscope, and is proportional to the velocity of the steel ball. The square of the probe output voltage is therefore proportional to the energy transferred to it. Measurements have also shown that there is a linear correlation between lithotripter pulse energy and the amount of synthetic stone destruction. Recent results would seem to reinforce this, and indicate also that the probe responds directly to cavitation activity [69].

### 6. Semi-quantitative techniques

With the exception of thermal probes, the majority of the devices described above represent state-of-the-art measurement techniques, and tend to be expensive. With this in mind, Sarvazyan et al. have developed a technique that requires the bare minimum of conventional laboratory supplies and reagents, and in principle, can be calibrated to provide reproducible acoustic data [70]. The technique is based upon the ability of ultrasound to increase the diffusion rate of liquids into porous media. When a piece of white paper is placed in a tank to which a few drops of water-soluble dye (0.1% methylene blue) have been added, and the transducer switched on, the rate of diffusion of dye into the paper is proportional to the local ultrasonic intensity: this was assessed over a wide range of exposure times. The authors correlated the technique with measurements made using a thermocouple probe. In theory, the technique may be calibrated by assessing the optical density of the exposed indicator paper.

The hostile conditions produced by ultrasonic cleaning baths have prompted studies on rugged, semi-quantitative devices for assessing the spatial distribution of the acoustic field. An example [71] is based on the principle of piezoelectricity, but consists of a waveguide attached to a conventional transducer. The device hence comprises an exponential horn with a tip diameter of 1 cm, attached to a PZT crystal. The bandwidth of the system was thought to be in the range 20–40 kHz. The probe is essentially a sonochemical horn, operating in receive mode. Assuming that the horn acted as a perfect waveguide, the authors used the output voltage to derive relative intensity values in making measurements of the

**Table 1**  
Summary of key measurement techniques for high power ultrasound fields

Property	Device	Membrane hydrophone	Needle hydrophone	Discrete thermal probe	Multi-element thermal probe	Fibre-optic hydrophone	Heterometric methods
Physical effect	Piezoelectricity	Piezoelectricity	Thermal absorption	Thermal absorption	$\text{d}I/\text{d}P$	Membrane or pellicle movement	
Parameter	Acoustic pressure	Acoustic pressure	spat acoustic intensity (relative)	spat acoustic intensity (relative)	Acoustic pressure	Particle displacement or velocity	
Spatial resolution	40 μm	75 μm	10 μm	Spatial averaging	0.1 mm	50 μm	
Bandwidth	100 MHz	30 MHz	Dependent on absorbing material	Dependent on absorbing material	Potentially >3 GHz	up to 100 MHz	
Sensitivity	$20 \text{ nV Pa}^{-1}$	$40 \text{ nV Pa}^{-1}$	$0.1 \text{ mV Jm}^{-3}$ (increases as $f^2$ )	$4 \text{ nV Pa}^{-1}$	$60 \text{ nV Pa}^{-1}$		
Pressure range	Up to 100 MPa	Up to 100 MPa	Not proven	Not proven	50 MPa	Potentially large	
Comment	Can be damaged by cavitation. Expensive	Can be damaged. High sensitivity. Frequency response unpredictable	Cheap. Easy to use. Subject to cavitation erosion damage in high intensity fields.	Can be subject to cavitation damage in high intensity fields. Patent refers to device suitable for use in 20 kHz fields only perhaps shielding and streaming effects	Upper frequency limit determined only by $\lambda$ of light used	Figures taken from [44,49]. High power capabilities not yet fully tested	
Refs.	[17–20,26]	[8, 13–16,28,29]	[50–58]	[59,60]	[34–43]	[44–49]	

spatial distribution of two commercially available cleaners. The device is not without its merits, as it is simple to use and durable. However, the extent to which it perturbs the field must be of concern.

Ultrasonic cleaning bath manufacturers have also developed semi-quantitative methods for characterising their devices. One example of this is the Ultraprobe [72], developed by Zenith Manufacturing in the US. The device consists of a column of 'ultrasonic wave energy responsive fluid medium' in which 'ultrasonic wave energy responsive visible particles' are suspended. It works on the principle of particulate movement: when the probe is placed in an ultrasonic cleaning bath, the suspended particles migrate to the standing wave nodes produced, thereby giving a visual indication of the standing wave field distribution in the cleaning bath.

## 7. Summary

This review has shown that although high power ultrasound has a wide variety of applications, varying from health care to welding, there are comparatively few measurement techniques that have been developed specifically for characterising the acoustic fields produced. Table 1 summarises the techniques described in this report that are applicable to high power field characterisation, with some comparison of their attributes.

The majority of the accurate, reliable techniques that have been reported relate to the medical uses of ultrasound, and have been limited in their adaptation to other applications. Most industrial applications (including sonochemistry and cleaning) are currently not subject to the same demand for control of exposure as in medicine, and the characterisation techniques uncovered reflect this. Researchers are using techniques which are simple and inexpensive to apply, but which yield information which is thought to relate to some aspects of the field which are relevant to the process: for example, in assessing the fields produced by sonochemistry processors, a calorimetry technique is used to provide a global indication of the power delivered to the sample. However, more recent literature is showing that information on spatial distributions is becoming essential, and the direction that current studies are taking is starting to reflect this.

This review has majored on conventional measurement techniques which have been or are being applied to high power cavitating fields. However, it is possible to envisage alternative methods being developed. For example, research on the measurement of acoustic intensity at audio frequencies in air may also have application to waterborne ultrasound. Kuttruff and Schmitz [73] have developed two designs of intensity probe, based on multi-microphone technology in a geometry con-

sisting of a number of sensors located on the surface of an imaginary sphere. The devices measure the intensity vector.

Further developments in polymer technology will also influence sensor designs. Very thin films of PVDF are available, which enable construction of hydrophones with larger bandwidths, and of finer spatial resolution. A sensor that combines both field measurement capability and cavitation monitoring features could be possible, and may find extensive application with appropriate frequency-domain processing.

## Acknowledgements

The authors acknowledge the support of the National Measurement System Policy Unit (NMSPU) of the UK Department of Trade and Industry.

## References

- [1] B. Zegiri, M. Hodnett, T.G. Leighton, A strategy for the development and standardisation of measurement methods for high power cavitating ultrasonic fields: final project report, NPL Report CIRA (EXT) 016.
- [2] C.R. Hill, Calibration of ultrasonic beams for biomedical applications, *Phys. Med. Biol.* 15 (1970) 241-248.
- [3] International Electrotechnical Commission, IEC 1102:1991, Measurement and characterisation of ultrasonic fields using hydrophones in the frequency range 0.5 MHz-15 MHz.
- [4] International Electrotechnical Commission, IEC 1157:1992, Requirements for the declaration of the acoustic output of medical diagnostic ultrasound equipment.
- [5] Food and Drug Administration, FDA 510(k):1985, Guide for measuring and reporting acoustic output of diagnostic ultrasound medical devices.
- [6] International Electrotechnical Commission, IEC 1689:1992, Ultrasonics - Physiotherapy systems - Performance requirements and methods of measurement in the frequency range 0.5 MHz-5 MHz.
- [7] EC Medical Devices Directive (93/42/EEC), Official Journal of the European Communities, 36 (L 169).
- [8] P.A. Lewin, Devices for ultrasound field parameter measurements, *Proceedings of IEEE International Biomedical Engineering Days*, 1992, pp. 107-111.
- [9] B. Zegiri, in: R.C. Preston (Ed.), *Overview of measurement techniques. Output measurements for medical ultrasound*, London, Springer-Verlag, 1991, pp. 35-56.
- [10] B. Pugin, Qualitative characterisation of ultrasound reactors for heterogeneous sonochemistry, *Ultrasonics* 25 (1987) 49-55.
- [11] T.G. Leighton, A strategy for the development and standardisation of measurement methods for high power/cavitating ultrasonic fields: review of cavitation monitoring techniques, ISVR Technical Report No. 263, January 1997.
- [12] J. Curie, P. Curie, Développement par pression de l'électricité polaire dans les cristaux hémisphériques à faces inclinées, *C. R. Acad. Sci., Paris* 91 (1880) 294.
- [13] A.P.J.B. Walton, R.C. Chivers, in: M.G. Silk (Ed.), *The piezoelectric hydrophone for ultrasonic output assessment. The Evaluation and Calibration of Ultrasonic Transducers*, Guildford, IPC Science and Technology Press, 1978, pp. 96-104.

- [14] P.A. Lewin, R.C. Chivers, Two miniature ceramic ultrasonic probes, *J. Phys. E: Sci. Instrum.* 14 (1981) 1420–1424.
- [15] P.A. Lewin, Miniature piezoelectric polymer ultrasonic hydrophone probes, *Ultrasonics* 19 (1981) 213–216.
- [16] M. Platte, A polyvinylidene fluoride needle hydrophone for ultrasonic applications, *Ultrasonics* 23 (1985) 113–118.
- [17] K.C. Shotton, D.R. Bacon, R.F. Quilliam, A PVDF membrane hydrophone for operation in the range 0.5 MHz to 15 MHz, *Ultrasonics* 18 (1980) 123–126.
- [18] D.R. Bacon, Properties of a PVDF hydrophone with 100 MHz bandwidth for studying medical, nonlinear and other fields, *Proc. IEEE Ultrasonics Symposium*, 1980, pp. 582–585.
- [19] R.C. Preston, D.R. Bacon, A.J. Livett, K. Rajendran, PVDF membrane hydrophone performance properties and their relevance to the measurement of the acoustic output of medical ultrasonic equipment, *J. Phys. E: Sci. Instrum.* 16 (1983) 786–796.
- [20] A.J. Coleman, J.E. Saunders, A survey of the acoustic output of commercial extracorporeal shock wave lithotripters, *Ultrasound in Med. And Biol.* 15 (1989) 213–227.
- [21] S. Meeks, R. Ting, The evaluation of static and dynamic stress on the piezoelectric and dielectric properties of PVDF, *J. Acoust. Soc. Am.* 74 (1984) 1010–1012.
- [22] A.J. Coleman, Private communication.
- [23] D. Cathignol, PVDF hydrophone with liquid electrodes for shock wave measurements, *Proc. IEEE Ultrasonics Symposium*, 1990, pp. 341–344.
- [24] R.L. Bedi, A.R. Selfridge, Spot poled reflector style hydrophone for shock wave measurements, *Proc. IEEE Ultrasonics Symposium*, 1990, pp. 1141–1145.
- [25] L. Filipczynski, J. Etienne, Capacitance hydrophones for pressure determination in lithotripsy, *Ultrasound in Med. And Biol.* 16 (2) (1990) 157–165.
- [26] P.A. Lewin, M.E. Schafer, J.M. Gilmore, PVDF sensors for quantitative acoustic shock wave measurements, *Proc. Ultrasonics International*, 1989, pp. 548–553.
- [27] B. Granz, PVDF hydrophone for the measurement of shock waves, *IEEE Trans. Elect. Insulat.* 24 (3) (1989) 499–502.
- [28] N. Inose, M. Ide, A miniature hydrophone for high acoustic pressures, *Jap. J. Appl. Phys.* 31 (Supplement 31-1) (1992) 272–273.
- [29] L. Gaete-Garréton, Y. Vargas-Hernández, S. Pino-Dubreuil, F. Montoya-Vitini, Ultrasonic detectors for high-intensity acoustic fields, *Sensors and Actuators A* 3738 (1993) 410–414.
- [30] M.E. Schafer, A. Broadwin, Acoustical characterisation of surgical devices, *Proc. IEEE Ultrasonics Symposium*, 1994, pp. 1903–1906.
- [31] A.D. Walmsley, W.R.E. Laird, A.R. Williams, Displacement amplitude as a measure of the acoustic output of ultrasonic scalers, *Dent. Mater.* 2 (1986) 97–100.
- [32] A.R. Williams, A.D. Walmsley, Exposimetry of low-frequency ultrasonic dental devices, *IEEE Trans. Ultrason. Ferroelec. Freq. Contr.* 35 (2) (1988) 264–269.
- [33] International Electrotechnical Commission, IEC 1205:1993, Ultrasonics – Dental descaler systems – Measurement and declaration of the output characteristics.
- [34] R. Reibold, P. Kwiek, Optical near-field investigation into the Raman–Nath and KML regimes of diffraction by ultrasonic waves, *Acustica* 70 (1990) 223–229.
- [35] B.D. Cook, Measurement of the optical near-field of an ultrasonically produced phase grating, *J. Acoust. Soc. Am.* 60 (1976) 95–99.
- [36] R. Reibold, W. Molkenstruck, Light diffraction tomography applied to the investigation of ultrasonic fields. Part I: Continuous wave, *Acustica* 56 (1984) 180–192.
- [37] W.A. Riley, L.A. Love, D.W. Griffith, Observation of Raman–Nath optical diffraction in the phase grating plane, *J. Acoust. Soc. Am.* 71 (1982) 1149–1154.
- [38] J.A. Bucaro, H.D. Dardy, E.F. Carome, Optical fibre acoustic sensor, *Applied Optics* 16 (7) (1977) 1761–1762.
- [39] Y. Wu, P.M. Shankar, P.A. Lewin, D.P. Koller, Fiber-optic ultrasonic sensor using Raman–Nath light diffraction, *IEEE Trans. Ultrason. Ferroelec. Freq. Contr.* 41 (2) (1994) 166–171.
- [40] Y.Q. Wu, P.M. Shankar, P.A. Lewin, Characterisation of ultrasonic transducers using a fiberoptic sensor, *Ultrasound in Med. And Biol.* 20 (7) (1994) 645–653.
- [41] P. Huber, J. Debus, A. Lorenz, E.W. Hahn, P. Peschke, W.J., Lorenz, A laseroptic hydrophone for high energy ultrasound, *Proc. IEEE Ultrasonics Symposium*, 1991, pp. 1147–1150.
- [42] J. Staudenraus, W. Eisenmenger, Fibre-optic probe hydrophone for ultrasonic and shock-wave measurements in water, *Ultrasonics* 31 (1993) 267–273.
- [43] T. Reuner, G. Buchholz, J. Oesterle, U. Schätzle, The fibre-optic hydrophone – a new quality in measuring lithotripter shock waves, *Proceedings of World Congress on Ultrasonics* 1995, pp. 939–942.
- [44] P.C. Beard, T.N. Mills, Extrinsic optical-fibre ultrasound sensor using a thin polymer film as a low-finesse Fabry–Perot interferometer, *Applied Optics* 35 (4) (1996) 663–675.
- [45] J.J. Alcoz, C.E. Lee, H.F. Taylor, Embedded fibre-optic Fabry–Perot ultrasound sensor, *IEEE Trans. Ultrason. Ferroelec. Freq. Contr.* 37 (1990) 302–305.
- [46] D. Royer, N. Dubois, M. Fink, Optical probing of pulsed, focused ultrasonic fields using a heterodyne interferometer, *Appl. Phys. Lett.* 61 (2) (1992) 153–155.
- [47] D.R. Bacon, Primary calibration of ultrasonic hydrophones using optical interferometry, *IEEE Trans. Ultrason. Ferroelec. Freq. Contr.* 35 (1988) 152–161.
- [48] C. Koch, R. Reibold, Interferometric fibre-optic sensor for measurement of lithotripter shock waves, *Proceedings of World Congress on Ultrasonics*, 1995, pp. 931–934.
- [49] P.C.M. Galloway, R.C. Preston, D.R. Bacon, Velocity interferometer for measurement of high amplitude acoustic pulses, *Proceedings of World Congress on Ultrasonics*, 1995, pp. 935–938.
- [50] W.J. Fry, R.B. Fry, Determination of absolute sound levels and acoustic absorption coefficients by thermocouple probes, *J. Acoust. Soc. Am.* 26 (1954) 294–317.
- [51] C.J. Martin, A.N.R. Law, The use of thermistor probes to measure energy distribution in ultrasound fields, *Ultrasonics* 18 (1980) 127–133.
- [52] C.J. Martin, A.N.R. Law, Design of thermistor probes for measurement of ultrasound intensity distributions, *Ultrasonics* 21 (1983) 85–90.
- [53] M. Romdhane, C. Gourdon, G. Casamatta, Thermosensitive probe based technique of local investigation of ultrasonic reactors, *Proceedings of Ultrasonics International*, 1993, pp. 739–742.
- [54] M. Romdhane, C. Gourdon, G. Casamatta, Development of a thermoelectric sensor for ultrasonic intensity measurement, *Ultrasonics* 33 (1995) 139–146.
- [55] M. Romdhane, C. Gourdon, G. Casamatta, Local investigation of some ultrasonic devices by means of a thermal sensor, *Ultrasonics* 33 (1995) 221–227.
- [56] I.P. Marangopoulos, C.J. Martin, J.M.S. Hutchison, Measurement of field distributions in ultrasonic cleaning baths: implications for cleaning efficiency, *Phys. Med. Biol.* 40 (1995) 1897–1908.
- [57] I. Paniwnyk, T.J. Mason, J.P. Lorimer, A. Barr, D. Martin, K. Hutt, R. Hanas, Methods of mapping power in sonochemical reactors, *Proceedings of World Congress on Ultrasonics*, 1995, pp. 655–658.
- [58] Y. Renaudin, N. Gondrexon, P. Boldo, C. Pétrier, A. Bernis, Y. Gonthier, Method for determining the chemically active zones in a high frequency ultrasonic reactor, *Ultrasonics Sonochemistry* 1 (1994) S81–S85.
- [59] International Electrochemical Commission, IEC Document

- SC29D/WG1(Secretary) 11, October 1977. Report on results of preliminary evaluation of the integrating probes.
- [60] R.G. Pohlman, T.J.M. Herbertz, A new instrument for measuring the ultrasonic energy density in liquids, *Ultrasonics for Industry Conference Papers*, 1970.
- [61] T.K. Saksena, Methods of reliable measurement of ultrasonic power and cavitation in liquids, *J. Acoust. Soc. India* VIII (1980) 1 January.
- [62] J. Zieniuk, R.C. Chivers, Measurement of ultrasonic exposure with radiation force and thermal methods, *Ultrasonics* 14 (1976) 161-172.
- [63] G.R. Torr, D.J. Watmough, A constant-flow calorimeter for the measurement of acoustic power at megahertz frequencies, *Phys. Med. Biol.* 22 (3) (1977) 444-450.
- [64] T.L. Zapf, M.E. Harvey, M.T. Larsen, R.E. Stoltenberg, Ultrasonic calorimeter for beam power measurements, *NIST Technical Note* 686, 1983.
- [65] T.A. Delchar, R.J. Melvin, A calorimeter for ultrasound total power measurements, *Meas. Sci. Technol.* 5 (1994) 1533-1537.
- [66] Ratoarinoro, F. Contamine, A.M. Willhelm, J. Berlan, H. Dehnas, Power measurement in sonochemistry, *Ultrasonics Sonochemistry* 2 (1995) S43-S47.
- [67] T. Hasegawa, K. Yoshioka, Acoustic radiation force on a solid elastic sphere, *J. Acoust. Soc. Am.* 46 (1969) 1139-1143.
- [68] S.D. Pye, N.J. Parr, E.G. Munro, T. Anderson, W.N. McDicken, Robust electromagnetic probe for the monitoring of lithotripter output, *Ultrasound in Med. and Biol.* 17 (1991) 931-939.
- [69] S. Pye, Private communication.
- [70] A.P. Sarvazyan, T.N. Pashovkin, G.V. Shilnokov, An extremely simple and rapid method for registration of ultrasonic field patterns, *Proceedings of Ultrasonics International*, 1985, pp. 324-328.
- [71] S.R. Soudagar, S.D. Samant, Semiquantitative characterisation of ultrasonic cleaner using a novel piezoelectric pressure intensity measurement probe, *Ultrasonics Sonochemistry* 2 (1995) S49-S53.
- [72] E.A. Pedziwiatr, Ultrasonic wave energy and identification, US Patent No. 4433102.
- [73] H. Kuttruff, A. Schmitz, Measurement of sound intensity by means of multi microphone probes, *Acustica* 80 (1994) 388-396.